University
of
St Andrews

A Dynamic Combinatorial Approach to the Recognition-Mediated Acceleration of Chemical Reactions

By

Mairead J. Minto

A Thesis Presented for the Degree of

Doctor of Philosophy

in the

School of Chemistry

University of St Andrews

St Andrews **February 2005**

(i) I, Mairead Minto, hereby certify that this thesis, which is approximately 67 000 words in length, has been written by me, that it is the record of work carried out by me and that it has not been submitted in any previous application for a higher degree.

Signature of candidate . . Date 3/5/05...

(ii) I was admitted as a research student in September 2001, and as a candidate for the degree of Doctor of Philosophy in September 2001; the higher study for which this is a record was carried out in the University of St Andrews between 2001 and 2004.

Signature of candidate . Date 3/5/05...

(iii) I hereby certify that the candidate has fulfilled the conditions of the Resolution and Regulations appropriate for the degree of Doctor of Philosophy in the University of St Andrews and that the candidate is qualified to submit this thesis in application for that degree.

Signature of supervisor ....Date 3/5/05

In submitting this thesis to the University of St Andrews I understand that I am giving permission for it to be made available for use in accordance with the regulations of the University Library for the time being in force, subject to any copyright vested in the work not being affected thereby. I also understand that the title and abstract will be published, and that a copy of the work may be made and supplied to any *bona fide* library or research worker.

Signature of candidate . Date 3/5/05..

Abstract

The field of dynamic combinatorial chemistry has emerged as a useful tool for the selection of receptors and substrates since its conception nine years ago. To date, no dynamic combinatorial system has been reported which utilizes recognition processes such as those adopted so effectively within the field of supramolecular catalysis in order to amplify members kinetically within a dynamic library. This thesis describes an investigation into the effect that recognition processes have on the rate and the stereo- and/or regiochemical outcome of reactions within a dynamic combinatorial context. The design of systems capable of kinetic amplification of library members within a dynamic library by either linear or non-linear methods is described.

Chapter 1 sets the work presented within this thesis in context. The role of molecular recognition in self-assembly, dynamic combinatorial chemistry and supramolecular catalysis are discussed in detail.

Chapter 2 describes the design of a system which utilizes the recognition properties within library building blocks in order to facilitate kinetic amplification within a dynamic library. We describe the rational design and synthesis of a system which has the potential to amplify the most stable member of the library *via* AB methodology.

Chapter 3 describes the rational design of a system in which a symmetrical cofactor, acts as a template for the preferential formation of library members which are the most suitable fit. Significant rate enhancement and diastereochemical control is achieved for individual recognition-mediated reaction processes over their bimolecular counterparts. The full library was studied *via* predictive kinetic modeling studies, two library members are shown to be preferentially selected from a possible eight structures.

Chapter 4 describes the design and synthesis of systems capable of probing the interplay between direct and reciprocal replication.

Chapter 5 reviews the work presented in this thesis and discusses the future of dynamic combinatorial chemistry.

Chapter 6 presents the experimental procedures used for the synthesis of library building blocks described within this thesis.

Acknowledgements

Firstly, I would like to thank my supervisor Dr Douglas Philp for giving me the opportunity to work in his laboratory for the past three years, on such a challenging and stimulating project. On a more personal note, I'd like to thank Doug for supporting me throughout my time in St Andrews and would like to take this opportunity to wish him every success in his future career. I would also like to thank the Organic Chemistry Lecturers at the University of St Andrews, for inspiring me to undertake this PhD and for their encouragement throughout the three years. I would also like to acknowledge Dr Markus Dobler for teaching me the practical-side of organic chemistry whilst on industrial placement in his laboratory.

Special thanks must go to the technical staff at the University of St Andrews, without their hard work and dedication this PhD would have been impossible to complete. Thanks to Caroline Horsburgh for Mass Spectrometry, Catherine Botting and Robin Antrobus for assistance with HPLC, Sylvia Williamson for Elemental Analysis and Melanja Smith for NMR assistance. I can't thank Mel enough, for not only for providing technical support in NMR, always with a smile, but for being a great friend throughout my PhD.

There are many people to thank for making the completion of this PhD easier, without the help, support and friendship of each of these people, the last three years would have been far more difficult. Firstly, 'The Dream Team' – The Glory Years – 2001-2002/3. Team members: (Dr) Rosalyne 'There's nothing to *worry* about' Cowie, (Dr) Eleftherios 'You've got to want it' Kassianidis, Dr 'Eh-up duck, Chemistry, you've gotta love it' Pearson and Dr Julie 'Mummy' Quayle. Thanks guys, you have all been fabulous friends and colleagues.

Thanks also to past group members: Dr Vikki Allen, Dr Lindsey Greig, Dr Sarah Howell and Dr Heidi Rowe for making me so welcome during my undergraduate project that I stayed! Thanks also to remaining group members: (Dr) Peter Donnelly (thanks for managing to live with a stressed 3rd year) and (Dr) Evan Wood. Also thanks to post-doc Simon Turega, enjoy your *interesting chemistry*! I have also been lucky enough to work along-side some lovely and talented undergraduate students during my PhD. Thanks to Amy Gradwell, Neil Keddie, Angus Roy and our 'puppy' Ewan McNeil for helping to making the lab a lively, fun place in which to work.

I must thank the Gannochy Crew: Steven Cobb, Cristina Lucas Lopez, Joanne 'twinkletoes' Richie, Charlotte Ryan and Gareth 'Big Bro' Knight, we survived it bed-bugs and all! Special thanks must go to Gareth for being my 'rock' throughout my PhD, I couldn't have asked for a better friend, thanks for always taking care of me Gareth. Thanks also to the 'girlies' Kate Philp and Kathryn Evans for helping the homeless! Special thanks also to Charlotte and Stephen (and the furry babies!) for making me so welcome in their home – I couldn't have finished this thesis without their generosity. Thanks to those who have supported me from afar; Iain Wellington, Erin Stewart and Laura Hardie, thanks for being fabulous friends.

Finally, I would like to thank my parents, Allyson and Derek for their constant love and support in everything I do. And it is to my parents, that I dedicate this thesis.

Abbreviations

Ac	acetyl
Ach	acetylcholine
Ala	alanine
B	binding region
Bn	benzyl
Bu	butyl
CA	carbonic anhydrase
CL	combinatorial library
COSY	correlation spectroscopy
d	doublet
DCC	dynamic combinatorial chemistry
dd	doublet of doublets
DCL	dynamic combinatorial library
DCM	dichloromethane
DMF	dimethyl formamide
DMSO	dimethylsulfoxide
DNA	deoxyribonucleic acid
E	enzyme
EM	effective molarity
eq	equivalent
Et	ethyl
ESI-MS	electrospray ionization mass spectrometry
FTICR ESI-MS	fourier transform ion cyclotron resonance electrospray ionization mass spectrometry
h	hour(s)
HOMO	highest occupied molecular orbital
HPLC	high-performance liquid chromatography
IR	infra-red
ITC	isothermal titration micro-calorimetry
k	rate constant
K_a	association constant
m	meta

MALDI-TOF	Matrix assisted laser desorption/ionization time of flight
Me	methyl
LAH	lithium aluminium hydride
LUMO	lowest unoccupied molecular orbital
Lys	lysine
MA	maleic anhydride
min	minute(s)
NAC	near attack conformation
NBS	*N*-bromosuccinimide
nOe	Nuclear Overhauser Effect
NOESY	Nuclear Overhauser Effect spectroscopy
o	ortho
p	para
Ph	phenyl
ppm	parts per million
Pr	prenyl
q	quaternary
QQQ ESI-MS	triple quadrupole electrospray ionization mass spectrometry
quant	quantitative
quat	quaternary
R	reactive region
RCM	ring closing metathesis
RNA	ribonucleic acid
rt	room temperature
s	singlet
S	substrate
t	triplet
TCNE	tetracyanoethylene
TFA	trifluoroacetic acid
THF	tetrahydrofuran
TMV	tobacco mosaic virus
TSA	transition state analogue
UV	ultraviolet

Contents

Chapter 1

Introduction

1.1 Molecular Recognition leading to the 'birth' of Supramolecular Chemistry

1.1.1 Pederson's Discovery

In 1967, Charles Pedersen[1] published methods of synthesizing cyclic polyethers (crown ethers). The first polyether macrocycle described, dibenzo[18]crown-6 **1 (Scheme 1)**, was found to have unexpected properties. When suspended in methanol crown ether **1** was sparingly soluble, however in the presence of any sodium salt it became freely soluble. Pederson discovered that a sodium ion had 'fallen' into the centre of the molecule and was held there by electrostatic interactions, to afford complex **2 (Scheme 1)**.

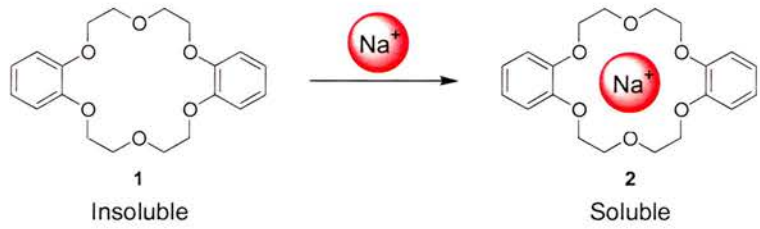

Scheme 1: Properties and structure of the first crown ether, dibenzo[18]crown-6 **1**.

Pederson's new class of molecules[2] could bind to specific metal ions and ignore all others. This pioneering research was outstanding from many perspectives. Any selectivity in the realm of inorganic chemistry was rare, but preference for the alkali and alkaline earth metals was particularly unusual. The alkali and alkaline earth metals are involved in many physiological processes, such as the responses of nerve cells. Therefore, it was plausible that this new class of compound, with such specific discriminatory properties for group I and II metals would have pharmaceutical potential.

1.1.2 Building upon an idea - The Cryptates

Lehn's studies on ionophores for nerve signalling enabled him to appreciate the significance of the properties of crown ether complexes. Lehn recognised that although the ring structures described by Pederson were very selective, as the ions sitting within them were three dimensional and spherical, therefore three dimensional spheroidal cavities would enhance the strength and selectivity of binding to metal ions. And so, the synthesis of macrobicylic cryptand cavity compounds was initiated and the selective inclusion of alkali cations yielded

the cryptates[3-4] **3 (Figure 1)**. This class of compound display special complexation properties, resulting from their macropolycyclic nature, defined as the *crypate effect*, characterized by high stability and selectivity, slow exchange rates and efficient shielding of the bound ion from the external environment. Many classes of macrocyclic ligand with efficient complexation properties have since been developed,[5] including spherands **4** by Cram and calixarenes **5** by Gutsche **(Figure 1)**. However, a detailed discussion of these compounds is outwith the scope of this report.

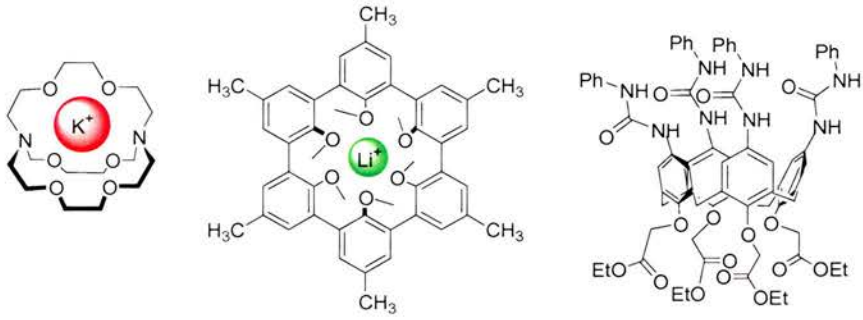

3 **4** **5**

Figure 1: Host-guest molecules: Cryptate **3** binding K^+ cation, Spherand **4** binding Li^+ and Calixarene **5** which can bind NaCl.

1.1.3 Defining Supramolecular Chemistry

At the beginning of the 1970's, ideas which would later form the basis of supramolecular chemistry were beginning to develop. Cryptates and crown ethers were known to distinguish between the alkali earth metals. This selectivity became defined[5] as molecular recognition the "...specific recognition of (and interaction with) one molecule by another." In order for recognition to occur it was understood that an interaction between 'host' and 'guest'[6] must occur. Jean-Marie Lehn proposed that the phenomenon of selectivity observed in the crown ethers and cryptates was linked to their ability to 'recognise' ions through weak interactions. This proposal was the beginning of Supramolecular Chemistry. A chemical discipline based on the non-covalent bond, defined by Lehn[7] in 1978 as *"chemistry beyond the molecule, whose goal is to gain control over the intermolecular non-covalent bond."* In general terms 'Supramolecular Chemistry'[8] **(Scheme 2)** relates to the organization and properties observed by collections of molecules held together by weak interactions: host-guest complexes,[3-5] self-assembled objects,[9-10] metal-ligand binding,[11] π-π interactions[12-14] and hydrophobic effects.[15] The resulting supramolecular entities have potential as catalysts, sensors or as new materials.[16-23]

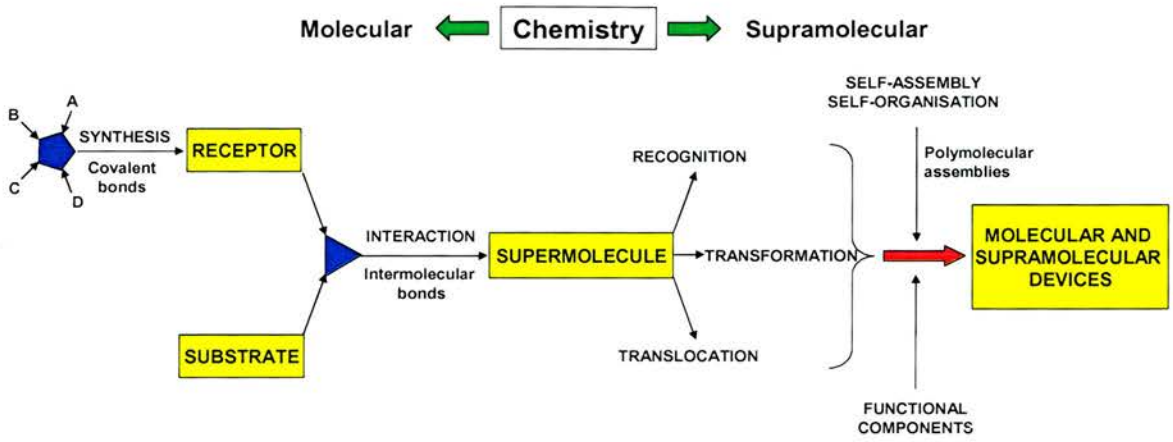

Scheme 2: From molecular to supramolecular chemistry: molecules, supermolecules, molecular and supramolecular devices. Taken from Ref. 7.

1.2 Hydrogen Bonding Examples of Molecular Recognition

Of particular relevance to the work presented in this thesis is use of hydrogen bonding for the recognition[25-26] of substrates. Weak interactions between molecules containing hydroxyl groups were noted by Nernst[27] as early as 1892. Although the interaction was nameless at that time, Werner[28] also included them in his concept of "Nebenvalenz" (minor valence). In 1936, Huggins[29] finally proposed the term "hydrogen bond." A hydrogen bond[30] is a type of attractive intermolecular force that exists between two partial charges of opposite polarity.

Figure 2: Hydrogen bond donor (D) and acceptor (A) atoms.

The hydrogen involved in bonding must be attached to a strongly electronegative heteroatom, such as oxygen, nitrogen or fluorine, which is called the hydrogen-bond donor (D) **(Figure 2)**. This electronegative element attracts the electron cloud from around the hydrogen nucleus and, by delocalising the cloud, leaves the atom with a partial positive charge. As a result of hydrogen's relatively small size, the resulting charge, though only partial, represents a large charge density. A hydrogen bond results when the strong positive charge density interacts with a lone pair of electrons on another heteroatom - the hydrogen-bond acceptor (A) **(Figure 2)**. The strength of the H-bond increases with an increase in the dipole moment of the D-H bond and the electron density on the acceptor atom. Hydrogen bonding can be described by five different contributions; electrostatic energy, exchange repulsion, polarization energy, covalent bonding and dispersion forces. Most theories relating to the strength of hydrogen bonds, claim angle dependence to be of importance in hydrogen bond energy, with a maximum value for a linear bond. The thermodynamic stabilities of hydrogen

bonded complexes in solution are also solvent dependent. Stabilities are highest in apolar solvents without hydrogen bonding properties, such as alkanes, whilst stability is lower in solvents which can themselves act as hydrogen bond donors or acceptors.

The Jorgensen Model[31] **(Figure 3)** gives a guide to the relative strengths of hydrogen bonded arrays. The model shows that the stability of hydrogen bonded molecules can be attributed to attractive and repulsive secondary interactions. Stabilisation arises from electrostatic attraction between positively and negatively polarized atoms in adjacent hydrogen bonds, whereas destabilization is likely to result from electrostatic repulsion between two positively or negatively polarized atoms. The effect of secondary interactions on hydrogen bonding systems was later proven experimentally by Murray and Zimmerman.[32]

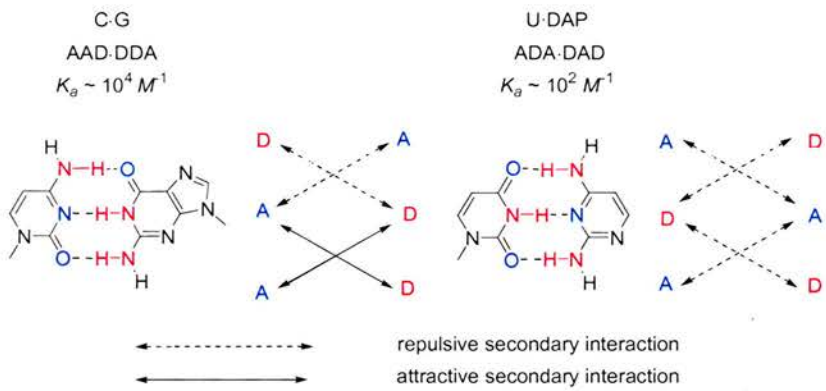

Figure 3: Attractive secondary interactions account for the difference in thermodynamic stability for the 1-methylcytosine·9-methylguanine (C·G) dimer and the 1-methyluracil·2,6-diaminopyridine (U·DAP) dimer. Where A = hydrogen bond acceptor and D = hydrogen bond donor. K_a is a measure of the stability of binding within the system. Taken from Ref. 30.

Complementary base pairing in nucleic acids provides an excellent example of molecular recognition.[31-33] The DNA bases **(Figure 4a)** contain all of the 'ingredients' required for hydrogen bond formation, having both nitrogen and oxygen atoms with lone pairs, and hydrogen atoms attached to nitrogen atoms. Watson and Crick[34] proposed that each base pair had a complementary partner, which was held together *via* hydrogen bonds on a sugar-phosphate backbone structure. The resulting structure formed a perfect double helix **(Figure 4b)** with one strand complementary to the other. Molecular recognition allows each base to specifically pair with its complementary partner in preference to all other bases during DNA replication.

a) **b)**

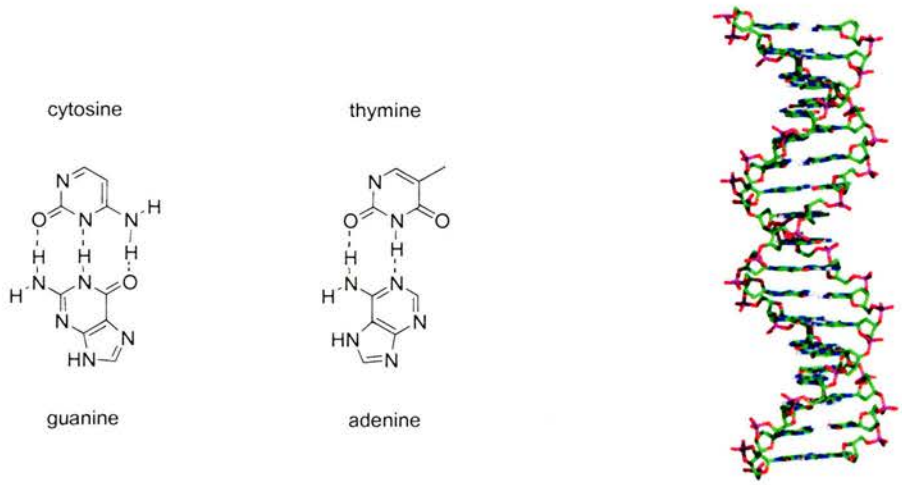

Figure 4: **a)** The bases in nucleic acids; **b)** DNA double helix.

Hydrogen bonding has been used as a tool[35] for synthetic molecular recognition. In designing a receptor, the steric and electronic features[36-37] required to complement the substrate must be considered. In addition, a flexibility/rigidity balance must also be met, depending upon the required function of the receptor. How well things fit together depends on their predisposition or pre-organisation, or a combination of these two effects. Specific recognition on a molecular level requires a close correspondence between the shape of the receptor and the substrate molecule.

Rebek and co-workers[38] have studied synthetic molecular receptors extensively. One such example, based upon the structure of Kemp's triacid[39] is receptor **6 (Figure 5)**. Rebek's[40] simple receptor consisting of two imides separated by a naphthyl spacer achieved extraordinary affinity (K_a = 50000 M^{-1}) for adenine derivatives.

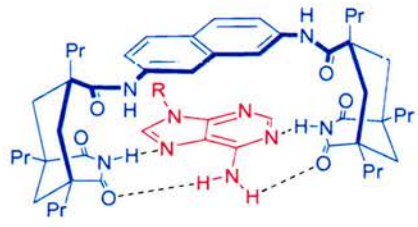

6

Figure 5: Adenine bound by hydrogen bonds to a synthetic receptor.

Mendoza and co-workers[41] in collaboration with Rebek developed a structure which incorporated both a receptor site with high affinity for adenine and a phosphate binding site

based upon guanidinium **(Figure 6a)**. Receptor **7** incorporates two Kemp triacid derivatives linked by a carbozole unit which acts as a nucleobase binding site. The electron-rich spacer renders possible π-stacking interactions with heterobases and positions the imide functions at an adequate distance for simultaneous Watson-Crick and Hoogsteen-base pairing **(Figure 6b)**. Receptor **7** therefore provides hydrogen bonding, π-stacking and salt bridge forms of molecular recognition.

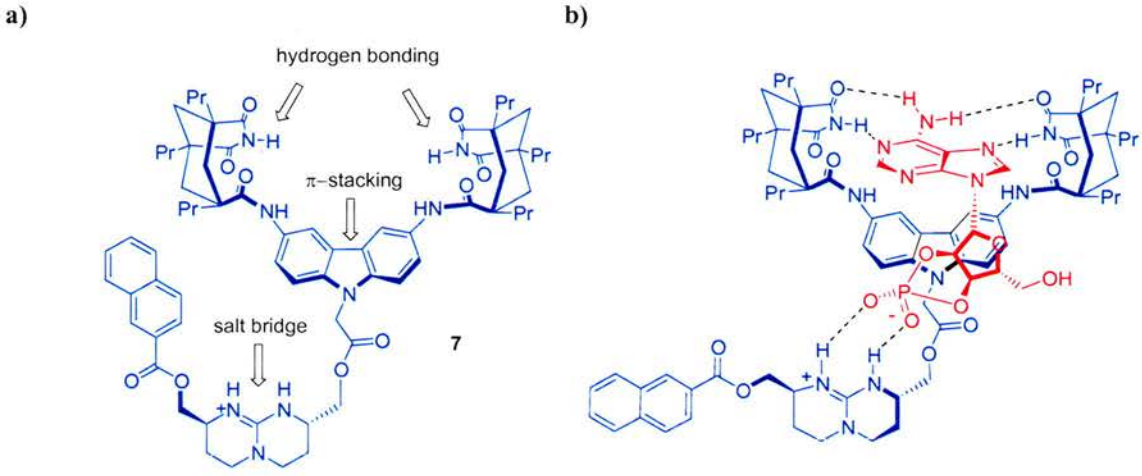

Figure 6: **a)** Receptor **7**, containing potential hydrogen bond, π-stacking and salt-bridge recognition sites. **b)** Adenine derivative bound to synthetic receptor **7**.

Hamilton and co-workers[42] have designed artificial receptors for the selective complexation of barbiturates through molecular recognition **(Figure 7)**. The widespread use of barbiturates as sedatives and anticonvulsants makes them attractive targets for molecular recognition studies.

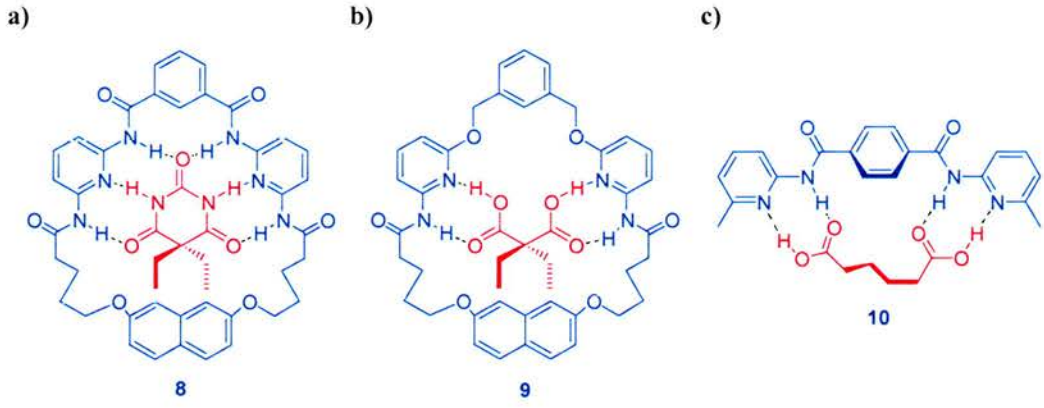

Figure 7: **a)** The hydrogen bonding motif of receptor **8** and barbiturate; **b)** The hydrogen bonding motif of receptor **9** and diethylmalonic acid; **c)** Simple receptor **10** binding adipic acid.

Receptor **8 (Figure 7a)** is based upon two 2,6-diaminopyridine groups linked through an isophthalic acid spacer. X-ray crystallographic, ^{1}H NMR spectroscopic and substrate binding studies confirmed that six hydrogen bonds are formed between the receptor and its substrate. This complementarity between host and guest results in a strong binding affinity, a value of $K_a \approx 10^5\ M^{-1}$ was calculated. Further studies by Hamilton[43] replaced the two phthalamide groups on receptor **8** by benzyl ethers, yielding receptor **9 (Figure 7b)**. Receptor **9** proved to be a relatively poor host for diethylmalonic acid and ethylmalonic acid ($K_a \approx 10^3\ M^{-1}$), this was perhaps as a consequence of the unfavourable, planar conformation of the diacid which was required to allow binding within the cavity. In order to overcome this problem, a wider separation of the two hydrogen-bonding regions was devised to minimise repulsive interactions between the carboxylate groups. Model compound **10 (Figure 7c)** was identified as a suitable candidate by molecular modelling studies. The relative position of the amide NH (~6.0 Å) and pyridine N (~10.7 Å) groups on receptor **10** were calculated to be suitable for the complexation of dicarboxylic acids separated by three or four methylene groups. Addition of adipic acid to a $CDCl_3$ solution of **10**, led to the rapid dissolution of the normally insoluble guest. Integration of the ^{1}H NMR spectrum of the mixture established a 1:1 stoichiometry between host and guest, and large downfield shifts (2.6 ppm) of the amide NH resonances indicated that a hydrogen-bonded complex had indeed been formed. NMR dilution experiments were carried out and the association constant for the simple complex was calculated to be of the order of $>10^5\ M^{-1}$.

Self-assembly occurs when molecules interact with one another through a balance of attractive and repulsive interactions in the same manner as described in molecular recognition. Therefore, the boundaries between molecular recognition and self-assembly are a matter of semantics.

1.3 Self-Assembly

1.3.1 Self-Assembly in a Natural System

Many synthetic self-assembled systems have been reported and the field has been extensively reviewed.[44-46] Viruses represent some of the best natural examples of self-assembly from which the chemist can learn. The tobacco mosaic virus (TMV)[47] **(Scheme 3)** is perhaps one of the best understood. TMV is composed of a single strand of RNA composed of 6400 base pairs encased in a protein sheath, which is formed from 2130 identical monomers. Fraenkel-Conrat and Williams[48] showed that TMV could be dissociated into constituent parts and that when the isolated components were reintroduced *in vitro*, reformation of the complete virus was observed. This reassembly process exhibited concentration, time and pH dependencies characteristic of a typical chemical reaction. This virus re-forming experiment showed that all the information needed to assemble the full virus was built into its constituent parts. Through the studies of such viruses the properties of self-assembled systems were uncovered; (i) Using only one or a few repeating subunits in building a large structure greatly reduces the amount of genetic information required, (ii) Self-assembly processes are potentially very efficient, as accurately assembled products can be obtained without the need for complete accuracy in subunit construction as defective subunits are not incorporated in the growing structure, (iii) Self-assembly processes generally use reversible interactions or reactions. Therefore, as the assembly process is always at, or close to dynamic equilibrium, the synthetic pathway will be error checking. It is for these reasons that the study of self-assembly processes are of great interest to the synthetic chemist.

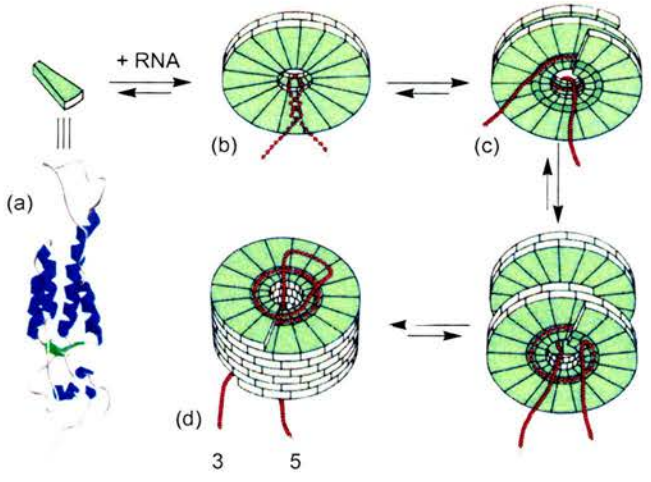

Scheme 3: The assembly of the Tobacco Mosaic Virus. Protein sub-units **(a)** associate with viral RNA to form a double disk structure **(b)**. Conformational change results in the formation of a slipped double disk **(c)** and initiates viral assembly **(d)**. Taken from Ref. 46.

1.3.2 Synthetic Self-Assembly

In an attempt to develop nanoscale structures, there has been huge interest in using an 'engineering-up' self-assembly approach. This approach transfers the concepts used in nature **(Section 1.3.1)** to the laboratory, where the ultimate goal is the fabrication of nanoscale devices. The 'engineering-up' approach has developed from the realization that the 'bottom-down' approach to the miniaturisation of circuits was reaching the physical limit of feasibility. Applying the principles from biological paradigms to synthetic systems allows the chemist to assemble artificial superstructures on the nanometer scale.[44-46] Synthetic self-assembled systems constructed to date range from knots to rings,[49] ladders,[50] helices,[51-53] capsules,[54-55] grids[56-57] to boxes[58] and many more.[11, 44-46] Presented below is an example of self-assembly in which linear components aggregate through metal-ligand interactions to facilitate helical structures. During the study of this helical self-assembled system, a new area of supramolecular chemistry became defined.

1.3.3 Non-Covalent Self-Assembly in a Synthetic System – Helicates

Helicates[59-60] consist of ligands which extend over adjacent metal centres, the ligands wrap around each other, generating an inorganic double-helical structure which bears resemblance to double-stranded DNA **(Figure 8)**.

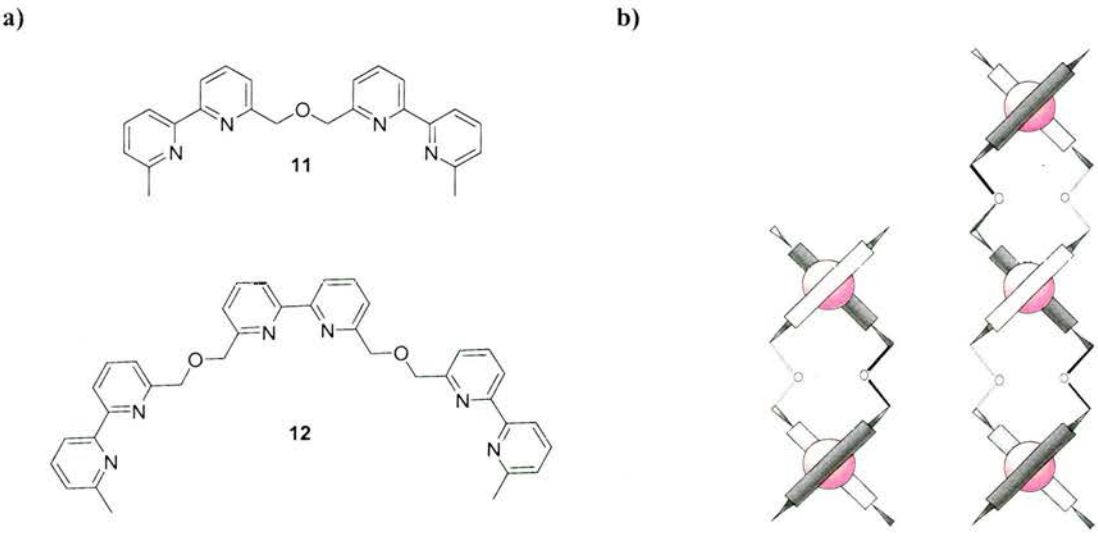

Figure 8: **a)** The structure of oligobipyridine ligands **11** and **12** which undergo complexation with metal ions to form an inorganic double helix; **b)** Schematic representation of the double stranded helicates formed by the complexation of two and three Cu^{+} cations respectively. Adapted from ref. 63.

Lehn and co-workers' research into helicates has spanned over two decades.[61-62] Initial studies[61, 63-64] focused upon the self-assembly of double-stranded helicates from oligobipyridine ligands **11** and **12** with copper (I) cations **(Figure 8)**. In 1993, Lehn[65] posed the question 'What will happen when a mixture of several oligobipyridine strands of different lengths is treated with Cu^{+}, will only helicates containing identical strands be formed or will ill-defined mixtures be obtained?' Complementary strands were indeed selected from the mixture of potential ligands **(Scheme 4)**. Lehn established that the self-assembly process of such helicate strands was instructed through self-recognition.

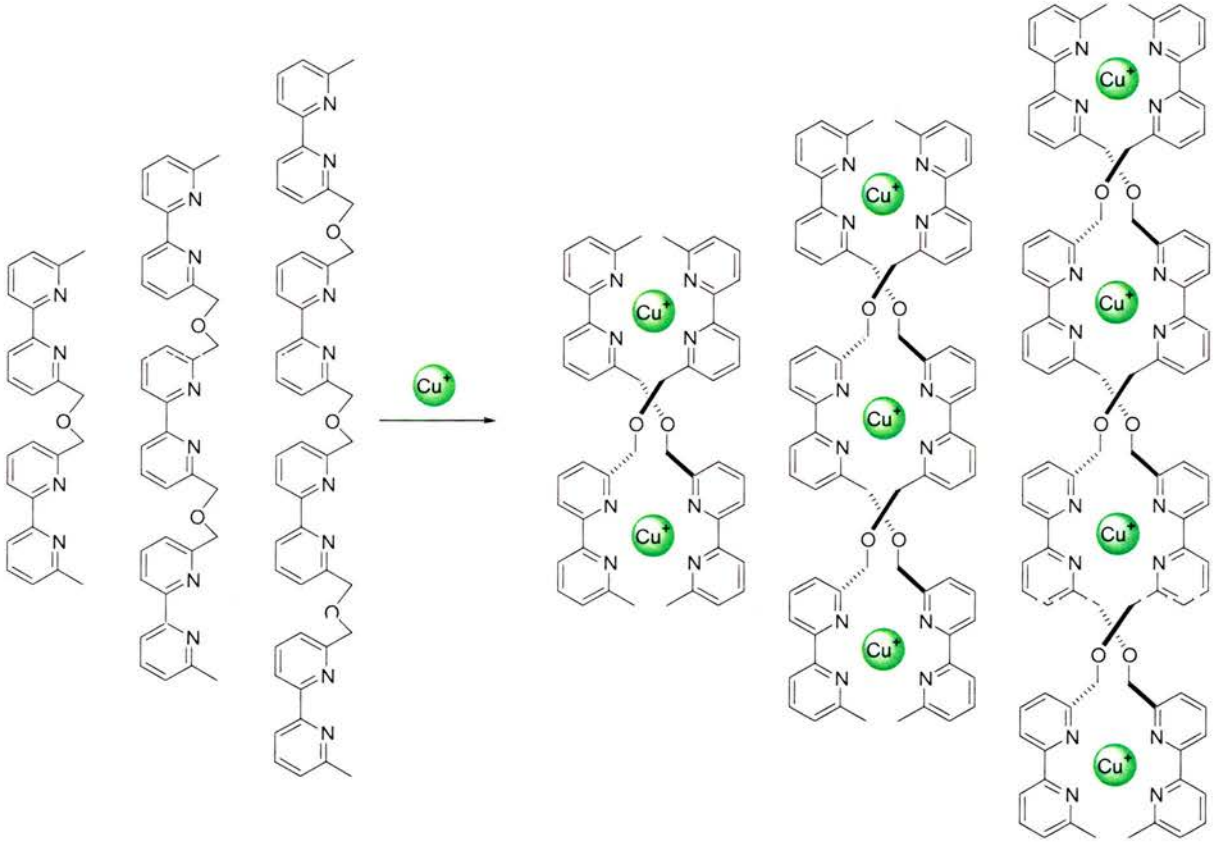

Scheme 4: Self-recognition in the self-assembly of double helicates. Adapted from Ref. 65.

Oligobipyridine strands were shown by Lehn[65] to also form a triple helix in the presence of Ni^{2+} ions. What would happen when the components for the formation of a double and triple helix were combined? Once again, metal ion-mediated selection occurred **(Scheme 5)**, the tetrahedrally coordinating Cu^{+} ions bound to the 6,6'-linked bipyridine ligand, whereas the octahedrally coordinating Ni^{2+} ion bound the 5,5'-linked tris(bipyridine) strand, resulting in the formation of two well-defined helical complexes from a mixture of four components **(Scheme 5)**.

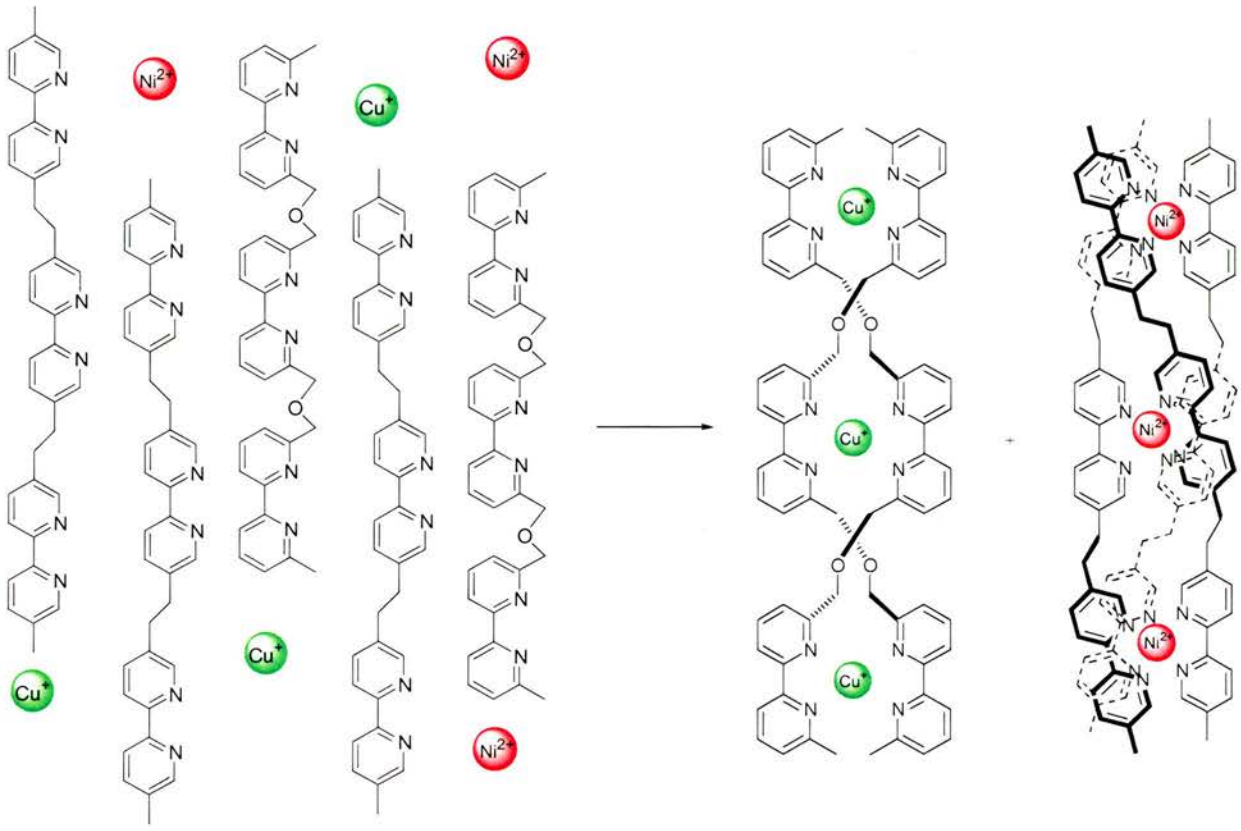

Scheme 5: Self-recognition in the self-assembly of a double helicate and a triple helicate from a mixture of oligobipyridine strands and Cu^{+} and Ni^{2+} ions. Adapted from Ref. 65.

This study was a turning point in supramolecular chemistry, it indicated that it was possible to program a system composed of mixtures of instructed components capable of spontaneously forming well-defined superstructures through self-recognition/assembly.

The term dynamic combinatorial chemistry (DCC) was coined in 1996 by Jean-Marie Lehn,[66] to describe the effect of varying the features of a metal salt on the nature of helicate species generated.[67] In the presence of the smallest anion, Cl^{-}, self-assembly generated the pentanuclear circular helicate **14 (Scheme 6)**. With larger anions such as SO_4^{2-}, BF_4^{-} and SiF_6^{2-} the hexanuclear species **13 (Scheme 6)** was formed, whereas, the Br^{-} anion yielded a mixture of both architectures. From these studies it was concluded that anionic charge had little influence on the structure formed. The formation of such structures was shown to depend upon a self-assembly process, wherein the size of the anion determines which components are selected from all possible combinations of constituents. This was the beginning of a new type of chemistry, known as dynamic combinatorial chemistry,[68] drawing upon influences from combinatorial chemistry, as the name suggests, and encompassing two of supramolecular chemistry's main themes; (i) self-assembly **(Section 1.3)**, in the generation of the library constituents, and (ii) molecular recognition **(Sections 1.1-1.2)**, in their interaction with the target molecule.

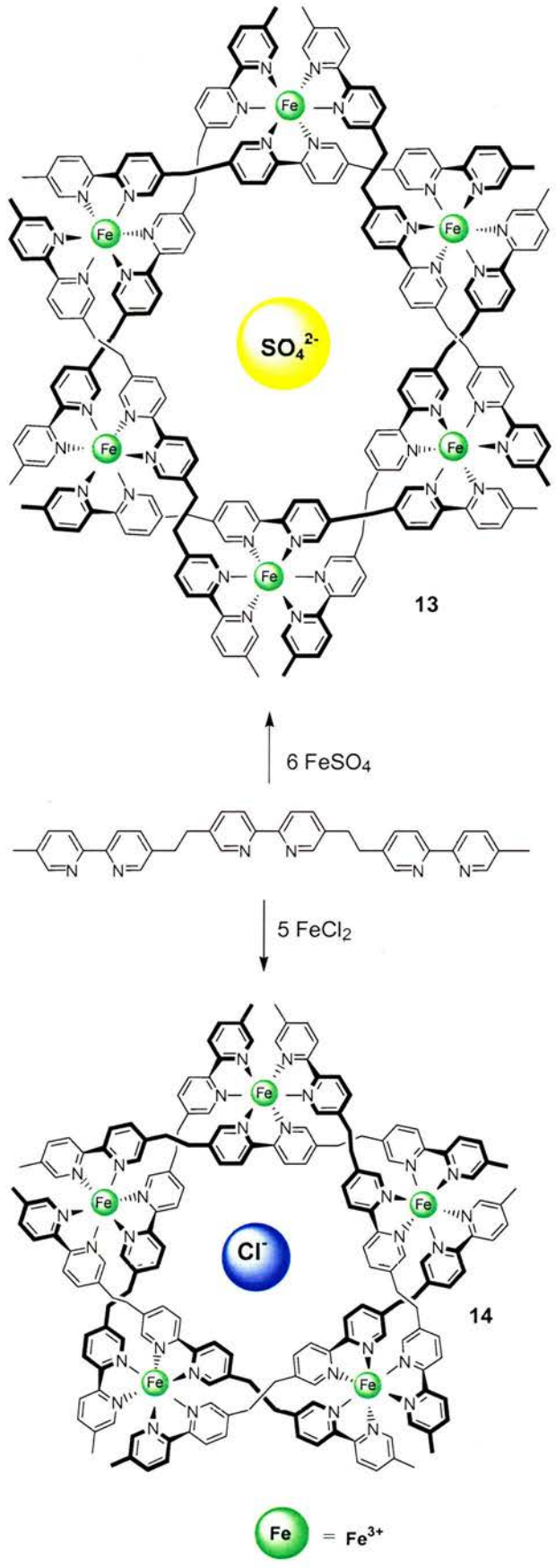

Scheme 6: Circular helicates **13** and **14** are the thermodynamic products of an assembly process which involves linear helicates as intermediates. The metal salt affects the size of helicate formed. Adapted from Ref. 46.

1.4 Combinatorial Chemistry *vs* Dynamic Combinatorial Chemistry

Combinatorial chemistry[69] allows the synthesis of large arrays of compounds in a short period of time, however, each individual compound needs to be prepared, often over several synthetic steps, and then characterised. Automated synthetic techniques in conjunction with solid-phase synthesis and high-throughput analytical methods have enabled the development of the process. If the target substance itself could be used to select an active ligand/inhibitor directly from a library pool, then the screening process would be more efficient and greatly simplified. In addition, if the library pool itself were able to undergo changes in composition during this process, adapting to the target constraints, then the screening signal would be amplified, facilitating detection and characterization. Furthermore, if the active species could be analysed directly whilst bound to the receptor site, several synthetic steps could be avoided, this is where dynamic combinatorial chemistry would confer a significant advantage over its counterpart - combinatorial chemistry. Considering combinatorial chemistry in terms of Fischer's Lock and Key hypothesis;[70] one can think of the formation of such substrates in terms of the fabrication of a large collection of keys, with the goal that one of them will fit the target lock (receptor) and be retrievable from the mixture. On the other hand, a substrate dynamic combinatorial library can potentially assemble a large set of keys from a set of parts which reversibly assemble in a spontaneous manner, one of which could fit the target lock (receptor). An overview of the important differences between real combinatorial chemistry and dynamic combinatorial chemistry are highlighted in **Table 1**.

Table 1: Static and dynamic combinatorial chemistry; comparative basic features of real and dynamic virtual combinatorial libraries. Adapted from Ref. 68.

Combinatorial Library (CL)	***Dynamic Combinatorial Library (DCL)***
Molecular constituents	Molecular or supramolecular constituents
Real set	Virtual set
Collection of molecules	Collection of components
Covalent	Covalent or non-covalent
Non reversible	Reversible
Neutral, uninformed	Instructed
Systematic	Recognition induced
Absence of target molecule	Presence of target molecule
Preformed by synthesis	Self-assembled

1.5 Dynamic Combinatorial Chemistry – How does it work?

Dynamic combinatorial chemistry[68] exploits reversibility within chemical systems in order to generate combinatorial libraries which are under thermodynamic control. Library members interconvert through equilibrium processes, therefore, any stabilisation of a given member will result in the thermodynamic redistribution of that equilibrium (Le Châtelier's principle), thus amplifying the concentration and favouring the formation of the most stable library member above all others. Molecular evolution within dynamic combinatorial systems is selection analogous to a Darwinian style 'survival of the fittest' strategy. Those molecules which bind to the template molecule are amplified/survive, whereas weak candidates, which do not bind the template well, are consumed/die, in preference of the stronger candidates.

Library constituents are formed from components either by covalent assembly, through reversible chemical reactions to give molecular dynamic combinatorial libraries or by self-assembly, through reversible non-covalent binding interactions to give supramolecular DCLs. The constituents within these systems may not, and need not exist in significant amounts in the absence of the target molecule, it is for this reason that they may be termed *virtual*.

Reversibility is a necessity in a dynamic combinatorial system as it leads to the spontaneous generation of diversity through the reversible combination of each library component. The degree of diversity achieved within a library depends upon the extent to which all possible combinations of geometrical and interactional spaces of the target site are explored. Only a handful of reversible reactions are suitable for use within dynamic combinatorial chemistry **(Table 2)**.

Table 2: A selection of potentially reversible reactions, interactions and intramolecular processes for the dynamic generation of virtual molecular and supramolecular combinatorial libraries/diversity. Taken from Ref. 68.

Reversible Covalent Bond Formation

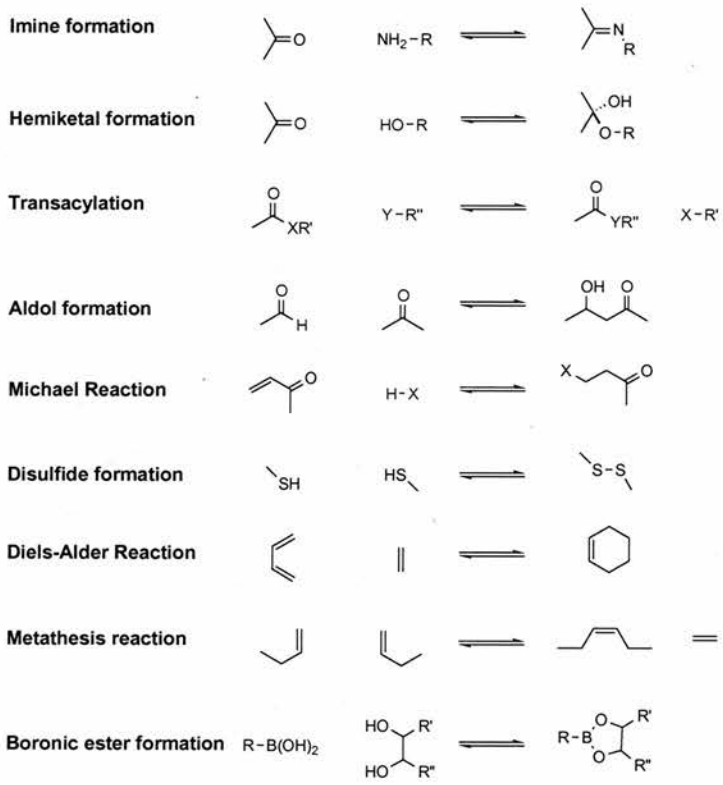

Reversible Interactions

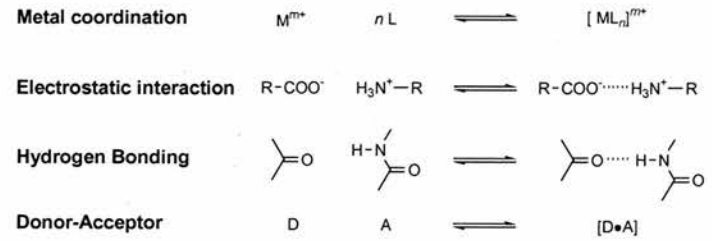

Reversible Intramolecular Processes

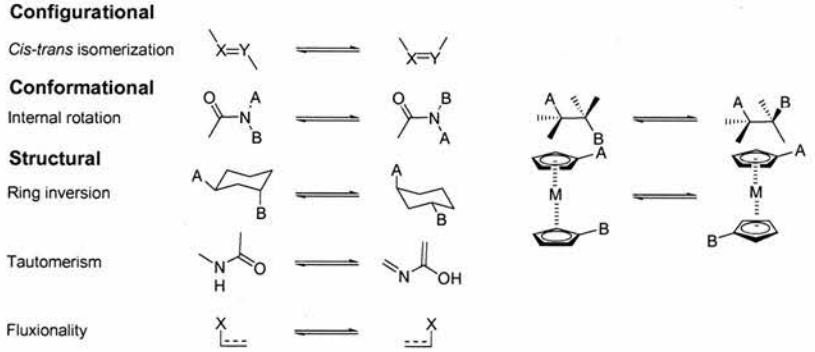

Within the framework of *virtual* combinatorial libraries two processes may be considered, depending on whether a receptor or a substrate acts as the target-template for the assembly of the other partner **(Scheme 7)**. Casting involves the receptor-induced assembly of a substrate. Conversely, moulding involves the substrate-induced assembly of a receptor that optimally binds the substrate.

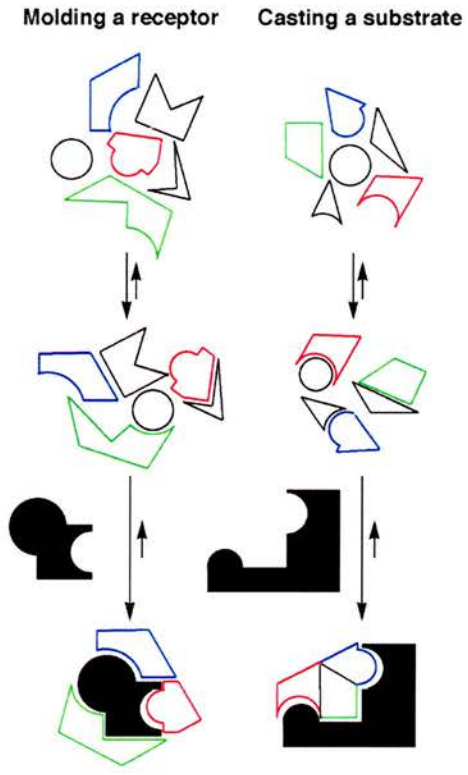

Scheme 7: Dynamic generation of virtual combinatorial libraries. Left: Moulding process – substrate induced self-assembly of the complementary receptor from a collection of structural components; it amounts to the selection of the optimal receptor from a virtual receptor library. Right: Casting process – receptor-induced self-assembly of the complementary substrate from a collection of components serving as building blocks; it amounts to the selection of the optimal substrate from a virtual substrate library. Adapted from Ref. 68.

1.6 How big a library can you generate?

In terms of a simple example, starting from n components of type A and m components of type B, a library of n x m constituents A-B can be generated. With ten components each (n = m = 10), a library of 100 constituents is produced. Larger and more diverse libraries can be generated using linkers and scaffolds. However, this is an over simplified view. What are the actual limits of a working DCL?

1.6.1 Limitations

The first theoretical analysis on the limitations of DCL amplification was conducted by Moore and Zimmerman.[71] Their studies considered a case in which an infinitely large dynamic library of polymeric chains had a log-normal distribution of affinity for a target molecule. Their findings indicated that the amplification in such a system was limited to two orders of magnitude and that amplification decreased with increasing target saturation.

More recently, Sanders and co-workers[72] have simulated DCLs using the same assumptions as Moore and Zimmerman, that of an idealized DCL situation. Under these circumstances, every host could interconvert with every other host and in the absence of a guest molecule all hosts were present at the same concentration. A large excess of template was also used in order to saturate the system, whereby almost all library members would be bound to the template. In making these assumptions, Sanders model ignored the effect of varying the concentration of host members upon the library, thus allowing the analysis of library size on amplification to be considered independently. Sanders used computer package DCLSim[73] designed specifically for the task of calculating the concentrations of compounds within a dynamic library in the presence and absence of a template. In a dynamic library of 10,000 members, each with a binding constant assigned on the basis of a log-normal distribution, at low binding constants Sanders simulated data matched Moore's distribution data. However, at the extreme of high binding, the shifted distribution was concentrated into a single compound which was amplified to become 8% of the complete library mixture.

In order to further probe the relationship between library size and amplification within a DCL, Sanders simulated libraries ranging from 10 to one million members. The results indicated, as expected that the best binding decreased with library size, but at a relatively slow rate. In general terms, it was observed that for large libraries, the concentration of the best compound for the target molecule appeared to be roughly inversely proportional to the square root of the library size. Why was there such a slow decay observed in the concentration of the best binding compounds upon increasing library size? Sanders proposed the answer to be two-fold; (i) as the size of the library increases the chance that it contains a good binder for the target increase, (ii) however, if there are a larger set of compounds the initial concentrations of each will be lower, which in turn suggests that the amplified concentrations will be lower. As the number of library members increases the effect of (ii) was observed to dominate the

effect of (i). Sanders concluded that even in libraries with 10^6 members, host-guest binding could induce the amplification of stronger binders to concentrations well within the detection limits of modern analytical equipment. Experimental conditions which would facilitate such a situation are however some way off.

Severin[74] has recently reported a numerical simulation which investigated the effects of varying target concentration and equilibrium constants upon DCLs. Severin found that it was not necessarily the assembly with the highest binding affinity to the given target which was amplified. In fact, it was possible that addition of a target molecule could lead to the decreased steady-state concentration of the best-binder. These studies suggested that in order to use DCLs for selection processes, it was desirable for the species with the highest binding constants to give the highest amplifications. Simulated numerical data suggested that this ideal dynamic library situation can be achieved through the appropriate design of a selection experiment.

1.7 Practical Considerations in the Design of a DCL

In order to design a DCL many factors have to be taken into consideration: (i) interconversion of library members is required to allow library evolution, and thus allow the library to be influenced by thermodynamics and therefore be error checking, (ii) library diversity allows the 'survival of the fittest' strategy to be tested and the geometrical and interactional spaces around a target molecule to be probed, (iii) within a dynamic library many species are rapidly interconverting therefore the processes by which evolving species are monitored is critical.

Many covalent, non-covalent, metal-induced and conformational DCLs[75-85] have been reported in the years following Lehn's discovery. The following specific examples span each of the aforementioned branches of dynamic combinatorial chemistry.

1.8 Covalent DCLs

The reversible covalent reactions studied in the context of dynamic combinatorial chemistry include, ester exchange,[86-88] transamination,[89] transimination,[90-99] exhange of oximes,[100-101] hydrazones,[102-107, 109, 111] and disulfides, [108, 113-120] olefin metathesis[121-122] and more recently transthioesterification.[123] The following examples give a flavour of the diversity within this research area.

1.8.1 Ester Exchange

Sanders and co-workers first proposed[86] the concept of thermodynamic templating of 'living' mixtures in 1996. A base-catalysed trans-esterification was employed as the reversible reaction within this DCL. Although base-catalysed ester exchange requires harsh conditions, such as potassium methoxide in refluxing toluene, template effects by alkaline cations were observed.[87] In 2000, Sanders[88] once more used the transesterification reaction to synthesize cyclic porphyrin dimers. In this study the reversible reaction of π-allyl palladium complexes was utilised to facilitate transesterification **(Scheme 8)**.

Scheme 8: Conditions for palladium-catalysed allyl transesterification: concentration of cinnamyl esters 10 m*M*, $Pd(PPh_3)_4$ 0.1 eq., R_2CO_2H < 0.1 eq., Et_3N, $CHCl_3$, 50 °C, 6 h.

Sanders determined that it was possible to synthesise cyclic porphyrin dimers **(Scheme 9)** using the reversible palladium-catalysed transesterification reaction. The reaction was templated by a bidentate pyridyl ligand **15** which improved the yield of cyclic product **16** 6-fold.

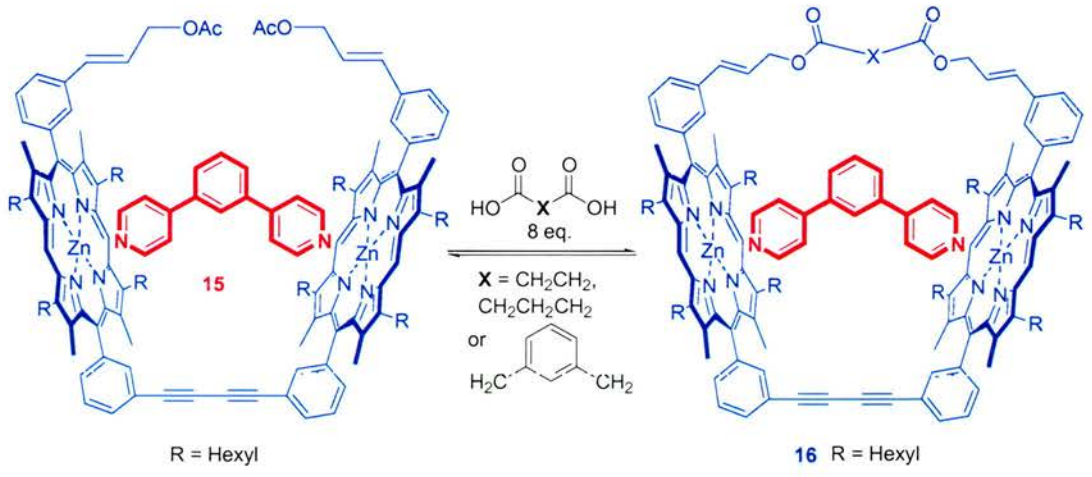

Scheme 9: Conditions for selection experiments: concentration of porphyrin dimer 5 m*M*, $Pd(PPh_3)_4$ 0.1 eq., Et_3N, $CHCl_3$, 50 °C, 6 h. Adapted from Ref. 88.

1.8.2 Transimination

Transimination has been used by many groups in order to generate DCLs.[90-99] Imines are however unstable, as they readily undergo hydrolysis under acidic conditions. Therefore, imine dynamic libraries are often reduced before screening. Hydrazones and oximes are structurally related to imines but have the advantage of being hydrolytically stable, therefore no reduction step is required.

In 1997, Lehn and Huc demonstrated[99] a practical application of the casting principle **(Section 1.5)** of dynamic combinatorial libraries, this involved the recognition-induced assembly of inhibitors for the enzyme carbonic anhydrase II (**CA**) **(Scheme 10)**. In their studies the reversible formation of imine bonds from aldehydes and amines under physiological pH and temperature conditions was exploited to give a dynamic library of fast interchanging species. On addition of the enzyme carbonic anhydrase II, the product equilibrium was shifted towards imine library member **17** which possessed features similar to those of known **CA** inhibitor **18**. These results show the products to be biased in favour of those with the highest binding affinity for the **CA** active site, thus proving the target-driven nature of this dynamic library. In this example the reversibility of imine formation can be switched off on reaching equilibrium. The imine(s) formed can be irreversibly reduced with $NaBH_3CN$, thus fixing the compound(s) generated in the form of amines, which in turn, facilitates the isolation and analysis of the final dynamic mixture.

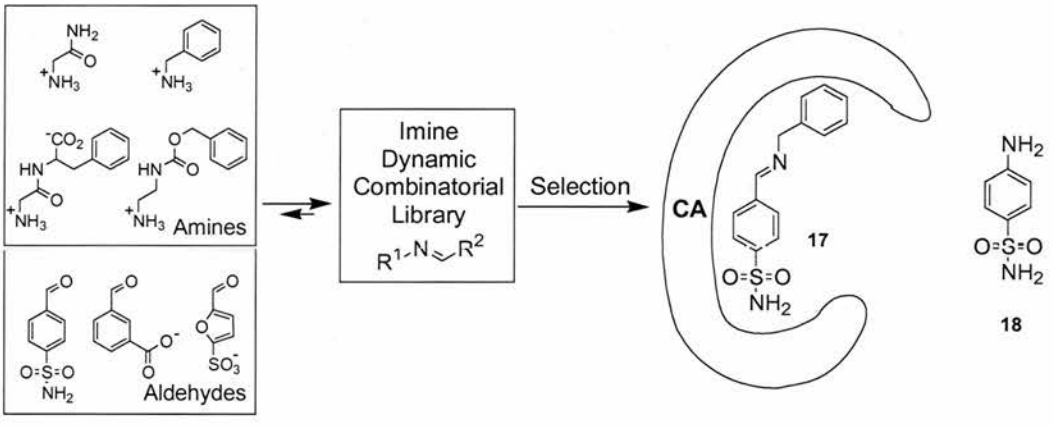

Scheme 10: Selecting an inhibitor for carbonic anhydrase from a dynamic combinatorial library of imines. The enzyme active site is represented by **CA**. The imine **17** selected is similar to known sulfonamide inhibitor **18**. Adapted from Ref. 99.

1.8.3 Exchange of Oximes

Eliseev and co-workers[100-101] have reported on the mechanism of transimination of oximes in water. Equilibration was rapid at higher temperatures and/or under acidic conditions, whereas ambient temperature and neutral conditions switched-off exchange.

1.8.4 Hydrazone Exchange

Sanders and co-workers[102] have developed the use of hydrazone exchange to prepare DCLs under mild exchange conditions. Hydrazone macrocycles of differing size were generated from bifunctional building block **19 (Scheme 11)** containing both a hydrazide and a protected aldehyde moiety separated by a spacer unit. The hydrazone exchange reaction is pH dependent. Addition of acid, switches on macrocycle formation whilst neutralisation of the reaction medium switches off the interconversion of species, allowing individual library members to be isolated and then characterised. After six hours, building block **19**, in chloroform and TFA affords macrocycles ranging from dimer **20** to 15mer including **21** and **22** as detected by ESI-MS. After a period of three days the product distribution drifts in favour of cyclic dimer **20**, which makes up about 88% of the dynamic library **(Scheme 11)**. Introduction of [18]-crown-6, **23**, into the macrocyclic library,[103] led to a decrease in the concentration of the higher oligomers, and the appearance of a new species, **24**, which was observed as the major component of the library. These results highlight the effect that a non-covalent interaction can have upon a hydrazone-based DCL. Molecular amplification of pseudo-peptide macrocycles *via* a templating effect with ammonium cations has also been reported.[104-105]

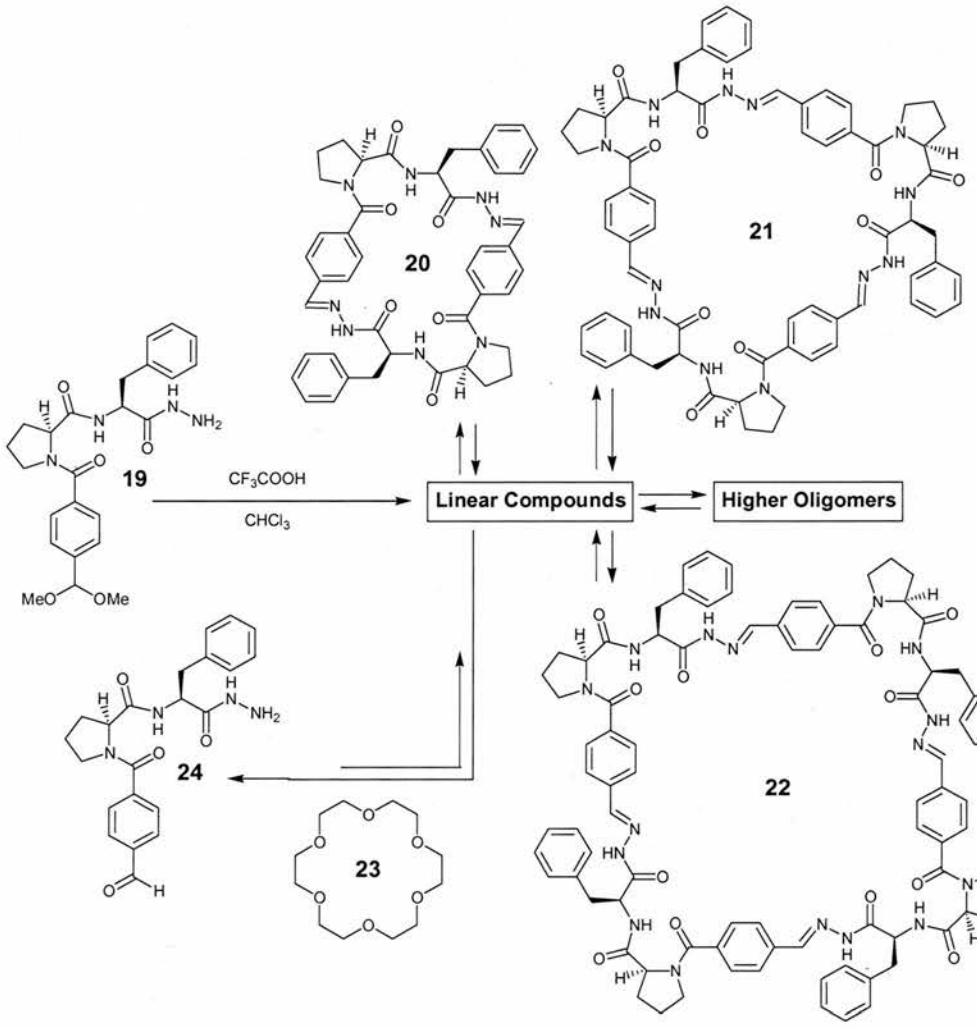

Scheme 11: The distribution of products formed by monomer **19** is influenced strongly by introduction of 18-crown-6 **23**.

Drawing upon studies by Kubik and co-workers,[106] Sanders postulated that ammonium salts **(Figure 9)** would bind cyclic trimer **21** strongly enough to template its formation leading to molecular amplification. On addition of salts containing three butyl or ethyl groups on the nitrogen, weak, non-specific amplification of higher oligomers occured. In experiments with tetra alkyl ammonium salts, binding was observed by ESI mass spectrometry, peaks corresponding to the complex 3mer-template were observed at *m/z* 817.5 (for 3mer: $EtMe_3N^+$), *m/z* 879.5 (for 3mer:$BnMe_3N^+$), *m/z* 855.5 (for 3mer:NMQ^+), and *m/z* 875.6 (for 3mer: ACh^+).

Figure 9: Tetraalkyl ammonium salts, guest molecules tested for their templating ability.

Binding constants were calculated for each library member complex and the extent of amplification was mirrored by the K_a values calculated: Acetylcholine (K_a = 230 M^{-1}) is the best template, NMQ (K_a = 150 M^{-1}) amplifies the trimer to a similar extent as $EtMe_3NI$ (K_a = 140 M^{-1}), and $BnMe_3NI$ possesses the smallest binding constant (K_a = 80 M^{-1}) and produced the weakest response from the system. In order to determine that the final product distribution in the presence of template did indeed represent the equilibrium of the system, the complexation effect of [18]-crown-6 **23** on the transient species was utilised in the hope that linear species **24** would be detected. Indeed, this effect did occur, both the cyclic trimer and linear species were amplified in the presence of template. It is noteworthy that, both of these effects are against the intrinsic thermodynamic preference of the system for the cyclic dimer. Further work has been carried out on this system and a *pseudo*-peptide receptor for Li^+ has been identified.[107] The cation converted the complex oligomeric mixture into one that contained 98% of the Li^+ receptor.

This in-depth study of a complex hydrazone DCL over several years highlights many of the important features of a working DCL: (i) the ability to control exchange process under mild conditions, (ii) ease of isolation and characterisation of DCL members, (iii) proof of the dynamic nature of the library at any moment, (iv) proof of principle, amplification of a receptor through a guest species and (v) the demonstration of mass spectrometry as a powerful technique for the analysis of complex DCLs.

1.8.5 Concanavalin A Lectin – Disulfide/Acyl Hydrazone DCL

Receptor-type proteins, such as lectins, can also be targeted by DCLs. Disulfide exchange was used as the reversible reaction of choice. Disulfides undergo an aqueous-phase compatible exchange process. A small disulfide-based carbohydrate library was developed and used in conjunction with the common Jack bean lectin Concanavalin A **(Scheme 12)**.[108] Library generation was undertaken at neutral to slightly basic pH, where redox exchange is rapid, the exchange could efficiently be stopped by lowering the pH. A bis-mannoside unit **(Scheme 12)** was selected on binding to the immobilized Concanavalin A, in accordance with known ligands for this lectin.

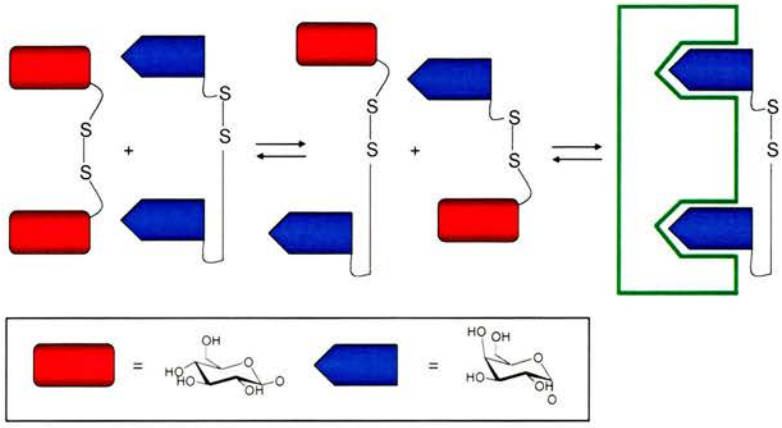

Scheme 12: Dynamic Library of disulfide containing carbohydrate structures. An example of thiol-disulfide exchange is shown. A bis-mannoside was selected by Concanavalin A. Taken from Ref. 82.

More recently, acyl hydrazone exchange was used in the generation of carbohydrate libraries to probe the binding site of Concanavalin A Lectin.[109]

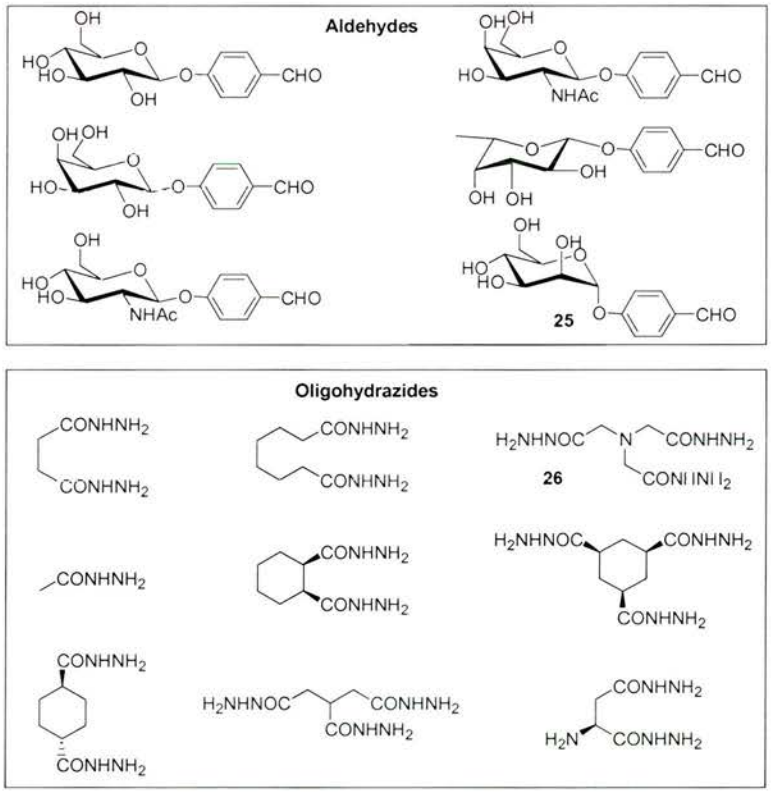

Figure 10: Components of the acylhydrazone library. Aldehydes contain carbohydrate moieties, solubilising the otherwise insoluble non-polar benzaldehyde fragment. Oligohydrazide core building blocks explore the geometrical and interactional space in the lectin binding site. Adapted from Ref. 109.

Acylhydrazone libraries were generated from the dynamic assembly of a series of oligohydrazide core building blocks **(Figure 10)** which were used to arrange the interactional components in a given geometry, with a set of aldehyde counterparts **(Figure 10)** potentially

capable of interacting with the binding site of the species. Generation of the dynamic libraries was accomplished at a moderately acidic pH of 4, with gentle agitation overnight. A complete acylhydrazone library resulting from these 15 components amounts to at least 474 different constituents. In order to identify the active compounds within the library, a previously described[110] dynamic deconvolution protocol was utilized. This methodology relies on the removal of a single building block from the complete library, resulting in the redistribution of the remaining components and suppression from the equilibrating pool of all constituents containing the removed components. Thus, when using this strategy a decrease in inhibitory effect reveals the importance of the removed component in the identification of active compounds from the dynamic library. This strategy was found to be highly efficient for targeting active species. On analysis of the dynamic deconvolution results compounds **25** and **26** were detected. The IC_{50} value for compound **27 (Figure 11)** was estimated to be in the micromolar range (22 μM). As a control, methyl-α-D-mannoside was used (IC_{50} = 0.8 mM), resulting in a 36-fold binding difference in favour of compound **27**. This value is comparable to the natural trimannoside ligand which shows a 60-fold higher affinity than the methyl-α-D-mannoside. This study enabled the efficient identification of a novel tritopic mannoside, showing potent binding to Concanavalin A.

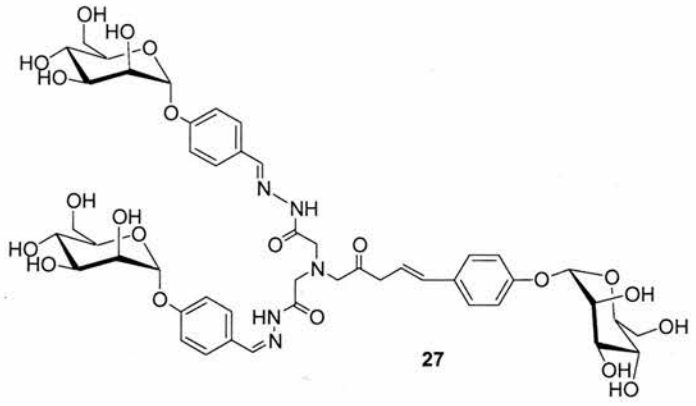

Figure 11: Potent ligand **27** for binding to Concanavalin A.

An acyl hydrazone library has also proved useful in the identification of a potent ditopic inhibitor for *Bacillus subtilis HPr kinase/phosphatase.*[111] Once more, a dynamic deconvolution approach proved successful in identifying the most potent inhibitor.

1.8.6 Disulfide DCLs

Disulfide exchange[112] is one of the most promising reactions for generating dynamic combinatorial libraries. Mechanistic studies indicate that: (i) in solution, thiols readily

oxidize to disulfides upon exposure to air; (ii) disulfide exchange takes place under mild conditions in the presence of catalytic amounts of thiol, (iii) the exchange is switched-off under slightly acidic conditions.

1.8.6.1 Solid-phase Disulfide DCL

A solid phase disulfide DCL[113] was reported by Hioki and Still.[114] Fluorescence microscopy was used to screen a 3375 member *N*-acetyl tripeptide library immobilised on polystyrene beads. A number of peptides were shown to bind selectively to fluorecent disulfide A-SS-A formed from A-SH **(Figure 12)**. Incubation of the disulfide with thiophenol resulted in an equilibrium mixture of 65% of the A-SS-A and Ph-SS-Ph and 35% of A-SS-Ph. When the equilibrating mixture was exposed to immobilized tripeptide ligand (Ac(D)Pro(L)Val(D)Val-PS) the composition shifted to 95% of A-SS-A. The beads to which A-SS-A were bound could be readily identified by the fluorescent tag incorporated into A-SH. The bound compound was isolated in 99.5% yield by washing the resin beads with $CHCl_3$ and then DMF. These studies have shown that binding to a peptide substrate can significantly shift the equilibrium of receptor molecules to enrich the mixture with the most effective substrate-binding receptor. This practical example describes the 'moulding' strategy described[69] by Lehn **(Section 1.5)**.

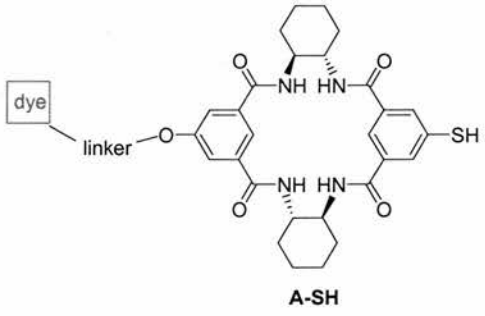

A-SH

Figure 12: Thiol A-SH contains a fluorescent probe for the identification of good binding species to the eight potential H-bond donor sites and the eight H-bond acceptor sites which will be available on disulfide A-SS-A.

1.8.6.2 Disulfide Macrocycles

Sanders[115] and co-workers have conducted extensive studies on the preparation of structurally diverse disulfide macrocycles in water. A dynamic library was achieved by mixing a selection of structurally diverse dithiol building blocks **28-31 (Figure 13)**.

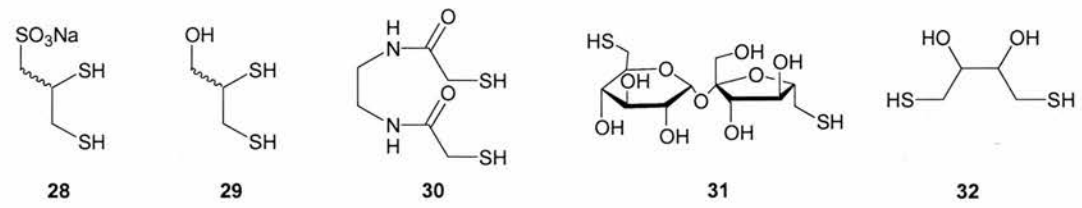

Figure 13: Dithiol building blocks for the generation of a disulfide macrocyclic library.

After stirring the dithiols in an open vial at 10 m*M* and at pH 7.5 the formation of 119 different macrocyles was recorded by both triple quadrupole electrospray ionization mass spectrometry (QQQ ESI-MS) and fourier transform ion cyclotron resonance (FTI-CR ESI-MS). In order to ascertain whether the library was under thermodynamic control, a set of control experiments were undertaken in which the same library was generated *via* two distinct routes. Firstly, one library contained mixtures of all thiol building blocks **28-31** and a mixture of disulfide macrocycles was formed directly by oxidation. Secondly, two separate libraries were generated by oxidising mixtures of thiols **28** and **29** and then **30** and **31**. These two libraries were later mixed and 15 mol% of dithiol **32** was added to partially reduce the library members, subsequent oxidation resulted in the identical distribution of disulfide macrocycles as in the direct oxidation case. In order to isolate compounds from a DCL it is advantageous to have control over the exchange process, to have conditions where exchange does not occur. Otto and co-workers found that the disulfide exchange reaction becomes very slow on increasing the acidity of the library medium.

This proof of principle study was further expanded in 2002 when Otto and co-workers[116] discovered two receptors for two different guests from a single DCL. Dithiols **33-35 (Figure 14)** incorporate hydrophobic aromatic surfaces that are well separated from the carboxylate groups, a requirement in order for the compounds to be water soluble.

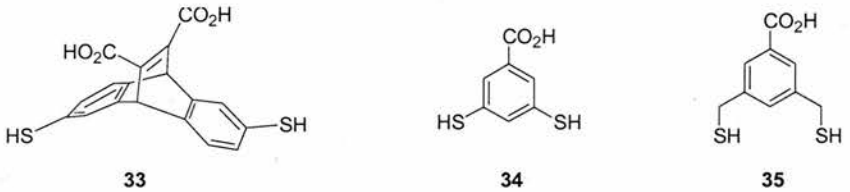

Figure 14: Building blocks **33**, **34** and **35** for the generation of a macrocyclic disulfide library.

The DCL was generated by mixing equimolar amounts of dithiols **33**, **34** and **35** under basic aqueous conditions (pH 8-9) in an open vial. The library was analysed by ESI-MS and 45

different macrocyclic disulfides of unique mass were identified. Quantitative information was obtained by high-performance liquid chromatography (HPLC) analysis. In the absence of any guest molecule, two major products, **36** and **37 (Figure 15)**, were detected.

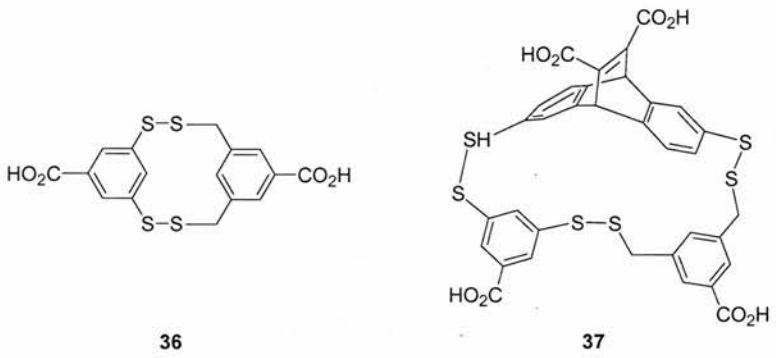

Figure 15: Major macrocyclic products detected in the absence of any templating molecule.

In the presence of 2-methylisoquinolinium iodide **38** as guest **(Figure 16)**, a dramatic shift in the library composition was detected. One of the previously minor components in the initial undoped library was amplified at the expense of the majority of other library members. The selected host was mixed trimer **39**. The same library was also exposed to *N*-methylated morphine **40** as a guest, this once again led to the amplification of one of the minor species from the original library, homotrimeric host **41**.

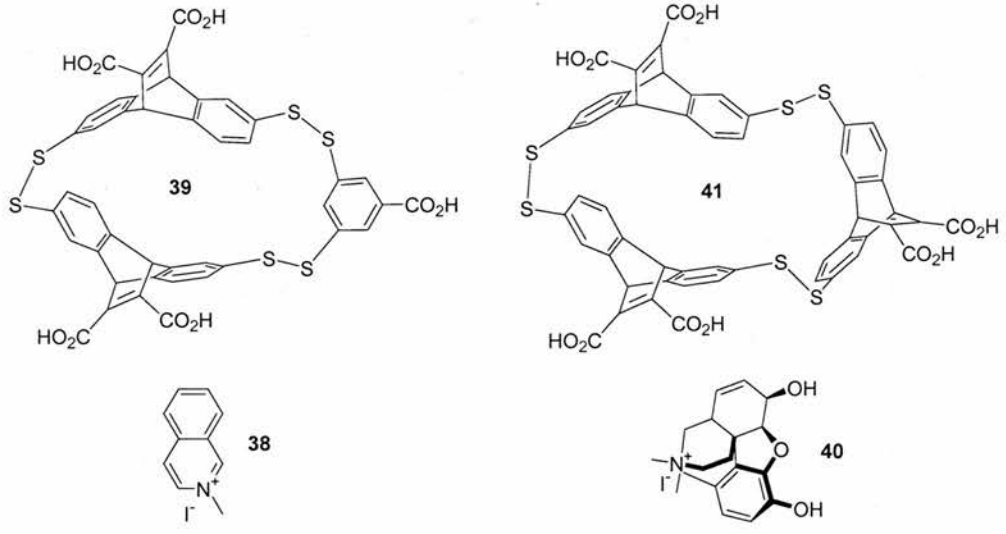

Figure 16: Library members **39** and **41** amplified on addition of 2-methylisoquinolinium iodide **38** and *N*-methylated morphine **40** respectively.

Otto and co-workers have also demonstrated the efficient synthesis of macrocycles **39** and **41** through the formation of a second generation of biased libraries, composed only of the

building blocks known to be selected by the host. In the presence of guest **38**, macrocycle **39** could be produced in 60-65% yield. Macrocycle **41** was obtained in an impressive > 95% yield on addition of template **40**. These are impressive yields for macrocylisation reactions, which are notorious for producing only small quantities of the desired product. The binding constants for the optimal host-guest pairs were found to be 6-25 times higher than those for the mismatched pairs. The guests therefore appear to be able to select a tightly binding host from a number of closely related structures. Perhaps more significantly within this study, relatively small differences in binding energies were shown to be sufficient to lead to large differences in the extent of selection. This study also demonstrated that molecular recognition-induced shifts in the composition of libraries of realistic size and diversity can be impressive.

In 2003, Otto and co-workers reported[117] the selection and amplification of a catalyst from a dynamic combinatorial library. Aformentioned dithiol library members **33-35 (Figure 14)** were used to search for catalysts to enhance the Diels-Alder reaction between acridizinium bromide **42** and cyclopentadiene **43 (Scheme 13)**. The transition state analogue utilized in this study was product **45** as its structure is similar to the activated complex **44**.

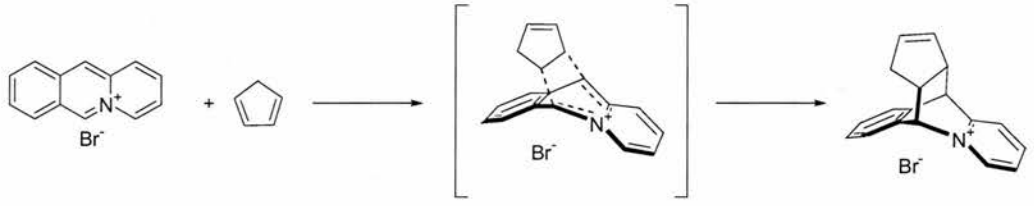

42 **43** **44** **45**

Scheme 13: Diels-Alder reaction between dienophile acridizinium bromide **42** and diene cyclopentadiene **43** demonstrating the similarity between the transition state and the product.

The product distributions of the library in the absence and presence of the transition-state analogue (TSA) were analysed by HPLC and mass spectrometry. Addition of the TSA to the library, resulted in the selection of macrocycles **39** and **41(Figure 16)**, the same receptors selected in the previous study.

The binding of dienophile **43** and Diels-Alder product **45** to hosts **39** and **41** were studied by isothermal titration microcalorimetry (ITC). Heterotrimer **39** was found to bind dienophile **43** more strongly than it bound Diels-Alder product **45**. In contrast, homotrimer **41** bound product **45** more strongly than it did starting material dienophile **43**. This suggested that heterotrimer **39** would be catalytically inactive and homotrimer **41** catalytically active.

Indeed, this was the case, macrocycle **41** induced a modest acceleration of the Diels-Alder reaction. As the reaction product was templated by the TSA only limited turnover observed for the reaction. Trimer **39** was found to be catalytically inactive. Although the efficiency of this system is modest, this study established dynamic combinatorial chemistry as a potential tool for catalyst development.

Otto and Kubik reported[118] studies on the dynamic optimisation of a neutral receptor, which binds inorganic anions in an aqueous solution. This study was designed to optimize the linking unit between two cyclopeptide rings. The library was constructed with 1 eq. of disulfide **52 (Figure 17)** and 0.33 eq. of each of the dithiol linkers **46-51** in a 2:1 (v/v) mixture of acetonitrile/water at a pH of 8-9 in the presence of air over 7 days.

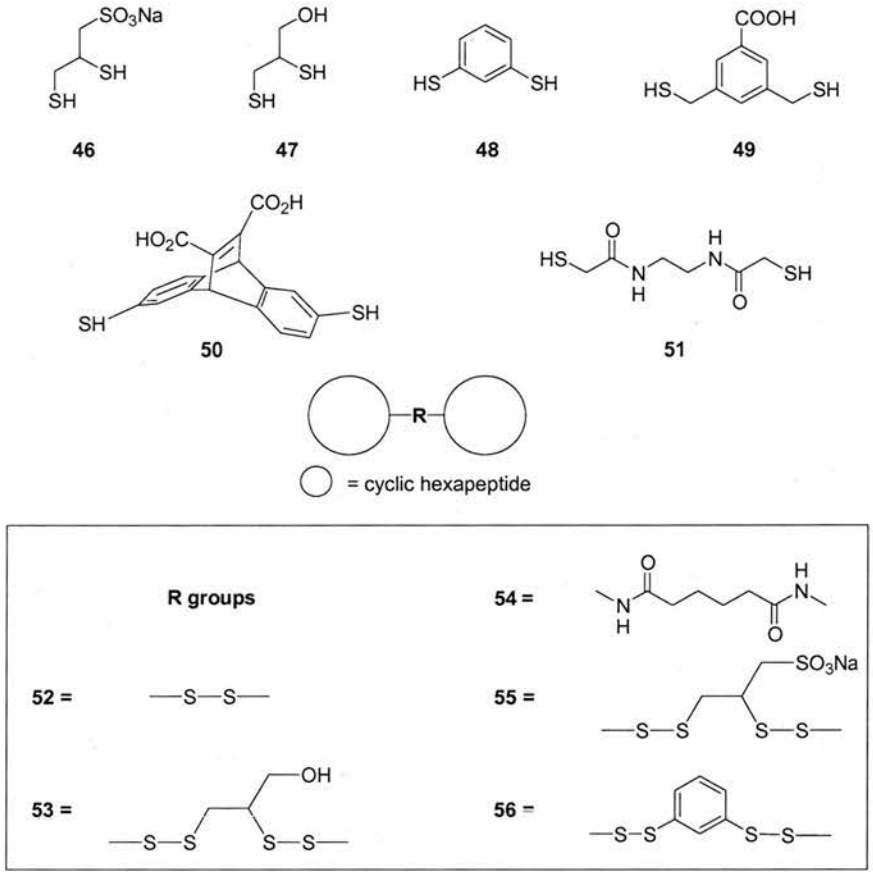

Figure 17: Dithiol spacers **46-51**. Cyclic hexapeptide receptor, with varying spacer units **52-56**. Adapted from Ref. 118.

In the absence of any template, the library was found to be composed mainly of starting disulfide **52**. Exposure of the dynamic library to KI and K_2SO_4 resulted in the selection of three different receptors (studies involving KBr, led to a decrease in selection using the same set of receptors, whereas NaCl and KF had no effect on the library composition). The

selected compounds were disulfides **53**, **55** and **56**, all of which contain short linker units. Binding studies were carried out in order to access the effectiveness of receptors **53** and **56** in comparison with previously studied receptor **54**. The results showed that receptors **53** and **56** can bind sulfate and iodide ions an order of magnitude more effectively than receptor **54**. Unprecedented binding affinities were also observed for iodide and sulfate anions with receptors **53** and **56**.

Disulfide exchange has also been utilized by Balasubramanian and co-workers.[119] Their studies on the formation of a disulfide-linked β-hairpin mimic from a small library found that under thermodynamic control, one disulfide β-sheet assembly was favoured over any other. More recently, the same group have extended their research in disulfide dynamic libraries to use a G-quadruplex as a target.[120] Within this library 4- and 5-fold amplifications were seen in specific library members with the greatest binding affinity for the target DNA molecule.

1.8.7 Olefin Metathesis DCLs

Vancomycin is a member of the glycopeptide class of antibiotics. In the past it has been used to treat infections caused by Gram-positive bacteria. The rise in vancomycin-resistant strains of bacteria is causing serious health concerns and therefore there is renewed interest in obtaining vancomycin analogues with restored activity for prevalent bacterial strains. Vancomycin's antibacterial activity arises from inhibitory effect on peptidoglycan biosynthesis in the bacterial cell wall. Specifically, vancomycin binds to the terminal Lys-D-Ala-D-Ala fragment **(Figure 18)** of the growing peptidoglycan biosynthetic precursor, through a network of five hydrogen bonds, thereby inhibiting cell wall growth and cross-linking.

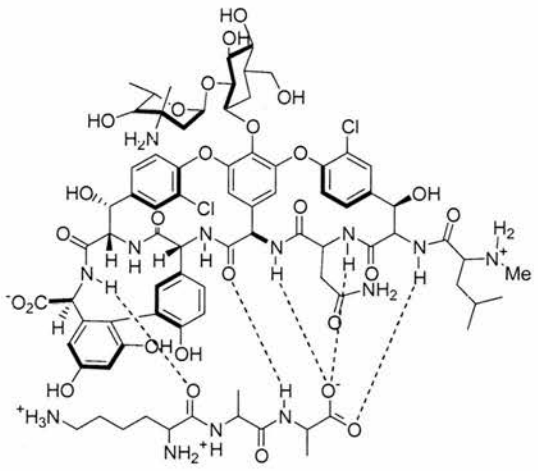

Figure 18: Vancomycin binding to the terminal Lys-D-Ala-D-Ala peptidoglycan fragment, showing five hydrogen bonds.

The vancomycin dimer is known to bind to its ligand more effectively than the monomer, due to strengthening of hydrogen-bonding interactions in the 'back-to-back' dimer. The increased affinity of the dimer also corresponds also to an increase in activity. Therefore, Nicolaou[121] and co-workers wished to utilize the enhanced activity found in the back-to-back dimer structure. The easiest way to achieve the desired dimer structure was to construct a bridge across the saccharide domains of two vancomycin molecules. This recent study was designed with two objectives in mind; firstly, the DCL would probe which dimer had strongest affinity for the target D-Ala-D-Ala fragement, and secondly the DCL would probe the most appropriate tether length required to allow the desired back-to-back dimer arrangement. The library of vancomycin analogues would then be allowed to self-assemble giving the most favoured assembly for the target and then a latent functionality would be used to covalently dimerize the selected species **(Scheme 14)**. As with all biological DCLs many factors have to be considered in terms of pH and temperature, this limits the number of reversible reactions available for use. Nicolaou identified the olefin metathesis and the disulfide exchange reaction as suitable reversible reactions for this library. Ultimately the olefinic compounds were chosen over their disulfide counterparts due to their greater metabolic stability. Earlier studies by Brändli and Ward had demonstrated[122] that the cross-metathesis of two di-subsituted internal olefins could generate up to 20 compounds.

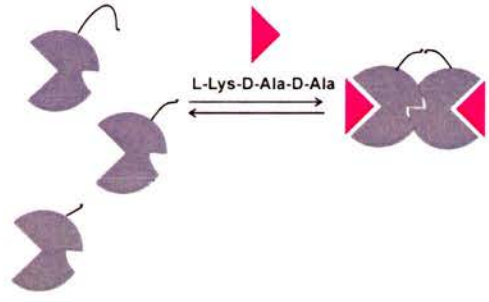

Scheme 14: Receptor library screened against bacterial cell wall building block D-Ala-D-Ala. Taken from Ref. 82.

An eight component target-accelerated combinatorial experiment employing the olefin metathesis reaction was carried out. Thirty-six library members were expected, and thirty were observed by mass spectrometry, due to the degeneracy of six dimers. Dimers were also synthesized individually and tested for biological activity. The results from the target-accelerated dimerization reaction corresponded to the results from the individual biological activity of the library members. The library identified three compounds as highly potent antibacterial agents, effective against both vancomycin-susceptible and vacomycin-resistant

strains. This study shows the usefulness of a target-accelerated synthesis in predicting biological activities at a pre-screening stage of drug discovery.

1.8.8 Transthioesterification

Ramstrom and co-workers[123] have recently studied the transthioesterification reaction to produce a prototype DCL **(Scheme 15)**.

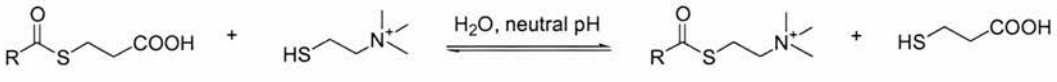

R = Me, Et, *n*Pr, *n*Bu, *n*Pe

Scheme 15: DCL generation by transthioesterification under mild conditions.

Acetylcholinesterase in conjunction with transthioesterification allowed the rapid generation and screening of the DCL, a process which resulted in the complete amplification of only the best binding substrates, acetate and propionate. This study has demonstrated once more that an enzyme catalyst may be used to assist the dynamic self-screening of its substrates (see **Section 1.8.2** on carbonic anhydrase).

1.9 Non-covalent Dynamic Combinatorial Libraries

1.9.1 Hydrogen Bonding DCLs

Reinhoudt and co-workers reported[124] the first example of guest-templated selection of a receptor in a non-covalent dynamic combinatorial mixture, in which the different receptors equilibrated through the reversible formation of multiple hydrogen bonds. Reinhoudt had previously reported[125-126] the non-covalent synthesis of a family of hydrogen-bonded assemblies, held together by 36 cooperative hydrogen bonds. However, none of the assemblies in this mixture contained a functional binding site for guest complexation. In order to probe the guest-templated selection of receptors within this 'family' of non-covalent receptors, a dimelamine was synthesised with two opposed zinc-porphyrin moieties, designed to bind tripyridines. It was postulated that the four assemblies within the dynamic mixture would each have very different binding affinities for the tripyridine depending on the number of zinc porphyrin centres that were incorporated in the binding process. Studies showed that the receptor with the maximum number of zinc porphyrin centres was indeed selected from the mixture, as detected by ^{1}H NMR spectroscopy.

Reinhoudt also reported[127] the 'covalent capture' of dynamic hydrogen-bonded assemblies. This involved converting libraries of dynamic hydrogen-bonded assemblies into covalent analogues for ease of characterization. The ring-closing metathesis (RCM) reaction was employed as it was compatible with the hydrogen bonded network within the assemblies. Covalent capture of the 4-component dynamic library described previously, occurred under standard RCM reaction conditions. HPLC analysis showed the formation of all four possible trimers. Covalent capture of hydrogen-bonded assemblies was shown to occur with high efficiency for this system and illustrates how libraries of this type can be monitored by conventional techniques such as HPLC and mass spectrometry.

Work in the field of non-covalent dynamic libraries has also been conducted by Rebek and co-workers. Rebek[128] generated tetrameric capsules, self-assembled in the presence of a methylquinuclidinium cation guest. From a possible six structurally different tetrameric capsules, one represented 69% of the observed mixture, eleven times the amount predicted by statistics. When this library was expanded to encompass more monomers, there was the possibility of generating up to 613 receptors (70 of these were capsules). Although selection for a single capsule was less marked than in the previous example, from a possible 70 capsules, only 11 were formed in any significant amount.

1.10 Metal-Ligand VCLs

Metal-ligand exchange has been used successfully in a variety of dynamic combinatorial systems.[129-138] Two specific examples from this field are described below.

1.10.1 Metalloporphyrin Tetramer Amplification

In 2002 Sanders and co-workers first reported[139] their studies on mixed-metal porphyrin cages from DLCs. Sanders had previously reported the synthesis of such porphyrin complexes, both in their template-assisted formation **(Section 1.8.1)** and in their ability to enhance the rate and selectivity of a Diels-Alder reaction **(Section 1.14.3)**. However, this study was the first example of selection and virtually quantitative amplification of a thermodynamically stabilised tetraporphyrinic construct from a DCL **(Scheme 16)**. The structure was stabilized by orthogonal metal-ligand coordination. In this system, reversible metal-ligand binding was used for two roles simultaneously, firstly to form the DCL and secondly to induce a templating effect. The library was composed of a bis-diphenylphosphine substituted zinc porphyrin **57** and rhodium porphyrin **58**, when mixed in $CDCl_3$, a mixture of

coordination compounds was formed. The mixture contained *cis/trans* linear, and cyclic species of variable length and ring size **(Scheme 16)**.

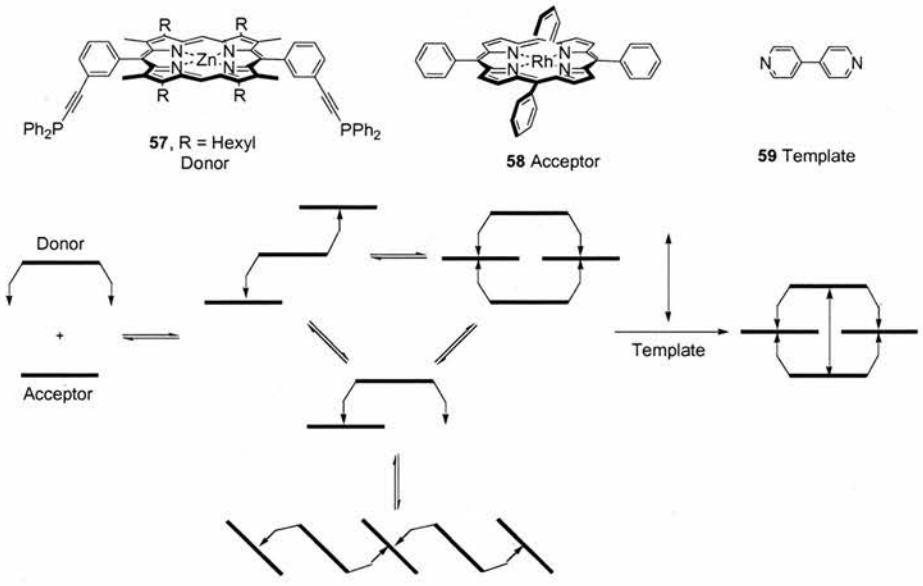

Scheme 16: A schematic representation of porphyrin DLC formation.

A tetraporphyrin was ultimately stabilised on addition of template 4,4'-bpy **59** to the DCL, through orthogonal Zn^{II}-nitrogen and Ru^{III}-phosphorus binding **(Scheme 16)**. Sanders has further extended this study to include a selection of different Rh^{II}/Ru^{III} porphyrins which can be selected and amplified by different templates.[140]

1.10.2 DNA and RNA binding Compounds Generated from a DCL

Miller[141] and co-workers have extensively studied DNA-binding compounds by selection and amplification from self-assembled combinatorial libraries. The utility of modified organotransition metal coordination complexes binding to oligonucleotides has been investigated. Salicylaldimines are well known to form coordination complexes with a wide variety of transition metals. Divalent zinc, as a consequence of its tetrahedral coordination geometry with salicylaldimines and compatibility with nucleic acids was chosen for initial studies.

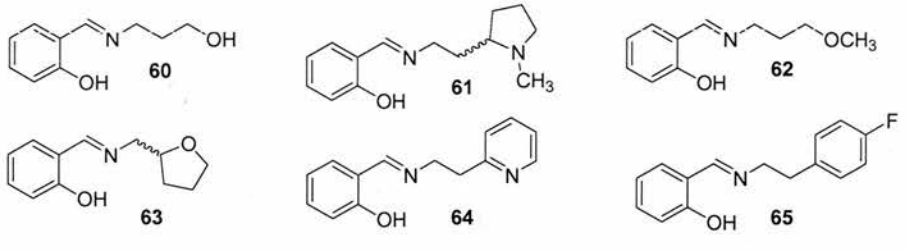

Figure 19: Six salicylaldimines **60-65** for use in a self-assembled library.

Six salicylaldimines **60-65 (Figure 19)** each with different side-chain functionalities were used in the formation of this library. From these six salicylaldimines a maximum of 36 unique bis(salicylaldiminato)zinc complexes could be produced. Selection from the library was achieved by incubation with a dA oligonucleotide bound solid-phase poly(dT)-cellulose resin for two hours, followed by elution and lyophilization. Analysis of the mixture was carried out by hydrolysis of the complexes with TFA, followed by the derivatisation of the amines with excess 2-naphthoyl chloride (to allow for UV detection) and separation by reverse-phase HPLC. Results showed that library member **66 (Scheme 17)** had the highest affinity for DNA (1 μM).

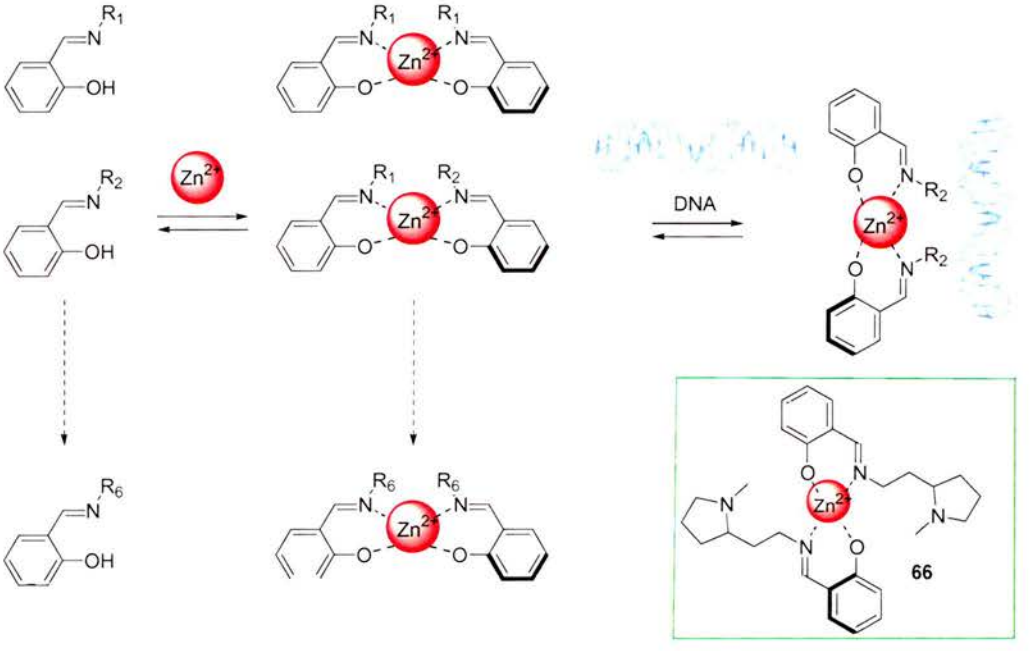

Scheme 17: Library of Zn^{2+} complexes with duplex DNA. Adapted from Ref. 82. R_1-R_6 represent various substituents.

Miller and Klekota[142] later expanded upon the strategy of selection and amplification in salicylaldimine and Zn^{2+} libraries. During the course of their initial studies on this system[141] Lehn and co-workers had published their work on imine libraries.[99] This suggested to Miller that a multi-stage equilibration process may be utilized within these systems. The presence of amine, salicylaldehyde and imine components in buffer would provide a very complex mixture, as each of these materials would be in equilibrium with one another, as well as in various complexed forms. A situation in which four-coordinate zinc in complex with an equilibrating mixture of two amines, salicylaldehyde, and water can produce a staggering mixture of at least 1,521 components, all of which can potentially participate in DNA binding.

A library was constructed with six amines **67-72 (Figure 20)**, salicyaldehyde **73**, and Zn^{2+} using double-stranded oligo(dA·dT)-cellulose resin **(Scheme 18)**.

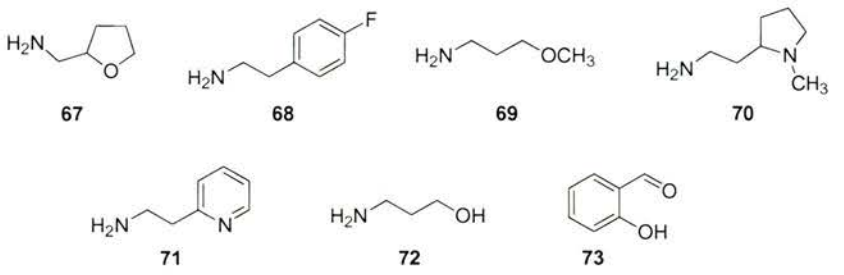

Figure 20: Components for an imine DCL, amine library building blocks **67-72** and aldehyde **73**.

Libraries were allowed to pre-incubate for one hour in order to reach an initial equilibrium before addition to the DNA resin. Samples were then incubated for three hours before being eluted, hydrolyzed, and derivatized with 2-naphthoyl chloride. Derivatized samples were then analyzed by HPLC. Similarly to previous results, Miller and co-workers observed that zinc complexes incorporating salicylaldehyde **73** and *N*-methyl 2-aminoethylpyrrolidine **70** had the highest affinity for oligo(dA·dT).

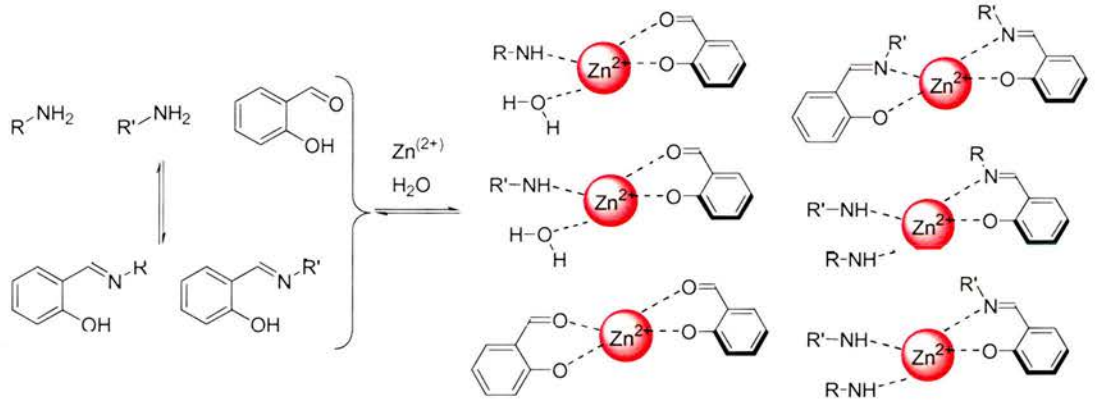

Scheme 18: A subset of the complexes that might be formed in a multistage evolution equilibration. Taken from Ref. 141. R and R' represent various substituents.

Subsequently in 2001, Karan and Miller reported[143] their studies upon RNA-selective coordination complexes identified *via* dynamic combinatorial libraries. Salicylimides were again selected as ligands in this RNA-binding library as a result of their metal binding properties. Functionality was incorporated into the library using amino acids as the 'R' group side-chains to afford compounds **74-79 (Figure 21)**. Cu^{2+} was selected as the metal of choice for the selection experiments.

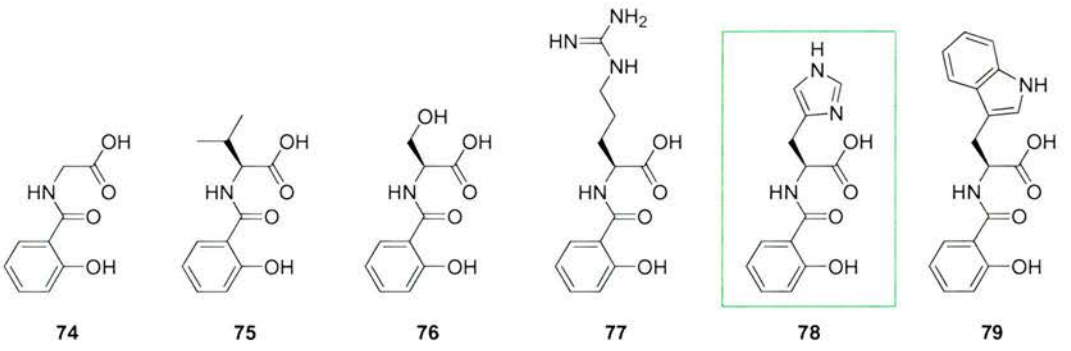

Figure 21: Salicylamide ligands **74-79** for the construction of RNA-binding library.

Selection experiments were carried out **(Scheme 19)** and compound **78** was selected above all other library members with an incredible affinity for the RNA hairpin (152 n*M*). This affinity showed more than 300-fold selectivity over the homologous DNA sequence. These results suggest that DCL experiments will be useful for the identification of novel RNA-binding compounds.

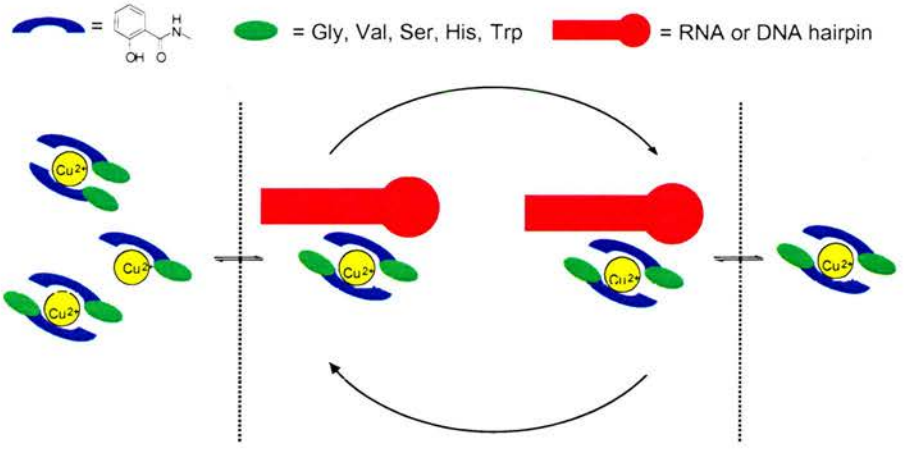

Scheme 19: Schematic representation of Miller's approach to the discovery of novel RNA-binding Cu^{2+} complexes. The receptor selects the best ligand. The template is dialyzed in the presence of the library to select the best binder and in the absence of the library to wash out the selected compound. Taken from Ref. 81.

1.11 Intramolecular VCLs

1.11.1 Induced Fit Selection of a Receptor – *cis-trans* isomerisation DCL

Lehn and co-workers reported the induced fit of a barbiturate receptor from a dynamic structural and conformational/configuration library.[144] The induced-fit process is the specific structural adaptation of a host molecule upon interaction with a guest molecule to form a more stable complex. The study involved the equilibration between different condensation

products of 5,5-dimethyl-1,3-cyclohexanedione **80** and 2-hydrazino-pyridine **81 (Scheme 20)**. Photo-isomeriation of the mono- and dihydrazone products generated diversity within the system. The library yielded the (*Z*/*Z*), (*E*/*E*), and (*E*/*Z*) dihydrazone isomers and also contained a substantial amount of the (*E*) and (*Z*) isomers of the monohydrazone, as well as the hydrazine-enone tautomer. Therefore, a number of equilibration processes can be envisaged: tautomerism, *cis/trans* isomerisation, hydrolysis to the monohydrazone monoketone, or transamination by the remaining 2-hydrazino-pyridine.

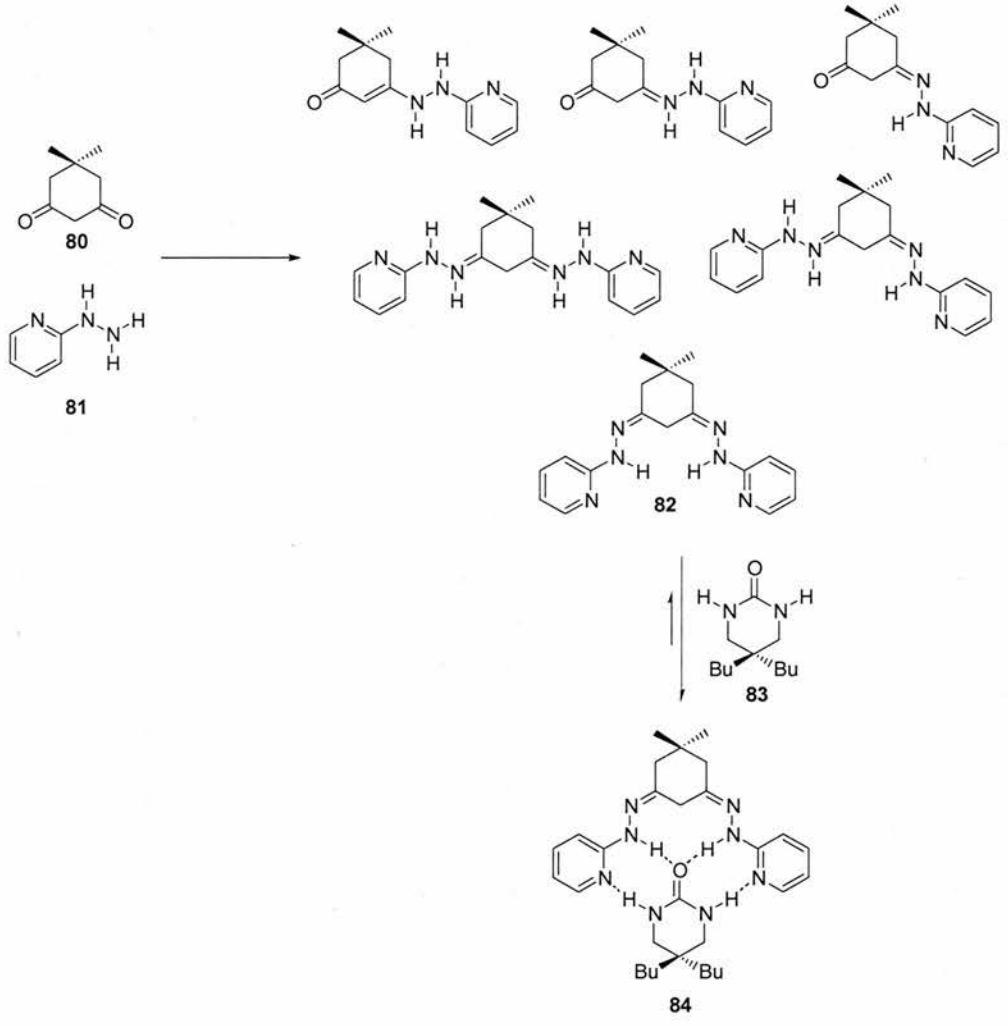

Scheme 20: Equilibrating library produced from **80** and **81**. The binding motif of optimal receptor **82** to the barbiturate **83**.

Addition of dibutylbarbiturate **83** to the equilibrating library led to a dramatic change in the ^{1}H NMR spectrum. The ^{1}H NMR spectrum became simpler, the disappearance of many products was coupled with the emergence of a single new species. The new species was determined to be a 1:1 complex between dibutylbarbiturate **83** and symmetrical dihydrazone as the (*Z*/*Z*) isomer, compound **82**. Addition of barbiturate **83** enforces a quantitative shift in the equilibrium of the library towards the dihydrazone (*Z*/*Z*) isomer **82**. Barbiturate **83** also

promotes the reaction of the monocondensation products with the remaining hydrazine-pyridine **81**. Complex **84** was amplified from the mixture of library members as a consequence of strong and specific hydrogen-bonding, the association constant was calculated as > 6400 M^{-1}. This study demonstrated the effectiveness of the substrate-driven selection of an optimal receptor from a dynamic library.

1.11.2 Internal Photoinduced Supramolecular DCL

In 1997 Eliseev and Nelen reported[145] an internal photoinduced supramolecular DCL. Molecular scaffolds **85**, **86** and **87**, **(Scheme 21)** each contain two double bonds and were designed to undergo a *cis-trans* isomerisation on irradiation with UV light. As defined by the symmetrical structure of the scaffolds, three isomers, *trans,trans* (**87**), *cis,trans* (**86**), *cis,cis* (**85**), co-exist in the irradiated solution. Arginine ligand **88** was chosen as the target, as a result of its ability to engage in supramolecular recognition, primarily through the formation of non-covalent salt bridges and hydrogen bonding interactions. It was shown by molecular modelling studies that the *cis,cis* receptor would have the most favourable binding for the ligand due to the proximity of its two arms, defined by its isomerisation motif. The arginine ligand **88** was attached to a silica stationary phase which had a high affinity for the *cis,cis* isomer. The irradiated solution was passed through the column, selection allowed to occur and the eluent is subsequently passed back through the apparatus for re-irradiation and selection. After thirty cycles of mutation the bound receptor was washed from the column a dramatic shift towards *cis,cis* isomer **85** was observed.

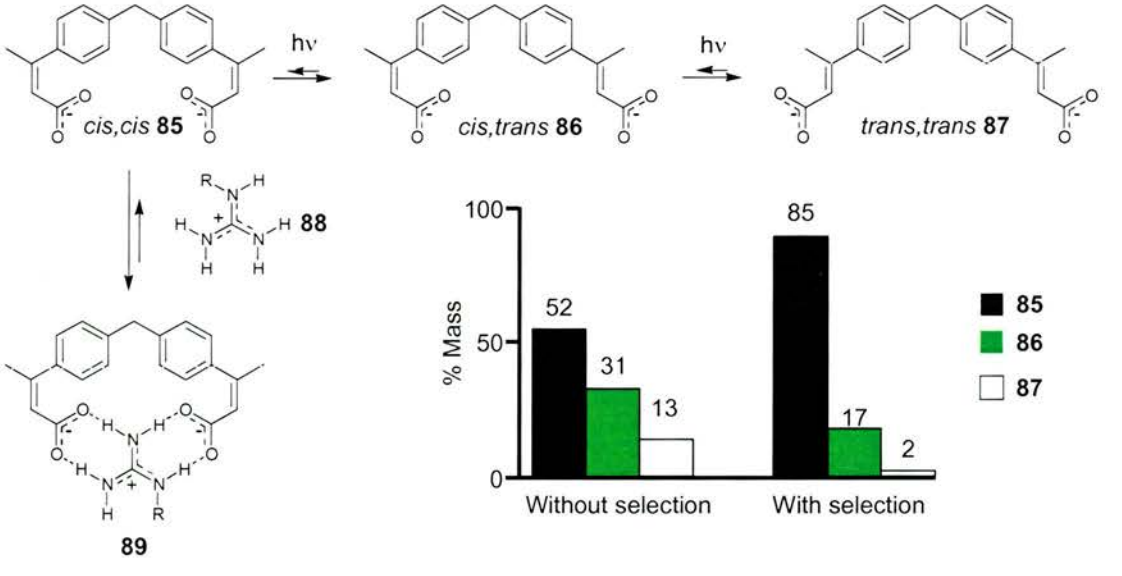

Scheme 21: Dynamic equilibrium shifting in action. Irradiation and complexation with a polymer-bound guanidinium salt shifts the equilibrium distribution of double bond stereochemistry strongly towards *cis-cis* complex **89**.

1.12 Orthogonal Dynamic Combinatorial libraries

Enhanced levels of diversity can be achieved by combining different connective chemistries, provided that they can be controlled independently. Eliseev and co-workers[146] first demonstrated an orthogonal approach to DCC using ligands containing imine moieties around a central cobalt ion **(Figure 22)**. Co-ligand exchange and imine exchange can be manipulated independently. Co-ligand exchange is rapid but can be frozen on oxidation to form kinetically inert Co(III) complexes. Imine exchange is efficient under acidic conditions but inactive under neutral conditions. Therefore, this library can work independently on two-levels. This orthogonal approach to DCLs has also been adopted by Choudhary and Morrow.[147] The reversiblity of acyl hydrazone ligands and metal-ligand exchange within one library has been employed in order to develop more efficient methods of metal extraction.

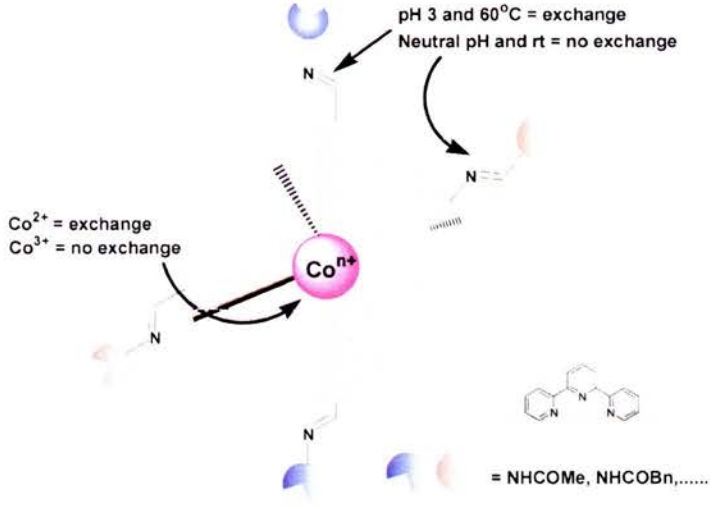

Figure 22: An orthogonal approach to a dynamic combinatorial library.

1.13 The Origin of Rate Enhancements in Enzymatic and Intramolecular Reactions

In order to discuss supramolecular catalysis in terms of design and function **(Section 1.14)**, it is first important to understand the explainations for rate accelerations in enzymatic and intramolecular reactions.

In 1948, Pauling proposed[148] the theory of transition state stabilisation as a means of explaining the mode of action in enzymatic reactions. He stated "the entire and sole source of catalytic power is the stabilization of the transition state; reactant-state interactions are by nature inhibitory and only a waste of catalytic power." This elegant theory was further expanded and is now termed "transition state stabilization."

Figure 23: Free energy diagrams for enzyme-catalyzed reactions in which **E**=enzyme, **S**=substrate, **E·S**=enzyme/substrate complex, and **TS**=transition state.

Within this model, two situations must be considered. In situation **I (Figure 23)**, where the concentration of substrate is low relative to the Michaelis-Menten dissociation constant (K_d) **(Scheme 22)**. The free energy diagram (**Figure 23**) illustrates that a change in the free energy of [**E•S**] will have no effect on the reaction rate, as it is dependent upon the free energy difference between **TS** and **E+S**.

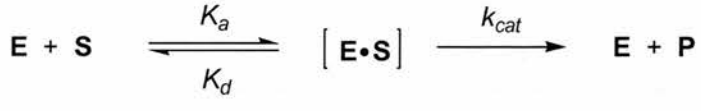

Scheme 22: The Michealis-Menten equation where **E**, **S**, [**E·S**] and **P** represent the enzyme, substrate, enzyme-substrate complex and product, respectively. K_a and K_d represent the association and dissociation constants. k_{cat} represents the forward rate of the chemical reaction.

Conversely, in situation **II (Figure 23)** where the concentration of substrate is high compared with the dissociation constant (K_d), lowering the free energy of [**E•S**] will lead to a decrease

in rate. This 'fundamentalist' approach was expanded by Menger,[149] he agrees that the classical Pauling theory is valid. However, introduces the "split-site" model **(Scheme 23)** and states that there is a further effect capable of inducing rate acceleration in enzymatic reactions. In the case of situation **II**, where we have stated that stabilisation of the [**E•S**] always leads to decrease in rate, the split-site enzyme theory suggests that one can accelerate the reaction by means of stabilising the binding region (ES_B) while destabilising the reactive region (ES_R) to a smaller extent.

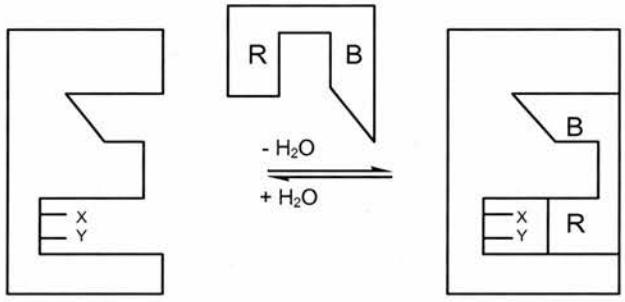

Scheme 23: Split-site enzyme model in which the active site is subdivided into a binding region and a reactive region. These regions associate with B and R of the substrate, respectively. Catalytic groups on the enzyme (X and Y) are brought into contact distances with the labile group of the substrate when the enzyme/substrate complex is formed. It is assumed that the total ES free energy equals the sum of the parts (*i.e.*, $ES = ES_R + ES_B$). Adapted from Ref. 148.

The first step in an enzyme-catalysed reaction is the complexation of the substrate and the enzyme. This binding process brings the reacting groups on the enzyme and substrate into close proximity allowing the reaction to occur. It was proposed in 1962 by Koshland[150] and later shown experimentally by Bruice[151-152] that holding reacting groups in close proximity does indeed lead to an increase in reaction rate. One useful concept which allows a quantitative understanding of the effect that proximity has on the rate of reactions is that of effective concentration (effective molarity, EM).[153] The effective concentration of the participating group is defined thus, as the concentration of reagent present in the intermolecular (bimolecular) reaction required to achieve comparable rate to the intramolecular (unimolecular) reaction. Comparison between intra- and intermolecular reactions in flexible systems can give maximum EM values of between 10^8-10^9 *M*. Higher figures are possible in reactions where ground state strain is relieved as part of the reaction. Bruice[151-152] studied the intramolecular nucleophilic displacement of a *para*-bromophenol group and compared these results with analogous intermolecular reactions **(Table 3)**. A clear trend between higher rates in intramolecular reactions was observed as the conformational flexibility was reduced.

Table 3: The rate constants for intramolecular nucleophilic displacement of a *para*-bromophenol ester by a carboxylate anion. Adapted from Ref. 151.

	k_{rel}
CH_3COO^- + $CH_3COOC_6H_4Br$	1.0
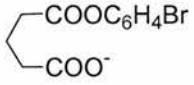	~ 1 x 10^3 *M*
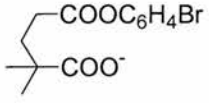	~ 3.6 x 10^3 *M*
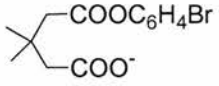	~ 1.8 x 10^5 *M*
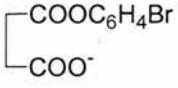	~ 2.3 x 10^5 *M*
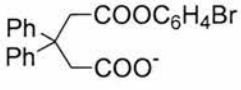	~ 2.7 x 10^5 *M*
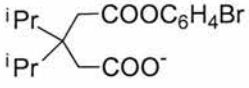	~ 1.3 x 10^6 *M*
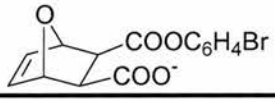	~ 8 x 10^7 *M*

Within this study Bruice states that geminal substitution is one cause of the rate accelerations observed. The acceleration of cyclisation reactions as a consequence of substitution of alkyl substituents for hydrogen atoms on the carbon backbone linking two reacting groups was first postulated by Ingold and Beesley.[154] It was suggested that the addition of such alkyl substituents to the central methylene would lead to angle deformation **(Figure 24)** and would therefore, bring chain ends closer together, thus favouring ring closure. This hypothesis, later to be termed the 'Thorpe-Ingold effect', although still valid, has been shown to play a minor role within the *gem*-dialkyl effect.[155]

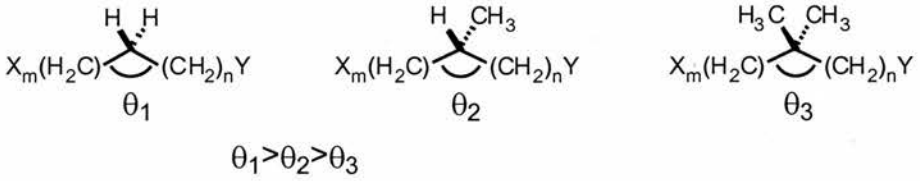

Figure 24: The Thorpe-Ingold effect. Alkyl substitution at the central methylene unit compresses the internal bond angle. X and Y represent reactive sites, whereas m and n indicate the number of methylene spacers between the reactive sites and the central methylene unit. Adapted from Ref. 155.

Bruice, also cited the 'Reactive Rotamer effect', in order to explain the rate enhancements shown within his study. Jung and co-workers[156-157] studied the reactive rotamer effect using intramolecular Diels-Alder reactions **(Scheme 24)**. This effect has been shown to be of greater significance to intramolecular rate enhancements than angular compression.[152]

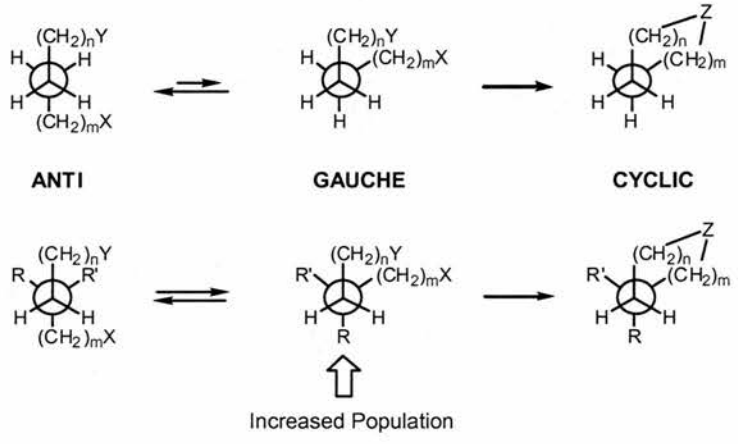

Scheme 24: The reactive rotamer model proposed by Jung *et al.* to explain the increase in intramolecular reactivity on geminal substitution. X and Y represent the two reactive sites, whereas n and m represent the number of methylene spacers attached to the central C-C bond. Adapted from Ref. 156.

The 'common sense phenomenon' of propinquity was refined by Menger[158-159] in his 'spatiotemporal postulate' to include a time component. He states that 'the rate of reaction between functionalities A and B is proportional to the time that A and B reside within a critical distance.' Page interprets[160-161] the spatiotemporal theory as a euphemism for entropy, as it is entropy which determines the time spent at the critical distance.

Complexation of two molecules is accompanied by a negative change in entropy as the volume of space available to the reactants is reduced. Comparing the losses of translational and rotational degrees of freedom between intra- and intermolecular reactions it is possible to appreciate the impact of entropy on the rate of reactions **(Tables 4 & 5)**. The change in entropy contributes to unfavourable rates and equilibria within bimolecular reactions.

Unimolecular reactions, which do not undergo such entropic variation are therefore expected to proceed at comparably faster rates.

Table 4: Table showing the changes in degrees of freedom associated with an intermolecular reaction.

	A + B ⇌ P	
Translation	3	3
Rotation	3	3
Vibration	$3n$-6	$3n$+$3n'$-6

Table 5: Table showing the changes in degrees of freedom associated with an intramolecular reaction.

	A—B ⇌ P	
Translation	3	3
Rotation	3	3
Vibration	$3n$-6	$3n$-6

However, entropy alone cannot explain the rate enhancements within intramolecular reactions. The concept of angular dependence on reaction rate was first introduced through the 'orbital steering hypothesis.'[162-164] This theory is based on the premise that rate accelerations can be achieved by enzymes and intramolecular structures by steering the reacting atoms in preferred orientations. Koshland stated that there was a 'window' of 10° to give the ideal alignment of orbitals on reacting species which could lead to large rate enhancements. Menger[165] carried out further experiments which showed that an angular displacement a few degrees either side of this optimum 'window' did not in fact dramatically effect the rate of reaction despite Koshland reporting otherwise.

It has been argued that this theory is incomplete, as it also does not appreciate the role of orientation and strain on reaction dynamics. One hypothesis encompassing the theories of proximity, angular dependence, entropy trap and transition state stabilisation; is the concept of a Near Attack Conformation (NAC).[166-169] Bruice and Lightstone propose that in order to enter the transition state, reacting species must first achieve a specific ground state conformation. The NAC is defined as a genuine ground state conformation where reactive

centres are separated by about 3Å, van der Waals overlap has yet to begin, no bond making or breaking steps have begun and the approaching nucleophile is within a 30° cone **(Figure 25)**.

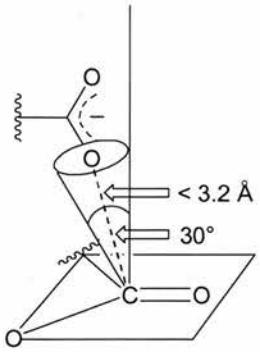

Figure 25: The geometry of a NAC for intramolecular carboxylate anion interaction with a carbonyl ester. Adapted from Ref. 165.

The above theories attempt to rationalise enzyme selectivity and reactivity, however as many as twenty-one hypotheses [170] have been proposed. As a consequence it is fair to comment that the phenomenon of enzyme and intramolecular rate acceleration is still not fully understood.

1.14 Supramolecular Catalysis

Molecular recognition **(Section 1.2)** is inextricably linked to supramolecular catalysis, in the process of substrate binding to form reactive complexes. Supramolecular catalysis endeavours to utilize molecular recognition in order to enhance chemical reactions. Synthetic enzyme mimics have been designed which reproduce some of the features of enzyme catalysis, a brief review of a selection of supramolecular catalysts is presented.

1.14.1 Partial Transacylase Mimics

Chymotrypsin **(Figure 26a)** is a serine protease and catalyses the hydrolysis of proteins. The active site of all serine proteases contain four common elements **(Figure 26b)**; a binding site, a nucleophilic hydroxyl group that is part of a serine residue in the polypeptide chain, an imidazole ring that is part of a histidine residue and an aspartate group that is part of an aspartic acid residue.

a) **b)**

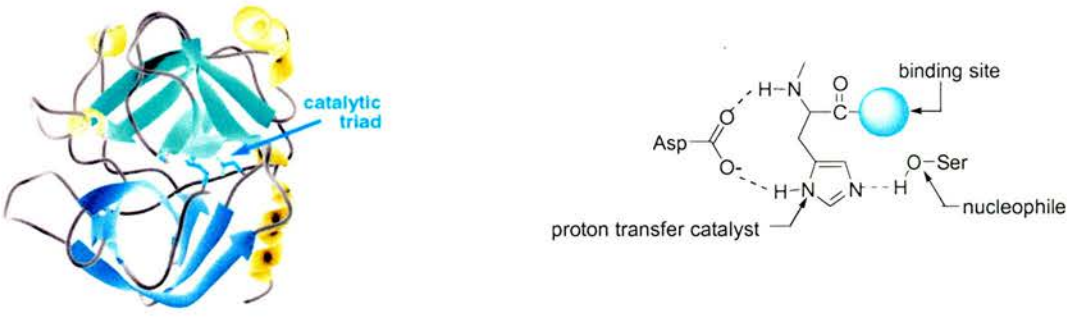

Figure 26: **a)** Protein crystal structure of chymotrypsin showing the active site and the important catalytic residues; **b)** A simplified diagram of the essential features required in a serine protease.

Cram[24] posed the question, "What are the minimum structural features required to observe "chymotrypsin-like" catalytic activity?" Molecular modeling studies demonstrated compound **90 (Figure 27)** to be the ultimate enzyme mimetic host, possessing groups in the optimal configuration for catalysis.

a) **b)**

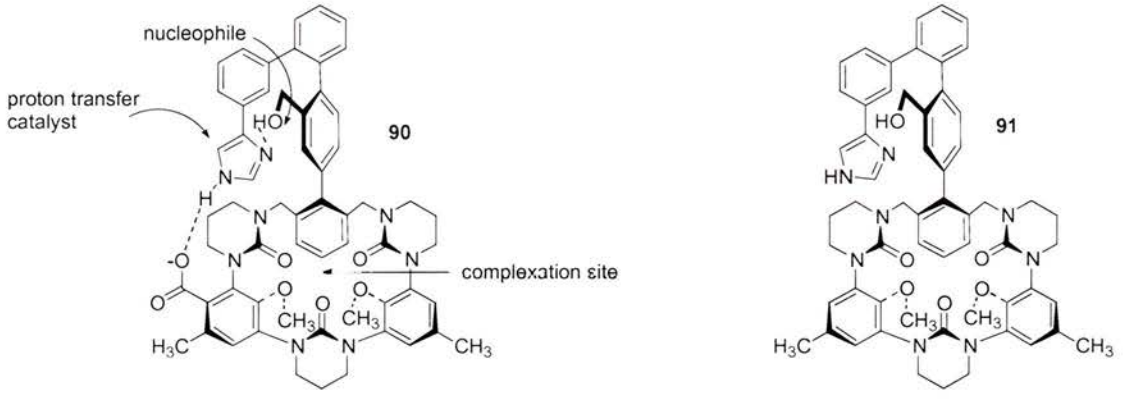

Figure 27: **a)** Ideal host for acylation of **90**; **b)** Simplified host structure **91** for the study of acylation reactions.

Such a complex structure was a difficult synthetic target, therefore before embarking on such a project Cram investigated simpler systems before finally using host **91** as a model compound. Compound **92** was acylated by **93** to give **94** and *p*-nitrophenol **95 (Scheme 25a)**. Kinetic measurements were conducted in $CHCl_3$ and the rate of acylation of host **91** by **93 (Scheme 25b)** was calculated as ~ 10^{11} higher than for the non-complexed model. This remarkable rate enhancement was as a result of the specific orientation of reactants through a highly ordered host-guest complex. The $-NH_3^+$ group can complex to the binding site of the host **(Scheme 25b)**, the coulombic attraction between the positive charge on the nitrogen atom and the lone pairs of electrons on the oxygen atoms holds guest **93** in the correct orientation so that reaction with host **93** may occur more readily.

This investigation demonstrated that a fully synthetic system can be designed and prepared which mimics an enzymes ablility to use complexation to enhance the rate of a reaction. This early example of supramolecular catalysis is still one of the most efficient to date.

a)

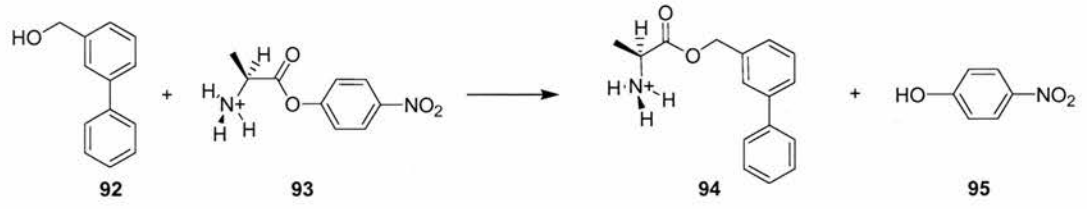

b)

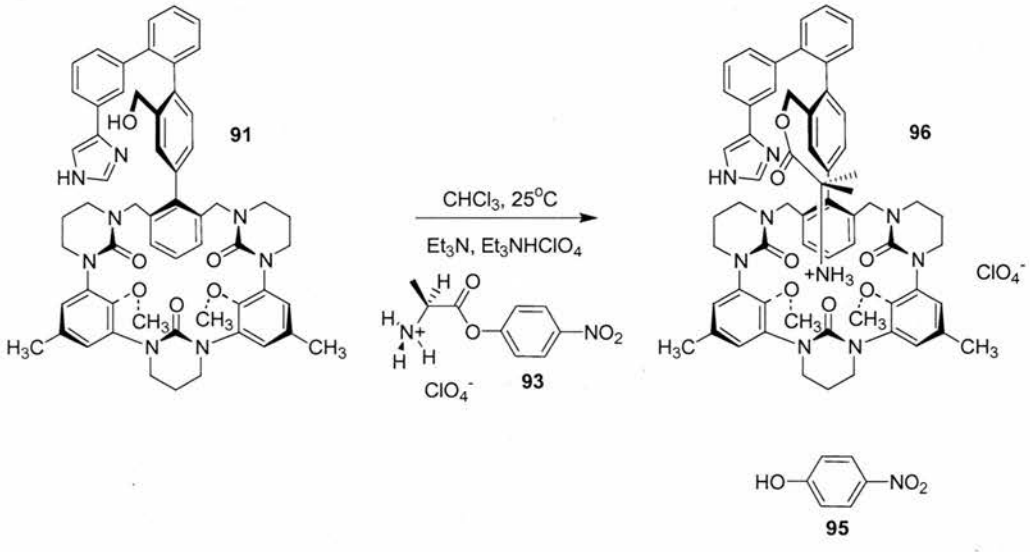

Scheme 25: **a)** The 'control' study reaction between 3-phenylbenzyl alcohol **92** and 1-(4-nitro-phenoxy carbonyl)-ethyl-ammonium **93**; **b)** The host-guest acylation reaction between host **91** and guest **93**.

1.14.2 Ternary Complex Methodology

Kelly and co-workers reported[171] the first example of a fully synthetic system which uses hydrogen bonding to simultaneously bind two substrates. A ternary complex was formed, which positioned the substrates in an orientation that facilitated the reaction between them. The reaction chosen for the study was the the S_N2 amination of an alkyl halide **99** by an amine **98** in $CDCl_3$ at room temperature. The presence of template **97** accelerated the formation of the product **100** by about 12-fold over the analogous bimolecular process **(Scheme 26)**.

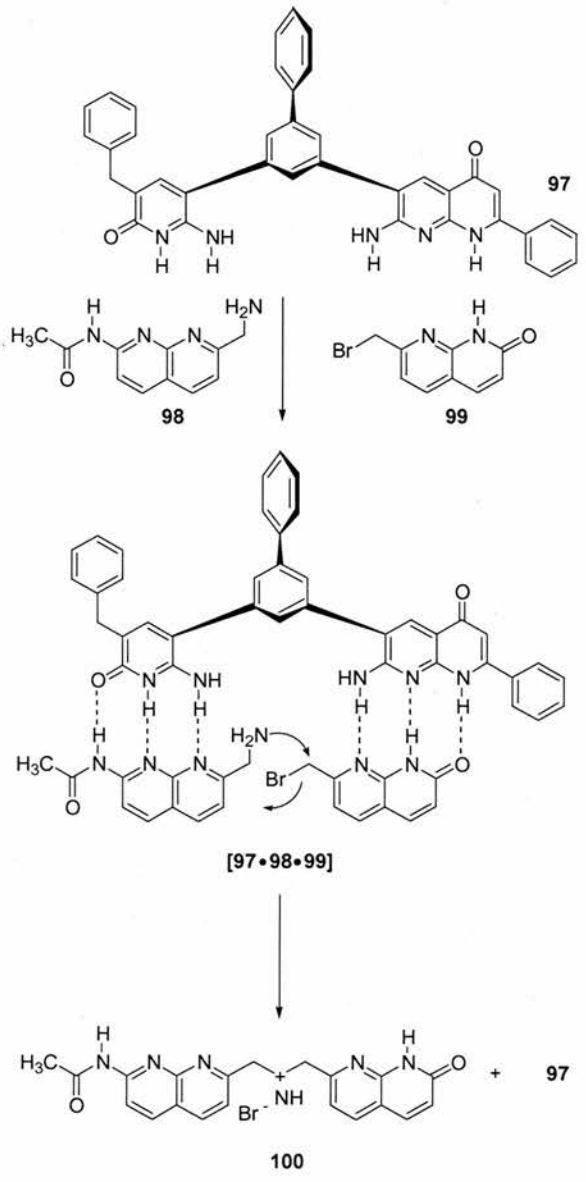

Scheme 26: Templated alkylation of amine **98**.

1.14.3 A Synthetic Supramolecular Catalytic System

Sanders studied[172] the Diels-Alder cycloaddition between the furan-based diene **102** and maleimide-based dienophile **101**. At 60 °C this reaction was unselective forming initially the kinetic *endo* isomer **103** and subsequently the thermodynamic *exo* **103** isomer **(Scheme 27)**.

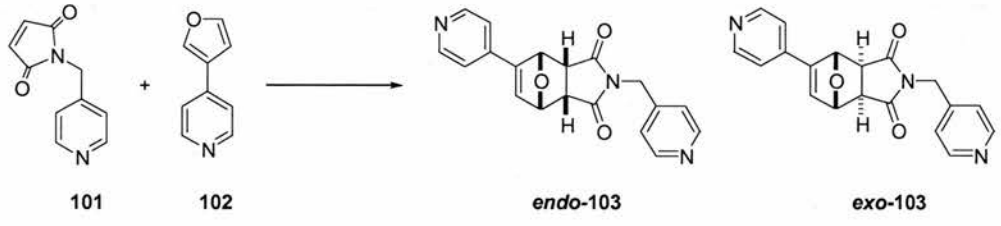

Scheme 27: The Diels-Alder reaction between **101** and **102** to give ***endo*-103** and ***exo*-103**.

However, the reaction between diene **101** and dienophile **102**, under identical reaction conditions in presence of the [2,2,2]-porphyrin trimer **104 (Figure 28)** only the *exo* cycloadduct **103** was observed throughout the reaction.

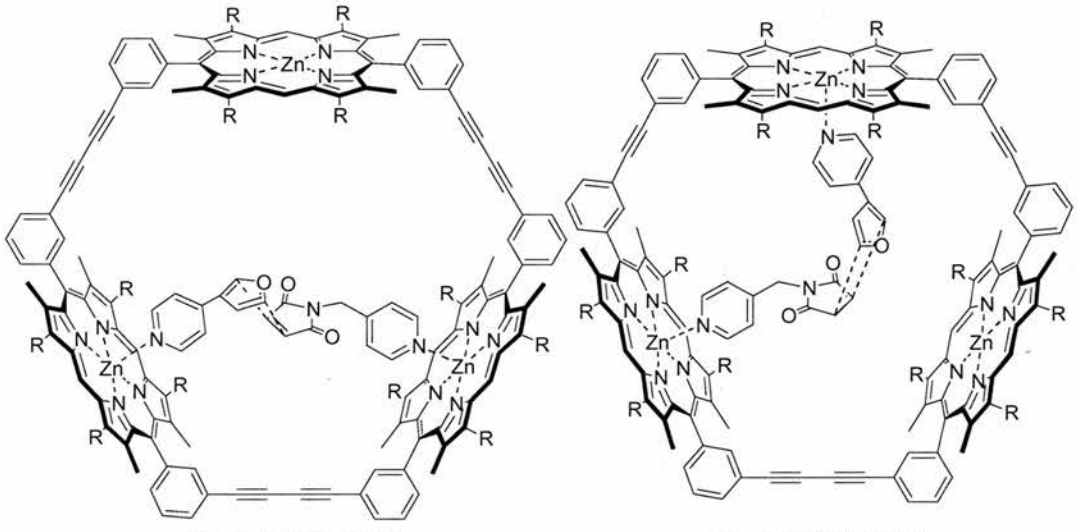

Figure 28: **a)** Representation of the *exo* transition state prior to the Diels-Alder cyloaddition reaction between the diene **101** and the dienophile **102** within the [2,2,2]-porphyrin trimer **104** cavity; **b)** Representation of the *endo* transition state prior to the Diels-Alder cycloaddition between **101** and **102** within the [1,1,2]-porphyrin trimer **105** cavity.

This selectivity arises from the hosts geometrical complementarity to the *exo* cycloadduct and the transition state of the reactive complex **(Figure 28)**. The original bimolecular cycloaddition reaction between **101** and **102** became *pseudo*-intramolecular in the presence of the trimer **104**, accelerating the formation of ***exo*-103** by 6000-fold. However no catalytic turnover was observed or expected as the product bound strongly to the host inhibiting further substrate binding.

Sanders later studied the effects of altering the porphyrin trimer in terms of shape and cavity size.[173] The [1,1,2]-trimer **105 (Figure 28)**, which has a rigid smaller cavity than the [2,2,2]-trimer **104**, favoured the production normally disfavoured *endo* cycloadduct by a factor of 500 over the analogous bimolecular reaction at 30 °C, thereby reversing the natural stereochemistry of the reaction.

1.15 Objectives

The initial aim of this research was to investigate the effect that various molecular recognition processes have on both the rate of, and/or stereo/regiochemical control of chemical reactions within a dynamic combinatorial context.

Firstly, we wish to investigate the control and acceleration of a Diels-Alder reaction mediated by the formation of a binary complex between two reagents. This investigation will involve:

- The identification of a suitable reversible bond forming reaction for this study
- The identification of a suitable covalent bond forming reaction for this study
- The rational design of a potential binary complex using molecular mechanics
- The subsequent synthesis of the desired building blocks
- The investigation into suitable reversible library conditions
- The full kinetic analysis of the reactivity and diastereochemical outcome of individual recognition-mediated reactions by ^{1}H NMR spectroscopic techniques, followed by kinetic simulation and fitting of the experimental data
- The investigation into the effect of small structural modifications upon library building blocks upon the outcome of the Diels-Alder reaction
- The study of a Diels-Alder/Disulfide library under reversible reaction conditions employing suitable monitoring techniques

We then wish to extend this methodology, to design and study a system which uses the ternary association between two reagents and a cofactor molecule in order to enhance the rate and influence the diastereoisomeric outcome of a Diels-Alder reaction within a dynamic combinatorial context. This study will involve:

- The identification of a reversible covalent bond forming reaction suitable for this study
- The rational design of a suitable cofactor molecule and building blocks containing complementary recognition sites which will allow ternary complex formation
- The subsequent synthesis of the desired building blocks and cofactor
- The full kinetic analysis of all of the systems including the kinetic simulation and fitting of the experimental data

- The investigation of the ability of ternary complex methodology to influence the diastereochemical outcome of each Diels-Alder reaction
- The investigation into the effect that small structural changes within the system have upon the diastereoisomeric outcome and the rate of the Diels-Alder reactions
- The investigation of kinetic modelling studies as a potential tool for the prediction of dynamic library evolution
- The investigation of molecular modelling studies as an indicator of dynamic library selection

Finally, the rational design of a system which can potentially replicate within a dynamic combinatorial library will be investigated. This study will involve:

- The rational design of a potentially replicating system based upon the Diels-Alder reaction
- The subsequent synthesis of the desired building blocks
- The full kinetic analysis of all of the systems, employing ^{1}H NMR spectroscopic techniques including kinetic simulation and fitting of the experimental data

Chapter 2

The Design of an AB-Mediated Dynamic Library

2.1 The Diels-Alder Reaction

The Diels-Alder reaction was discovered[174] in 1928 by Otto Diels and Kurt Alder, the reaction that bears their names has since become of great synthetic importance, recognised by their joint award of the nobel prize for chemistry in 1950. The Diels-Alder reaction[175-176] is a $[_{\pi}4_s + _{\pi}2_s]$ cycloaddition in which a conjugated diene (4π electrons) undergoes a stereospecific addition reaction with a dienophile (2π electrons) to form a six-membered ring **(Scheme 28)**. The Diels-Alder reaction is a member of the pericyclic family of reactions and is thought to proceed *via* a concerted mechanism.

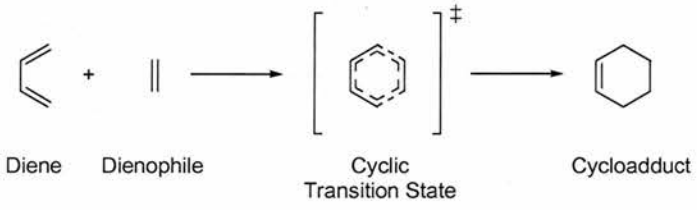

Scheme 28: Schematic of the Diels-Alder cycloaddition reaction.

The terminal π lobes of the cyclic diene and dienophile overlap when the molecular orbitals interact suprafacially. The Diels-Alder reaction can give rise to diastereoisomeric products, the *endo* and *exo* cycloadducts. Which product is formed depends upon the orientation of the approaching diene to the dienophile **(Scheme 29)**.

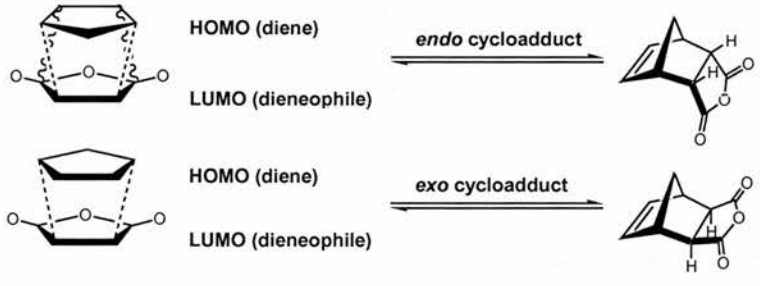

Scheme 29: *Endo* and *exo* cycloadducts resulting from the Diels-Alder reaction between cyclopentadiene and maleic anhydride. The curly and dashed lines represent the secondary and primary bonding interactions respectively which are present in the transition state.

2.1.1 The Dienophile

The Diels-Alder reaction is usually more rapid if the dienophile is suitably substituted. **Figure 29** describes the effect of substituents upon the energy gap between the HOMO and LUMO of the dienophile.

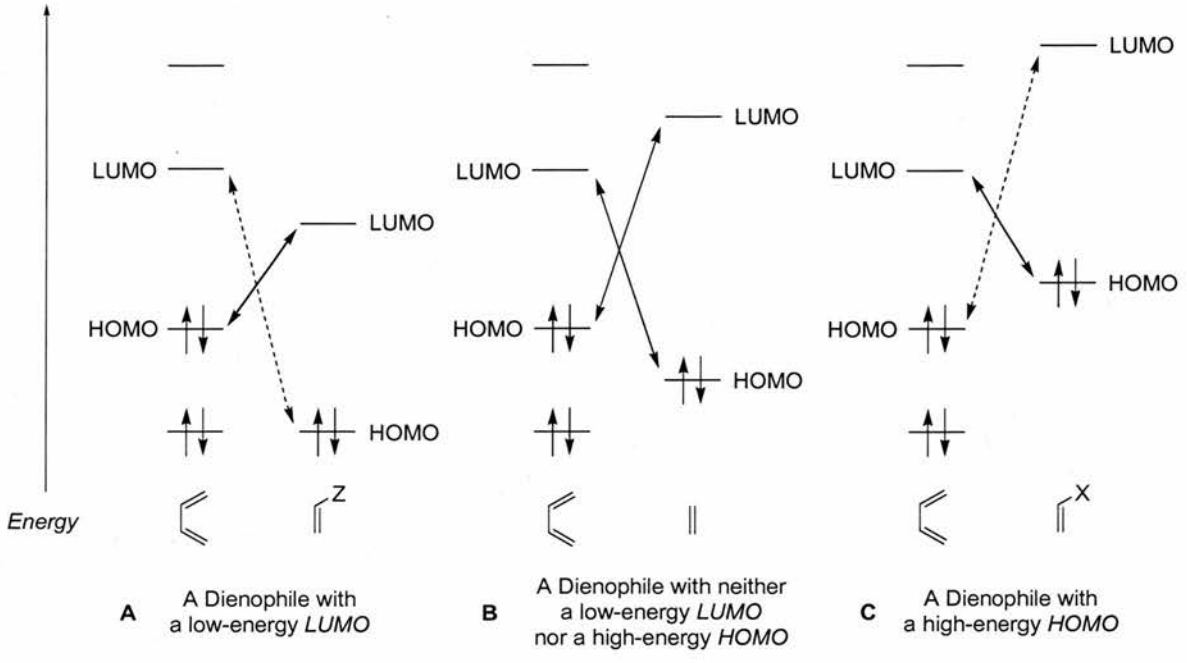

Figure 29: Substituent effects upon the dienophile energy.

Three situations are presented: 'normal' electron demand, 'inverse' electron demand and 'neutral' electron demand Diels-Alder reactions. Example A **(Figure 29)**, describes the majority of Diels-Alder reactions and is an example of a 'normal' electron demand reaction. The dienophile has been substituted with an electron-withdrawing group, consequently, the dominating orbital interaction results from the $HOMO_{diene}$-$LUMO_{dienophile}$ overlap. By contrast, example C **(Figure 29)** describes an inverse electron demand Diels-Alder cycloaddition, in which the dienophile is substituted with an electron-donating group, this reaction is now governed by the lower energy separation between the $LUMO_{diene}$ and the $HOMO_{dienophile}$. In the situation of a non-functionalised dienophile (neutral electron demand, example B, **Figure 29**), neither frontier orbital interaction dominates.

2.1.2 The Diene

Adding electron donating or withdrawing substituents onto the diene also influences the rate at which the Diels-Alder reaction proceeds. Electron donating and withdrawing substituents

promote normal and inverse electron demand cycloaddition reactions respectively. In a study by Sustmann[177] the Diels-Alder reactions of various diene derivatives with either maleic anhydride (MA) or tetracyanoethylene (TCNE) were investigated. A correlation was observed between $HOMO_{diene}$ and $LUMO_{dienophile}$ energy separations and the logarithm of the rate constants calculated for the cycloaddition reactions **(Figure 30)**.

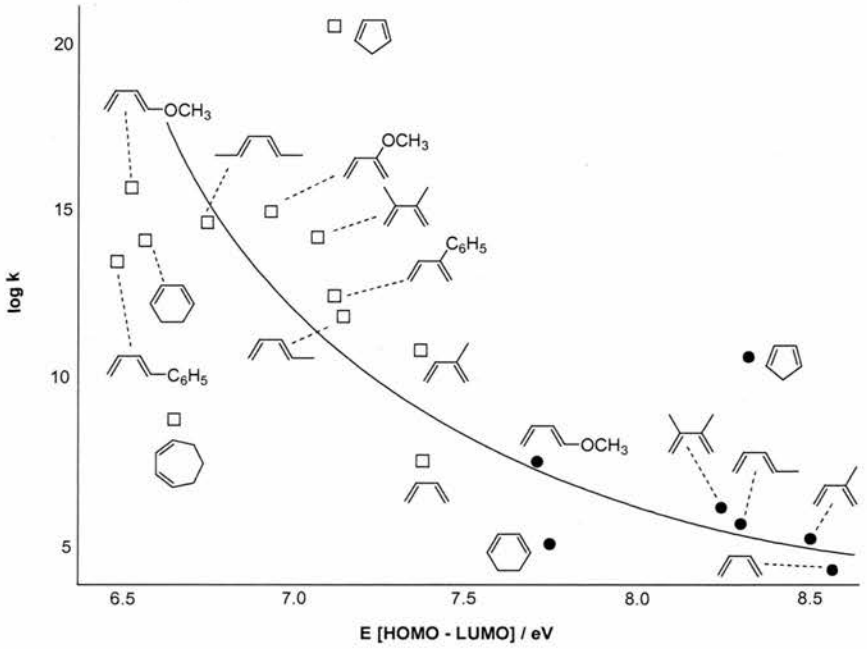

Figure 30: The solid line represents an approximate correlation of the Diels-Alder rate constants of TCNE (□) and MA (•) to substituted butadienes depending upon the HOMO-LUMO energy gap. k represents the rate constant associated with each cycloaddition reaction. Adapted from Ref. 177.

Diene conformation can also influence the rate of reaction. The diene can only react in the *s-cis* conformation. This orientation is essential in order to obtain overlap of the p-orbitals in the diene and dienophile. Cyclic dienes **106-108 (Figure 31)** are constrained by their cyclic nature to adopt a *s-trans* conformation and do not react with dienophiles, cyclic *s-cis* dienes **109-111** however are reactive.

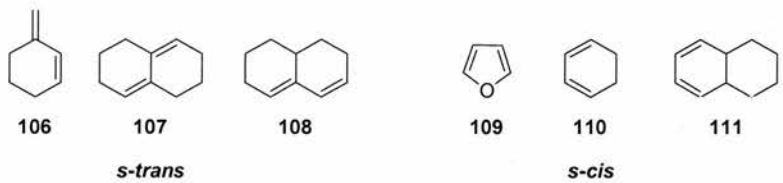

Figure 31: Unreactive *s-trans* cyclic dienes **106-108**, reactive *s-cis* cyclic dienes **109-111**.

2.2 AB-Complex Systems

The location of complementary recognition sites on both reactive partners **A** and **B (Scheme 30)**, can allow rate enhancement and achieve regio- and/or stereochemical control of various chemical reactions. **Scheme 30** displays the two alternate pathways open to starting materials **A** and **B**.

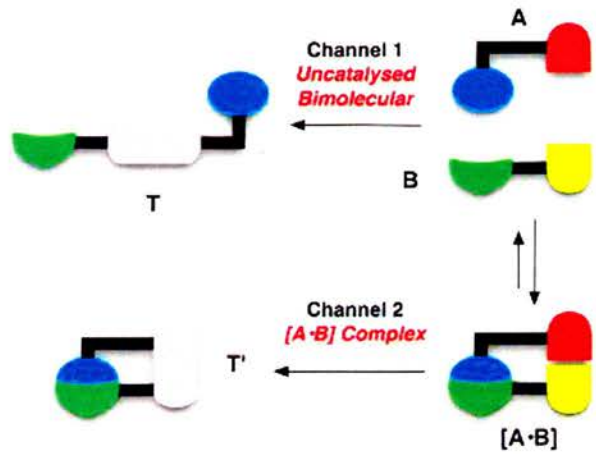

Scheme 30: Schematic representation of an AB-system where the green and blue blocks represent the complementary recognition groups, the black lines represent the spacer units and the reactive sites are represented by the yellow and red blocks.

Firstly, an uncatalysed bimolecular reaction, between two building blocks **A** and **B**, can form product **T**. Secondly, there is an accelerated pathway, in which **A** and **B** can bind reversibly together *via* their complementary recognition sites to form an [**A**·**B**] complex. Reactive partners **A** and **B** can be orientated in such a manner that the original bimolecular process becomes *pseudo*-intramolecular. Therefore, for entropic[160-161] reasons, we might expect rate enhancement over the unaccelerated bimolecular route. It is the effect of proximity[150] of the reactive sites on **A** and **B** within the [**A**·**B**] complex which allows the acceleration of the covalent bond forming process to form product **T'**. Association occurs *via* the recognition sites, and therefore renders the chemical reaction between the reagents effectively intramolecular as opposed to intermolecular. In addition, the use of specific recognition to pre-associate the reactive partners should also permit the control[178] of the stereo- and/or regiochemical outcome of the reaction, through the orientation of reagents. These effects evolve when the reaction in question is under kinetic control and selective stabilisation of one transition state with respect to another serves to accelerate the formation of a specific product. Whilst under thermodynamic control, the molecular recognition present within reactive

complex [**A·B**] may serve to influence the stability of the final product. It should be noted that AB systems are not catalytic since the recognition used to assemble an [**A·B**] complex persists in the final product. It is for this reason that the term acceleration, rather than catalysis, is used to described the increase in rate observed *via* this recognition-mediated route.

2.3 Thermodynamic and Kinetic Control of a Reaction

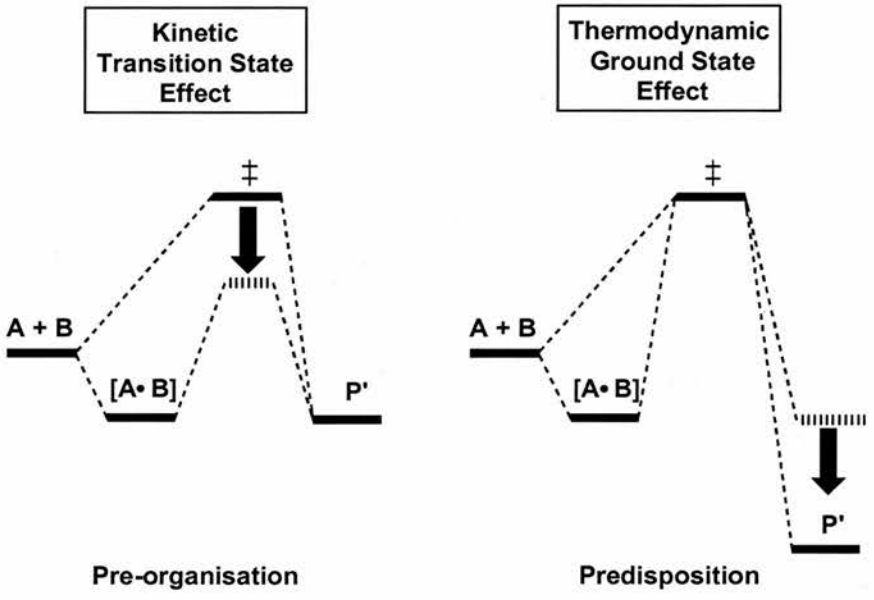

Figure 32: A schematic representation of a kinetic transition state effect and a thermodynamic ground state effect.

Kinetic and thermodynamic effective molarities (*kEM* and *tEM*) are quantitative ways of determining whether transition state stabilisation or product stabilisation **(Figure 32)** is the most influential effect within a system. The kinetic effective molarity **(Equation 1)** compares the forward rate of the recognition-mediated reaction (k_{funi}), to the forward rate of the bimolecular control reaction (k_{fbi}) **(Equation 1)**.

$$kEM = \frac{k_{funi}}{k_{fbi}} = \frac{s^{-1}}{M^{-1}s^{-1}} = M$$

Equation 1: Kinetic effective molarity (*kEM*) expressed in *M* and where k_{funi} and k_{fbi} represent the forward rate of the recognition-mediated and bimolecular reaction, respectively.

Effective molarities can be thought of as the concentration required for one of the reagents present in the bimolecular reaction, to allow the bimolecular pathway to proceed at the same rate as the recognition-mediated process. The thermodynamic effective molarity **(Equation**

2) compares the equilibrium constant (K_{uni}) resulting from the recognition-mediated reaction with the equilibrium constant (K_{bi}) derived from the bimolecular reaction.

$$tEM = \frac{K_{uni}}{K_{bi}} = \frac{k_{funi}}{k_{runi}} \times \frac{k_{rbi}}{k_{fbi}} = \frac{s^{-1} \times s^{-1}}{s^{-1} \times M^{-1}s^{-1}} = M$$

Equation 2: Thermodynamic effective molarity (tEM), where K_{uni} *and* K_{bi} represent the equilibrium constant of the recognition-mediated and bimolecular reaction, respectively. k_{fbi}, k_{rbi} and k_{funi}, k_{runi} represent the forward and backward rates constant associated with the bimolecular and recognition-mediated reactions, respectively.

2.4 Determining the Position of a Transition-State

A statistical treatment of activated complex theory is difficult as rarely anything is known about the structure of the activated complex.[179] The Bell-Evans-Polanyi principle states that for similar reactions, the more exothermic the reaction the lower its activation energy will be. Conversely, the more endothermic the reaction the higher its activation energy will be. The Hammond postulate relates this exothermicity to the position of the transition state. The corollary derived from the Hammond postulates states that, for similar reactions the more exothermic the reaction, the earlier (more reactant-like) the transition state. Conversely, the more endothermic the reaction the later (more product-like) the transition state becomes. The Marcus equation quantitatively encompasses the Bell-Evans-Polanyi principle and the Hammond postulate. We can define a reaction coordinate running from reactant (x = 0) to product (x = 1) **(Figure 33)**. The energy of the reaction as a function of x is taken as a parabola ($y = x^2$), with a force constant of a (shown in blue, **Figure 33a**). The energy of the product can be described as a parabola with the same force constant, offset by the reaction energy ΔE_o (shown in red, **Figure 33a**). The location of the transition state is assumed to be at the point where the two parabolas intersect. The transition state position can be calculated by equating the two energy expressions **(Equations 3-5, Figure 33b)**. Solving **Equation 6 (Figure 33b)** for $x^{\neq}$, when $\Delta E_o = 0$ (thermoneutral reaction) the location of the transition state, is exactly halfway between reactant and product. When ΔE_o is negative the earlier (more product-like) the transition state, conversely, when ΔE_o is positive the transition state is later (more starting-material-like).

a)

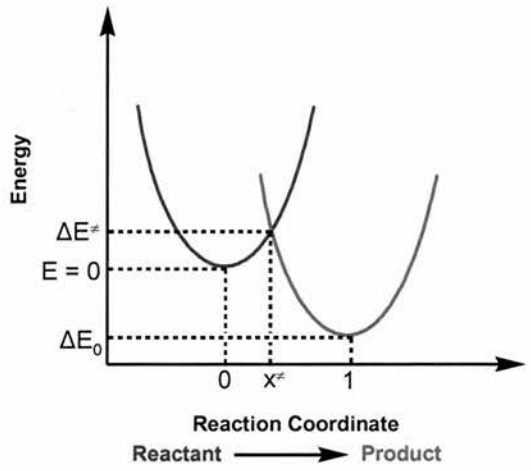

b)

$$E_{reagent} = a(x)^2 \quad (3)$$

$$E_{product} = a(x-1)^2 + \Delta E_0 \quad (4)$$

$$a(x^{\neq})^2 = a(x^{\neq}-1)^2 + \Delta E_o \quad (5)$$

$$x^{\neq} = \frac{1}{2} + \frac{\Delta E_0}{2a} \quad (6)$$

Figure 33: **a)** Graph comparing the location of a transition state of a reaction with the exothermicity of the reaction. **b)** Equations **3-6** described the position of the transitions state in a thermoneutral reaction.

Diels-Alder reactions are known to have late, product-like transition states, where ΔE_0 is positive. The position of the transition state is important in our studies as there are two possible paths open within our recognition-mediated reactions; (i) recognition features could stabilise the transition state, pre-organising reactants, leading to the production of one product over another, or (ii) recognition could stabilise the product ground state, leading to an energetically more stable product which is predisposed to form. A third situation could also occur where the recognition properties within the starting materials which initially serve to stabilise the transition state, also persist in the product, allowing both pre-organisation and predisposition of the Diels-Alder reaction.

2.5 Reaction of Molecules with Complementary binding sites

Rate acceleration of Diels-Alder reactions *via* AB-complex methodology has been successfully utilized[180-186] by Philp and co-workers. They have studied[182] the recognition-induced control of a Diels-Alder reaction using a 2-amidopyridine·carboxylic acid motif (K_a = 170 M^{-1}; **Scheme 31**). The reaction between **112** and **113** was carried out at 5 m*M* of each reagent in $CDCl_3$ at 30 °C. The reaction preceded with very high ***endo*-114** selectivity (6000:1). The kinetic effective molarity (*kEM*) achieved for the recognition-mediated reaction was only 63 m*M*. The high diastereoselectivity was as a result of the persistence of the two hydrogen bonds used to assemble the [**A**·**B**] complex exclusively in the *endo* cycloadduct.

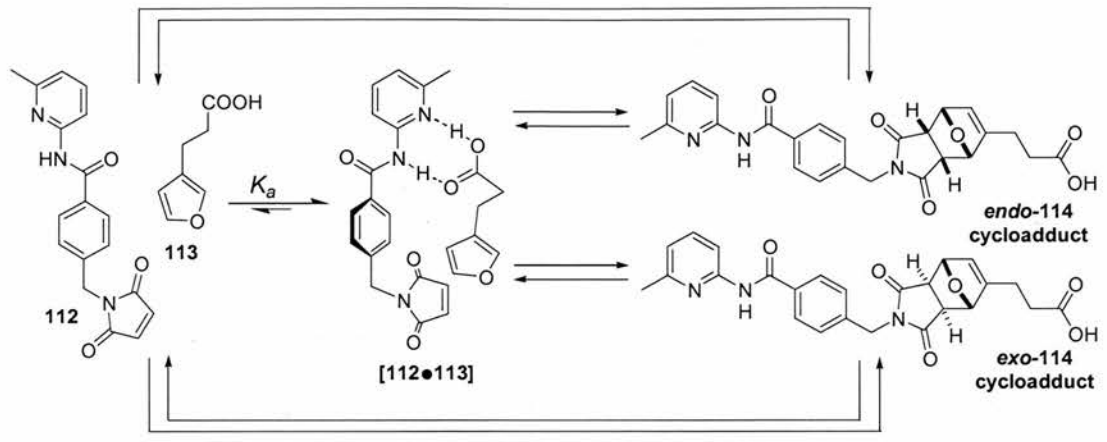

Scheme 31: Recognition-mediated schematic of the Diels-Alder reaction between diene **113** and the dienophile **112**.

Similar studies[181] were conducted for the [2+3] dipolar cycloaddition reaction between azide **115** and maleimide **116 (Scheme 32)** with reagents at initial concentrations of 100 m*M* in $CDCl_3$ at 50 °C. A large kinetic effect was observed for the reaction (*kEM* = 2.2 *M*), although the stability of the reactive complex was much lower ($K_a \sim 28\ M^{-1}$). These results illustrated that the magnitude of the association within a reactive complex does not necessarily correlate with the observed rates.

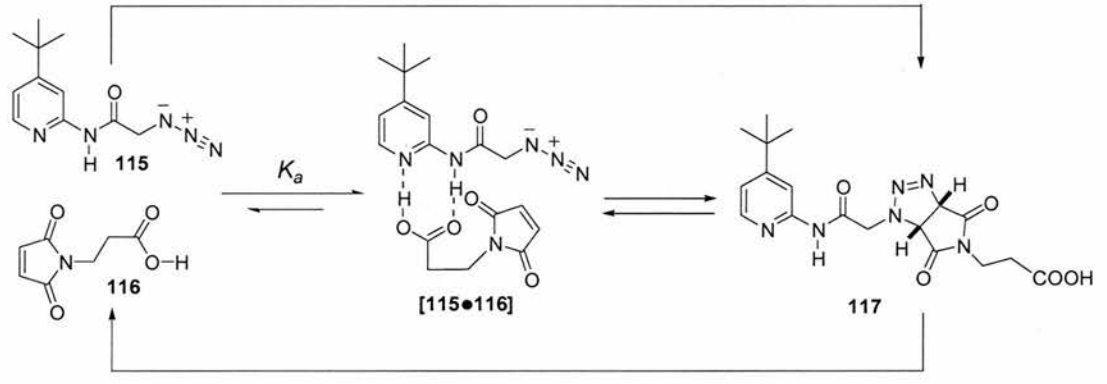

Scheme 32: Recognition-mediated schematic of the [3+2] dipolar cycloaddition between azide **115** and maleimde **116**.

Philp and co-workers have recently reported[186] studies on an AB system which accelerated the Diels-Alder reaction between amide **118** and maleimide **119 (Scheme 33)** at 35 °C in $CDCl_3$ at 25 m*M* of each starting reagent. In this study, the observed rate acceleration in the recognition-mediated reaction was as a result of stabilization of the reagents within the transition state rather than the ground state as in the previous example ($K_a = \sim 250\ M^{-1}$, *kEM* = 2.6 *M*, *tEM* = 68 m*M*). We wished to utilise such AB recognition-mediated systems within a dynamic combinatorial library.

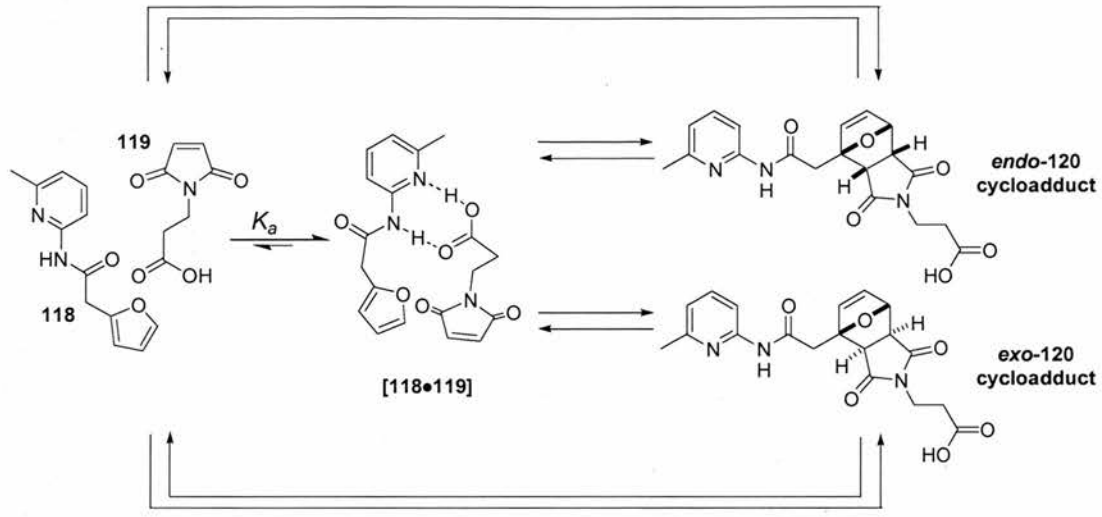

Scheme 33: Recognition-mediated schematic depicting the Diels-Alder reaction between diene **118** and dienophile **119**.

2.6 Project Outline

Several groups have demonstrated[75-85] the efficiency of DCLs in selecting the most suitable receptor or substrate from a collection of components. We wished to design a system which would encompass the rate accelerating features of AB-methodology with the reversibility and subsequent selection properties of dynamic combinatorial libraries. Thus, the aim of this project was to design and synthesize a dynamic combinatorial library capable of selection and rate acceleration simultaneously.

In recent years, disulfide exchange reaction has emerged[108, 113-120] as a useful dynamic combinatorial reaction, the reader is directed to a summary of the work conducted on disulfide libraries **(Section 1.8.6)**. The following target molecules were therefore proposed **(Figure 34)**. Recognition thiol molecules **121** and **122** have tagging groups incorporated. These are bulky solubilising isovaleryl and tolyl groups. A phenyl ring was chosen as a rigid spacer unit. Diene **124** is commercially-available, while the 3-substituted isomer **123** can be synthesized readily. Dienophile components **125** and **126** both contain carboxylic acid recognition moieties and vary in carbon spacer chain length.

This dynamic system was designed to work on two levels and therefore is analogous to the orthogonal libraries described in **Section 1.12**. The Diels-Alder and disulfide exchange reactions were chosen as the reversible reactions of choice within our system.

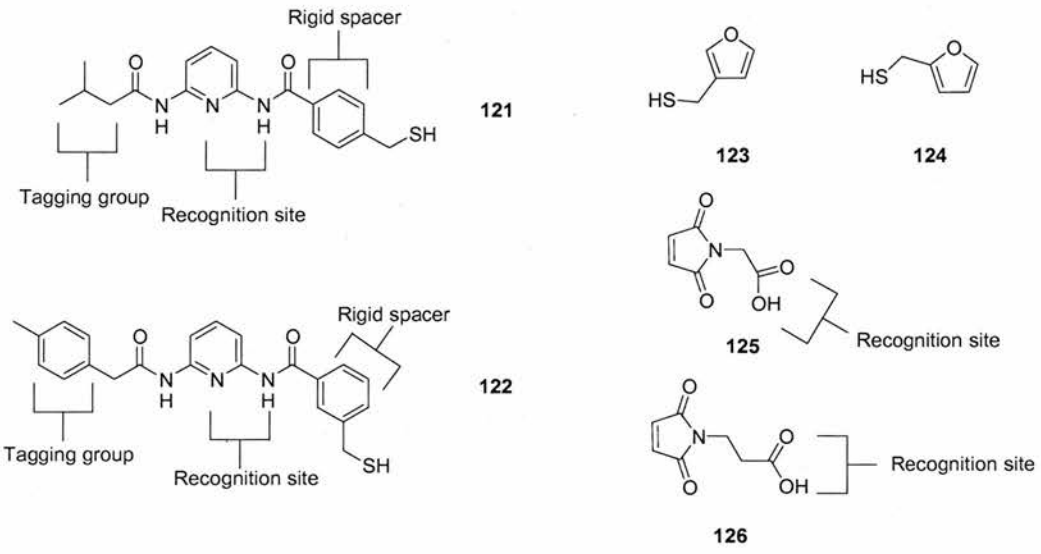

Figure 34: Recognition thiols **121** & **122**; note aminopicoline recognition motif, also isovaleryl and tolyl tagging groups. Dienes **123** and **124** – furan thiols with thiol moiety in the 2- and 3- position. Dienophiles **125** & **126** – maleimides with carboxylic acid recognition site.

Within this library diversity is acquired in four areas; (i) the recognition thiols **121-122** are para- and meta- substituted, (ii) furfuryl mercaptans **123** and **124** contain a thiol moiety in the 2- or 3- position, (iii) spacer chain length is varied on the maleimide, either one or two carbons - compounds **125** and **126** respectively, (iv) the Diels-Alder reaction can give rise to *endo* and/or *exo* cycloadduct products. In total, a maximum of 16 products may be formed. As result of reversibility inherent within the system, it is hoped that the library mixture will be under thermodynamic control, and therefore, the most thermodynamically stable product will be assembled from all library components.

The previously successful hydrogen bonding motif of carboxylic acid:2-amidopyridine[180-186] was selected to provide recognition within the system. The addition of recognition sites to a diene and dienophile[186] has been shown to control both the rate and the diastereochemical outcome of a Diels-Alder reaction **(Section 2.5)**. Therefore, within our system we hope to accelerate the Diels-Alder reactions and enforce diastereochemical control *via* an AB-mediated pathway **(Section 2.2)**.

Within our library many species will be generated over time, it is important that the formation of each product can be monitored effectively. Recognition thiol amides **121** and **122** would be isomers of each other and therefore indistinguishable by mass spectrometry without the incorporation of tagging groups, thus changing their masses, allowing the evolution of library species to be easily monitored by electrospray mass spectrometry.

2.7 Synthesis of Library Building Blocks

2.7.1 Synthesis of Thiol 121

Thiol **121** was prepared in five high-yielding steps **(Scheme 34)**. Isovaleryl chloride **127** was coupled[187] to 2,6-diaminopyridine **128** in 93% yield after purification by column chromatography. Amine **129** was coupled to 4-chloromethylbenzoylchloride **130**, under standard conditions,[188] to afford chloride **131** in 71% yield. The use of hexamethyldisilathiane to convert an alkyl chloride to a thiol[189] has been used successfully within the group and therefore this method was employed. Chloride **131** was reacted with hexamethyldisilathiane and TBAF in dry THF. However, after work-up and recrystallisation, the ^{1}H NMR spectrum of the product did not contain any resonances corresponding thiol **121**, thiol **121** had been oxidised to disulfide **132**. A new approach was therefore required. Chloride **131** was reacted with potassium thioacetate[190-191] in acetone, to afford thioacetate **133** in good yield after purification *via* flash column chromatography. The de-*S*-acetylaction step was then carried out using 1*M* KOH in methanol to afford thiol **121** in virtually quantitative yield.

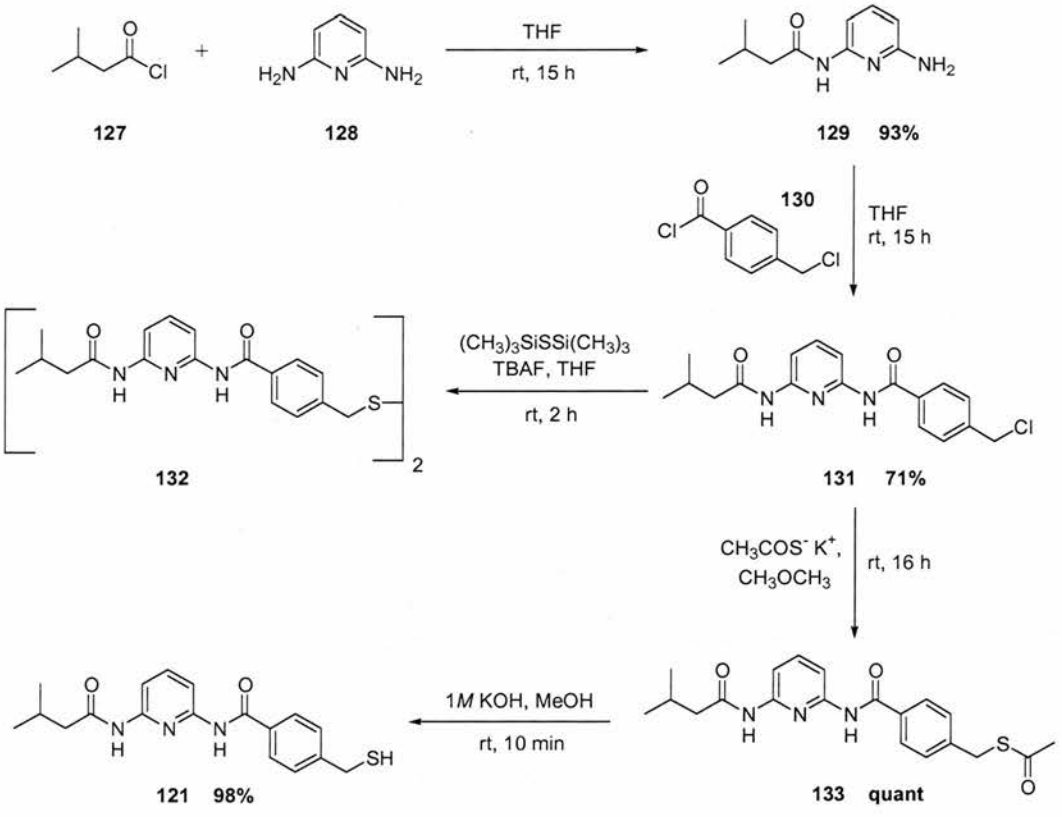

Scheme 34: Synthetic pathways attempted in the formation of 4-mercaptomethyl-*N*-[6-(3-methyl-butyrylamino)-pyridin-2-yl]-benzamide **121**.

2.7.2 Synthesis of Thiol 122

Thiol **122** was prepared in five steps **(Scheme 35)**. A procedure for the conversion of carboxylic acids to acid fluorides has been developed within the group, based upon methodology described[192] by Kilburn and co-workers. This method of synthesising reactive acid halide intermediates proved to be more versatile and higher yielding than the corresponding thionyl chloride route. *p*-Tolylacetic acid **134** was converted to acid fluoride **135** using cyanuric fluoride. Intermediate **135** was identified by ^{19}F NMR spectroscopy, through the appearance of a diagnostic triplet at +44 ppm. Crude acid fluoride **135** was used without further purification. Amine **136** was prepared in good yield by coupling 2,6-diaminopyridine **128** to crude acid fluoride **135**. The reaction of 3-chloromethylbenzoyl chloride **137** with amine **136** under standard conditions yielded benzoyl chloride **138** in 97% yield after purification *via* column chromatography. Chloride **138** was then reacted with potassium thioacetate to give protected thiol **139** in good yield, which was then de-*S*-acetylated using 1*M* KOH in MeOH to give free thiol **122** in virtually quantitative yield within ten minutes.

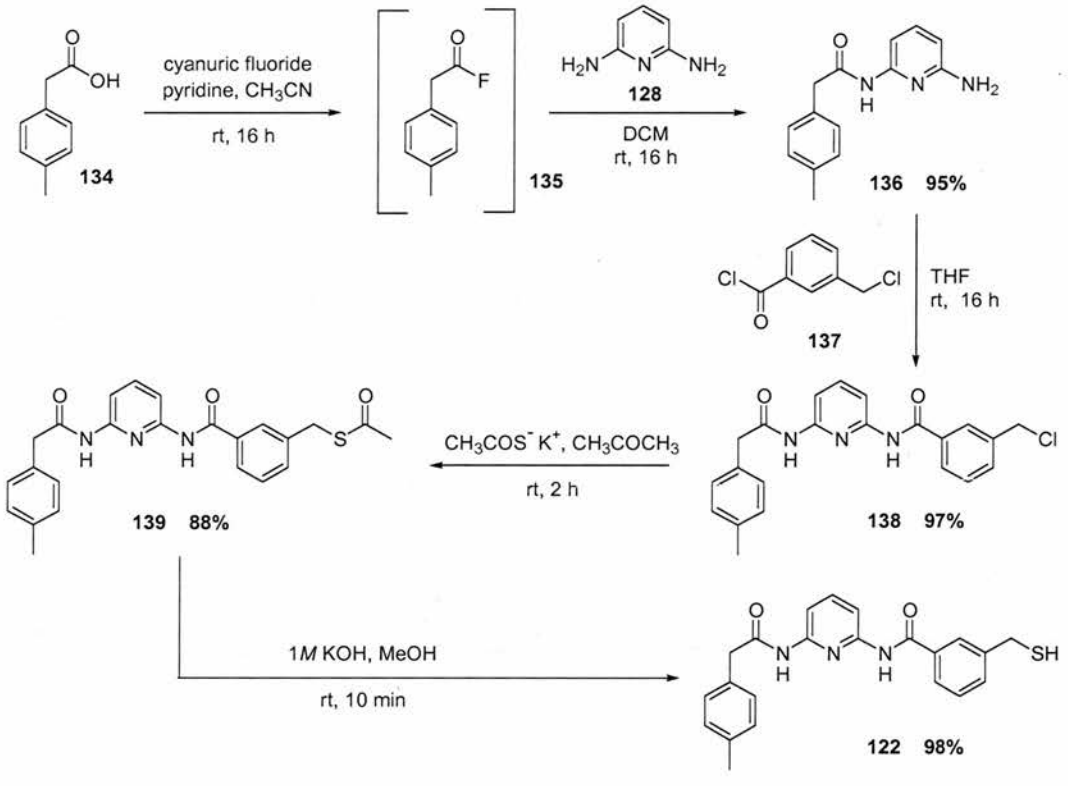

Scheme 35: Synthetic route for the preparation of 3-mercaptomethyl-N-[6-(2-p-tolyl-acetylamino)-pyridin-2-yl]-benzamide **122**.

2.7.3 Synthesis of Furan Thiol 123

Furan-3-yl-methanethiol **123** was prepared **(Scheme 36)** in two steps from commercially available 3-furan methanol **140**. Alcohol **140** was chlorinated using carbon tetrachloride and tributylphosphine in acetonitrile. Chloride **141** was not isolated, but instead, reacted *in situ* with potassium thioacetate. After stirring overnight, protected furan thiol **142** was isolated in 57% yield. Thioester **142** was then deprotected to give the free furan thiol **123** in 85% yield.

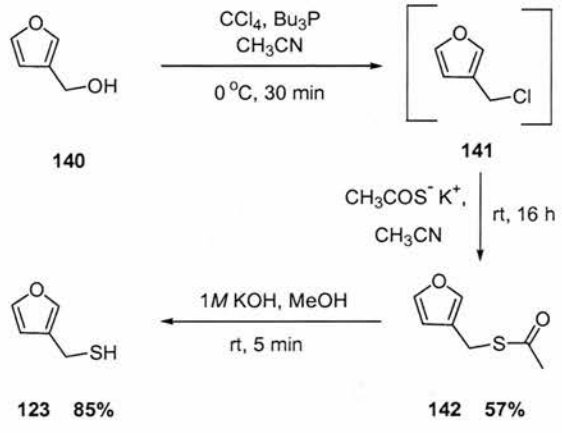

Scheme 36: Synthetic strategy for the synthesis of furan-3-yl-methanethiol **123**.

2.7.4 Synthesis of Maleimide Acids 125 & 126

Maleimide **125**, containing a one carbon chain, was prepared in a one-pot reaction[193] **(Scheme 37)**, *via* intermediate **146** which was not isolated. Commercially-available maleic anhydride **143** and glycine **144** were stirred together in acetic acid for 8 hours to form intermediate **146** and then refluxed to give maleimide **125** in 22% yield after recrystallisation. Maleimide **126** containing a two carbon chain was prepared from maleic anhydride **143** and β-alanine **145** affording maleimide **126** in 47% yield after purification.

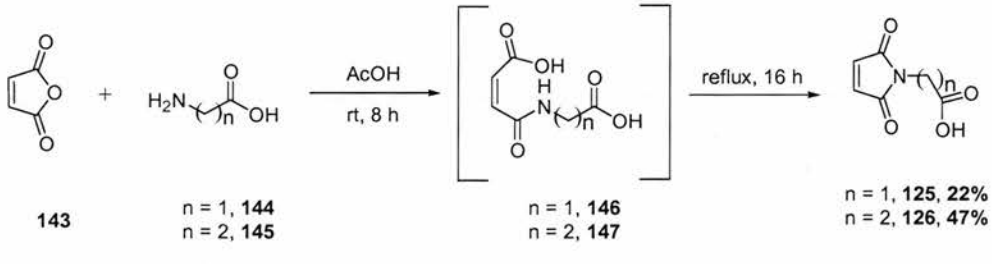

Scheme 37: Synthesis of maleimide acids, (2,5-dioxo-2,5-dihydro-pyrrol-1-yl)-acetic acid **125** and (2,5-dioxo-2,5-dihydro-pyrrol-1-yl)-propionic acid **126**.

Maleimide acids **125-126** contain carboxylic acid moieties designed to promote a recognition-mediated reaction *via* an AB complex pathway. A control reaction where no recognition sites are present must be carried out in order to assess the effect of recognition upon the Diels-Alder reaction. Control reactions have been conducted previously within the group, where methyl esters **148-149** are substituted in place of maleimide acids **125-126**. Maleimide acids **125** and **126** were converted in one step to their methyl ester equivalents[194] **148** and **149** **(Scheme 38)**. Acids **125** and **126** were methylated using cesium carbonate and methyl iodide to yield control compounds **148** and **149** in 87% and 60% respectively.

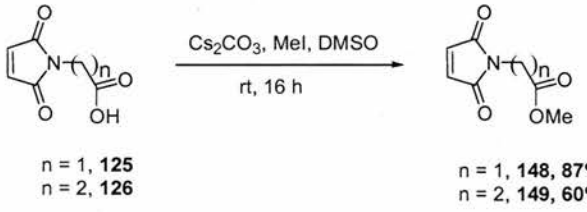

Scheme 38: Synthetic pathway for the synthesis of maleimide esters **148** & **149**.

2.8 Optimisation of Reversible Reaction Conditions

As discussed previously in **Section 1.7** reversibility within a dynamic system is crucial, as it allows the library to be under thermodynamic control. The exchange of thiol library constituents is imperative, therefore ideal exchange conditions for our system were determined as our first priority. Thiols can be oxidised to their disulfide counterparts on exposure to air **(Scheme 39)**.

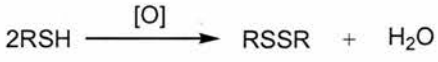

Scheme 39: Oxidation of two moles of thiol to one mole of disulfide and water in the presence of oxygen.

The oxidation process can be influenced greatly by the addition of base and/or halogen. The following reactions have been described[195] for the oxidation of thiol to disulfide by halogens **(Scheme 40)**.

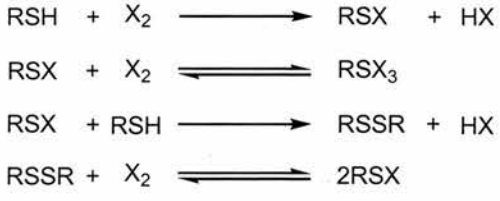

Scheme 40: Reactions postulated for halogen oxidation of a thiol to its disulfide counterpart.

Studies[195] upon the oxidation of thiols under basic conditions postulate the reaction profile shown in **Scheme 41**.

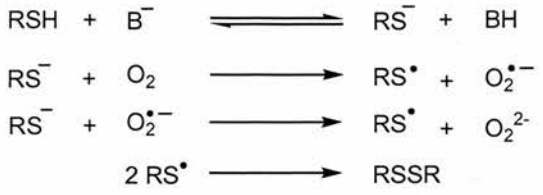

Scheme 41: Reaction sequence proposed for the catalysis of disulfide formation by strong base.

Firstly, the oxidation of two thiol molecules to a disulfide molecule was followed using commercially available thiol, furfuryl mercaptan **124 (Scheme 42)**. Disulfide formation under basic conditions alone can be slow, but addition of an oxidising agent can speed up the reaction as described previously. The oxidising reagent of choice was I_2, as this would not interfere with reaction monitoring by ^{1}H NMR spectroscopy, nor would it interfere with the recognition sites within our final system. Previous work had also been reported[196] on a similar oxidation reaction.

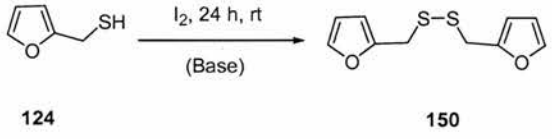

124 **150**

Scheme 42: Synthetic route for the conversion of furan-3-yl-methanethiol **124** to equivalent disulfide **150**.

NMR scale experiments were carried out in accordance with the procedure outlined in the experimental section **(Chapter 6)**. As disulfide formation occurs at pH > 7, in order to assess the basicity required for oxidation of thiols to occur, varying amounts of base were added to the reaction. Furfuryl mercaptan **124** (1 eq.), I_2 (1 eq.) were reacted at 25 m*M* in $CDCl_3$ with base at 10, 50 and 100 mol % at 25 °C. After 16 hours, a ^{1}H NMR spectrum was recorded. The formation of disulfide **150** could be easily distinguished by ^{1}H NMR spectroscopy. The furyl ring protons associated with furfuryl mercaptan **124** appeared as a distinctive set of two multiplet resonances and on conversion of thiol **124** to disulfide **150**, a second set of multiplet resonances corresponding to the disulfide furyl ring protons were observed. The concentration of disulfide and thiol present after 16 hours was calculated using the deconvolution tool available within 1D WINNMR and the results are shown in **Table 6**. These results demonstrate that using 50/100 mol % collidine **151** as base, all of thiol **124** was converted to disulfide **150**. Amide **152** which had been previously synthesised within the

group was used as a base in order to gauge whether the basicity inherent within recognition thiols **121** and **122** would be sufficient to facilitate disulfide formation. Furfuryl mercaptan **124** was converted entirely to disulfide **150** after 16 hours using 100 mol % of amide **152**. These results suggest that there would be no need for an external base to be present within our system.

Table 6: Results for the conversion of thiol **124** to disulfide **150**.

Base	10 mol % disulfide:thiol / m*M*	50 mol % disulfide:thiol / m*M*	100 mol % disulfide:thiol / m*M*
 **151**	22:3	25:0	25:0
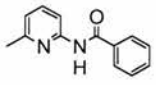 **152**	-	23:2	25:0

The next logical step in the optimization process for the dynamic system was to attempt the exchange of two different thiols to give a mixed disulfide. This process was modelled using heptane thiol **153** and furfuryl mercaptan **124** under optimized thiol oxidation conditions described previously. The experiment was carried out on an NMR scale with furfuryl mercaptan **124** (1 eq.), heptane thiol **153** (1 eq.) and iodine (1 eq.) at 25 °C at 25 m*M* in $CDCl_3$ **(Scheme 43)**. A ^1H NMR spectrum was recorded after 16 hours. Thiol/disulfide exchange had indeed occurred, this was evident by the appearance of a diagnostic set of resonances in the ^1H NMR spectrum, corresponding to the furyl ring protons associated with mixed disulfide **154**.

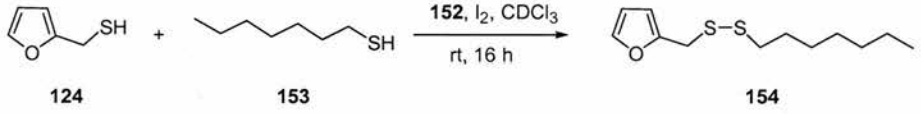

124 **153** **154**

Scheme 43: Exchange of thiols **124** and **153**.

It is important that, within a dynamic combinatorial library, all components are soluble and therefore able to exchange freely. For this reason, the exchange of thiol **122** to its disulfide counterpart was investigated **(Scheme 44)**. However, on mixing equivalent quantities of recognition thiol **122** with iodine (1 eq.) in $CDCl_3$ a precipitate of disulfide **155** was formed.

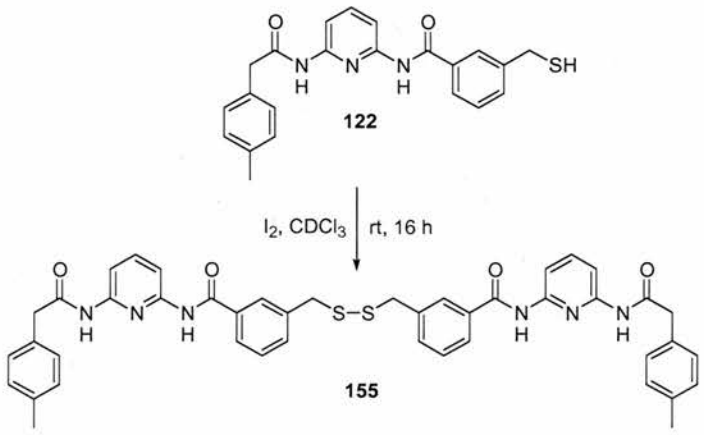

Scheme 44: Proposed conditions for disulfide **155** formation.

Many reactions were carried out to assess whether a drop in the concentration of one or both of the reactants would allow disulfide **155** to remain in solution. However, on varying the concentration of both thiol **122** and iodine there was no increase in solubility. Disulfide **155** was insoluble in $CDCl_3$, even at low concentrations of 1 m*M*. It was hoped that on exchange of furan thiol **124** with thiol **122**, mixed disulfide **157 (Scheme 45)** would be more soluble in $CDCl_3$ than disulfide **155 (Scheme 44)**. Takata and co-workers[197] had shown that thiols can be exchanged using thiol exchange agents, it was hoped that mercaptopyridine **156** would act as an exchanging agent within our system. A set of ^1H NMR spectroscopy experiments were performed varying the amount of furan thiol **124**, iodine, thiol **122** and mercaptopyridine **156** in $CDCl_3$ at room temperature **(Table 7)**. However, in all instances disulfide **157** precipitated out of solution within 10 minutes of mixing the reagents.

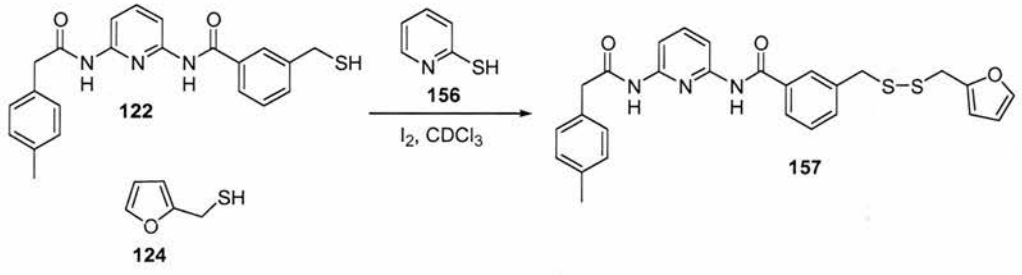

Scheme 45: Proposed conditions for thiol exchange using an exchanging agent **156**.

As a result, the order of reagent addition was investigated. Furan thiol **124**, iodine and mercaptopyridine **156** were mixed together before introducing thiol **122**, the concentrations of reacting species **(122, 124 & 156)** were also varied in a parallel set of experiments **(Table 8)**.

Table 7: Time taken for disulfide precipitation on addition of thiol **122** to thiol **124** under exchange conditions.

Experiment [a]	$[I_2]$ / m*M*	[156] / m*M*	[124] / m*M*	[122] / m*M*	Time / min [b]
1	75	25	50	50	immediate
2	75	0	50	50	immediate
3	75	10	50	50	5
4	25	25	25	25	10

a All reactions were carried out on an NMR scale, at room temperature in $CDCl_3$.
b The time taken for the formation of precipitate **157**, these times are approximate.

Table 8: Time taken for disulfide precipitation on addition of thiol **124** to thiol **122** under exchange conditions.

Experiment [a]	[124]:$[I_2]$:[156] / m*M*	[122] / m*M*	Time / min [b]
5	25:20:12.5	25	30
6	25:12.5:12.5	25	90
7	12.5:6.25:12.5	12.5	90

a All reactions were carried out on an NMR scale, in $CDCl_3$ at 45 °C.
b Time in minutes taken for precipitate **157** to be formed, these times are approximate.

Statistically a quarter of the product produced would be the insoluble disulfide **157**. Therefore, the purpose of the optimisation work was to limit the amount of disulfide **157** formed. These studies revealed that the optimum conditions for the exchange of thiols **122** and **124** was using thiol **124** (25 m*M*), iodine (25 m*M*), mercaptopyridine **156** (12.5 m*M*) and thiol **122** (25 m*M*), as no disulfide **157** precipitate was formed over the initial one and a half hours of the reaction.

2.9 Diels-Alder Reaction Conditions

Using the optimized thiol exchange conditions desribed in **Section 2.8**, a Diels-Alder cycloaddition reaction was attempted using maleimide **126 (Scheme 46)**. The reaction was conducted in $CDCl_3$ at 45 °C for 16 hours. After this time, a ^1H NMR spectrum was recorded. No peaks corresponding to the maleimide ring protons were observed and no peaks for the Diels-Alder cycloadduct **127** were detected. At this time, it was thought that I^- generated during may have been attacking maleimide **126** by conjugate addition.

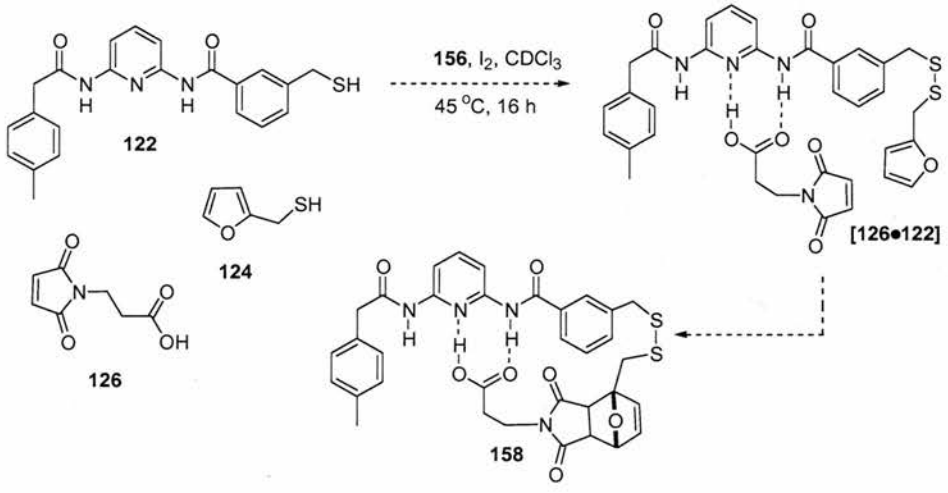

Scheme 46: Proposed conditions for the Diels-Alder cycloaddition reaction.

2.10 Re-optimisation of Thiol Exchange Conditions

A strategy was now required for the conversion of thiol to disulfide which did not include a strong nucleophile as an oxidizing agent. It was hoped that furfuryldisulfide **150** would freely interconvert with thiol **122 (Scheme 47)**.

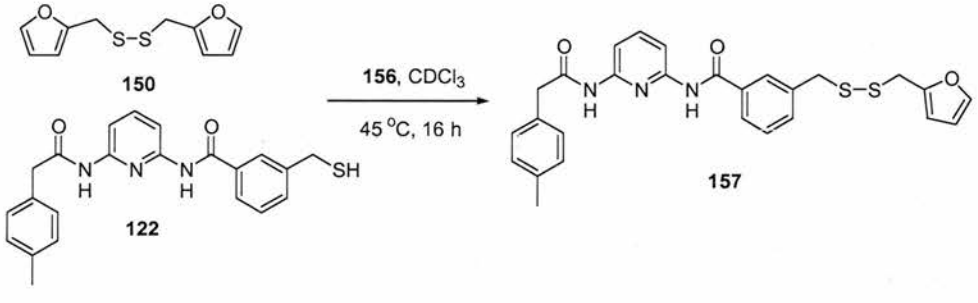

Scheme 47: Synthetic route for the preparation of 3-furan-2-ylmethyldisulfanylmethyl)-*N*-[6-(2-p-tolyl-acetylamino)-pyridin-2-yl]-benzamide **157**.

Without the presence of I_2 to drive the oxidation reaction, no exchange between thiols occurred over 16 hours at 45 °C. It is known that pH is a major factor in disulfide formation and exchange, as a result a series of experiments were set up to investigate the effect, if any, that the addition of base would have upon the exchange reaction. Benzene thiol **159** was added in place of mercaptopyridine **156** as an exchanging agent. In reactions with triethylamine, pyridine and *t*-butylammonium iodide, exchange did not occur by ^{1}H NMR spectroscopy, however in the experiment with imidazole exchange occurred at 45 °C over 16 hours. This was confirmed by peaks corresponding to all possible combinations of thiol/disulfide in the MALDI-TOF mass spectrum **(Figure 35)**.

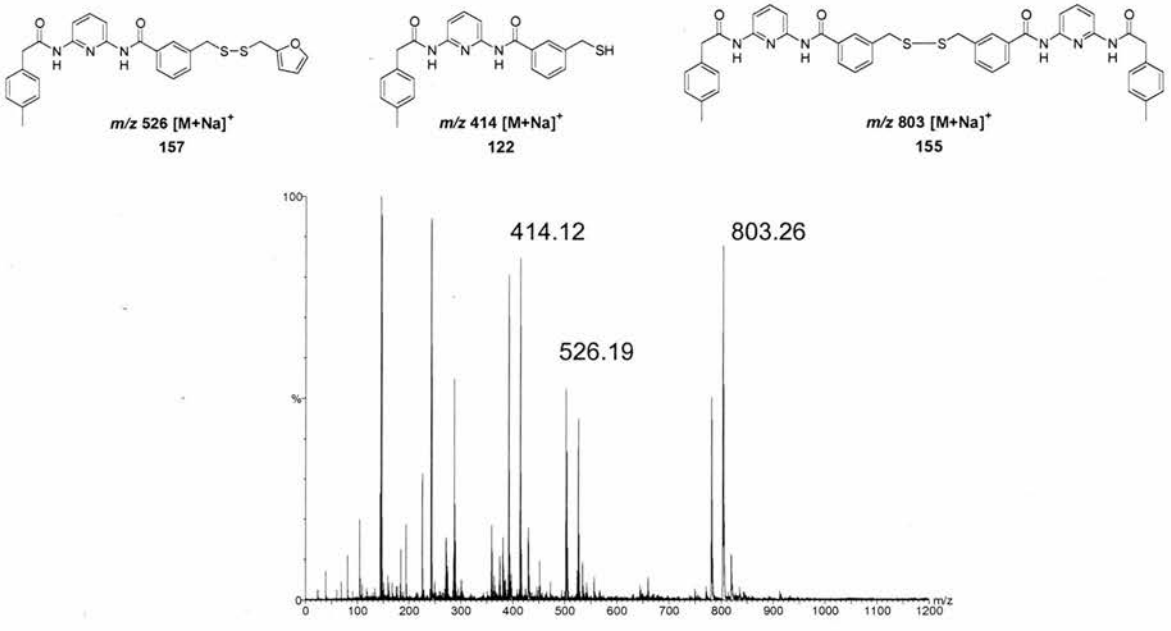

Figure 35: MALDI-TOF mass spectrum showing; *m/z* 803.26 representative of the recognition disulfide **155**, *m/z* 526.19 representative of mixed disulfide **157**, *m/z* 414.12 representative of thiol **122**.

2.11 Re-optimisation of Diels-Alder Reaction Conditions

Optimized thiol/disulfide exchange conditions **(Section 2.10)** were used with maleimide **126** in an attempt to provoke a Diels-Alder cycloaddition reaction **(Scheme 48)**. After 16 hours, analysis of the ^{1}H NMR spectrum, revealed once again, that no Diels-Alder cycloadduct **158** had been formed. It appeared by ^{1}H NMR spectroscopy that Michael addition of the deprotonated recognition thiol **122** to maleimide **126** was occurring to give adduct **160** **(Figure 36)**.

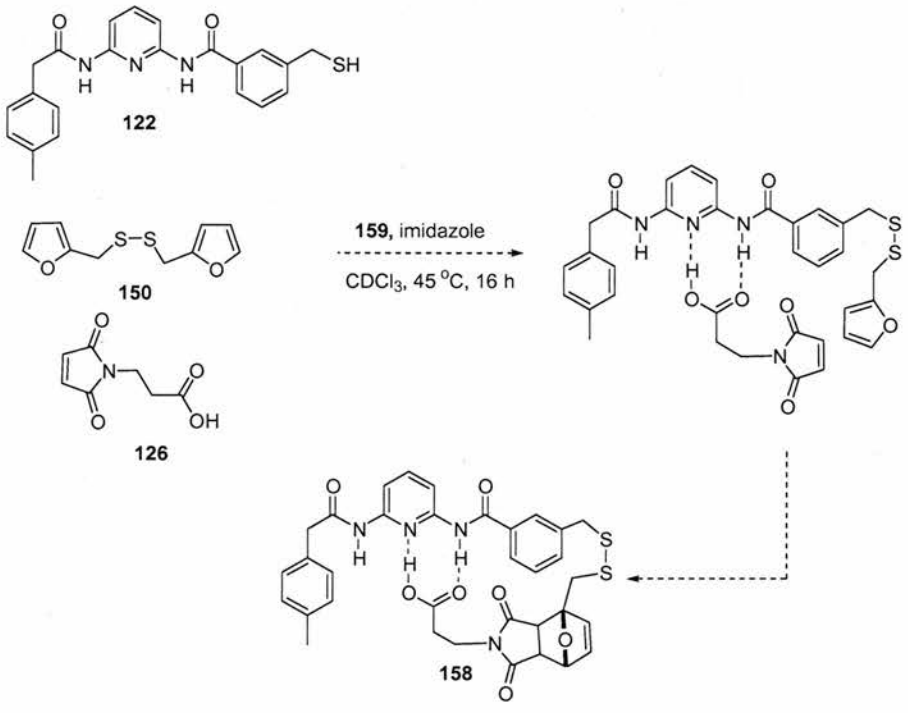

Scheme 48: Proposed synthetic route for the synthesis of Diels-Alder cycloadduct **158**. The reaction was conducted under optimized conditions **(Section 2.13) 122**, **126** & **150** (25 m*M*) and **159** (12.5 m*M*).

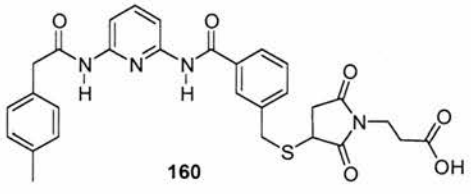

Figure 36: Michael adduct **160** formed from the reaction between **122** and **126**.

The outcome of the reaction is not surprising as α,β-unsaturated carbonyl compounds can also act as Michael acceptors. Maleimide **126** can act as the electrophilic partner in the conjugate addition reaction **(Scheme 49)**. Thiol **122** acts as a nucleophile, attacks the β-carbon atom of the maleimide alkene and produces a stable enolate, which is then converted back to the carbonyl with concomitant protonation to give Michael adduct **160**.

1,4-Conjugate addition reactions, or Michael addition reactions,[198-199] occur with α,β-unsaturated carbonyl compounds in the presence of a nucleophile, as in the example above. The conjugated system leads to the weakening of both π bonds *via* polarisation. The reaction between the nucleophile and electrophile is governed by two factors; (i) electrophilic attraction between the positive and negative charges, and (ii) orbital overlap between the HOMO of the nucleophile and the LUMO of the electrophile. Successful reactions tend to result from a combination of the two factors.

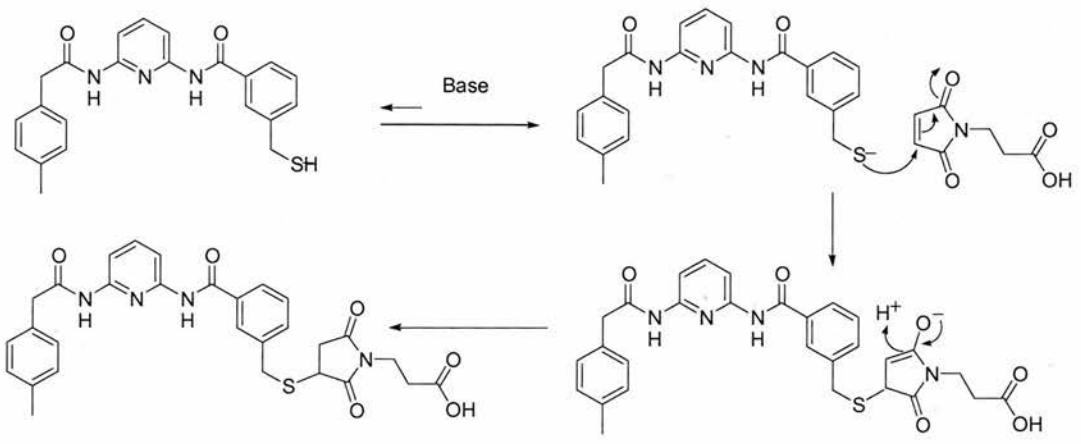

Scheme 49: Representation of the Michael Additon pathway followed by thiol **122** and maleimide **126** under basic conditions.

Nucleophiles which contain small, electronegative atoms (O or Cl) predominately react under electrostatic control and are termed hard nucleophiles. Whereas nucleophiles containing large atoms, such as sulfur within thiols, P, I, and Se are predominantly controlled by orbital overlap and are termed soft nucleophiles. The concept of 'hard' and 'soft', can also be applied to electrophiles, H^+ is hard as it is charge dense and Br_2 is soft as its orbitals are diffuse and uncharged. This theory is important when evaluating the likelihood of a conjugate addition reaction to occur, as hard nucleophiles prefer to react with hard electrophiles, and similarly, soft nucleophiles prefer to react with soft nucleophiles. In our case, where we have an α,β-unsaturated carbonyl compound, the β-carbon is a soft electrophile and will therefore react quickly with the soft thiol nucleophile.

As the Diels-Alder reaction had proven to be not viable within our system, our attention turned to the potential of Michael addition reactions as dynamic reactions using our original library members.

2.12 Rates and Equilibria of Michael-Addition Reactions of Benzene Thiol to 2-Cyclopentane-1-ones

Mandolini and co-workers reported[200] the reversible Michael addition reaction between benzene thiol **159 (Figure 37)** and 2-cyclopenten-1-one **161** catalysed by triethylamine to afford adduct **162** as the product. The reaction of benzene thiol in the presence of base resulted in the unexpected occurrence of small amounts of unreacted enone at infinite time, thus suggesting the existence of an equilibrium **(Scheme 50)**. An equilibrium constant in the range of between 3 and 5 x 10^3 M^{-1} was calculated.

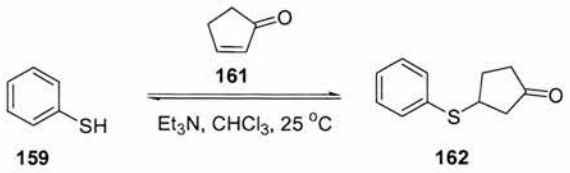

Figure 37: Reaction conditions under which enone **161** and thiol **159** undergo a Michael addition reaction to produce adduct **162**.

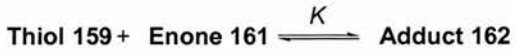

Scheme 50: The equilibrium observed in the Michael addition of thiol **159** to enone **161**.

The above studies suggested that this type of reaction can be reversible and therefore under thermodynamic control. We therefore proposed to attempt a dynamic approach to the Michael addition reaction using our original system building blocks **(Figure 38)**. Control compounds which will be used in order to assess the effect of recognition on the system are highlighted in **Figure 38**.

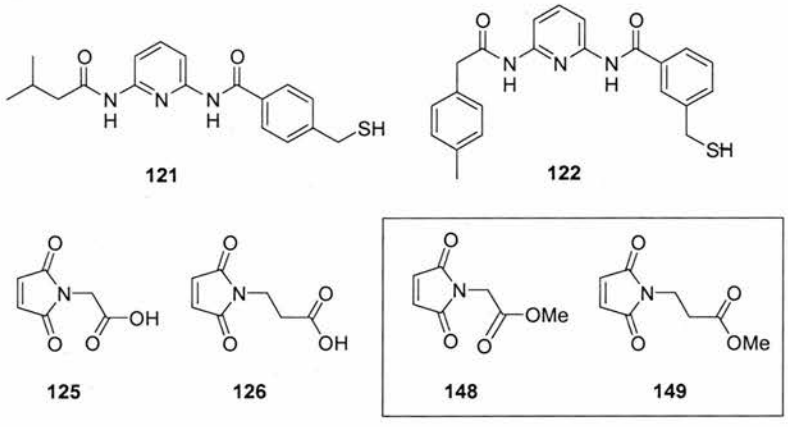

Figure 38: Building blocks for the study of reversible Michael addition reactions.

One could imagine maleimide **126 (Scheme 51)** being positioned through appropriately located hydrogen bonds, at a suitable orientation for the rate of reaction between electrophile **126** and nucleophile **122** to be enhanced.

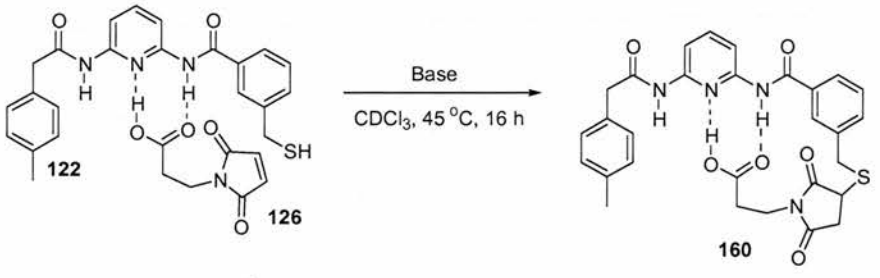

Scheme 51: Michael additon reaction proceeding *via* an AB pathway.

2.13 Initial Optimisation of Michael Addition Reaction Conditions

Initial investigations to assess the optimal conditions for Michael addition reactions between maleimides **125** and **126** and thiols **121** and **122** were undertaken. Reactions were conducted at a starting concentration of 25 m*M* for each reactant, in $CDCl_3$ at a temperature of 50 °C. A variety of bases were investigated at either 0.5 eq. (12.5 m*M*) or 1 eq. (25 m*M*) the results of the studies are shown in **Table 9**.

Table 9: The effect of varying the equivalence of various bases on the rate of reaction between maleimide **126** and thiol **122**.

Base	Equivalence	Rate of Reaction
t-butyl pyridine	0.5 eq. 1 eq.	No reaction No reaction
triethylamine	0.5 eq. 1eq.	Reaction instantaneous Reaction instantaneous
imidazole	0.5 eq. 1eq.	Reactions complete within ~ 8-16 hours Reactions complete within ~1-3 hours

These results demonstrate that 0.5 eq. (12.5 m*M*) of imidazole would facilitate the Michael addition reaction at a rate which was easily monitored by ^{1}H NMR kinetic studies. Therefore the conditions used for the study of each Michael addition reaction were as follows: 25 m*M* of each reactant and 12.5 m*M* of imidazole in $CDCl_3$ at a temperature of 25 °C. The samples were analysed by 500 MHz ^{1}H NMR spectroscopy. The course of each Michael addition reaction was monitored by the appearance of a distinctive multiplet at ~ 3ppm corresponding to a ring C-H formed during the reaction, this resonance was followed over a period of 16 hours. The concentration of product produced was calculated using the deconvolution tool available within 1D WINNMR.

2.14 Kinetic Experiments

2.14.1 Michael Addition Reaction between Thiol 122 and Maleimide 125

Reactants **122** and **125 (Scheme 52)** were reacted and monitored as described above. The rate profile for the reaction is shown as filled red circles in **Figure 39a**. In order to determine the

effect of recognition upon the reaction rate, a control experiment was undertaken in which the carboxylic acid recognition site was removed, disrupting the recognition-mediated pathway.

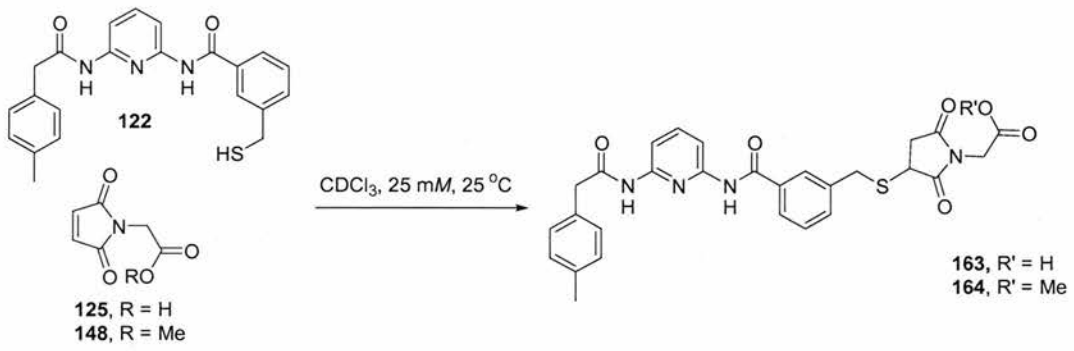

Scheme 52: Michael addition reaction between thiol and maleimides to yield Michael Adducts **163** or **164**.

The control reaction substituted methyl ester maleimide **148** in place of the carboxylic acid maleimide **125**. The rate profile (open circles, **Figure 39a**) for the control reaction indicated that, the reaction rate was practically unchanged. This result was surprising, as the recognition motif of amidopicoline:carboxylic acid groups are know to be sufficiently strong to mediate AB reactions.[186] We performed a series of molecular mechanics calculations to explore the conformations open to the Michael addition product. Monte Carlo conformational searches were performed form a variety of starting conformations using the AMBER* forcefield and the GB/SA solvation model for $CDCl_3$.

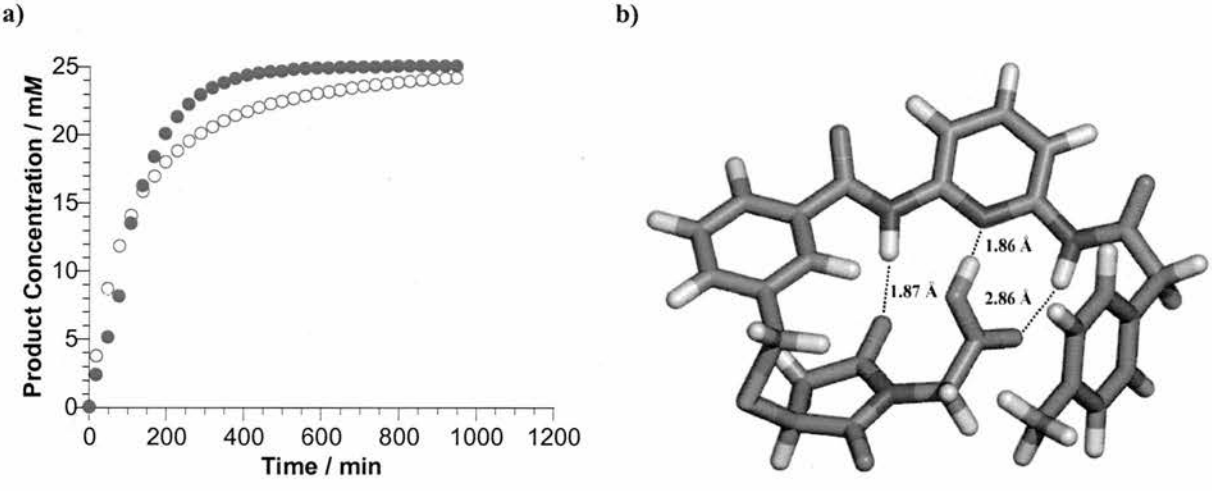

Figure 39: **a)** Rate profile for the bimolecular reaction, thiol **122** with maleimide **148** (shown as open red circles). Rate profile for the potential recognition-mediated reaction, thiol **122** with maleimide **125** (shown as filled red circles). **b)** Model representative of the minimum energy conformation of adduct **163** derived from molecular mechanics calculations. Carbon, oxygen, nitrogen, sulfur and hydrogen atoms are depicted in green, red, blue, orange and white respectively. Hydrogen bonds are represented by dashed lines and hydrogen bond donor and acceptor distances are given in Å.

These calculations suggested **(Figure 39b)** that Michael adduct **163** adopted a closed structure that could potentially react *via* a recognition-mediated pathway, the structure could be stabilised by up to three hydrogen bonds. However, on considering the reaction conditions in the potential recognition-mediated and control reactions respectively it became apparent that an additional factor must be considered in order to compare these two situations. If we consider the acid/base potential within the recognition-mediated reaction we have a system in which the recognition carboxylic acid and recognition thiol are in competition for deprotonation by the base. In the case of control reaction A **(Scheme 53)** where there is no carboxylic acid present, the base will only deprotonate the thiol and therefore the Michael addition reaction will precede faster. In order to combat this, the control reactions would be 'buffered' with 1 equivalent of acid (control reaction B, **Scheme 53**).

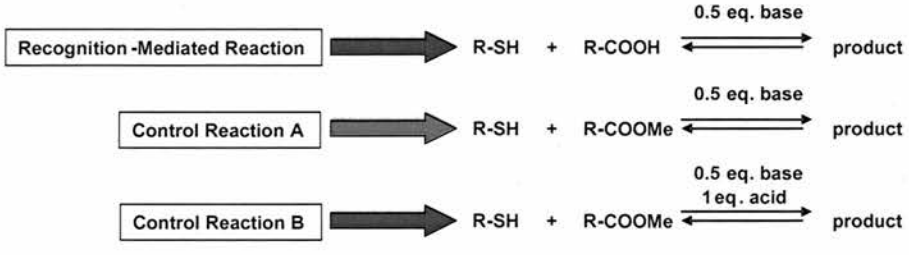

Scheme 53: Schematic representation of the stoichiometries required in order to maintain overall basicity within the control and recognition-mediated reactions.

The protocol for control reactions was therefore modified to: 25 m*M* of thiol and maleimide, 12.5 m*M* of imidazole, 25 m*M* of acetic acid in $CDCl_3$ at a temperature of 25 °C. It can be seen from the concentration/time profile **(Figure 40)** that the control reaction containing methyl ester **148** does indeed proceed slower than the corresponding reaction containing carboxylic acid **125**, suggesting that the reaction is indeed recognition-mediated.

In order to confirm whether the reaction was proceeding *via* an AB-complex pathway kinetic modelling studies were undertaken. Firstly, a kinetic model for the bimolecular reaction **(Scheme 54)** was established, comprising of the two starting materials **A** and **B** irreversibly forming Michael adduct product P, where k_1 represents the forward rate constant for the bimolecular reaction.

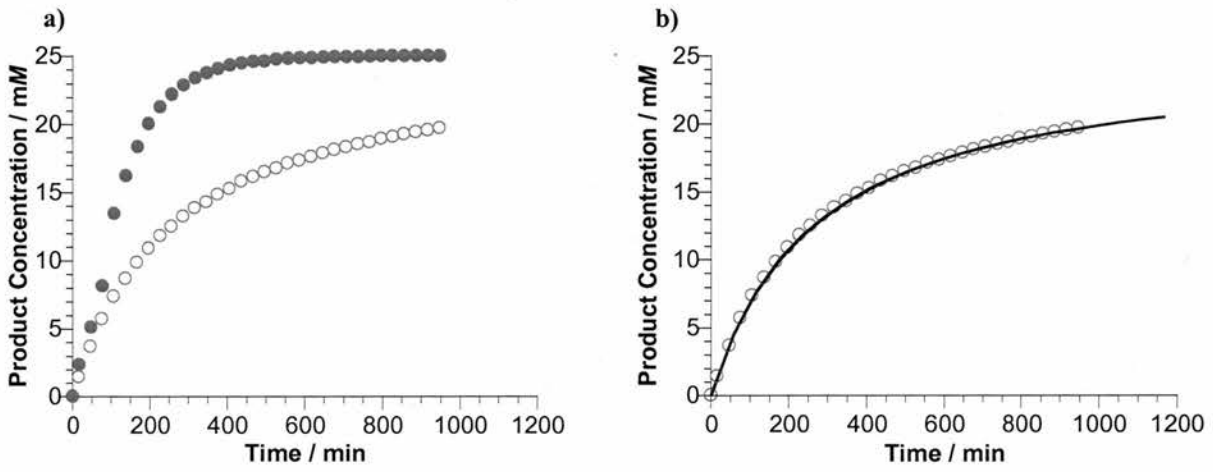

Figure 40: **a)** Rate profile for the bimolecular reaction, thiol **122** with maleimide **148** (shown as open red circles). Rate profile for the potential recognition-mediated reaction, thiol **122** with maleimide **125** (shown as filled red circles). **b)** The fitted profile of the bimolecular reaction is depicted, the experimentally determined rate profile is shown as open red circles, the solid line represents the best fit of the data to the bimolecular kinetic model.

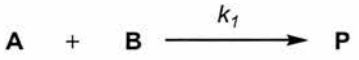

Scheme 54: Model used for the fitting of bimolecular rate data between a nucleophile **A**, and an α,β-unsaturated compound **B** in the irreversible production of product Michael adduct **P**.

This model was used in conjunction with the simulation and fitting package SimFit. SimFit was used to fit the experimental rate data obtained by numerical integration of the appropriate differential rate equations. An excellent fit between the experimental data and model was obtained **(Figure 40b)** which allowed the extraction of kinetic parameters from the observed rate profiles. The rate constant for the control reaction was calculated (k_1 = 2.67 x 10^{-3} $M^{-1}s^{-1}$). Secondly, a kinetic model for the *pseudo*-intramolecular reaction was derived **(Scheme 55)**. This model consists of the bimolecular rate equation, and in addition, equations representative of the *pseudo*-intramolecular reactions. The reversible association of reactants **A** and **B** in a reactive AB-complex are also described.

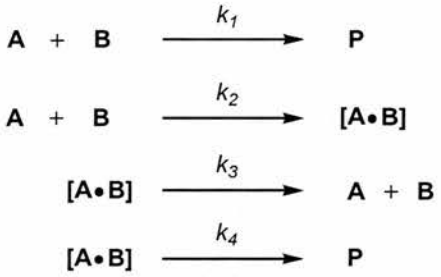

Scheme 55: Model used for the fitting of the AB-mediated data for reaction between a nucleophile **A**, and an α,β-unsaturated compound **B** in the irreversible production of product Michael adduct **P**.

The association constant (K_a) was estimated at ~ 150 M^{-1} based upon NMR binding study data acquired previously **(Section 3.12)**. The reaction was fitted approximately to an AB-mediated model, therefore an estimated value for the rate of the complex-mediated reaction was obtained (k_4 = 2 x $10^{-4}s^{-1}$). The lack of perfect fit to the model can be attributed to the very fast rate of the reaction. SimFit cannot accurately fit data which reach completion very quickly. However, the experimental kinetic results, molecular modelling studies and kinetic modelling studies, all suggest that the Michael addition reaction between **122** and **125** is recognition-mediated. Calculating the kinetic effective molarity **(Section 2.3)** from the calculated rate constants gives an estimated *EM* value of 75 m*M*, suggesting that the presence of hydrogen bonds in the transition state pre-organises reactants **122** and **125** allowing the reaction between them to proceed at a faster rate.

2.14.2 Michael Addition Reaction between Thiol 121 and Maleimide 125

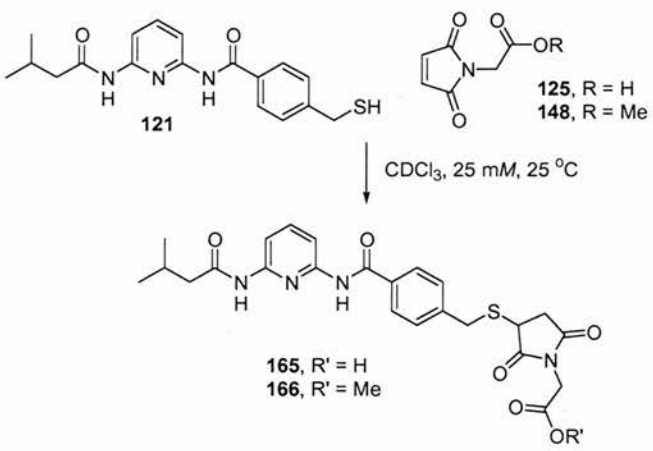

Scheme 56: Reaction conditions under which thiol **121** can undergo Michael addition with maleimides **125** and **148**.

The effect of changing the position of the thiol moiety on the recognition thiol was next investigated **(Scheme 56)**. The bimolecular control reaction between methyl ester **148** and thiol **121** and the recognition-mediated reaction between acid **125** and thiol **121** were carried out under reaction conditions previously described in **Section 2.14.1**. The reaction mixtures were monitored by ^{1}H NMR spectroscopy, over a period of 16 hours, the rate profiles obtained are shown in **Figure 41a**.

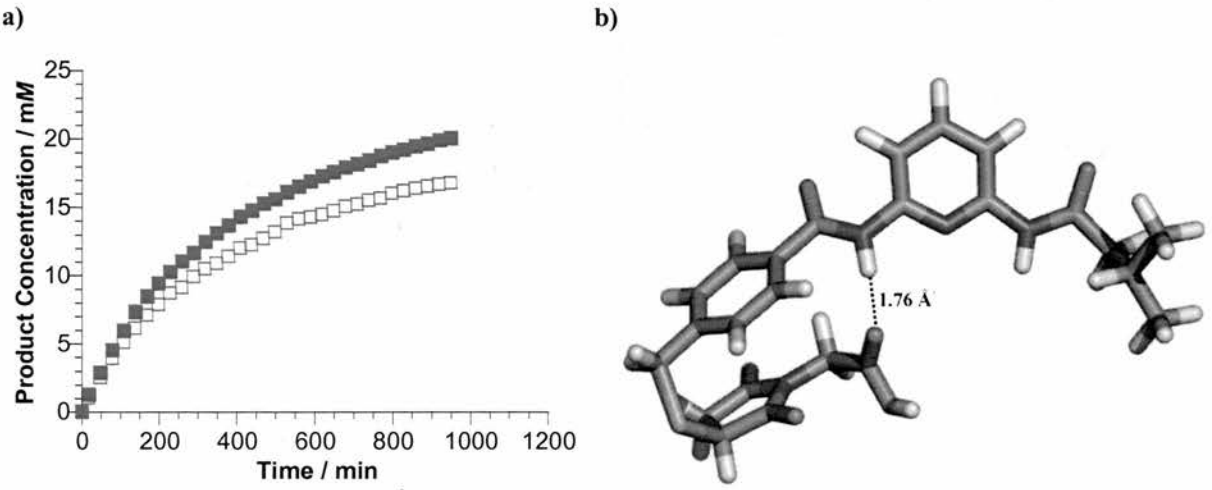

Figure 41: **a)** Rate profile for the bimolecular reaction, thiol **121** with maleimide **148** (shown as open red squares). Rate profile for the potential recognition-mediated reaction, thiol **121** with maleimide **125** (shown as filled red squares). **b)** Model representative of the minimum energy conformation of adduct **165**. Carbon, nitrogen, oxygen, sulfur and hydrogen atoms are depicted in green, blue, red, orange and white respectively. Hydrogen bonds are represented by dashed lines and hydrogen bond donor and acceptor distances are given in Å.

There is a moderate rate acceleration observed for the maleimide acid/thiol reaction relative to the methyl ester control reaction **(Figure 41a)**. These results indicate that although the reaction between **121** and **125** is recognition mediated, this does not appear to be the major chemical pathway used for the reaction. This hypothesis is substantiated by molecular modelling studies **(Figure 41b)** which suggest that the lowest energy conformations of Michael adduct **165** do not adopt a closed-AB structure.

Indeed, kinetic modelling studies confirmed this lack of AB-character. On fitting the bimolecular maleimide ester experimental data **(Figure 42a)** to the previously derived model, k_1 was calculated at $k_1 = 1.5 \times 10^{-3}\ M^{-1}s^{-1}$. The reaction between maleimde **125** and thiol **121** was fitted to an AB complex model and a reasonable fit obtained, the rate constant was estimated at $k_4 = 1.6 \times 10^{-5}\ s^{-1}$. A *kEM* value of 39 m*M* was calculated, this value is only marginally higher than the actual reaction concentration, indicating the minor influence of recognition-mediated pathway within this system. The change in position of the thiol group from meta- to para-substitution upon recognition nucleophiles has had a large impact upon the rate of the Michael addition reaction with maleimide **125 (Figure 42b)**. These results show that a minor change in the configuration of molecules within this system can govern whether a recognition-mediated or bimolecular pathway is favoured.

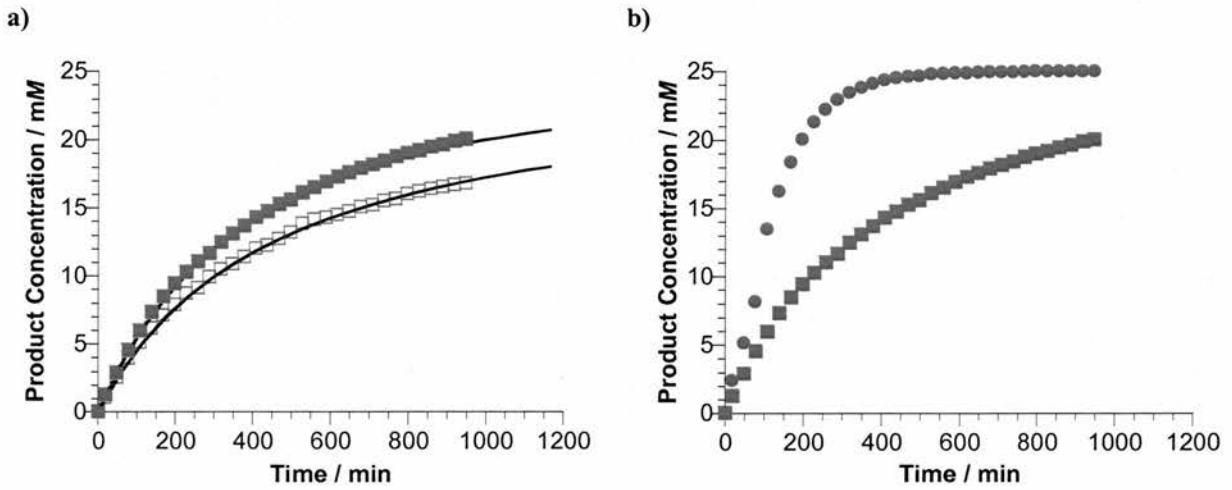

Figure 42: **a)** Rate profile for the bimolecular reaction, thiol **121** with maleimide **148** (shown as open red squares). Rate profile for the recognition-mediated reaction, thiol **121** with maleimide **125** (shown as filled red squares). The solid lines represent the best fit of the data to the appropriate kinetic model. **b)** Rate profile for meta-substituted thiol **122** with maleimide **125** shown as filled red circles, rate profile for para-substituted thiol **121** with maleimide **125** shown as filled red squares.

2.14.3 Michael Reaction between Maleimide 126 and Thiol 121

The Michael addition reaction between maleimide **126** and thiol **121 (Scheme 57)** allowed the investigation into the effect of varying the spacer length on the Michael acceptor moiety. The reaction conditions employed for both the control and recognition-mediated reactions were as described previously in **Section 2.14.1**, the rate profiles of the two reactions are shown in **Figure 43a**.

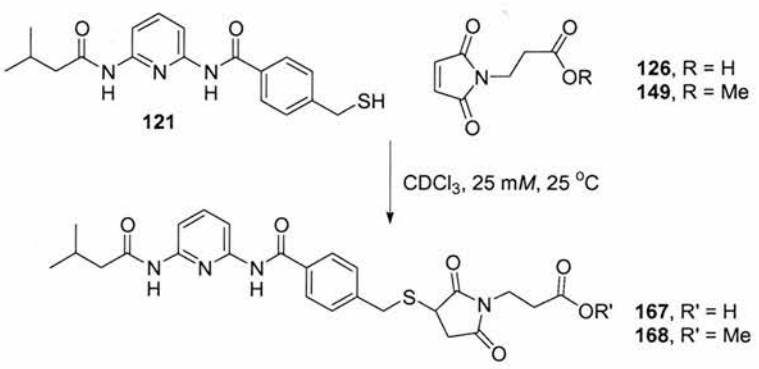

Scheme 57: The conditions under which Michael adducts **167** and **168** are formed.

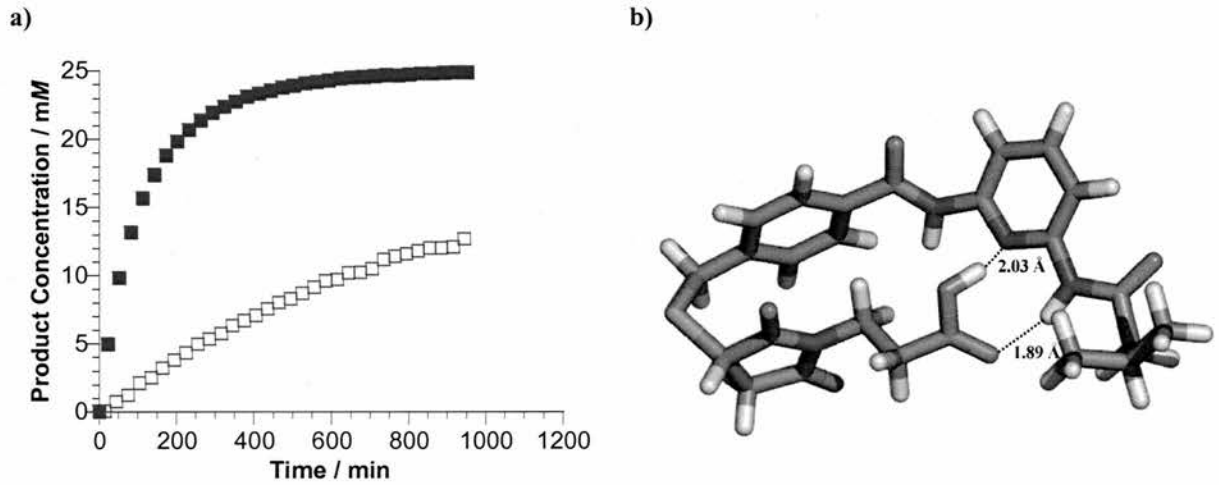

Figure 43: **a)** Rate profile for the bimolecular reaction, thiol **121** with maleimide **149** (shown as open blue squares). Rate profile for the potential recognition-mediated reaction, thiol **121** with maleimide **126** (shown as filled blue squares). **b)** Model representative of the minimum energy conformation of adduct **167** derived from molecular mechanics calculations using the AMBER* forcefield. Carbon atoms are depicted in green, oxygen atoms are coloured red, nitrogen atoms are shown in blue, hydrogen atoms are depicted in white and sulfur atoms are depicted in orange. Hydrogen bonds are represented by dashed lines and hydrogen bond donor and acceptor distances are given in Å.

A large rate enhancement can once again be observed in the rate profile of the acid/thiol reaction compared with the methyl ester/thiol reaction, suggesting that the reaction is indeed recognition-mediated. This assumption is also supported by molecular modelling studies **(Figure 93b)** which suggest that the lowest energy conformation of structure **167** adopts a conformation which has two hydrogen bonds present. The AB-character of the reaction was confirmed by kinetic modelling studies. The reaction rate for the bimolecular reaction and recognition-mediated reactions were once again calculated by fitting experimental data for the reaction between thiol **121** and maleimide ester **149 (Figure 44a)**, using SimFit, a good fit between experimental data and model was achieved and the rate constants and resulting kinetic effective molarity extracted **(Figure 44b)**. A value of ~ 400 m*M* was obtained for the kinetic effective molarity suggesting that the effect of recognition upon the reaction rate is significant. The recognition features incorporated into building blocks **121** and **126** leads to the stabilization of the transition state of the product which results in the observed rate acceleration of the Michael addition reaction.

a)

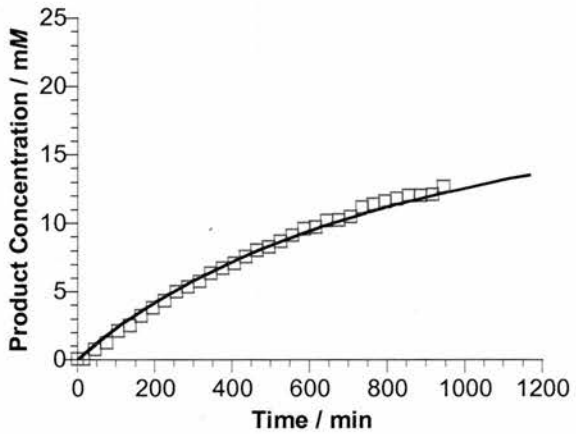

b)

k_1 / $M^{-1}s^{-1}$	k_4 / s^{-1}	kEM / mM
6.85×10^{-4}	$\sim 3 \times 10^{-4}$	~ 400

Figure 44: **a)** The fitted profile of the bimolecular reaction is depicted, the experimentally determined rate profile is shown as open blue squares, the solid line represents the best fit of the data to the bimolecular kinetic model. **b)** Values extracted from the fitting of a *pseudo*-intramolecular model to the experimental data for the Michael additional reaction between **121** and **149**.

2.14.4 Michael addition reaction between Thiol 122 and Maleimide 126

Once again, the effect of changing the position of the thiol moiety was studied in the reaction of thiol **122** with maleimide **126 (Scheme 58)**. Reactions were carried out as described in **Section 2.14.1**. The rate profiles of the two reactions are shown in **Figure 45a**.

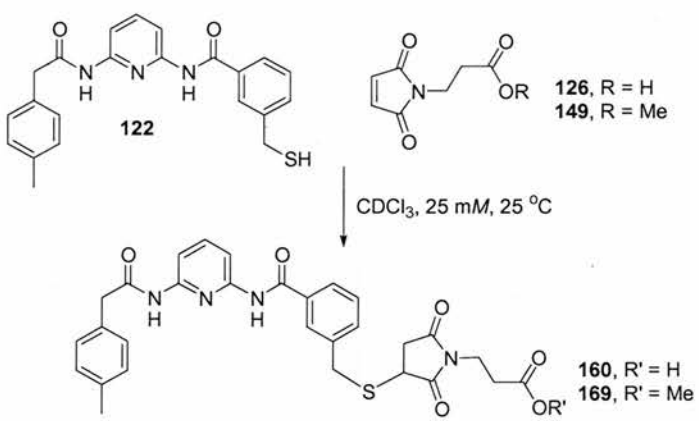

Scheme 58: The conditions under which Michael adducts **160** and **169** are formed.

The effect of recognition upon the reaction of thiol **122** and maleimide **126** is apparent. When comparing the bimolecular reaction to the recognition-mediated reaction, the extent to which the reaction proceeds and the rate at which the reaction proceeds is significantly faster in the reaction between carboxylic acid **126** and thiol **122**. Molecular modelling studies of adduct **160 (Figure 45b)** were conducted using the AMBER* forcefield and the GB/SA solvation model for $CDCl_3$. A representative minimum energy conformation is shown for adduct **160**.

It can be seen that the closed conformation adopted by adduct **160** allows the structure to be stabilised by three potential hydrogen bonds. These studies suggest that an AB-complex pathway may operate within this system.

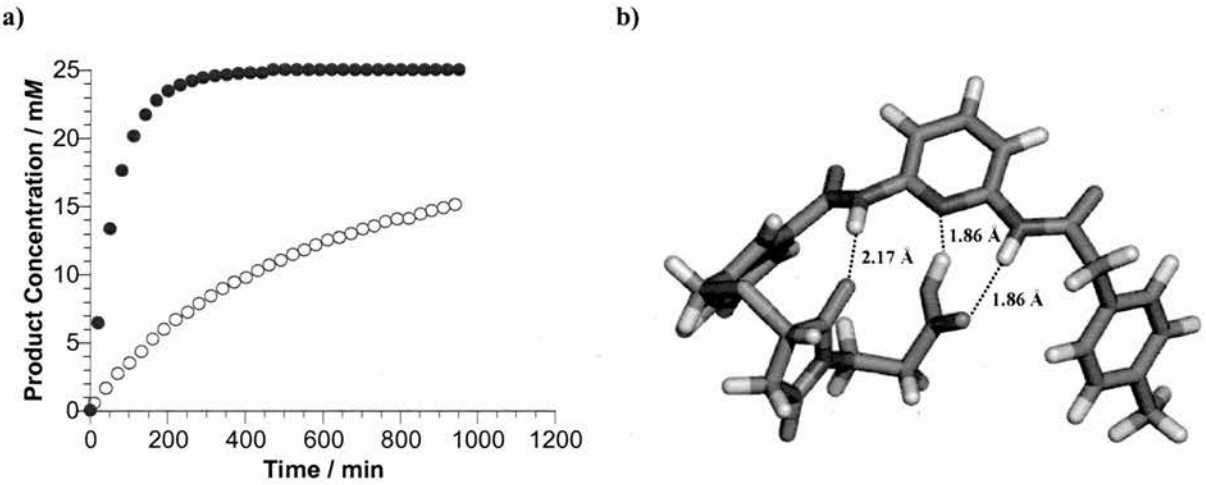

Figure 45: **a)** Rate profile for the bimolecular reaction, thiol **122** with maleimide ester **149** (shown as open blue circles). Rate profile for the potential recognition-mediated reaction, thiol **122** with maleimide acid **126** (shown as filled blue circles). **b)** Model representative of the minimum energy conformation of adduct **160** derived from molecular mechanics calculations using the AMBER* forcefield. Carbon atoms are depicted in green, oxygen atoms are coloured red, nitrogen atoms are shown in blue, sulfur atoms are depicted in orange and hydrogen atoms are depicted in white. Hydrogen bonds are represented by dashed lines and hydrogen bond donor and acceptor distances are given in Å.

The AB-character of the reaction was confirmed by kinetic modelling studies. The reaction rate for the bimolecular reaction and recognition-mediated reactions were once again calculated by fitting experimental data for the reactions to the appropriate model **(Schemes 54** and **55)** using SimFit. A good fit between experimental data and model was achieved **(Figure 46a)** and the rate constants and resulting values for the kinetic effective molarity extracted **(Figure 46b)**. A value of ~ 450 m*M* was obtained for the kinetic effective molarity suggesting that the effect of recognition upon the reaction rate is significant, the reactants are stabilized by their recognition features at the transition state.

We can conclude that the Michael Addition reactions between thiols **121** and **122** and maleimides **125** and **126** are recognition mediated. The extent to which the reactions are influenced by the AB-complex pathway is heavily dependent upon both the carbon spacer lengths on the maleimdes and also the orientation of the thiol moiety on the amide components. Our molecular modelling studies are consistent with the experimental kinetic results. Maleimides **125-126** only differ from enone **160** in one additional carbonyl moiety. However, enone **161** undergoes a reversible Michael addition reaction with thiols and

maleimides **125-126** do not. The additional carbonyl group present in our maleimides, must act in some way which alters their reactivity.

a)

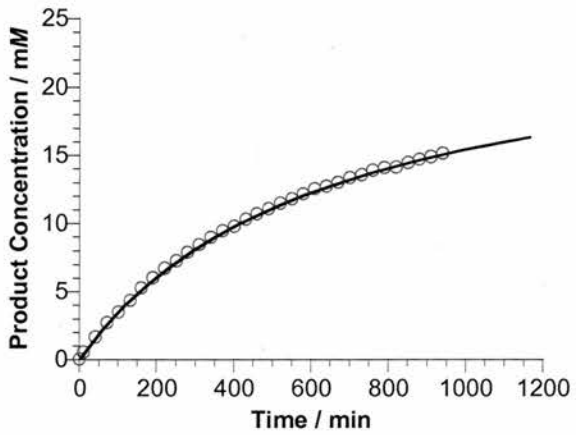

b)

k_1 / $M^{-1}s^{-1}$	k_4 / s^{-1}	kEM / mM
1.09×10^{-3}	$\sim 5 \times 10^{-4}$	~ 450

Figure 46: **a)** The fitted profile of the bimolecular reaction is depicted, the experimentally determined rate profile is shown as open blue circles. The solid line represents the best fit of the data to the bimolecular kinetic model. **b)** Values extracted from the fitting of a *pseudo*-intramolecular model to the experimental data for the Michael addition reaction between **122** and **149**.

The Michael addition reactions between our library building blocks are not reversible, this set of molecules is therefore not suitable to observe the effect of dynamic libraries in conjunction with recognition-mediated AB reactions. We looked into ways in which we could modify our library building blocks in order to facilitate reversible dynamic library conditions.

2.15 A New System

Mandolini and co-workers also described[200] the behaviour of methyl-substituted enones (2- and 3-methyl-2-cyclopent-2-ene-1-one, **170** and **171** respectively) with benzene thiol **159** **(Figure 47)**. The conjugate addition reaction between these compounds can result in the formation of adducts **172-173**.

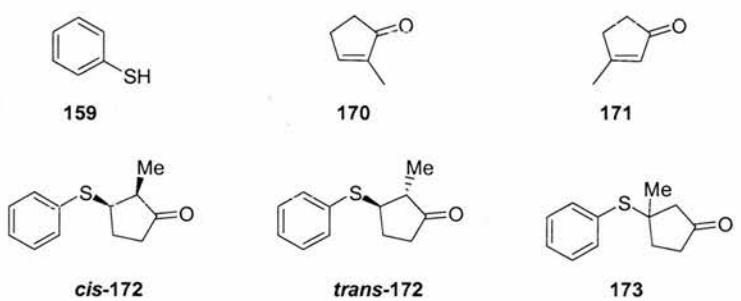

Figure 47: Benzene thiol **159**, 2-methyl-2-cyclopent-2-en-1-one **170**, 3-methyl-2-cyclopent-2-en-1-one **171**. The Michael adducts *cis* and *trans*-**172** are produced from the reaction between **159** and **170**. Michael adduct **173** is produced from the reaction between **159** and **171**.

Studies on 2-methyl-2-cyclopenten-1-one **170** revealed that the less stable *cis*-isomer **172** was formed about two orders of magnitude more rapidly than the more stable *trans*-adduct **172** as a result of the addition mode of the incoming proton as shown in **Scheme 59**.

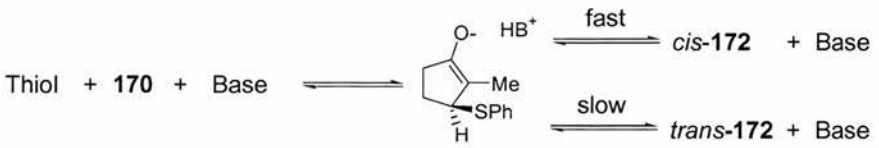

Scheme 59: The overall process in the generation of adducts *cis*-**172** and *trans*-**172**. The key step within this reaction sequence involves an enolate-ammonium ion pair. The re-protonation step determines which isomer is formed, depending upon whether attack occurs from the top or bottom face of the ring.

An equilibrium constant of 1.30 M^{-1} was calculated for the reaction, its low value is as a consequence of two factors; (i) stabilisation of the double bond by the methyl group, which is an electronic effect, and (ii) the presence of the methyl group results in an increase in bond eclipsing within the addition product. Studies upon 3-methyl-2-cyclopentene-1-one **171** also calculated a low equilibrium constant value of 6.10 M^{-1}, as a result of the presence of the methyl substituent. As reversibility is enhanced by the addition of methyl substituents to the alkene, we surmised that a similar effect would be observed within our system. The following molecules were proposed as Michael adduct building blocks **(Figure 48)**.

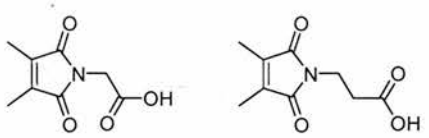

174 **175**

Figure 48: Target compounds dimethyl maleimides **174** and **175**.

2.16 Synthesis of Michael Acceptors 174 and 175

Dimethyl furan dione **178** was prepared *via* a two-stage synthetic procedure **(Scheme 60)**.[201] Maleic anhydride **143** was added to 2-aminopyridine **176** in acetic acid and the reaction mixture refluxed for two hours. After this time, the solvent was removed *in vacuo* and the resulting residue, intermediate 3,4-dimethyl-1-pyridin-2-yl-pyrrole-2,5-dione **177**, was dissolved in 2 M H_2SO_4 and refluxed for a further one hour. Upon cooling, the product crystallised from solution, it was isolated by filtration whilst washing with copious amounts of water. The desired product **178** was obtained in 72% after drying under vacuum over P_2O_5.

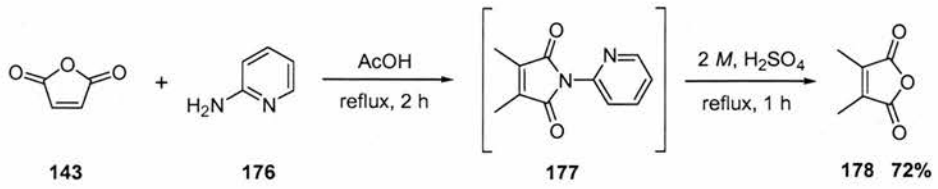

Scheme 60: Synthetic sequence in the preparation of dione **178** *via* intermediate **177**.

Maleimide **174**, containing a one carbon chain, was prepared in a one-pot reaction (**Scheme 61**), *via* intermediate **179** which was not isolated. Dione **178** and glycine **144** were stirred together in acetic acid for 8 hours to form intermediate **179** and then refluxed to give maleimide **174** in 45% yield after purification *via* silica gel column chromatography. Maleimide **175** containing a two carbon chain was prepared from dione **178** and β-alanine **145** affording maleimide **175** in 37% yield after purification *via* column chromatography.

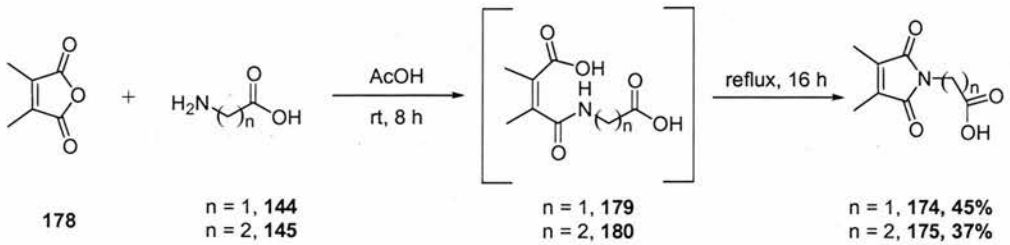

Scheme 61: Synthetic procedure for the preparation of dimethyl maleimides **174** and **175**.

2.17 Initial Studies

Initial studies were carried out on an NMR scale with donor and acceptor at initial concentrations of 25 m*M* in $CDCl_3$ at 25 °C. Different bases were tested at various stoichiometries to assess the optimal conditions for the Michael addition reaction to occur. However, disappointingly, no Michael adduct was observed after 24 hours in all cases. The lack of reactivity can be attributed to the steric hindrance of the two methyl groups around the α,β-unsaturated system. As reversibility was known to occur in the reaction between enone **170 (Figure 49)** and thiophenol **159**, we proposed the following maleimide building blocks **181-182** as our new target molecules.

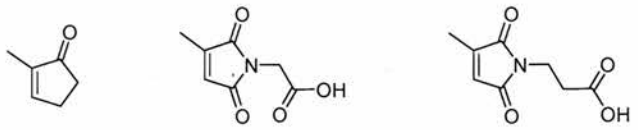

170 **181** **182**

Figure 49: Target building blocks **181** and **182** chosen as a result of the studies on enone **170**.

2.18 Synthesis of Maleimides 181 and 182

Maleimide **181**, containing a one carbon chain, was prepared in a one-pot reaction (**Scheme 62**), *via* intermediate **184** which was not isolated. Citraconic anhydride **183** and glycine **144** were stirred together in acetic acid for 8 hours to form intermediate **184** and then refluxed to give maleimide **181** in 67% yield after purification *via* column chromatography. Maleimide **182** containing a two carbon chain was prepared from citraconic anhydride **183** and β-alanine **145** affording maleimide **182** in 49% yield after purification *via* silica gel flash column chromatography.

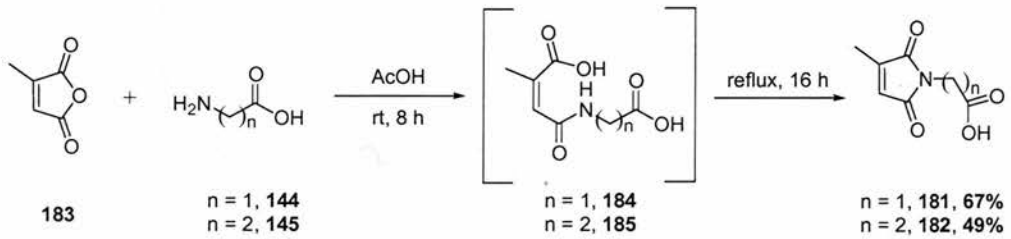

183 n = 1, **144** n = 2, **145** n = 1, **184** n = 2, **185** n = 1, **181**, **67%** n = 2, **182**, **49%**

Scheme 62: Synthesis of methyl maleimides **181** and **182** *via* intermediate compounds **184** and **185**.

2.19 The Reversibility of the System

Initial investigations upon the reversibility of the Michael addition reactions of maleimides **181** and **182** with thiols **121** and **122** were carried out on an NMR scale. Maleimide **182** and thiol **122** were reacted in $CDCl_3$ with 0.5 eq./1 eq. of imidazole. The Michael reaction between maleimide **182** and thiol **122** proceeded faster than the reaction between maleimide **175** and thiol **122** and slower than the reaction between maleimide **126** and thiol **122** by ^1H NMR spectroscopy after 24 hours. These results are as one would expect due to the effect of steric hindrance upon the reaction rate **(Figure 50)**.

The reaction between maleimide **182** and thiol **122** with 1 eq. of imidazole had reached 60% completion after 24 hours. After 66 hours, the reaction between maleimide **182** and thiol **122** had reached 70% and at 168 hours the reaction had reached 75% completion. At infinite time

5% of unreacted maleimide **182** was detected by ^{1}H NMR spectroscopy. These results suggest that an equilibrium is indeed in effect within this reaction.

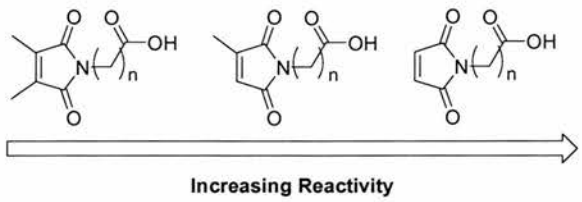

Figure 50: The increasing trend in reactivity shown from maleimides **175**, **182** and **126**. n = 1 or 2, carbon spacer chain.

The reversibility profile within the family of maleimides studied follow a trend **(Figure 51)**; dimethyl maleimides, **174** and **175** reactivity with thiol **122** lies in favour of the reactants, methyl maleimides **181** and **182** appear to undergo a reversible reaction with thiol **122** and maleimides **125** and **126** react irreversibly with thiol **122**.

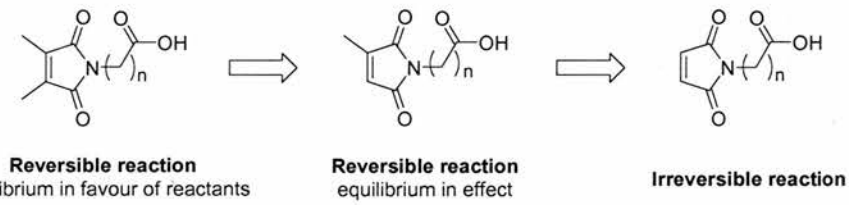

Figure 51: The trend in reversibility displayed by maleimides in their reaction with thiol **122**. n=1 or 2 carbon spacer chain length.

We have shown that the Michael addition reaction between methyl maleimides **181-182** is reversible. Further studies will be conducted to gauge the affect of AB-complex reactions within a dynamic library situation.

2.20 Conclusions

The initial aim of this project was to successfully blend the rate acceleration and diastereochemical control, known to occur in Diels-Alder reactions when AB-methodology is utilised, with the concept of dynamic combinatorial chemistry, where a 'survival of the fittest' strategy prevails when a library is under thermodynamic control. We successfully synthesised library of building blocks **121-126**. However, having successfully established appropriate conditions to facilitate thiol/disulfide exchange in $CDCl_3$, Diels-Alder reactivity was not observed within the system. Instead, a Michael addition reaction between recognition thiols **121-122** and maleimides **125-126** occurred.

At this juncture, our project strategy was altered to incorporate the Michael addition reactivity displayed by our library members. Kinetic studies upon each Michael acceptor **125-126** and donor **121-122**, have shown these reactions to be recognition-mediated. A combination of techniques have been successfully utilised to unequivocally confirm the AB-nature of these reactions. Experimental kinetic data, kinetic modelling and molecular modelling studies all substantiated that an AB-pathway was in operatation within the system.

Small changes in the structure of building blocks were noted to greatly influence the rate at which the recognition-mediated reactions occurred. However, Michael addition reactions between maleimides **125-126** and thiols **121-122** were shown to be irreversible. Thus, our original library building blocks were deemed unsuitable for further investigations as reversibility is a key requirement of dynamic combinatorial systems.

The addition of methyl groups to α,β-unsaturated carbonyl compounds was known to effect the position of equilibrium within similar Michael addition reactions. Addition of two methyl groups to our original maleimides yielded building blocks **174-175**, however, no Michael addition reaction was observed on their reaction with thiols **121-122**, this is presumably due to steric hindrance at the electrophilic acceptor. The reaction between compound **182** with only one methyl substituent and thiol **122** has been shown to be reversible.

Assuming that the AB-complex pathway which was followed by building blocks **121-122** is still open to our methyl substituted maleimides **181-182**, we have effectively designed a system in which the formation of Michael adducts shall be subject to both AB-complex methodology and dynamic combinatorial chemistry simultaneously.

This project has underlined some of the key challenges in designing a dynamic library. There were three key areas which needed to be controlled within our system in order for the project to be successful:

(i) reversibility - required to allow the library to evolve
(ii) recognition - allowing the reaction to proceed *via* the AB pathway
(iii) reactivity - the reaction we wished to accelerate

Our initial library studies had successfully achieved reversibility, however, under the conditions required for reversibility, the Diels-Alder reaction was not observed. Reversibility was the problem with our initial studies upon Michael addition reactions. Finally, on modifying library members, the three requirements of reversibility, recognition and reactivity have been met and will hopefully allow the selection and amplification of one library member in a dynamic combinatorial library.

Chapter 3

The use of Kinetic Modelling as a Predictive Tool in the Study of ABC-Mediated Dynamic Libraries

3.1 Natural Coenzymes

Cofactors and coenzymes[202] are non-protein entities which are required within an enzyme. Inorganic cofactors are metal ions which can bond through coordinate covalent bonds to the enzyme. Nutritional supplements contain transition metal cations such as Cu^{2+}, Fe^{3+} and Zn^{2+} mainly in order to act as coenzymes within enzymes. Organic cofactors are generally referred to as coenzymes, examples of this are NAD^+ and CoA. Cofactors/coenzymes generally assist in the transfer of electrons. Many enzymatic reactions cannot proceed in the absence of a cofactor **(Figure 52)**.

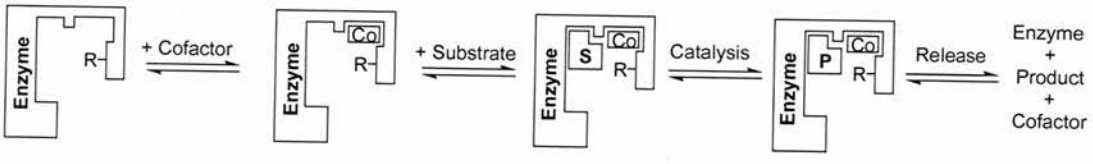

Figure 52: Schematic representation of an enzyme binding a cofactor and associating with the substrate. **S** and **P** represent the substrate and product, respectively. **Co** and **R** correspond to the cofactor and the reactive group of the enzyme. Taken from Ref. 202.

3.2 ABC Methodology

AB methodology, described in the previous Chapter, relies on the use of recognition sites located on two reacting entities allowing the formation of an [**A•B**] reactive complex. Thus, the reaction becomes *pseudo*-intramolecular, allowing rate acceleration and regio- and/or stereochemical control of the reaction. Within the Philp group a system has been developed which incorporates the recognition features of an AB system and with the added possibly of achieving catalytic turnover, this model is termed the ABC-mediated reaction pathway **(Scheme 63)**. In this model, recognition sites are once again located upon reactive partners **A** and **B**, however, they are not complementary to each other, but rather, are complementary to the recognition features incorporated into a third molecule, the cofactor **C**. Recognition between the three species can result in the formation of a reactive [**A•B•C**] complex. The formation of this complex renders the reaction between **A** and **B** effectively *pseudo*-intramolecular. Therefore, in an analogous fashion to AB complex reactions, significant rate

acceleration may be achieved by utilizing this methodology. As the reactive functionalities are held in a specific orientation with respect to one another, stereo- and/or regiochemical control of the reaction may also be possible. ABC-mediated reactions also have the potential to accomplish catalytic turnover. On completion of the bond forming reaction, there are two possible outcomes for the reaction cycle; (i) cofactor remains bound to the product (product inhibition) or, (ii) on completion of the reaction the cofactor is released back into solution, turnover is observed, catalysis has been achieved.

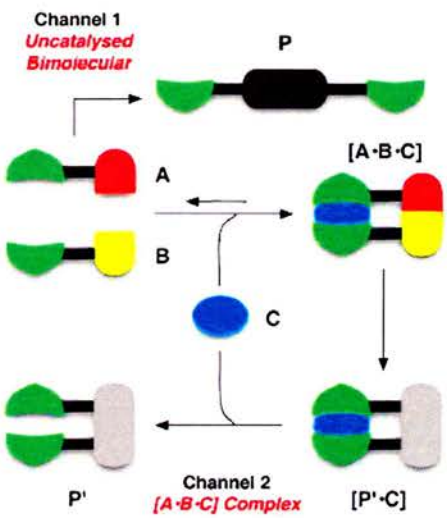

Scheme 63: Schematic representation of an ABC-mediated reaction pathway. Green and blue blocks represent the recognition sites, red and yellow blocks represent the reactive sites and the blue block represents the cofactor molecule.

3.3 Previously Studied ABC systems

In 2001, Philp and co-workers reported[203] a simple ABC system based upon the association between two benzo-15-crown-5 recognition sites and a potassium cation, this system accelerated a base-promoted aldol reaction using ABC methodology. A more complex system was reported in 2002.[204] The study investigated the effect of cofactors **186-189 (Figure 53)** upon the reaction between diene **190** and dienophile **191 (Scheme 64)**. Cofactors **186-189** all contained two carboxylic acid groups, which could potentially hold amides **190** and **191** in the correct orientation for the Diels-Alder reaction between them to become *pseudo*-intramolecular **(Scheme 64)**.

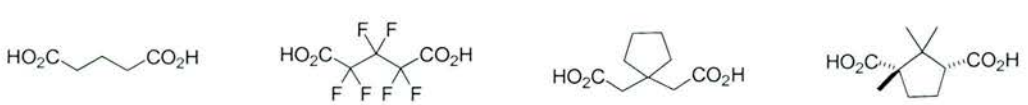

186 **187** **188** **189**

Figure 53: A variety of cofactor structures each with a glutaric acid core substructure.

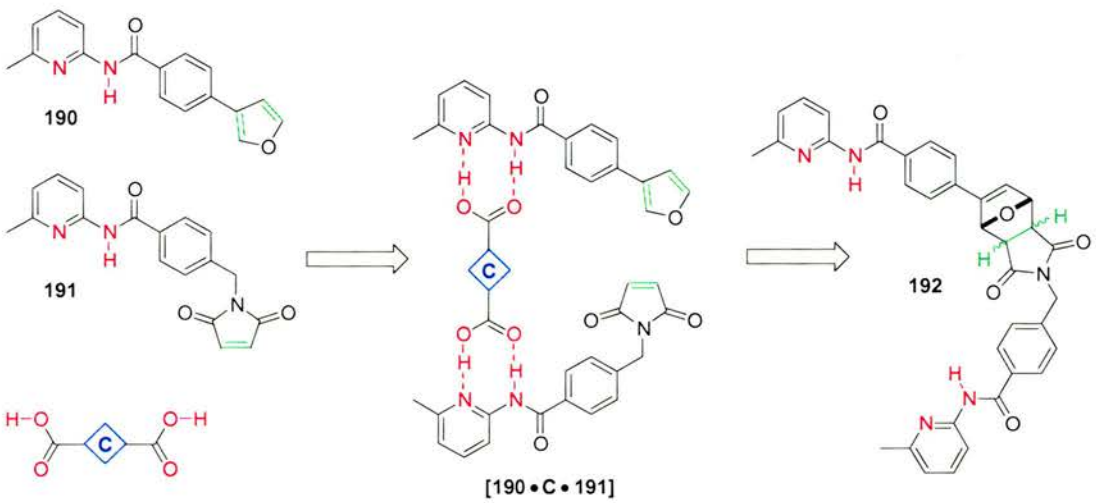

Scheme 64: Schematic representation of a Diels-Alder ABC-system.

Each cofactor **186-189** was tested to investigate what effect, if any, it had upon the rate of the reaction between diene **190** and dienophile **191**. Firstly, a control reaction was carried out in the absence of cofactor, with each starting reagent **190** and **191** at a concentration of 20 m*M*, in $CDCl_3$ at a temperature of 50 °C. The reaction was monitored by ^{1}H NMR spectroscopy over a period of 16 hours. On analysis of the ^{1}H NMR spectrum after 10 hours the *endo* and *exo* cycloadducts were present in a 1:1 ratio. Repeating the same reaction in the presence of glutaric acid **186** as cofactor, resulted in a large change in the *endo*:*exo* ratio and in the rate of reaction. The formation of the *exo* cycloadduct was enhanced by 80%, whereas, the formation of the *endo* cycloadduct was suppressed by 4%, compared with the control reaction. Cofactors **187-189** did not show similar activity. What was the reason for the difference in behaviour of cofactors **187-189** compared with cofactor **186**? The common structural feature within these non-reactive compounds was the addition of geminal non-hydrogen substitutents in the centre of the glutaric acid chain. Cofactor **193 (Figure 54)** was synthesised to investigate the effect of the presence of one substituent on the glutaric acid chain upon cofactor activity.

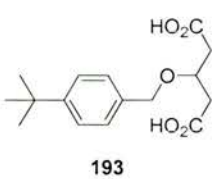

193

Figure 54: Cofactor **193**, 3-(4-t-butylbenzyloxy)pentanedioic acid.

The kinetic results obtained from the reaction between **190** and **191** in the presence of cofactor **193** gave a rate profile identical to the corresponding reaction with glutaric acid as cofactor. Once more, the *exo* cycloadduct was greatly enhanced and the *endo* cycloadduct suppressed. This result indicated that the system was tolerant of one substituent on the glutaric acid chain, but not two. Cofactor **193** also displayed greater solubility in comparison with glutaric acid. This increase in solubility can be attributed to the addition of the bulky *t*-butyl group. The system was studied further to assess the effect of varying the concentration of cofactor **193**. The reaction between **190** and **191** with 0.5 eq. of cofactor **193** resulted in a rate profile very similar to the profile obtained in the analogous reaction containing 1.0 eq. of cofactor **193**. Rate acceleration and diastereochemical control of the Diels-Alder reaction was also observed with only 0.1 eq. of cofactor **193**. These results[205] suggested that sub-stoichiometric amounts of cofactor **193** could induce a large change in the rate and the diastereochemical outcome of the Diels-Alder reaction, and indicated that the system was indeed catalytic.

3.4 A Dynamic ABC System

We wished to extend the previously conducted ABC methodology described in **Section 3.3** to encompass the theory of dynamic combinatorial chemistry. The library building blocks proposed for this study are shown in **Figure 55**.

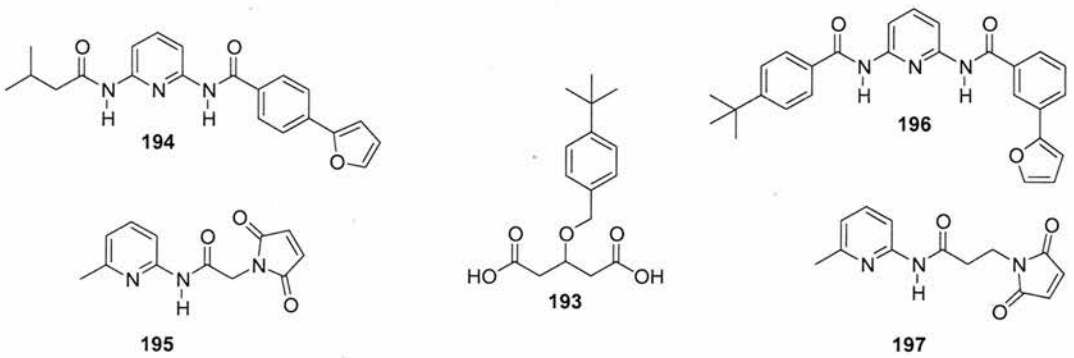

Figure 55: Library building blocks. Dienes **194** and **196**, dienophiles **195** and **197**, and cofactor **193**.

The Diels-Alder reaction would be used as the reversible reaction within the library. 2-Aryl furan amides **194** and **196** were chosen as a result of studies[183] previously conducted within the group on similar compounds. A recognition-mediated Diels-Alder reaction between a 2-aryl furan compound and a methyl protected maleimide **148** resulted in the reaction reaching 4% conversion. The analogous reaction containing carboxylic acid maleimide **125** was found to greatly enhance the rate and selectivity of the reaction *via* an AB-mediated pathway. We

therefore wished to determine whether 2-aryl furan compounds would also be suitable for use within ABC-mediated reactions. Diversity was incorporated into library members by varying both the carbon chain length on dienophiles **195** and **197**, and the position of the furyl diene moieties (*meta*- or *para*-substituted) upon dienes **194** and **196**. The previously successful hydrogen bond motif of carboxylic acid:2-amidopyridine was selected to provide the recognition within the system. It was hoped that the library would be under thermodynamic control, and therefore, the product which was the 'best fit' for the cofactor would be selected above other cycloadduct library members, in an approach analogous to the moulding strategy described by Lehn **(Section 1.5)**.

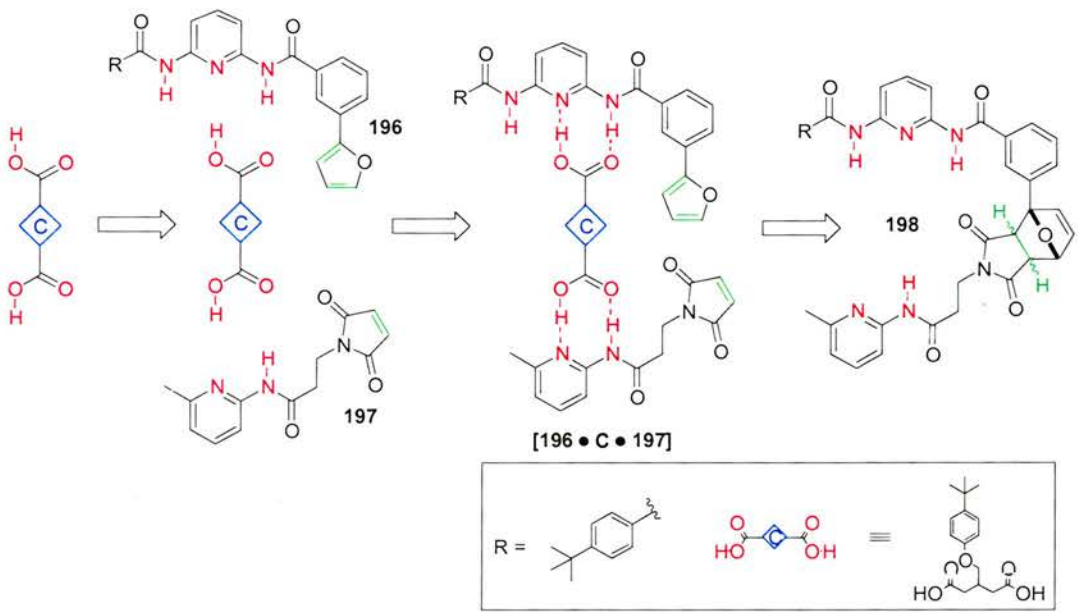

Scheme 65: A schematic representation of diene **196** and dienophile **197** assembling upon cofactor **193** and the resulting Diels-Alder reaction between the molecules.

Cofactor **193** has two carboxylic acid recognition groups. Dienes **194** and **196** and dienophiles **195** and **197** all contain amidopicoline recognition sites. Therefore, one could envisage cofactor **193** assembling diene **196** and dienophile **197** into a ternary complex [**196•C•197**], bound by hydrogen bonds between amidopicoline and carboxylic acid recognition sites **(Scheme 65)**. This binding event could render the subsequent Diels-Alder reaction between the diene and dienophile *pseudo*-intramolecular, leading to an increase in the rate of the reaction and the possibility of controlling the diastereochemical outcome of the reaction, as described in the previous section. As the Diels-Alder reaction can give rise to either *endo* or *exo* diastereoisomeric products, this small library can form a maximum of eight cycloadducts **(Figure 56)**.

It is hoped that the combination of ABC methodology with dynamic combinatorial chemistry will lead to the acceleration and control of the Diels-Alder reactions, leading to the production of one library member above all others.

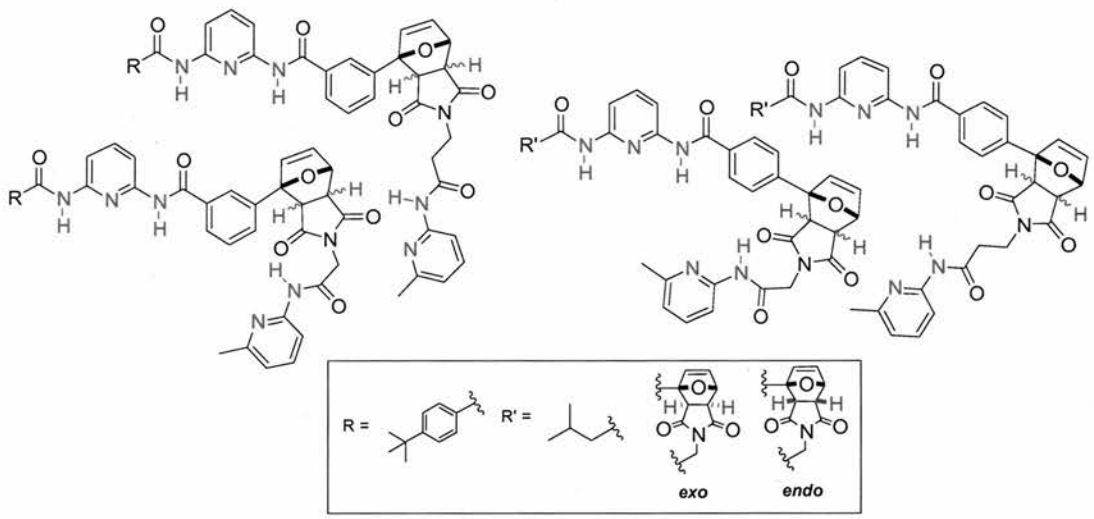

Figure 56: The eight possible Diels-Alder cycloadduct products which can result from the combination of diene **194** and **196** and dienophile **195** and **197** library members.

3.5 Synthesis of Library Building Blocks

3.5.1 Synthesis of Amides 194 and 196

Synthesis of amide **194** containing a diamidopyridine recognition sites and a diene furan moiety was undertaken in four steps **(Scheme 66)**.

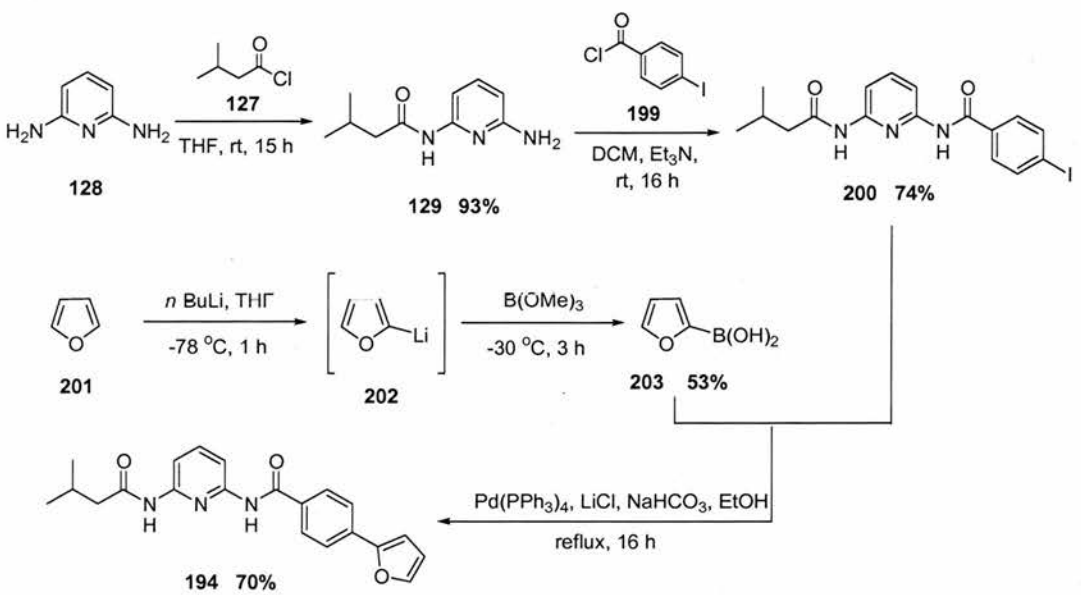

Scheme 66: Synthetic sequence for the production of amide **194**.

Amide **129 (Scheme 66)** was synthesised successfully as described previously **(Section 2.7.1)** in good yield. A further amine/acid-chloride coupling reaction was performed under standard conditions with 4-iodobenzoylchloride **199**. Amide **200** was obtained in 74% yield after purification by silica gel column chromatography. Boronic acid **203** was synthesised[206] from furan **201** *via* reaction with *n*-butyl lithium at -78 °C to yield intermediate **202**, subsequent reaction with trimethylborate at -30 °C, followed by an acidic work-up, afforded boronic acid **203** in 53% yield. Recognition amide **194** was prepared *via* a Pd^0 cross coupling reaction between aryl iodide **200** and boronic acid **203** using conditions developed by Suzuki,[207] subsequent purification on silica gel flash column, yielded desired amide **194** in 70% yield.

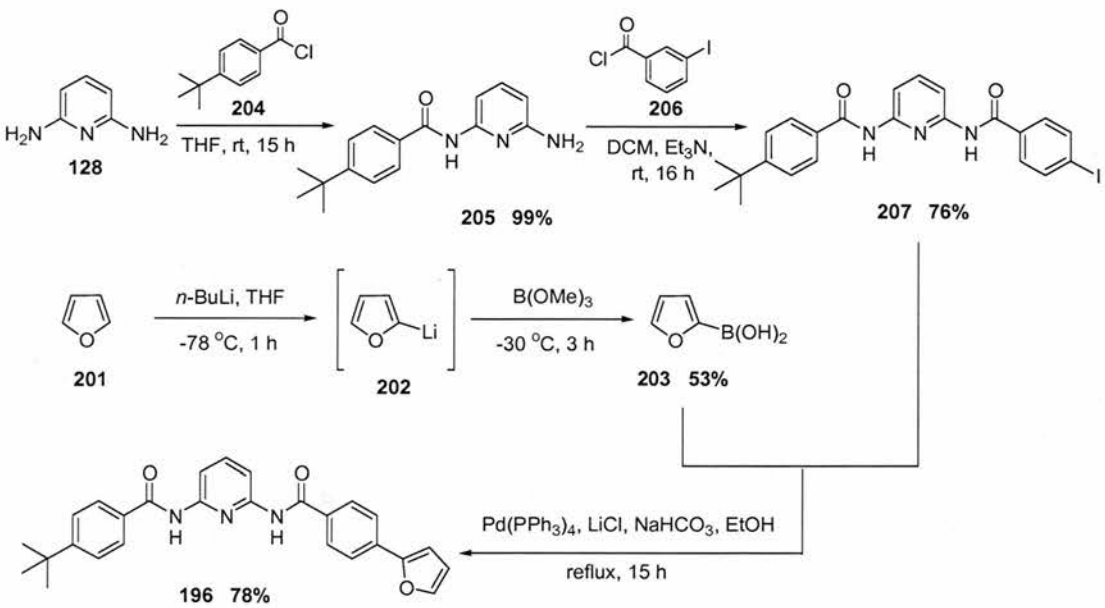

Scheme 67: Synthetic pathway for the production of amide **196**.

A further coupling reaction between amine **128 (Scheme 67)** and acid chloride **204** afforded amide **205** in 99% yield, after purification by silica gel column chromatography. Amide **205** was subsequently reacted with 3-iodobenzoyl chloride **206** to obtain amide **207** in good yield. Boronic acid **203** was synthesised[206] from furan **201** *via* lithiated intermediate **202**. The desired recognition amide **196** was prepared[207] *via* a Pd^0 cross coupling reaction between aryl iodide **207** and boronic acid **203** in 78% yield after purification on silica gel column.

3.5.2 Synthesis of Diacid Cofactor 193

Cofactor **193** was synthesised in an established three-step synthetic sequence **(Scheme 68)**. Trichloroacetimidate **210** was prepared[208] successfully *via* a two-stage base-catalysed condensation process.

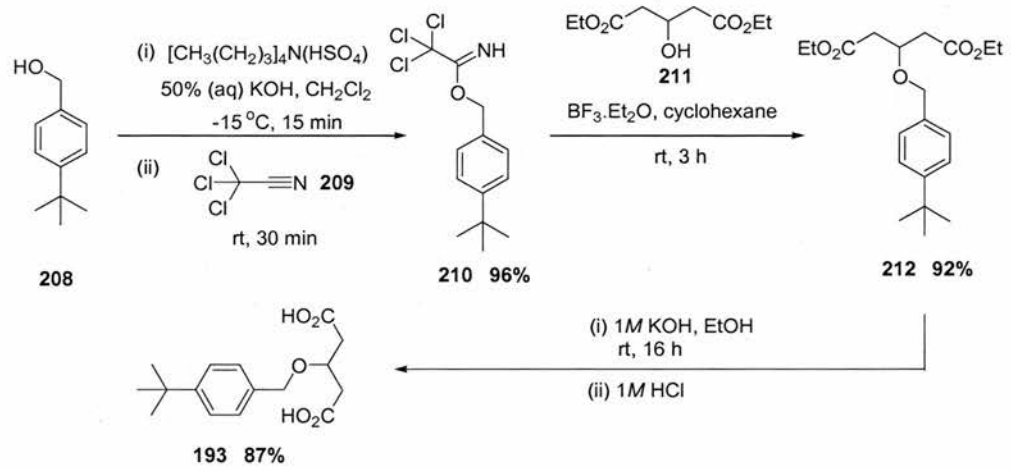

Scheme 68: Synthetic procedures for the preparation of carboxylic acid **193**.

Initially, aqueous potassium hydroxide and a catalytic amount of *tetra-n*-butylammonium hydrogen sulfate were added to 4-*tert*-butylbenzyl alcohol. After 15 minutes at -15 °C, trichloroacetonitrile was added, to yield the desired trichloroacetimidate **210** in 96% yield. Conversion[209] to the corresponding ether **212** was achieved 92% yield, through a Lewis-acid catalysed reaction with diethyl 3-hydroxyglutarate **211**. Diester **212** was hydrolysed under standard conditions to yield the desired diacid cofactor **193** in 87% yield after recrystallisation from from CH_2Cl_2/hexane.

3.5.3 Synthesis of Amides 195 & 197

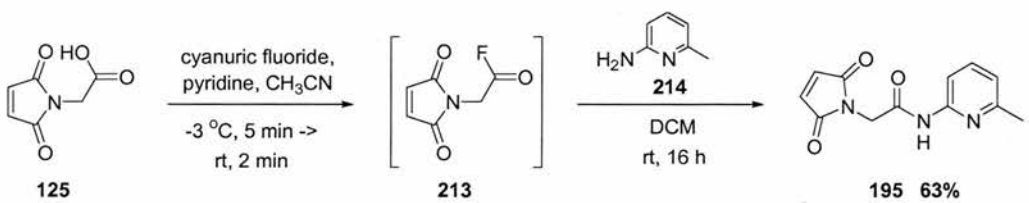

Scheme 69: Synthetic sequence for the production of 2-(2,5-dioxo-2,5-dihydro-pyrrol-1-yl)-*N*-(6-methyl-pyridin-2-yl)-acetamide **195**.

Amide **195** was synthesised in a one-pot reaction sequence **(Scheme 69)**. Maleimide **125** was first converted to the corresponding acid fluoride **213** with cyanuric fluoride. Reaction time

was crucial to the fluorination reaction, an increase in the reaction time led to the degradation of maleimide **125**. The organic phase was reduced *in vacuo* and 2-aminopicoline **214** added to the crude fluoride, the resulting reaction mixture was stirred for 16 hours. Target amide **195** was obtained in 63% yield over the two-step process after purification *via* flash column chromatography.

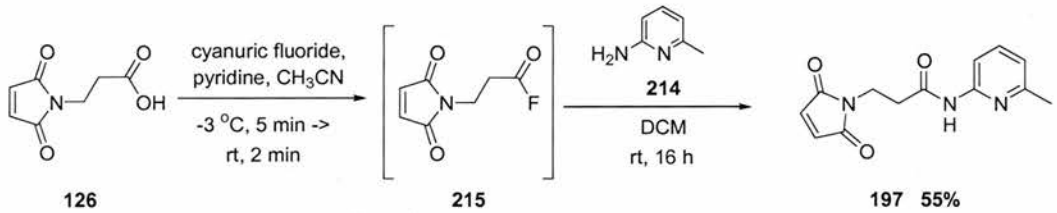

Scheme 70: One-pot synthetic procedure for the preparation of amide **197**.

Amide **197 (Scheme 70)** was synthesised in an analogous fashion to amide **195 (Scheme 69)**. Maleimide **126** was converted to amide **197** *via* fluoride intermediate **215**. Target amide **197** was obtained in 55% yield after purification by flash column chromatography.

3.6 The Reactivity of the Library

In order to determine whether cofactor **193** had any influence upon the equilibrium of the competing Diels-Alder reactions within the library **(Figure 55)**, four experiments were conducted;

(i) 1 eq. of each building block **194-197** (25 m*M*) at 25 °C
(ii) 1 eq. of each building block **194-197** (25 m*M*) with cofactor **193** (25 m*M*) at 25 °C
(iii) 1 eq. of each building block **194-197** (25 m*M*) at 50 °C
(iv) 1 eq. of each building block **194-197** (25 m*M*) with cofactor **193** (25 m*M*) at 50 °C

However, very little Diels-Alder product was detected by ^{1}H NMR spectroscopy after 16 hours. One explanation for the poor reactivity of the 2-aryl furan diene is as a result of the high level of π-conjugation which is disrupted in the formation of the cycloadduct **(Scheme 71a)**. These studies show the limitations of recognition-mediated reactions, similar compounds were previously shown to undergo recognition-mediated reactions *via* an AB pathway, however extending these studies to incorporate ABC methodology proved unsuccessful.

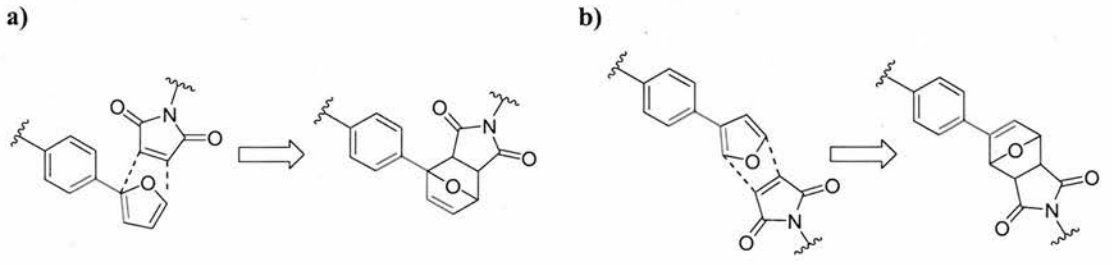

Scheme 71: **a)** The destruction of π-conjugation in the reaction between 2-aryl furyl dienes and maleimide dienophiles; **b)** The maintained level of π-conjugation in the reaction between 3-aryl furyl dienes and maleimide dienophiles.

This problem could be overcome using a 3-aryl furan derivative as π-conjugation is maintained in the formation of the corresponding 3-aryl furan cycloadduct **(Scheme 71b)**.

3.7 Revised Target Library

This revised library only differs from the system described previously, in the orientation of the furan moiety, substituting 2-furyl aryl diene compounds with 3-furyl aryl dienes which should exhibit greater reactivity **(Scheme 71)**. Once again, cofactor **193** has two carboxylic acid recognition groups, and dienes **216** and **217** and dienophiles **195** and **197** all contain amidopyridine recognition sites.

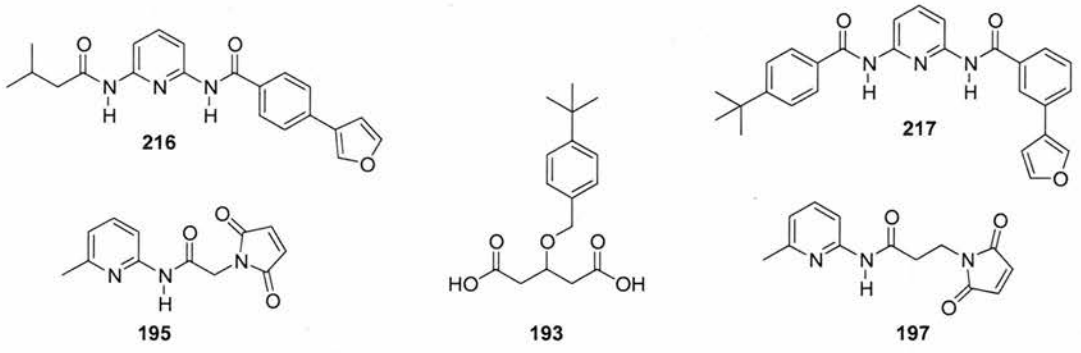

Figure 57: Revised library building blocks. Dienes **216** and **217**, dienophiles **195** and **197** and cofactor **193**.

Therefore, once again, one can envisage cofactor **193** assembling a diene and dienophile upon it, bound by hydrogen bonds between amidopicoline and carboxylic acid recognition sites **(Scheme 72)**. This binding event would render the subsequent Diels-Alder reaction between the diene and dienophile *pseudo*-intramolecular, leading to a possible increase the rate of the reaction and the influence upon the diastereochemical outcome of the reaction.

Our small library of building blocks **(Figure 57)** can, once again, result in a possible 8 cycloadduct products **(Figure 58)**. It is hoped however, that cofactor **193** will act in such a way to stabilise one product or the transition-state of one product, resulting in the amplification of a single cycloadduct library member.

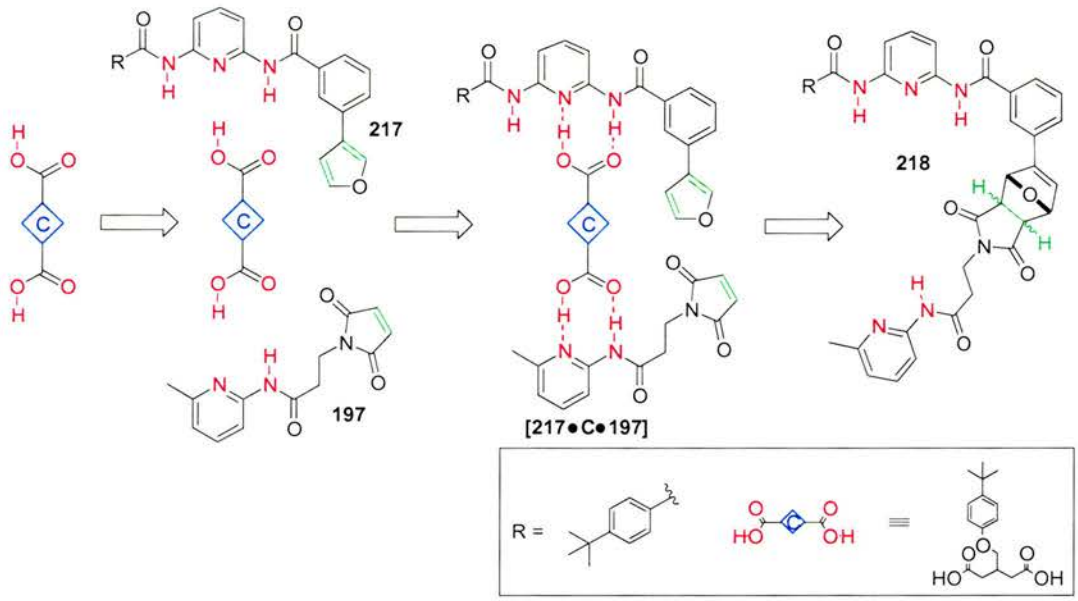

Scheme 72: A schematic representation of a diene **217** and dienophile **197** assembling upon a cofactor molecule **193**, and the resulting Diels-Alder reaction.

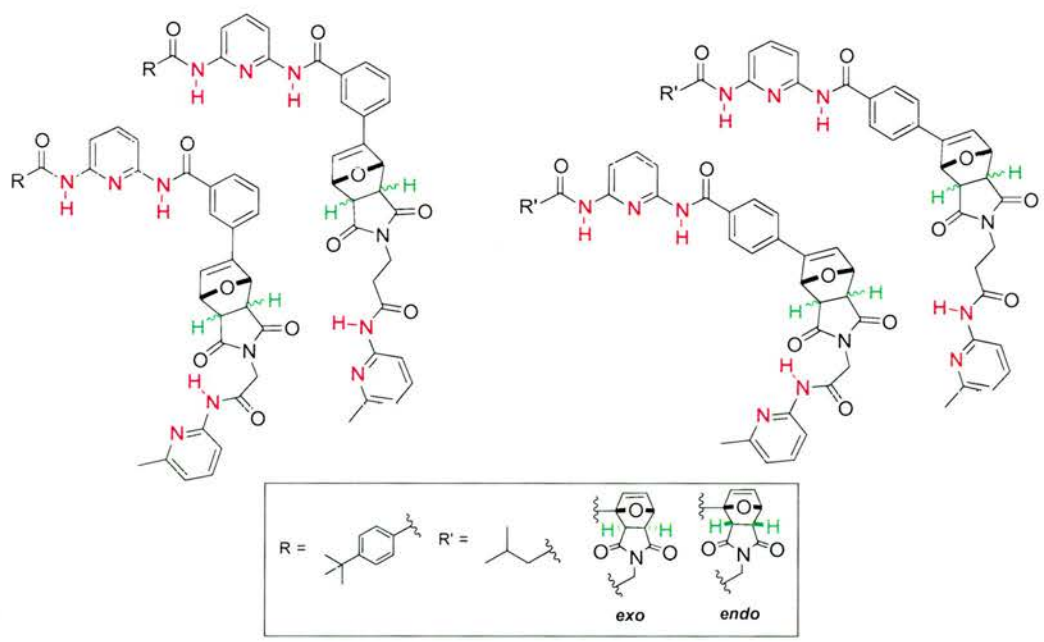

Figure 58: The eight possible Diels-Alder cycloadduct products which can result from the Diels-Alder reactions between dienes **216** and **217** and dienophiles **195** and **197**.

3.8 Synthesis of Amides 216 and 217

Recognition dienes **216** and **217** were synthesised in 5 steps **(Schemes 73 & 74)**. Amide **129** was synthesised as discussed previously **(Section 3.5.1)**. Boronic acid **221** was synthesised[206] from 3-bromofuran **219** *via* a lithium-halogen exchange reaction to yield intermediate **220**, addition of trimethylborate to the reaction mixture afforded boronic acid **221** in 46% yield after recrystallisation from Et_2O/hexane. Amide **216** was prepared *via* a Suzuki coupling reaction between aryl iodide **200** and boronic acid **221** in 74% yield after purification *via* silica gel flash column chromatography.

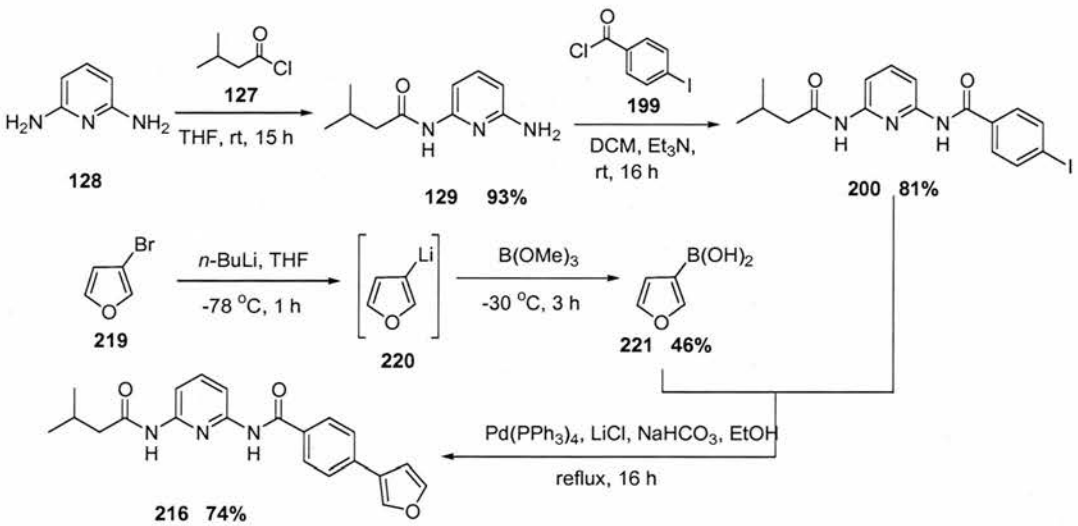

Scheme 73: Synthetic sequence for the formation of amide **216**.

Amide **207** was prepared as discussed previously in **Section 3.5.1**. Boronic acid **221** was synthesised[206] as discussed previously. Amide **217** was prepared *via* the Suzuki coupling reaction between aryl iodide **207** and boronic acid **221** in 78% yield after purification *via* silica gel flash column chromatography.

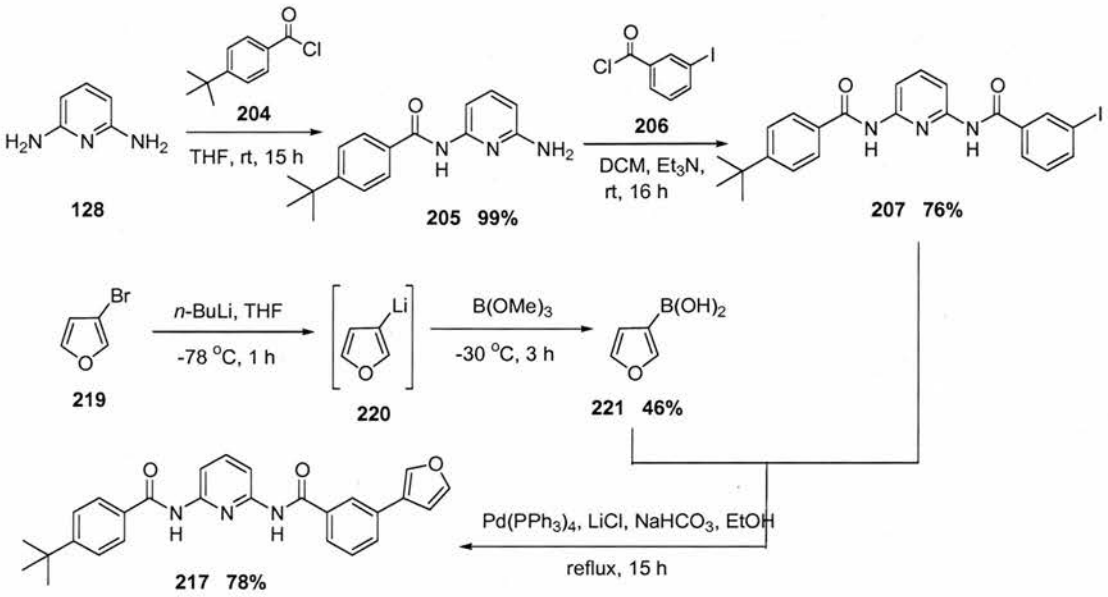

Scheme 74: Synthetic sequence for the production of amide **217**.

3.9 Kinetic Analysis of the System

3.9.1 Initial ^{1}H NMR Spectroscopic Studies

In order to determine whether cofactor **193** had any influence upon the equilibrium of the competing Diels-Alder reactions within the library **(Figure 57)**, four experiments were investigated;

(i) 1 eq. of each building block (25 m*M* in TCE) at 25 °C
(ii) 1 eq. of each building block with 1 eq. cofactor **193** (25 m*M* in TCE) at 25 °C
(iii) 1 eq. of each building block (25 m*M* in TCE) at 50 °C
(iv) 1 eq. of each building block with 1 eq. cofactor **193** (25 m*M* in TCE) at 50 °C

The solvent chosen for these studies was deuterated 1,1,2,2-tetrachloroethane ($Cl_2CDCDCl_2$, TCE). TCE was chosen for its non-polar characteristics and boiling point of 145 °C, rather than chloroform ($CDCl_3$), whose boiling point of 60 °C is very close to the temperature at which we wished to study our reactions (50 °C). Reactions were monitored by ^{1}H NMR spectroscopy over a period of two weeks. After 24 hours, differences were observed in the ^{1}H NMR spectra of samples with/without cofactor. The 'finger print' Diels-Alder bridgehead proton region (5-6 ppm) was decidedly simpler in the cofactor experiments. We decided to investigate whether the cofactor was selecting/enhancing the production of certain cycloadduct library members over others.

3.9.2 Conditions for Kinetic Studies

Before studying the full library, we first wanted to assess the effect, if any, that the cofactor had upon individual Diels-Alder reaction reactions. As little difference was apparent in the composition of the libraries at 25 °C and 50 °C **(Section 3.9.1)**, it was decided to monitor kinetic experiments at 50 °C in order to aid the retro Diels-Alder reaction, thus, facilitating dynamic conditions. Diene and dienophile initial concentrations were kept constant at 25 m*M*. Bimolecular rate data for each system was obtained by reaction of each diene and dienophile in the absence of cofactor **193**. Reactions were monitored by 500 MHz ^{1}H NMR spectroscopy. An identical reaction in which diacid cofactor **193** was added would allow the effect of recognition upon the rate and diastereochemical outcome of the reaction to be investigated.

3.10 Assignment of Diels-Alder Diastereoisomeric Products by ^{1}H NMR Spectroscopy

Before studying the Diels-Alder reactions *via* kinetic experiments it was important to determine the resonance patterns expected for the *exo* and *endo* products.

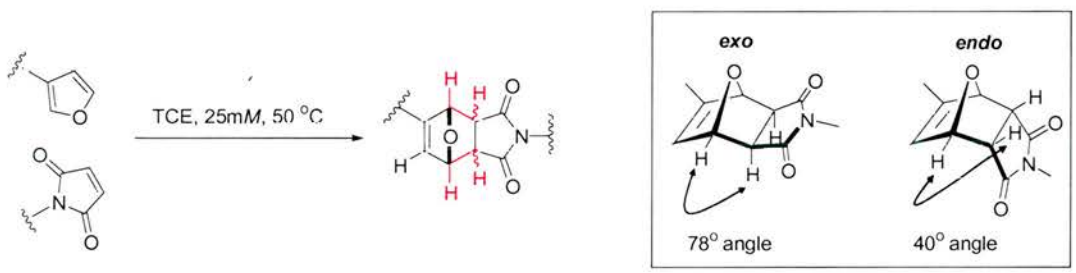

Scheme 75: The use of dihedral angles to assign diasteroisomeric Diels-Alder cycloadduct products.

The coupling between adjacent protons is strongly dependent upon the dihedral angle (H-C-C-H) between the two C-H bonds (shown in red, **Scheme 75**), this allows one diastereoisomer to be distinguished from another. For a three bond coupling, the size of the coupling constant ($^3J_{HH}$) is governed by the Karplus relationship.[210] The Karplus relationship states that the maximum $^3J_{HH}$ will occur when the dihedral angle is 0° or 180°, with 180° giving a larger coupling constant than 0°. The minimum coupling constant occurs when the dihedral angle is 90°. The dihedral angle in the *exo* cycloadduct was calculated at ~ 78°, thus, the $^3J_{HH}$ would be expected to be ~ 1 Hz. The *endo* adduct however, has a dihedral angle of ~ 40° and

therefore one would expect the $^{3}J_{HH}$ to be larger at ~ 5 Hz. Indeed, the bridgehead resonances can be clearly assigned for our diastereoisomeric Diels-Alder cycloadducts **(Figure 59)**.

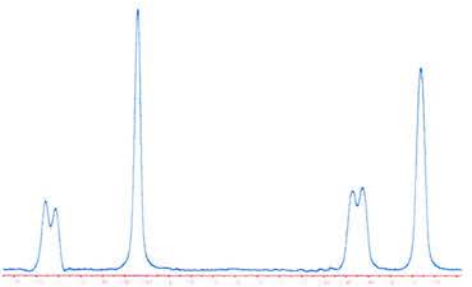

Figure 59: Partial 300 MHz ^{1}H NMR spectra showing the 'finger-print' Diels-Alder *endo* and *exo* regions. The *endo* adduct can be seen clearly as a doublet with a large *J* value, the *exo* adduct can be observed as an apparent singlet as the *J* value is small.

3.11 The Diels-Alder Reaction between Diene 216 and Dienophile 195 in the Absence and Presence of Cofactor 193

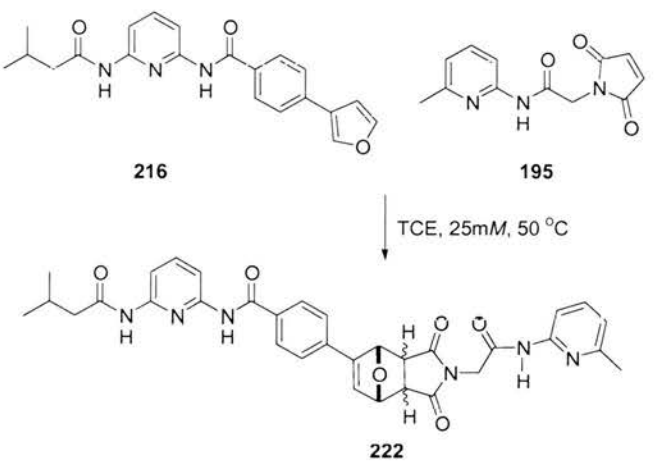

Scheme 76: The reaction conditions chosen to facilitate the Diels-Alder reaction between **216** and **195**.

Kinetic experiments were carried out in accordance with the procedure outlined in the general experimental section **(Chapter 6)**. The reaction mixture **(Scheme 76)** was monitored by 500 MHz ^{1}H NMR spectroscopy for 16 hours. The extent of reaction completion was determined using the deconvolution tool available in 1D WINNMR. The reaction between diene **216** and dienophile **195** at 50 °C and 25 m*M* of each reagent in TCE, led to the production of *exo*:*endo* cycloadducts in a 2:1 ratio of after 16 hours **(Figure 60)**.

a) b)

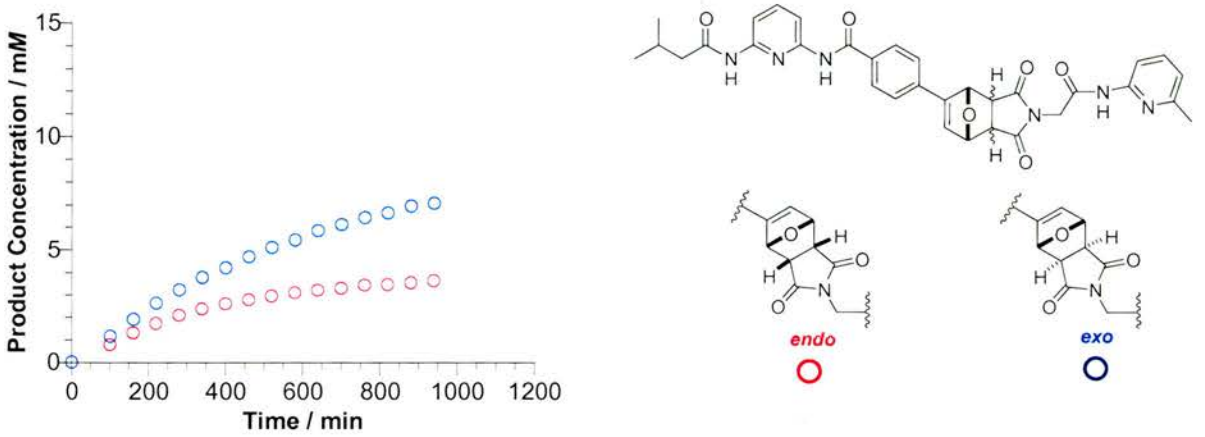

Figure 60: Rate profile for the reaction between **216** and **195** at 50 °C at 25 m*M* of each starting reagent. The resulting *endo* adduct product is depicted as open red circles and the *exo* adduct is depicted as open blue cicles.

In order to determine the rate constants for the bimolecular reaction, it was necessary to define a kinetic model that would describe the chemical pathways leading to the products. This kinetic model involves the reversible formation of the cycloadducts (*exo* and *endo*) from the reaction of the diene and dienophile **(Scheme 77)**.

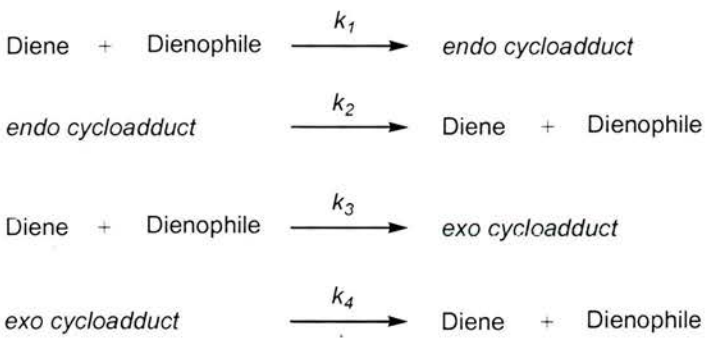

Scheme 77: A kinetic model for the bimolecular reaction between a diene and dienophile. k_1 and k_3 represent the forward rates resulting in the production of the *endo* and *exo* cycloadduct respectively, k_2 and k_4 describe the rate for the retro Diels-Alder reaction.

This model was used in conjunction with simulation and fitting package SimFit. SimFit is designed to simulate and fit experimental data by numerical integration of the appropriate differential rate equations as defined by a kinetic model, the programme allows the extraction of kinetic parameters from the observed rate profiles. **Figure 61a** shows the experimental data as open circles and the solid lines represent the fitted data. A good fit between experimental data and model, **(Figure 61a)** allowed the extraction of kinetic parameters from the observed rate profiles **(Figure 61b)**.

a)

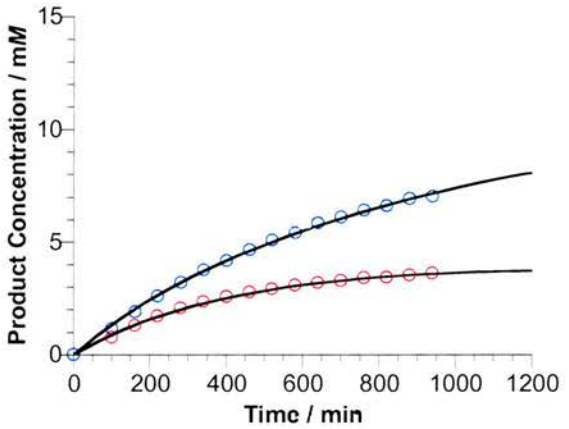

b)

cycloadduct	Control Reaction 216 + 195
endo	k_1 2.77 x 10^{-4} $M^{-1}s^{-1}$
	k_2 1.16 x 10^{-5} s^{-1}
exo	k_3 4.02 x 10^{-4} $M^{-1}s^{-1}$
	k_4 1.81 x 10^{-6} s^{-1}

Figure 61: **a)** Rate profile for the reaction between **216** and **195** at 50 °C at 25 m*M* in TCE of each starting reagent. The open blue circles represent the *exo* adduct, the open red circles represent the *endo* adduct. The solid black line represents the data obtained from fitting package SimFit. **b)** Table showing rate constant data for the bimolecular reaction between **216** and **195**.

The reaction between diene **216** and dienophile **195** in the presence of cofactor **193** was monitored by 500 MHz ^{1}H NMR spectroscopy (50 °C, 25m*M* initial concentration of each component in TCE). The reaction was followed over a period of 16 hours and the concentration of the two diastereoisomers formed was determined by deconvolution of the appropriate resonances **(Figure 62a)**.

a)

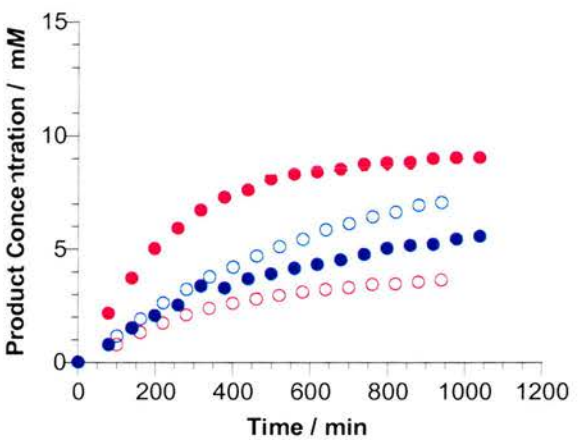

b)

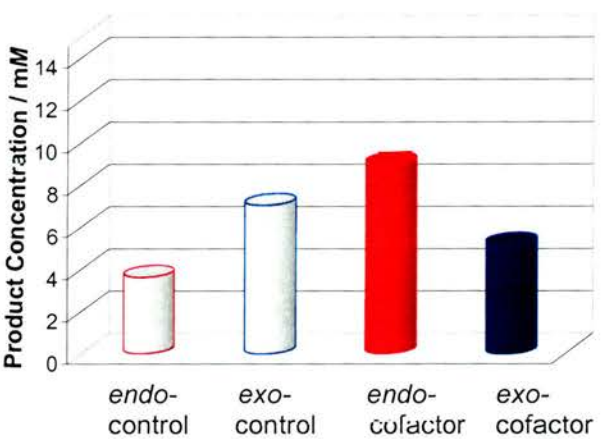

Figure 62: **a)** Bimolecular reaction data are shown as open circles, blue and red, *exo* and *endo* isomers respectively. The filled circles represent the reaction between **216** and **195** in the presence of cofactor **193** (*exo* - blue, *endo* - red), **b)** Distribution of products at 15 hours. Reactions with no cofactor are depicted as unfilled bars, outlined in red for the *endo* isomer and blue for the *exo* isomer. Filled bars represent the cofactor mediated reaction (red bars – *endo* isomer, blue bars – *exo* isomer).

In contrast to the bimolecular reaction, the *endo* cycloadduct is formed as the major isomer in a ratio of ~2:1 *endo*:*exo* cycloadduct **(Figure 62b)**, therefore, cofactor **193** has influenced the diastereochemical outcome of the reaction. The cofactor has enhanced the production of the *endo* adduct by 65% and suppressed the production of the *exo* adduct by 25%. In addition, it

can be seen that the cofactor has also led to an increase in the rate of production of the *endo* cycloadduct, suggesting that the reaction is recognition-mediated. In order to confirm whether the reaction between diene **216** and dienophile **195** was proceeding *via* an ABC complex mediated pathway **(Scheme 77)** we attempted to fit the observed rate data to the appropriate recognition-mediated kinetic model.

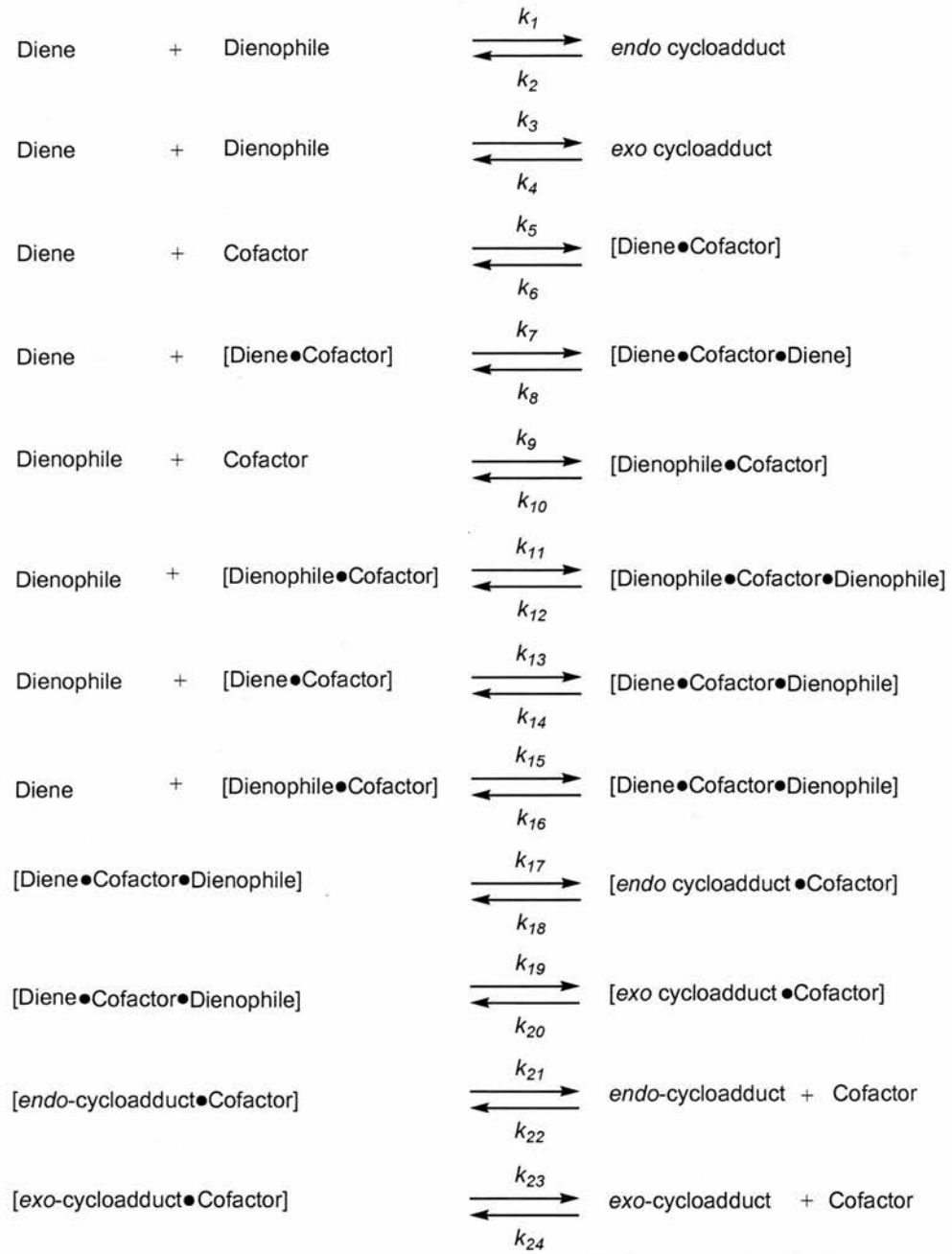

Scheme 78: Kinetic model for the cofactor-mediated *pseudo*-intramolecular reaction.

The model for an ABC system involves 24 rate constants **(Scheme 78)**, including the reversible formation of *exo* and *endo* cycloadducts as described in the simple bimolecular

reaction **(Scheme 77)**. Before calculating the rate constants for the *pseudo*-intramolecular reaction, it was necessary to define the association constant (K_a) for the association of an amidopyridine group with a carboxylic acid group. As complexes of this type are in fast exchange, we can assume that the rate, for example k_5, **(Scheme 78)**, is at the diffusion limit. The association constant for the complex can then be expressed as a ratio of the two rate constants.

3.12 Calculation of Association Constants, K_a

The association of building blocks **(Figure 57)** with the cofactor **193** were calculated *via* a series of binding studies, and the association constants, K_a, were determined using ^{1}H NMR spectroscopy titration methodology.[211] As cofactor **193** contains two acid functionalities, it can bind two molecules of amide **(Figure 63)**. It is therefore not possible to determine the value for one carboxylic acid and amidopyridine association; as a result, cofactor **193** was substituted with chloropropionic acid **223** for the subsequent binding studies.

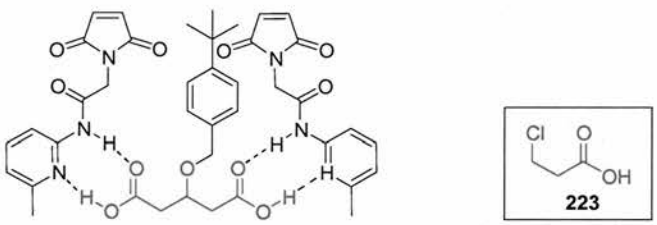

Figure 63: Representation of the binding motif of two amidopicoline units upon cofactor **193**, chloropropionic acid **223** mono-carboxylic acid substitute used for binding studies.

The concentration of amide **195** was kept constant at 10 m*M* and chloropropionic acid **223** concentration was varied between 1 m*M* and 50 m*M* at 50 °C in TCE. The shift in proton resonance (highlighted in blue, **Figure 64**) was monitored at each concentration of acid. On increasing the concentration of acid **223**, the fraction of bound amide **195** increased, shifting the proton resonance downfield.

The recorded data were then fitted using a non-linear curve fitting program, Solver, to provide an estimation of the association constant between acid **223** and maleimide **195**, a value of 264 M^{-1} was calculated.

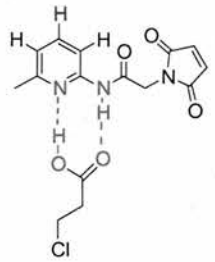

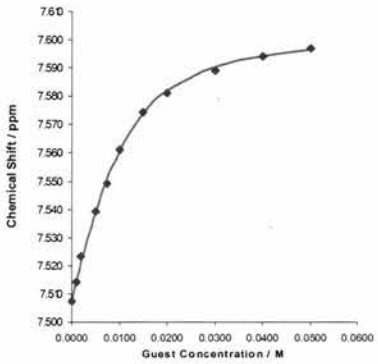

Initial Values:	
Δδ (sat)	0.098
[Amide Host] / *M*	0.010
Temperature / K	325
K_a / M^{-1}	264

Figure 64: Binding constant data for the association between amide **195** and chloropropionic acid **223**.

Following the same methodology as described above, the association constant for diene **216** with chloropropionic acid **223 (Figure 65)** was determined. However, on maintaining the concentration of amide **216** at 10 m*M* and varying the concentration of chloropropionic acid **223** between 1 m*M* and 50 m*M*, little change was detected in the resonances of the amide protons by 300 MHz ^{1}H NMR spectroscopy.

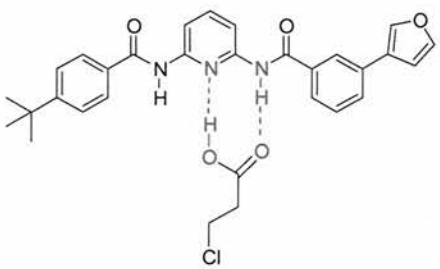

Figure 65: Association of diamide **216** and chloropropionic acid **223**.

In order to assess whether any binding event was occurring ^{13}C NMR binding studies were undertaken. Chemical shift changes were observed in the resonances for the pyridine ring C-H carbons. One carbon resonance was monitored whilst varying the concentration of acid **223**, the recorded data were fitted using the non-linear curve fitting program, Solver, to provide an estimation of the association constant between acid **223** and amide **216**. A K_a value of 34 M^{-1} was calculated.

The association constant for diene **216** containing a diamidopicoline recognition motif is far lower (K_a, ~ 40 M^{-1}) than the association constant for dienophile **195** (K_a, ~ 250 M^{-1}) containing an amidopyridine recognition motif. The very large difference in binding strength was somewhat surprising, we therefore decided to calculate the electrostatic potential energy

surfaces of our library amides. Semi-empirical molecular orbital (MO) calculations were performed using the PM3 Hamiltonion[212] as implemented in MOPAC 7.[213]

In order to analyse the electrostatic potential energy (ESP) calculations we must first define the parameters which have been used to generate the results. The electrostatic potential at a given point (x, y, z) on a molecule is defined by the electrostatic potential energy between itself and an imaginary positively charged ion at the same location. The potential energy of the two charged particles depends upon the nature of their charges and the distance between them. The energy, *E*, can be expressed in the form of **Equation 7**, where Q_1 and Q_2 are the charges on the two particles and r is the distance between them.

$$E = \frac{Q_1 \times Q_2}{r}$$

Equation 7: Equation relating the potential energy of charged particles to the charges upon them Q_1 and Q_2 and the distance between them r.

Solving **Equation 7** when r is large, *E* tends towards zero, conversely, when the distance between the charges is small, the energy *E*, becomes larger. The energy is especially large when both charges are large, and conversely, is small, if the charges are small. As the ion has a positive charge, it will be attracted to electron-rich regions of the molecule, and be repelled by electron-deficient regions. Therefore, electron-rich regions usually have negative potentials and electron-deficient regions normally have positive potentials. Electrostatic potential energy maps use different colours to identify the different potentials. Atoms coloured red have a negative potential and those coloured blue a positive potential, intermediate potentials are assigned colours according to the colour spectrum as shown in **Figure 66**.

Figure 66: A representation of the colour gradient used within electrostatic potential energy maps in order to depict electron deficient and electron rich atoms.

ESP maps were calculated for dienes **216** and **217** which contain diamidopyridine recognition motifs the results are shown in **Figure 67**. The electron deficient amide moieties can be

clearly seen in blue. The pyridine nitrogen appears yellow and is therefore neither electron rich, nor electron poor.

The picture is very different for amidopicoline containing dienophiles **195** and **197 (Figure 68)**. The electron deficient amide N-H can, once again, be seen clearly in blue. However, in this case, the pyridine nitrogen can be seen in bright red, showing its electron rich character, indicating hydrogen bond accepting potential. The hydrogen bond accepting potential of the pyridine nitrogen is diminished in diamidopyridine containing dienes **216** and **217**. Was the reduction in electron deficiency in recognition-amides **216** and **217** as a consequence of the bulky amide tagging groups, or was it as a result of the additional –NH attached to the pyridine ring? In order to ascertain what was governing the observed effect an additional electrostatic potential map was generated for *N*-(6-amino-pyridin-2-yl)-4-furan-3-yl-benzamide **224**, **(Figure 69)** which is identical to dienes **216** and **217**, however, does not contain a bulky amide group.

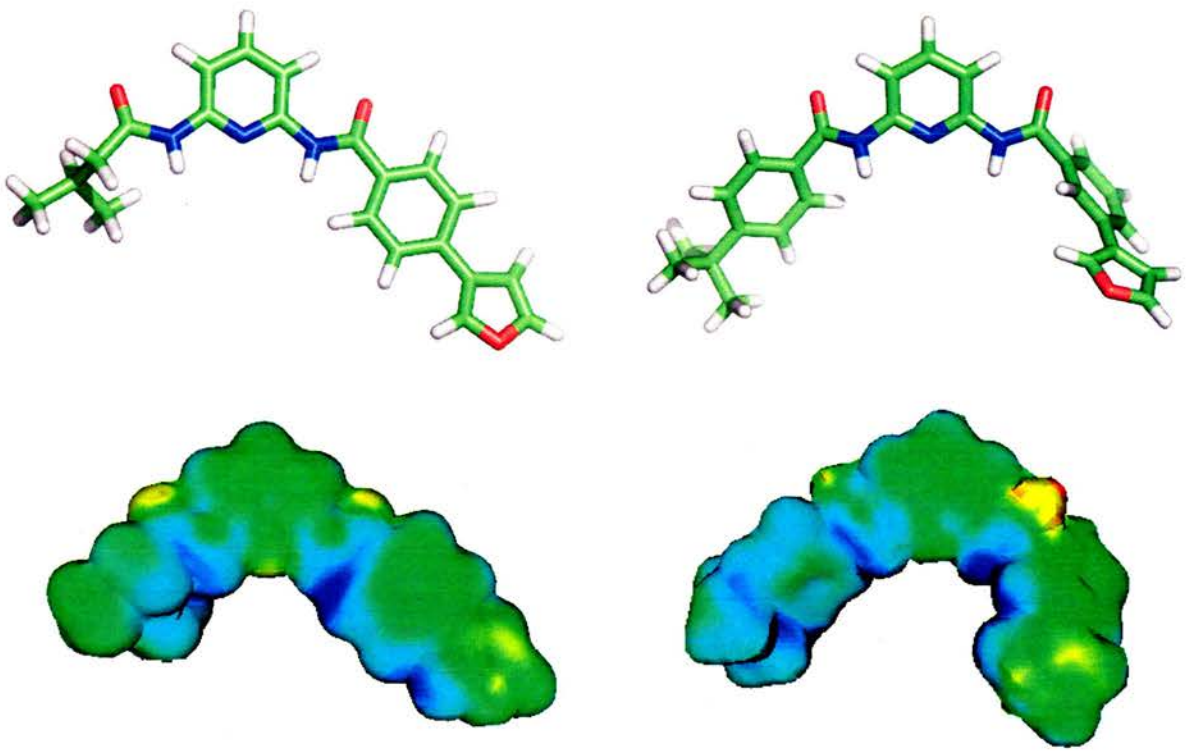

Figure 67: Electrostatic energy potential maps generated for dienes **216** and **217** containing diamidopyridine motifs. Blue regions indicated electron rich areas and red regions indicate electron deficient areas.

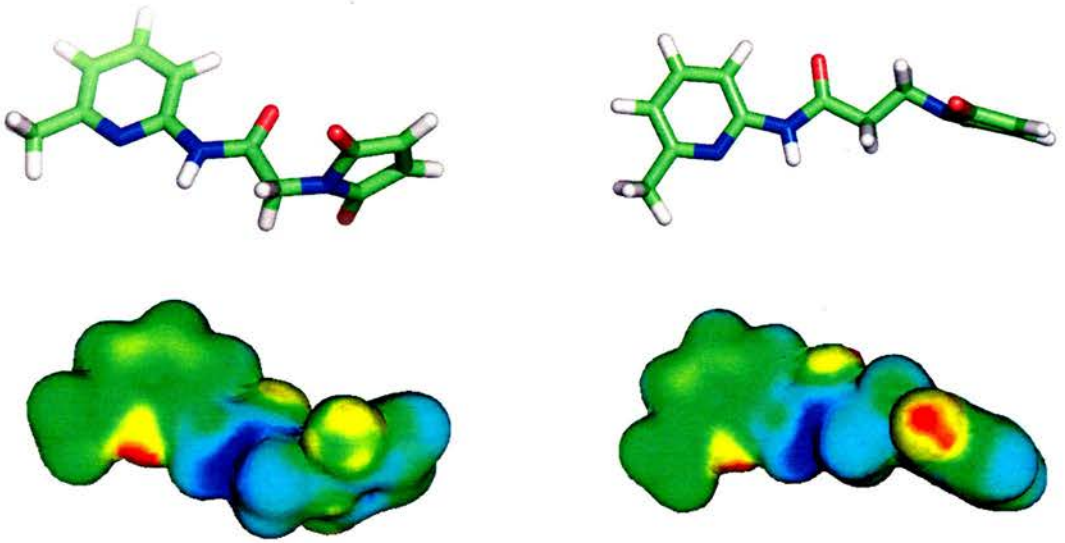

Figure 68: Electrostatic energy potential maps generated for diene **195** and **197** containing amidopyridine motifs. Electron rich areas are shown in blue and electron deficient areas are shown in red.

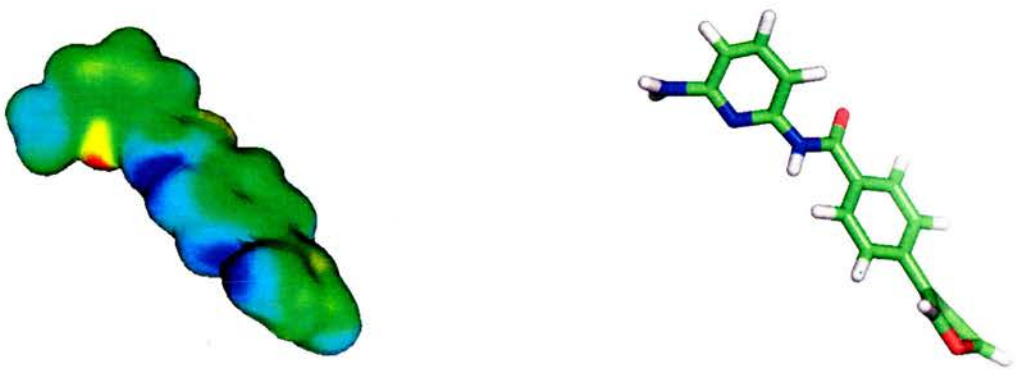

Figure 69: Electrostatic energy potential maps generated for amide **224** containing an amidopyridine motif and an amine moiety. Electron rich areas are shown in blue and electron deficient areas are shown in red.

The electrostatic potential map for amine **224** shows an electron density profile very different to that of the corresponding tagged molecule. In the case of amide **224**, the pyridine nitrogen appears red and is therefore electron rich. Therefore, we can conclude that the presence of the additional amide in molecules **216** and **217** results in the reduction in the electron accepting potential of the pyridine nitrogen, leading to a lower value for the association between carboxylic acid **223** and amides **216** and **217**.

Having calculated the association constants for the library members, these values were then entered into the kinetic model (k_5-k_{16}, **Scheme 78**), in conjunction with the bimolecular rate constant data calculated for reaction between diene **216** and dienophile **195** (k_1-k_4, **Scheme 78**). Thus, allowing the *pseudo*-intramolecular kinetic model to be fitted to the experimental data **(Figure 70a)**.

a) b)

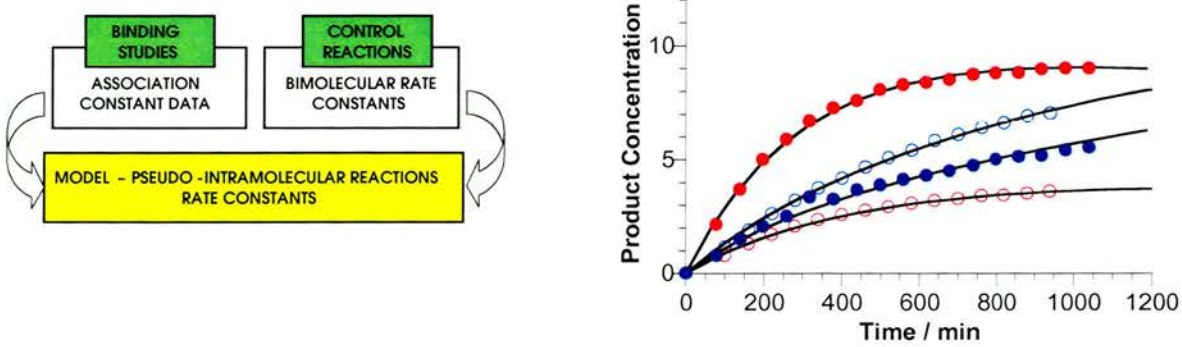

Figure 70: **a)** A cartoon representation of the parameters required in order to model a pseudo-intramolecular system, **b)** Rate profile for the reaction between **216** and **195** with cofactor **193** (filled circles, red – *endo* cycloadduct, blue, *exo* cycloadduct) and without cofactor (open circles, red – *endo* cycloadduct, blue – *exo* cycloadduct). Fitted data are shown as solid lines.

The simulation gave an excellent fit (solid line, **Figure 70b)** to the experimentally determined rate profiles, enabling the rate constants for the *pseudo*-intramolecular reaction to be extracted. The rate constant data product by SimFit for the reaction between **216** and **195** in both the bimolecular process and recognition-mediated pathways allowed the kinetic and thermodynamic effective molarities for the system to be calculated **(Section 2.3)**.

Table 10: Rate constant data for the *pseudo*-intramolecular reaction between **216** and **195**, *kEM* and *tEM* values for both the *endo* and *exo* isomers.

cycloadduct	Recognition-Mediated Reaction 216 + 195	*kEM* / m*M*	*tEM* / m*M*
endo	k_{17} 1.76 x 10^{-4} s^{-1} k_{18} 1.71 x 10^{-5} s^{-1}	625	431
exo	k_{19} 5.71 x 10^{-5} s^{-1} k_{20} 2.45 x 10^{-7} s^{-1}	142	1049

The EM figures calculated are shown in **Table 10**. The *endo* cycloadduct has a higher *kEM* (625 m*M*) compared with the *exo* cycloadduct (142 m*M*). The *endo* cycloadduct is produced preferentially in the initial stages of the reaction as a result of cofactor **193** pre-organising the reactants at the transition state. As time progresses the kinetic data suggests that the *exo* cycloadduct should prevail as a consequence of the high *tEM* value calculated (1049 m*M*). The effect of varying carbon spacer length on dienophile **195** upon the rate and selectivity of the Diels-Alder reaction with diene **216** was next investigated.

3.13 Diels-Alder Reaction between Diene 216 and Dienophile 197 in the Absence and Presence of Cofactor 193

The bimolecular rate data for the system were obtained by reaction of diene **216** with dienophile **197** in the absence of cofactor **(Scheme 79)**. The reaction between 25 m*M* of **216** and **197** in $CDCl_3$ at 50 °C leads to the production of the *exo* cycloadduct in 6.3 m*M* and the endo cycloadduct in 3.6 m*M* after 16 hours. Once again, the data were fitted to a bimolecular rate profile **(Scheme 77)** using the fitting package SimFit. A good fit was obtained between the experimental data and fitted data (solid line, **Figure 71**), allowing bimolecular rate constants k_1 to k_4 to be calculated **(Table 11)**.

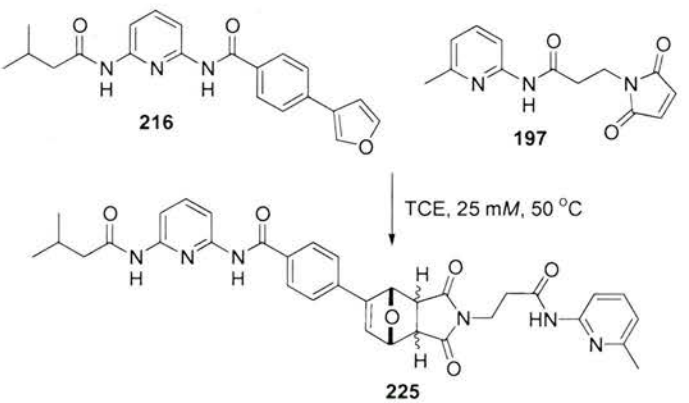

Scheme 79: Reaction conditions for the reaction between **216** and **197** resulting in the production of Diels-Alder cycloadduct product **225**.

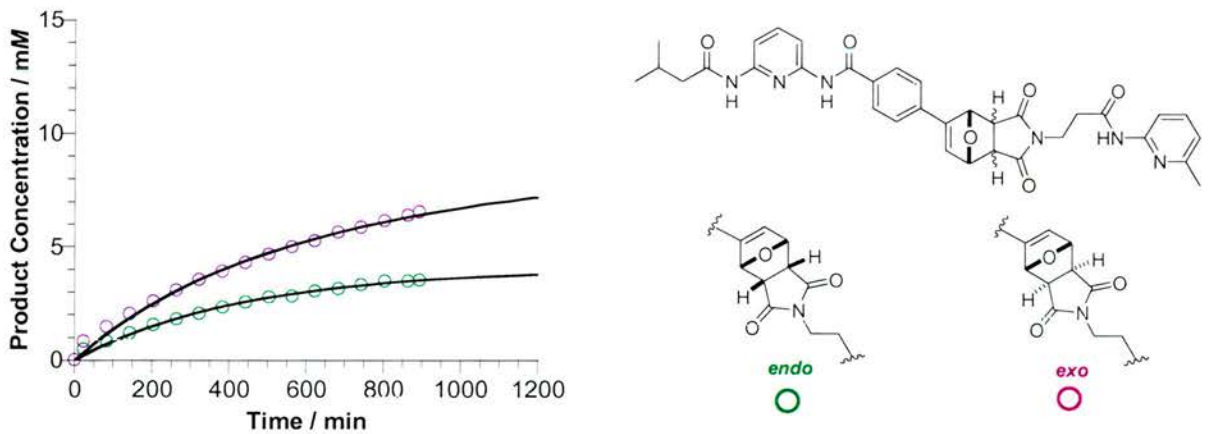

Figure 71: Rate profile for the reaction between **216** and **197** at 50 °C at an initial concentration of 25 m*M* of each starting reagent. The *endo* adduct is shown as green open circles, the *exo* adduct is shown as purple open circles. Fitted data are presented as a solid lines.

Table 11: Rate constant data for the bimolecular reaction between **216** and **197**.

cycloadduct	Control Reaction 216 + 197
endo	k_1 2.56 x 10^{-4} $M^{-1}s^{-1}$
	k_2 9.74 x 10^{-6} s^{-1}
exo	k_3 4.09 x 10^{-4} $M^{-1}s^{-1}$
	k_4 5.59 x 10^{-6} s^{-1}

The effect of cofactor **193** upon the reaction between diene **216** and dienophile **197** was studied at 50 °C and 25m*M* of each component in TCE. The reaction was followed over a period of 16 hours and the concentration of each diastereoisomer determined. The results **(Figure 72)** show that cofactor **193** has led to an increase in the rate of the reaction between **216** and **197**, suggesting that the reaction is recognition-mediated. In this case, cofactor **193** does not have any influence upon the diastereochemical outcome of the Diels-Alder reaction, the *exo* isomer predominates in both the control (no cofactor) and recognition-mediated reactions (with cofactor).

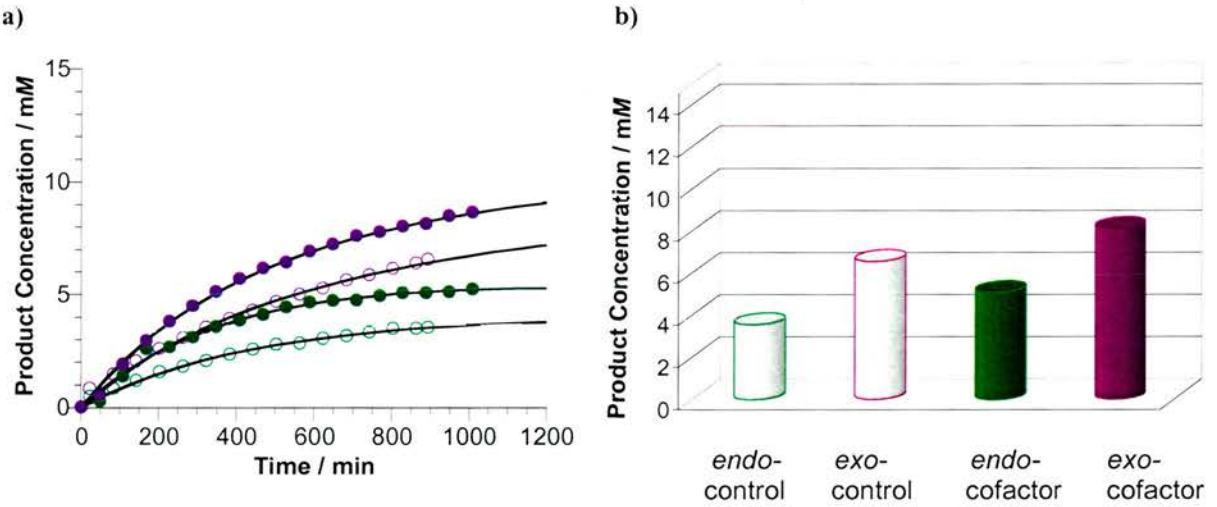

Figure 72: **a)** Rate profile for the reaction between **197** and **216** at 50 °C. Data for the bimolecular reaction are shown as open circles (*endo*-green, *exo*-purple). Data for the cofactor-mediated reaction are depicted as filled cicles (*endo*-green, *exo*-purple), **b)** Bar graph depicting the distribution of products at 15 hours. Data for the bimolecular reaction are shown as unfilled bars, outlined in green for the *endo* cycloadduct and purple for the *exo* cycloadduct. The cofactor-mediated reaction data are shown as filled in green for the *endo* cycloadduct and purple for the *exo* cycloadduct.

Once again, kinetic modelling of the chemical reaction pathways was undertaken, and rate constant data extracted. Effective molarities were calculated using the bimolecular and cofactor-mediated rate constant data **(Table 12)**. The effective molarities generated for this

system suggest that transition-state stabilisation is the main factor governing the moderate effect of cofactor **193** upon the reaction between **216** and **197**.

Table 12: Rate constant data for the cofactor mediated reaction between **216** and **197** and the *tEM* and *kEM* values calculated.

cycloadduct	Recognition-Mediated Reaction 216 + 197	*kEM* /m*M*	*tEM* / m*M*
endo	k_{17} 7.83 x 10^{-5} s^{-1}	288	163
	k_{18} 1.83 x 10^{-5} s^{-1}		
exo	k_{19} 1.02 x 10^{-4} s^{-1}	249	148
	k_{20} 9.46 x 10^{-6} s^{-1}		

The effect of varying the spacer chain length on the dienophiles had led to a striking change in the diastereochemical outcome of the reaction with diene **216**. On reaction of diene **216** with dienophile **197** which contains a one carbon chain spacer unit, the *endo* cycloadduct product is formed preferentially over the 16 hour monitoring period. Conversely, the reaction of diene **216** with dieneophile **197** which contains a two carbon chain spacer unit, produces the corresponding *exo* cycloadduct in greater concentration over 16 hours. Our next set of kinetic data relates to the variation in furyl diene moiety orientation from the *para* to the *meta* position.

3.14 The Diels-Alder Reaction between Diene 217 and Dienophile 195 in the Absence and Presence of Cofactor 193

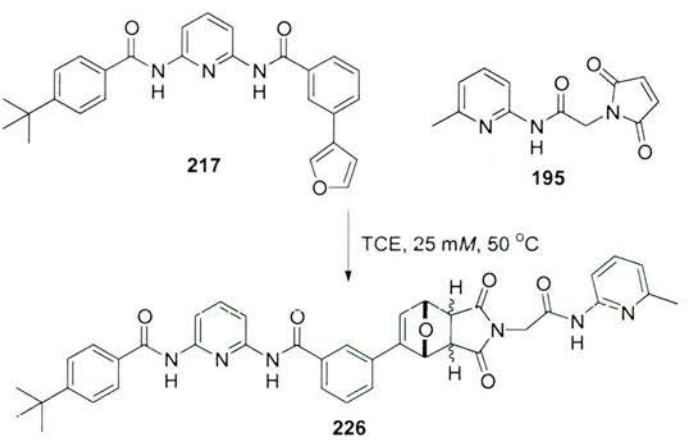

Scheme 80: Diels-Alder reaction between **217** and **195**.

The bimolecular data for the system were obtained by reaction of diene **217** with dienophile **195** in the absence of cofactor **193 (Scheme 80)**. The reaction between **195** and **217** at 50 °C

and 25m*M* in TCE, led to the production of *exo*:*endo* cycloadducts in a ratio of ~ 1:1 **(Figure 73)**. When the identical reaction was carried out in the presence of cofactor **193** little change was observed in the rate profile of the reaction **(Figure 73)**.

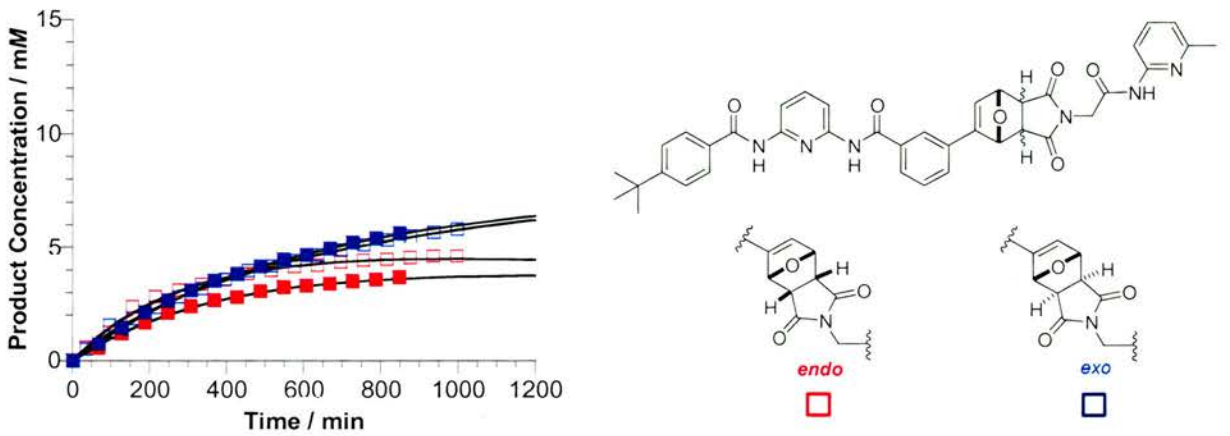

Figure 73: Rate profile for the reaction between **195** and **217** in the absence and presence of cofactor **193**. Bimolecular data are shown as open red squares for the *endo* cycloadduct and blue open squares for the *exo* cycloadduct. The data for the *pseudo*-intramolecular reaction are depicted as filled red squares for the *endo* cycloadduct and filled blue squares for the *exo* cycloadduct.

Table 13: Rate data for the reaction between **195** and **217**.

cycloadduct	Control Reaction 195 + 217
endo	k_1 4.99 x 10^{-4} $M^{-1}s^{-1}$
	k_2 2.40 x 10^{-5} s^{-1}
exo	k_3 3.91 x 10^{-4} $M^{-1}s^{-1}$
	k_4 7.53 x 10^{-6} s^{-1}

The rate constant data **(Table 13 & 14)** for the reaction between **217** and **195** in the absence and presence of cofactor gave effective molarities shown in **Table 14**. The effective molarities for this system are low, confirming the lack of a recognition-mediated effect.

Table 14: Rate constant data for the reaction between **195** and **217** in the presence of cofactor **193**, *kEM* and *tEM* values are presented.

cycloadduct	Recognition-Mediated Reaction 195 + 217	*kEM* / m*M*	*tEM* / m*M*
endo	k_{17} 4.95 x 10^{-5} s^{-1}	99	96
	k_{18} 2.45 x 10^{-5} s^{-1}		
exo	k_{19} 5.95 x 10^{-5} s^{-1}	152	64
	k_{20} 1.81 x 10^{-5} s^{-1}		

3.15 The Diels-Alder Reaction between Diene 197 and Dienophile 217 in the Absence and Presence of Cofactor 193

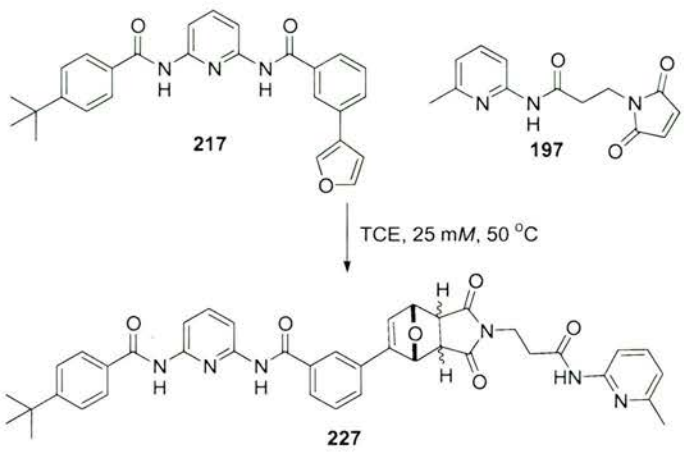

Scheme 81: Diels-Alder reaction between **217** and **197**.

The reaction between **217** and **197** at 50 °C and 25m*M* in TCE **(Scheme 81)**, led to the production of ~ 5 m*M endo* and ~ 5 m*M exo* cycloadduct **218** after 16 hours **(Figure 74)**. The reaction data was successfully fitted to a bimolecular kinetic model and the rate constants for the production of each diastereoisomer were calculated **(Table 15)**.

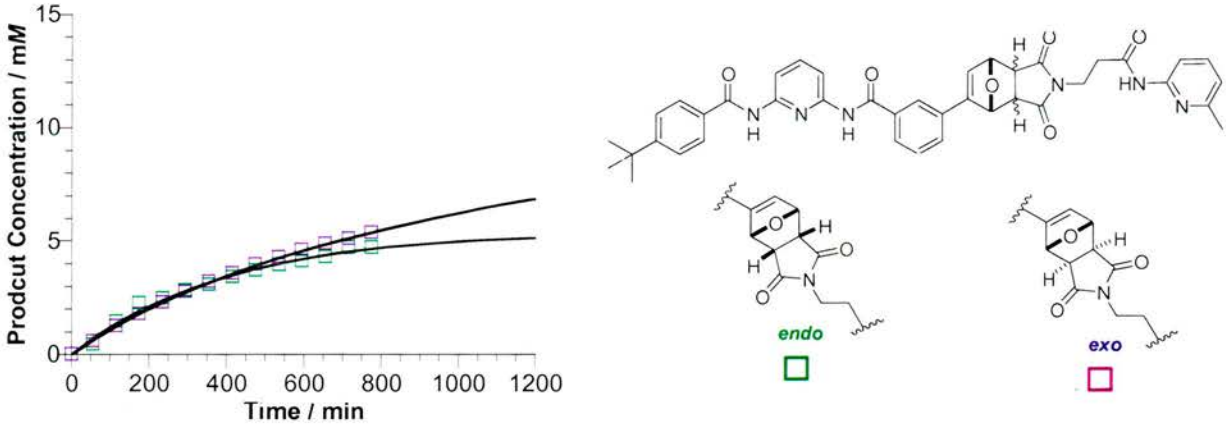

Figure 74: Rate profiles for the reaction between **217** and **197** over 16 hours. The *endo* cycloadduct is depicted as open green squares and the *exo* cycloadduct as open purple squares.

When the reaction between **217** and **197** is modified to incorporate cofactor **193** a large increase in the rate of production of *exo* cycloadduct was observed. On fitting the reaction data to a *pseudo*-intramolecular kinetic model, a good fit was obtained, allowing the rate constants for the reaction to be generated. On analysing the kinetic rate profiles **(Tables 15** &

16) of the bimolecular and cofactor-mediated reaction, kinetic and thermodynamic effective molarity data were extracted **(Table 16)**.

Table 15: Rate constant data for the bimolecular reaction between **217** and **197**.

cycloadduct	Control Reaction 217 + 197
endo	k_1 3.73 x 10^{-4} $M^{-1}s^{-1}$
	k_2 1.07 x 10^{-5} s^{-1}
exo	k_3 3.30 x 10^{-4} $M^{-1}s^{-1}$
	k_4 7.48 x 10^{-7} s^{-1}

It is apparent that the large amplification observed for the *exo* cycloadduct is a kinetic effect. The cofactor serves to stabilise the reactants at the transition state, holding them in a specific orientation in order to allow the reaction between them to occur in a *pseudo*-intramolecular fashion, and thus, diastereochemical control of the reaction is achieved. Cofactor **193** enhances the production of the *exo* diastereoisomer by 85% and suppresses the production of the *endo* isomer by 25%.

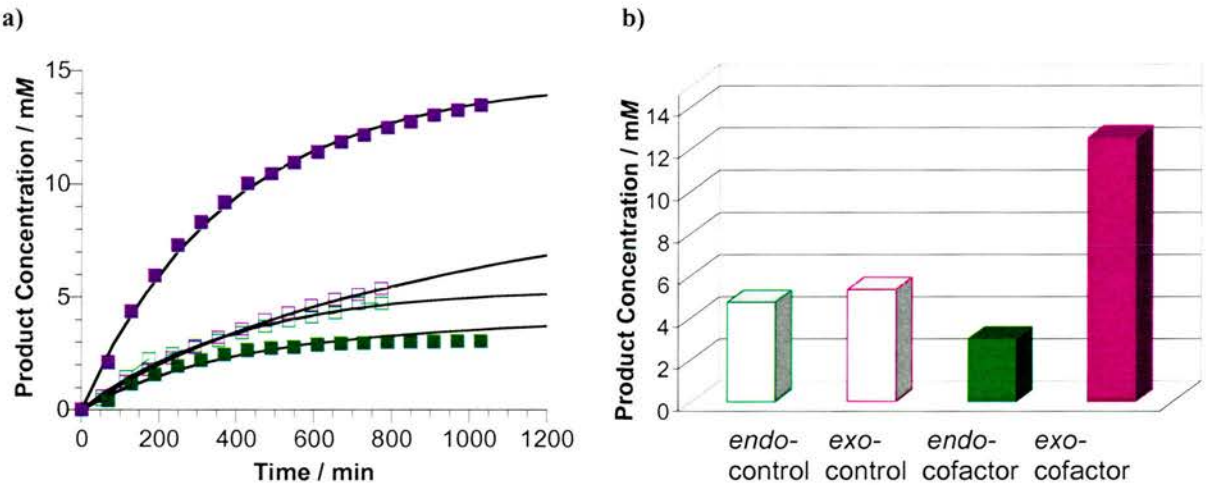

Figure 75: **a)** Rate profile for the recognition mediated reaction between **217** and **197** in the presence of cofactor **193**. Bimolecular data are shown as open squares (*endo* cycloadduct, green; *exo* cycloadduct, purple). Cofactor mediated data are shown as filled squares (*endo* cycloadduct, green; *exo* cycloadduct, purple).

Table 16: Rate constant data for the pseudo-intramolecular reaction between **217** and **197**, and the *tEM* and *kEM* values for both cycloadducts.

cycloadduct	Recognition-Mediated Reaction 217 + 197	*kEM* /mM	*tEM* / mM
endo	k_{17} 5.35 x 10^{-5} s^{-1}	143	115
	k_{18} 1.35 x 10^{-5} s^{-1}		
exo	k_{19} 2.08 x 10^{-4} s^{-1}	630	37
	k_{20} 1.28 x 10^{-5} s^{-1}		

Once again, a large effect has been observed on varying the spacer chain length on the dieneophiles. In the case of the reaction of diene **217** with dienophile **197** which contains a one carbon spacer unit, there is barely any effect induced by the addition of cofactor **193**. However, in the case of the cofactor-mediated reaction of diene **217** with dienophile **197** containing a two carbon spacer unit, the reaction clearly follows a recognition-mediated pathway.

The effect of varying the orientation of the furyl diene moiety on the rate and selectivity of the reaction should also be noted. The outcomes of the reactions between dienophile **195** with dienes **216** and **217** in the presence of cofactor **193** is somewhat different. In the case of reaction of dienophile **195** with *para*-substituted diene **216** the presence of cofactor **193** leads to the reaction following a recognition-mediated pathway. Thus, an increase in the rate and control of the diastereochemical outcome of the reaction was shown. The *endo* cycloadduct is favoured over the *exo* cycloadduct, the opposite diastereochemical outcome to the analogous bimolecular reaction. If however, the diene is substituted with the *meta*-amine **217** the reaction does not follow a recognition-mediated route, the reaction rate and diastereochemical distribution of products is very similar to that of the analogous bimolecular reaction.

The diastereochemical effect of varying the orientation of the diene upon the Diels-Alder reaction with dieneophile **197** containing a two carbon spacer is less prominent. Both the reaction of diene **216** and diene **217** with dienophile **197** result in the recognition-mediated formation of the *exo* cycloadduct product. However, the extent to which the reaction rate is influenced is considerable, *meta*-dienophile **217** is moderately accelerated *via* a pseudo-intramolecular reaction pathway, whereas dienophile **216** is considerably accelerated through an ABC-mediated pathway (*kEM* = 630 m*M*).

The minor structural variations between library members **195, 197 & 216, 217** leads to large differences in both the rates and diastereochemical outcomes of the Diels-Alder reactions between them, it is this selectivity for cofactor **193** which we hope to exploit within a dynamic library situation.

3.16 Library Simulation

The kinetic data calculated in **Sections 3.11** and **3.13-3.15** describes data collected over a period of 16 hours. It is unfeasible to monitor reactions over long periods of time *via* 500 MHz ^{1}H NMR spectroscopy. However, it would be advantageous to simulate the evolution of library members over longer periods of time. Work has recently been conducted[72-74] by two research groups on the limits of dynamic combinatorial libraries *via* predictive modelling packages. We proposed to use the rate constants previously calculated in conjunction with the simulation package available within SimFit to predict the outcome of reactions between a library of interacting and reacting species. Rate constant data derived for each diene (**216** & **217**) and dienophile (**195** & **197**) in the presence and absence of cofactor **193** were entered into the isosim simulation package within SimFit. Predicted data were simulated using the kinetic profiles derived from the previous eight kinetic experiments **(Sections 3.11, 3.13-3.15)** in conjunction with the association data (K_a) determined by ^{1}H/^{13}C NMR titration experiments **(Section 3.12)**. These parameters **(Scheme 82)** were entered into a model for competition experiments between the two dienes **216** and **217** and one dienophile **195** or **197**. The isosim program uses rate constant data, association constant data and the initial concentrations of library components to predict the evolution of the reacting species over a specified time period.

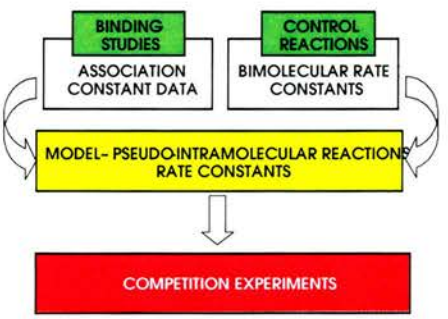

Scheme 82: A cartoon depiction of the data required to model a competition experiment over a period of days.

3.17 Competition Experiment with Dienes 216 and 217 and Dienophile 195 in the Absence and Presence of Cofactor 193

A kinetic simulation was run for the reaction between dienes **216** and **217** with dienophile **195** **(Scheme 83)**. The results from this competition experiment simulation over a ten day period in shown in **Figure 76a**.

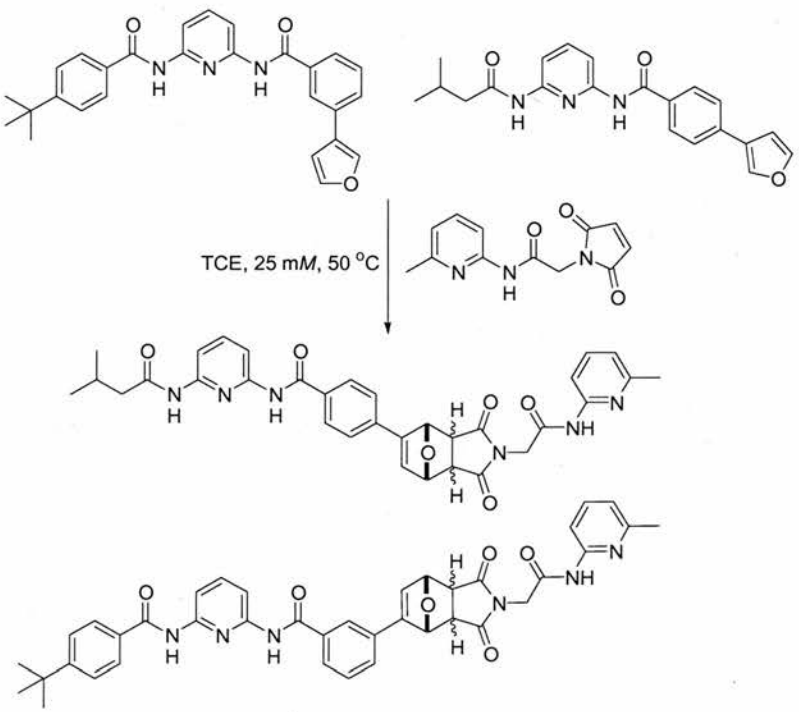

Scheme 83: Competition experiment where dienes **216** and **217** compete for building block **195**.

In order to determine whether the predicted data were correct, competition experiments were conducted on an NMR scale. Components **195**, **216** and **217** were reacted together at 50 °C at an initial concentration of 25 m*M* of each building block in TCE, the library was monitored by ^{1}H NMR spectroscopy every day for a period of 10 days **(Figure 76b)**. It can be seen that the predicted data and experimental data give a similar distribution of products.

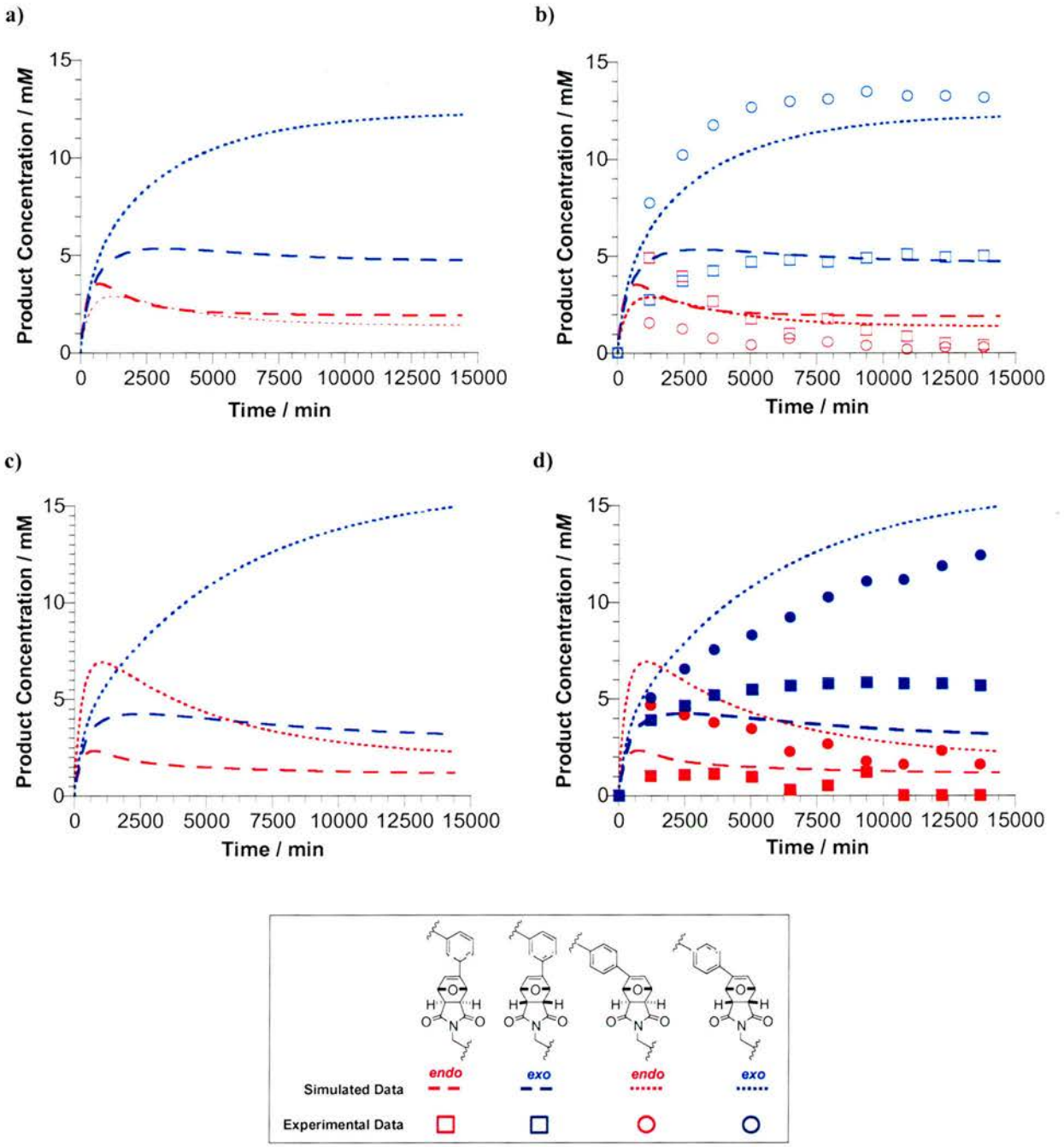

Figure 76: **a)** Simulated data using isosim programme within SimFit for the reaction of dienes **216** and **217** with dienophile **195**, **b)** Experimental data collected every 24 hours for 10 days, **c)** Simulated data using isosim program within SimFit for the reaction of dienes **216** and **217** with dienophile **195** in the presence of cofactor **193**, **d)** Experimental data collected every 24 hours for 10 days.

A kinetic simulation was also run for the reaction between dienes **216** and **217** and dienophile **195** in the presence of cofactor **193** the rate profile extracted from the simulation is shown in **Figure 76c**. Experiments were also conducted on an NMR scale, components **216**, **195** and **217** were present at initial concentrations of 25 m*M* in TCE at 50 °C in the presence of cofactor **193** (1 eq.). The library was monitored every 24 hours by ^{1}H NMR spectroscopy for a period of 10 days. **Figure 76d** shows experimental data collected every 24 hours for a

period of 10 days. Again, the predicted data follow the same distribution as the simulated data. However, the match between experimental data is not as accurate as that for the bimolecular reaction. This is no doubt as a consequence of the added complexity within the cofactor reaction, as 24 rate constants are used to generate this simulated data.

3.18 Competition Experiments between Dienes 216 and 217 and Dienophile 197 in the Absence and Presence of Cofactor 193

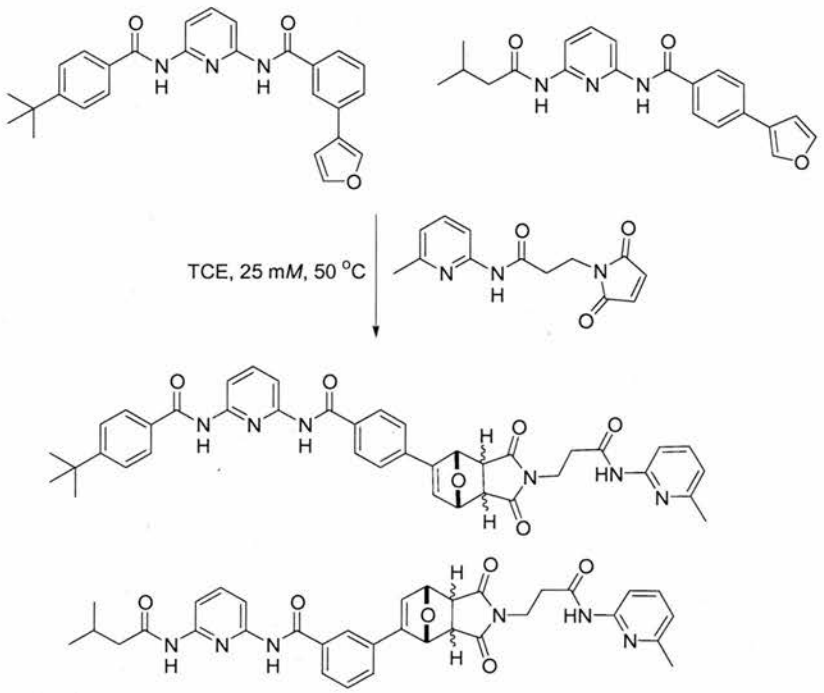

Scheme 84: Competition experiment between dienes **216** and **197** and dienophile **197**.

A kinetic simulation was run for the reaction between dienes **216** and **197** and dienophile **197** **(Scheme 84)** in the absence **(Figure 77a)** and presence of cofactor **(Figure 77c)**. Components **216**, **197** and **197** were reacted together in the absence and presence of cofactor **193** at 50 °C at an initial concentration of 25 m*M* of each building block in TCE, the library was monitored by ^{1}H NMR spectroscopy over a period of 10 days. **Figures 77b** and **77d** show the experimental data collected by ^{1}H NMR spectroscopy every 24 hours, over a period of 10 days in the absence and presence of cofactor respectively. Once again, there is a deviation from the simulated data when comparing with the experimental data, however, the distribution of products is not dissimilar. The reason(s) for the observed deviation from the predicted model will be discussed fully in the conclusions of this chapter.

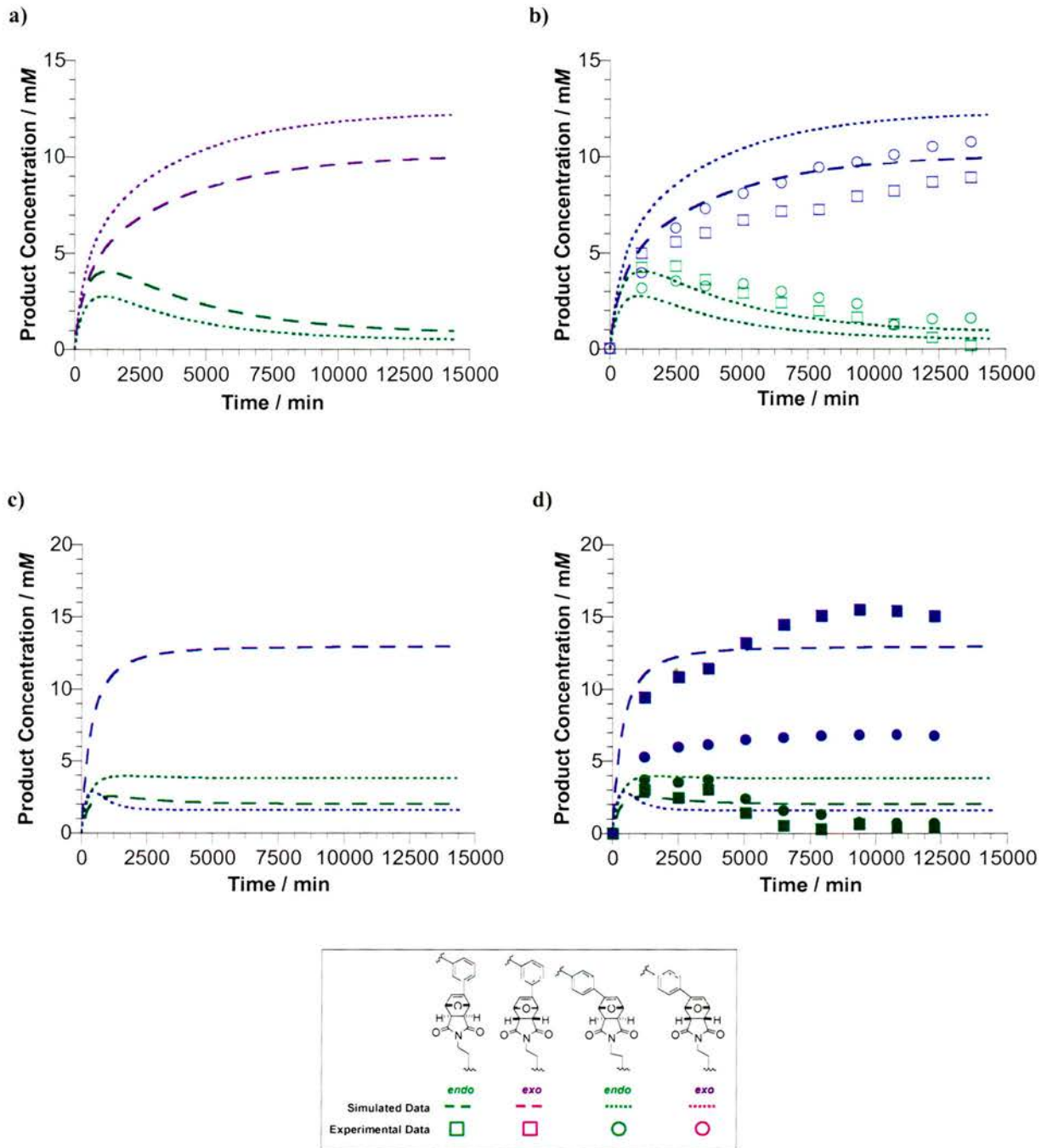

Figure 77: **a)** Simulated data using isosim programme within SimFit for the reaction of dienes **216** and **217** in the presence of dienophile **197**, **b)** Experimental data collected every 24 hours for 10 days, **c)** Simulated data using isosim program within SimFit for the reaction of dienes **216** and **217** in the presence of dienophile **197** and cofactor **193**, **d)** Experimental data collected every 24 hours for 10 days.

3.19 Full Library Studies

We had planned to simulate the outcome of our full library **(Scheme 85)** before following it experimentally by ^{1}H NMR spectroscopy. However, as a result of the reaction mixture

containing four building blocks and eight library members, monitoring of the evolving species by ^{1}H NMR spectroscopy proved impossible.

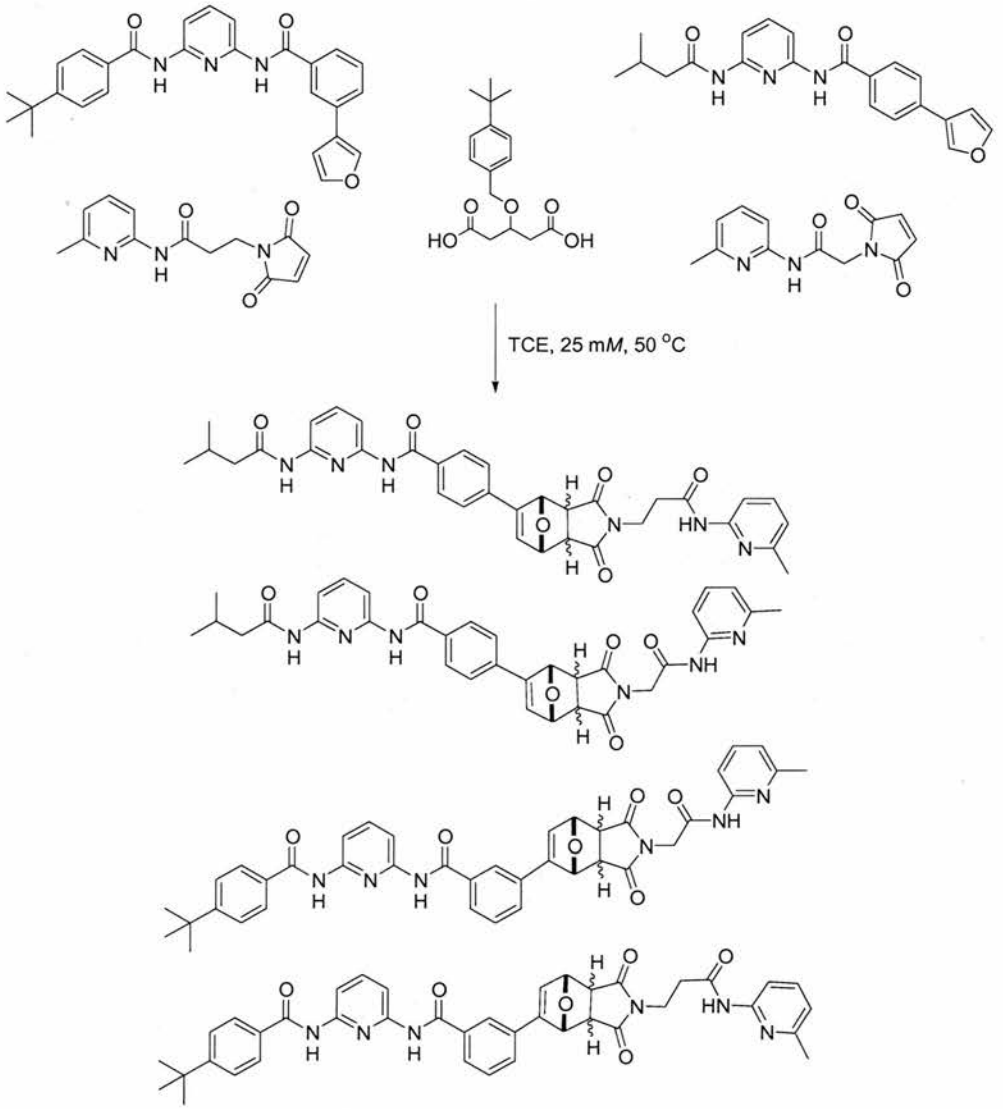

Scheme 85: Full library; two dienes **216** and **217** and two dienophiles **195** and **197** reaction between these components can lead to the production of eight possible Diels-Alder products.

As the predicted data for competition experiments fitted well with experimental data, we decided to simulated the outcome of the full library in the presence and absence of cofactor. The model for the full library was derived by fitting together the models used for the previously simulated competition experiments **(Scheme 86)**. This model was then run using the isosim package within SimFit the rate profiles generated are shown in **Figure 78**. It can be seen that under full library conditions cofactor **193** influences, both the products which are produced, and the rate at which those products are produced.

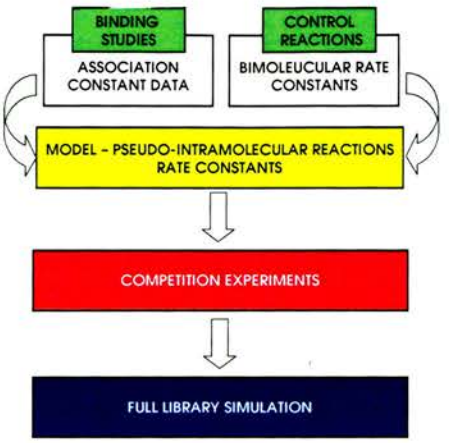

Scheme 86: A cartoon representation of the step-wise derivation of a full kinetic model simulation.

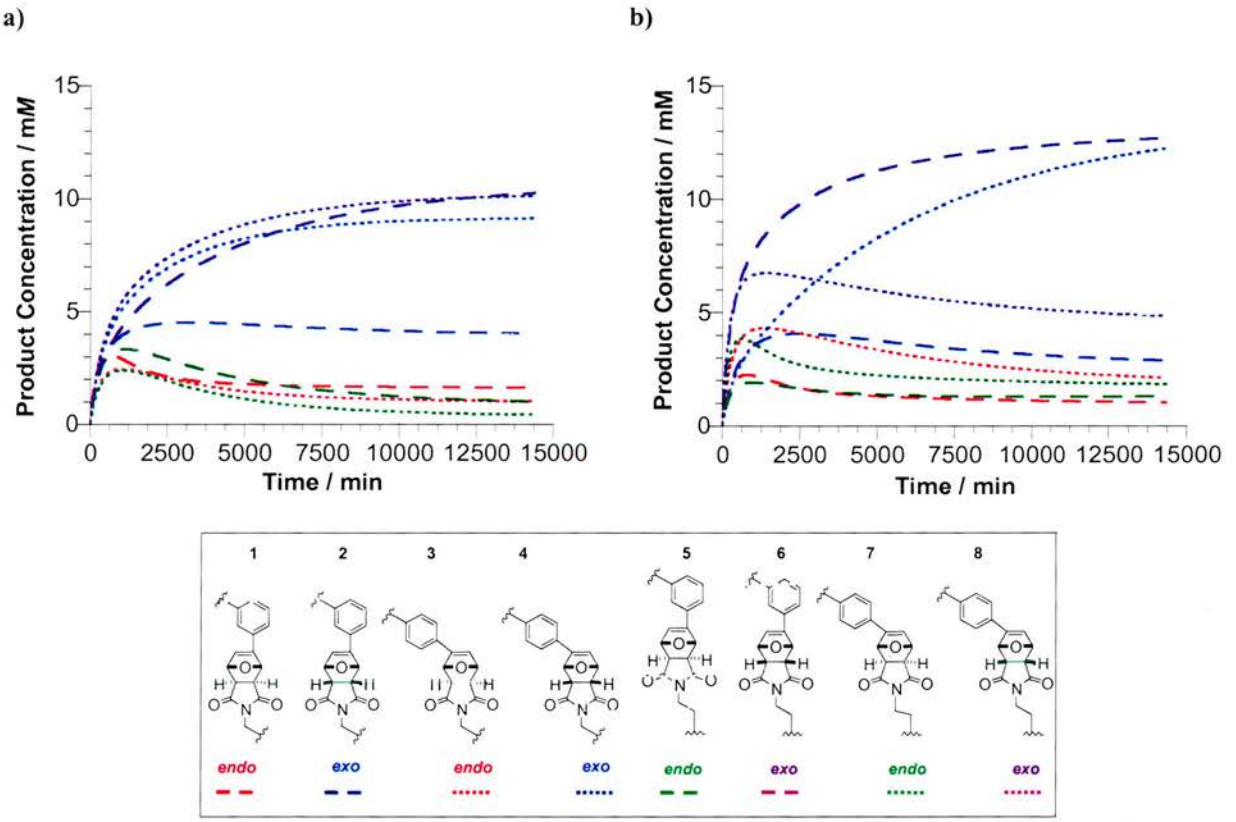

Figure 78: **a)** Full library simulation with no cofactor, **b)** Full library simulation with cofactor.

In order to appreciate the difference in the library composition on addition of cofactor at both the initital stages of library evolution (10 hours) and at final equilibration of the library mixture (10 days) the change in concentration of each library member on addition of cofactor has been plotted **(Figures 79** and **80)**. It can be observed more clearly from these data that the cofactor greatly influences the distribution of the library members within the mixture over both short time periods (10 hours, **Figure 79**) and longer time periods (10 days, **Figure 80**).

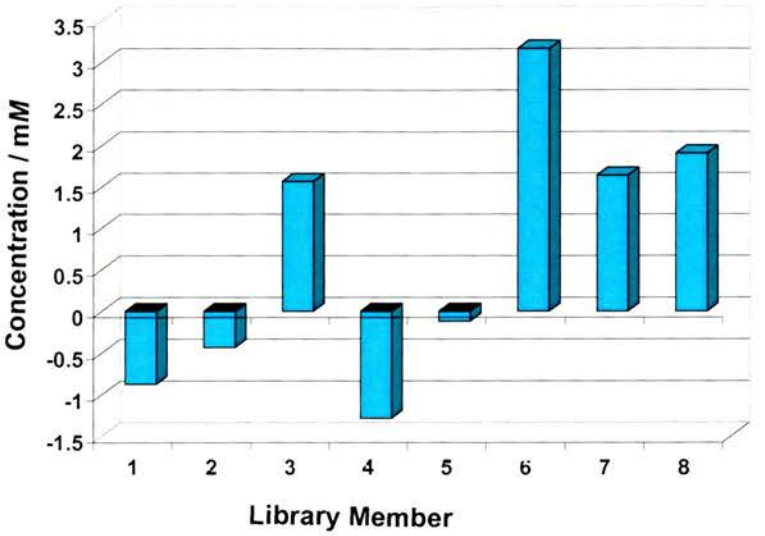

Figure 79: The concentration change on library members in the presence of cofactor at 10 hours.

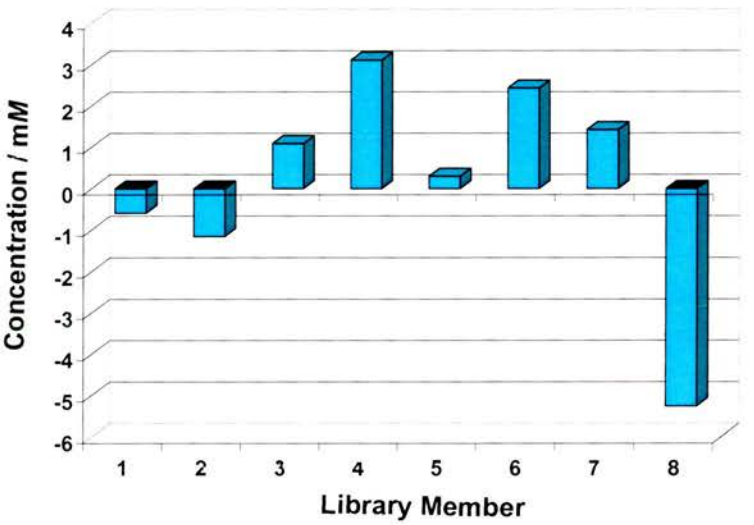

Figure 80: The concentration change on library members in the presence of cofactor at 10 days.

3.20 Molecular Modelling Studies

Molecular modelling calculations allow us to visualise the selection effect of cofactor **193**. A comprehensive molecular modelling study of each library member with cofactor **193** was undertaken using the AMBER* forcefield and the GB/SA solvation model for $CDCl_3$. Representative minimum energy conformations are shown in **Figure 81**. The conformations chosen represent five of the eight possible products and are shown in order of selection, from the adduct which is produced in the greatest concentration to the adduct produced in the lowest concentration in the presence of cofactor **193** at 10 days.

a)

exo cycloadduct, *meta*-substituted diene, 2 carbon spacer unit on dienophile

– –

b)

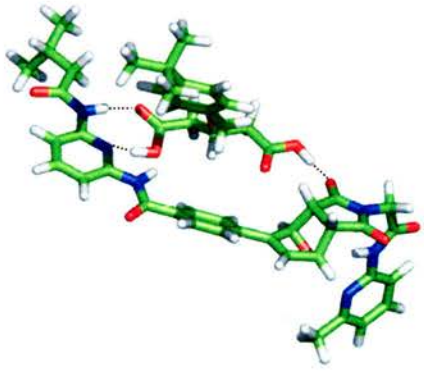

exo cycloadduct, *para*-substituted diene, 1 carbon spacer on dienophile

.....

c)

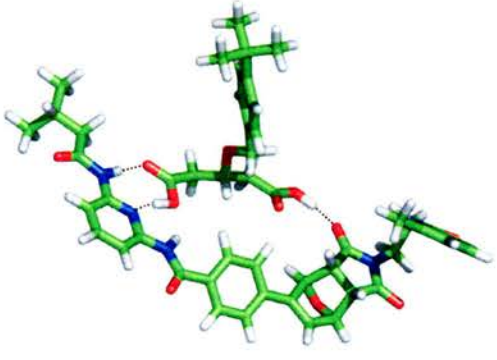

exo cycloadduct, *para*-substituted diene, dienophile containg a two carbon spacer chain

.....

d)

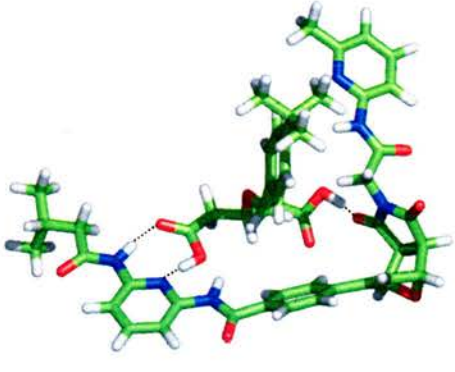

endo cycloadduct, *para*-substituted diene, one carbon spacer unit on dienophile

.....

e)

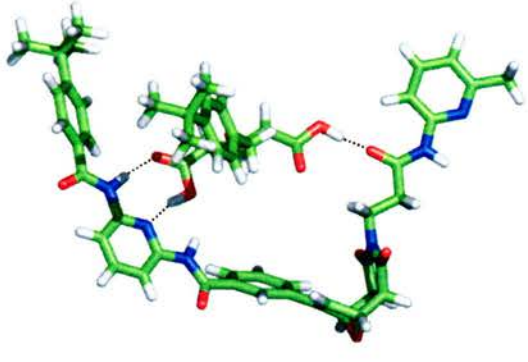

endo cycloadduct, meta substituted diene, two carbon spacer unit on dienophile

– –

Figure 81: Models representative of the minimum energy conformation of each adduct derived from molecular mechanics calculations using the AMBER* forcefield. Carbon, oxygen, nitrogen and hydrogen atoms are coloured green, red, blue and white respectively. Hydrogen bonds are represented by dashed lines. Models are presented in order of the highest to lowest concentration of cycloadduct produced as predicted by SimFit at 10 days. The coloured line below each model refers to the rate profile generated within the kinetic simulations.

The full library simulation calculates that the cycloadduct formed from diene **217** with furyl diene moiety in the *meta*-position and dienophile **197** with a two-carbon spacer chain length will be produced preferentially within the library. Molecular modelling studies suggest that the lowest energy conformation adopted by cycloadduct **218 (Figure 81a)** with cofactor **193** allows the formation of four hydrogen bonds, which would lead to the stabilisation of this product. Interestingly, no other library cycloadduct member adopts this optimal hydrogen bonding configuration with cofactor **193**.

As we move through the molecular modelling conformations **(Figure 81b–Figure 81e)** the number of potential hydrogen bonding interactions remains constant at three, however, in order to maintain the amidopyridine/carboxylic acid hydrogen bonding motif the cycloadducts structures become distorted and adopt unnatural conformations.

These studies show that although molecular modelling is a tool in which accuracy is often brought into questioned. When used as a means to gain a greater understanding of the selection effects observed within libraries of molecules it can be very effective tool.

3.21 Prediction Data Varying the Concentration of Cofactor

Section 3.3 described previous studies conducted with cofactor **193**, rate enhancement and diastereochemical control of a Diels-Alder reaction was shown to occur in the presence of sub-stoichiometric amounts of cofactor. We wished to investigate the effect of lowering and raising the equivalence of cofactor **193** on the concentrations of library members produced within our system.

Kinetic simulations were once again carried out using the isosim prediction tool available within SimFit. Concentration of library components were kept constant at 25 m*M* and the cofactor concentration varied at 10, 5, 2, 1, 0.5, 0.2 and 0.1 eq. the simulation predicted the evolution of the library over a ten day period of time. The data presented follows the effect of varying cofactor concentration on the three most abundant library members from our initial library simulations.

The data presented in **Figure 82** show the concentration of cycloadduct ***exo*-218** produced after 24 hours and 10 days in the presence of varying amounts of cofactor **193**. The data suggest that over a short time period of 24 hours there is a peak in the production of ***exo*-218**

with one equivalent of cofactor. However, over the ten day study period, the highest concentration of ***exo*-218** is formed in the presence of 0.5 eq. of cofactor.

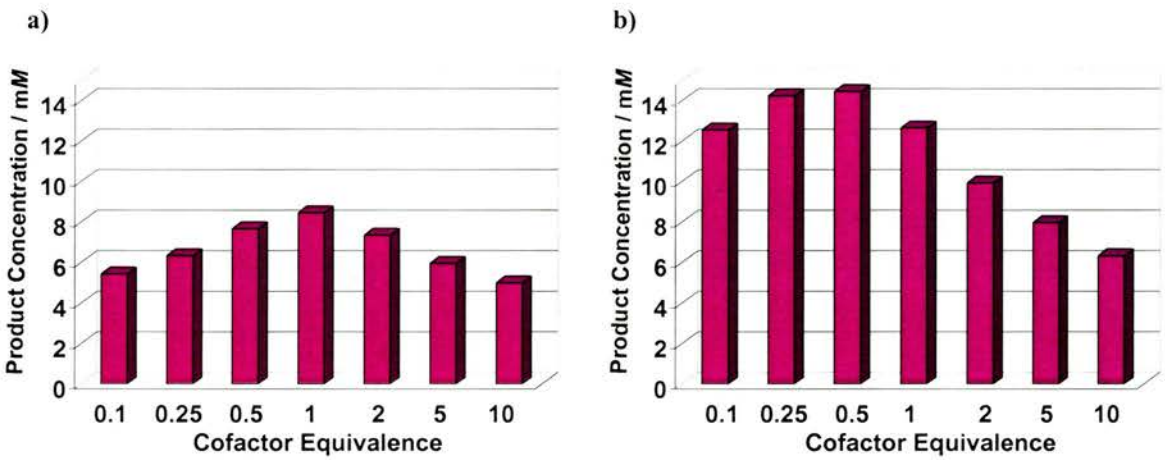

Figure 82: The concentration of library member ***exo*-218** produced over; **a)** 24 hours and **b)** 10 days, on varying the concentration of cofactor **193**.

The effect on the concentration of cycloadduct ***exo*-222** when the equivalence of cofactor **193** was varied is presented in **Figure 83**. The data suggest that in 24 hours the amount of ***exo*-222** produced increases steadily on decreasing cofactor concentration, the highest concentration of library member ***exo*-222** can be observed with catalytic amounts of cofactor. In comparison, over the ten day study period, the highest concentration of ***exo*-222** is formed in the presence of excess cofactor.

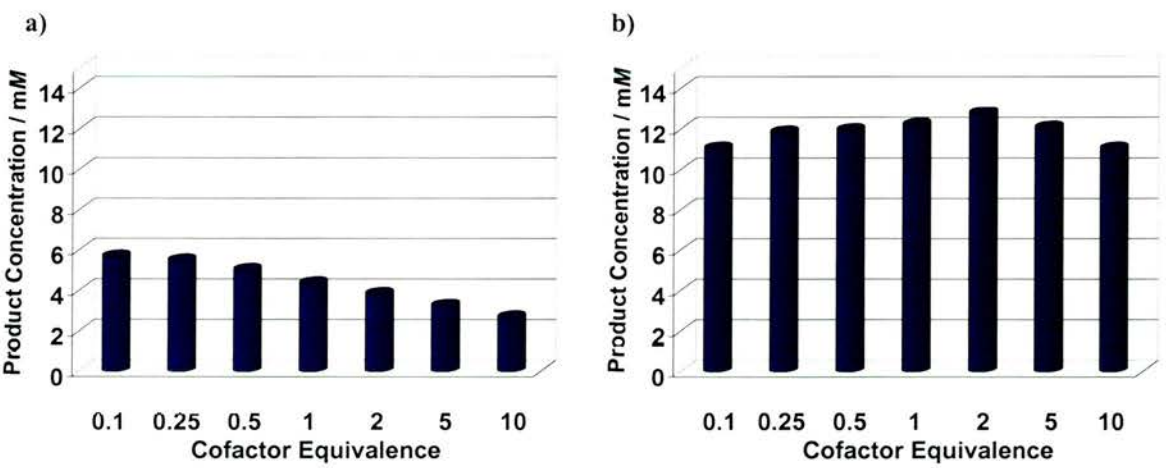

Figure 83: The concentration of library member ***exo*-222** produced over; **a)** 24 hours and **b)** 10 days, on varying the concentration of cofactor **193**.

Again, the effect upon the concentration of cycloadduct library member ***exo*-225** on varying cofactor concentration is presented in **Figure 84**. The data suggest that at 24 hours the amount of ***exo*-225** is highly dependent upon cofactor concentration, the amount of ***exo*-225**

produced increases initially as the cofactor concentration is lowered from 10 eq. to 5eq. and then steadily decreases, however when using a catalytic amount of cofactor the concentration of ***exo*-225** is seen to increase. This same pattern is observed for the production of cycloadduct ***exo*-225** after 10 days.

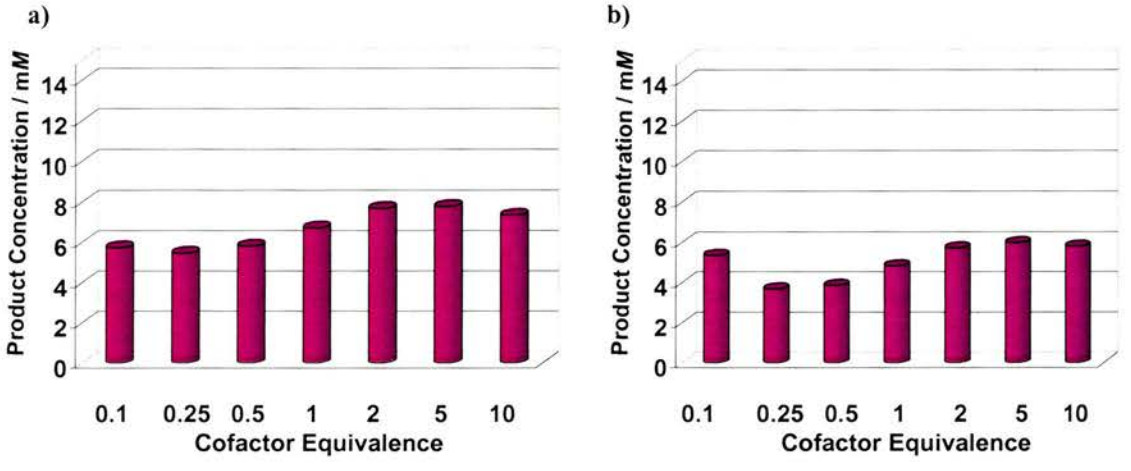

Figure 84: The concentration of library member ***exo*-225** produced over; **a)** 24 hours and **b)** 10 days, on varying the concentration of cofactor **193**.

These results suggest that our library is sensitive to the amount of cofactor present, each library member responds in a very different manner to the increase and decrease in stoichiometry of cofactor **193**. There would be no way of predicting the effect of cofactor concentration upon such a library, without the use of a predictive tool such as isosim.

We next wished to investigate the effect of the varying of cofactor concentration upon the selectivity of library members. The way in which this is shown is by using a 'selectivity factor'. The concentration of library member ***exo*-226** was used as a zero point, as its rate profile is relatively unaffected by addition of cofactor **193 (Figure 78)**. Therefore, using the previously recorded data, we obtained a ratio for the concentration of the three most abundant library members with respect to the concentration of ***exo*-226** at various concentrations of cofactor. Once again, the selectivity of each library member is shown after 24 hours and after 10 days.

The results **(Figure 85)** suggest that the selectivity of library member ***exo*-218** does indeed vary with cofactor concentration. After 24 hours there is a peak in selectivity at 5 eq. of cofactor. After 10 days the greatest selectivity is observed with sub-stoichiometric amounts of cofactor.

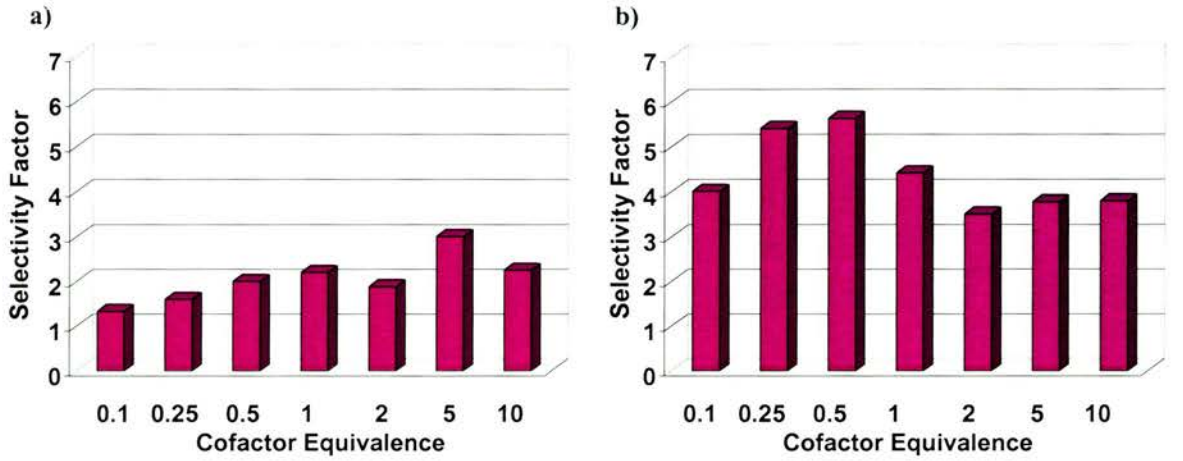

Figure 85: The selectivity calculated for library member ***exo*-218** with respect to ***exo*-226** at; **a)** 24 hours and **b)** 10 days, on varying the equivalence of cofactor **193**.

The selectivity results for ***exo*-222 Figure 86** suggest, once more, that cofactor concentration can have a large effect on the selectivity of the library member. The effect of cofactor equivalence upon the selectivity of ***exo*-222** after 24 hours is limited. However, after ten days there is a very large effect on selectivity by varying cofactor concentration.

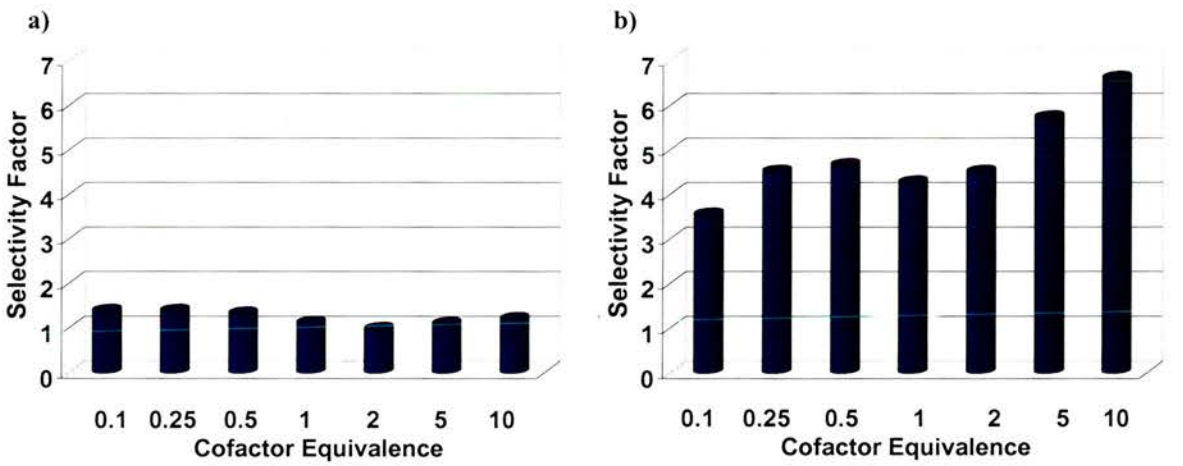

Figure 86: The selectivity calculated for library member ***exo*-222** with respect to ***exo*-226** at; **a)** 24 hours and **b)** 10 days, on varying the equivalence of cofactor **193**.

The results for ***exo*-225 Figure 87** suggest that on increasing cofactor concentration selectivity for ***exo*-225** increases at both 24 hour and 10 day intervals.

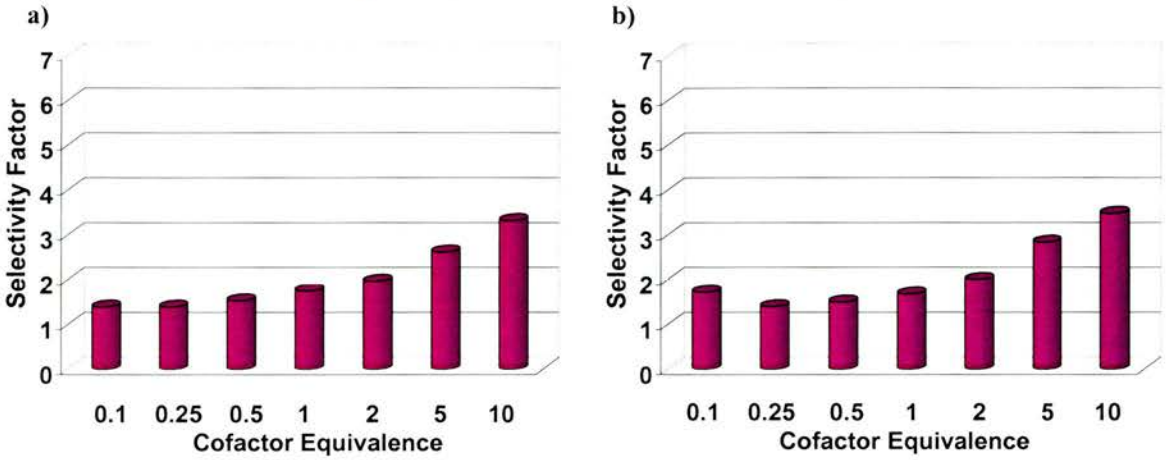

Figure 87: The 'selectivity' calculated for library member ***exo*-225** with respect to ***exo*-226** at; **a)** 24 hours and **b)** 10 days, on varying the equivalence of cofactor **193**.

3.22 Conclusions

Initial studies upon 2-aryl furan compounds determined there unsuitability for library studies, as a consequence of their limited Diels-Alder reactivity. This result is probably as a consequence of the disruption which would occur to the π-conjugated system on forming the cycloadduct product. Substitution of 2-aryl furan dienes with 3-aryl furan dienes generated Diels-Alder cycloadducts on reaction with our maleimides.

Cofactor **193** has been shown to influence each Diels-Alder reaction within our system. The extent of this effect varies greatly between library building blocks, this is somewhat surprising given the similarities in their structures. We have shown that minor changes in configuration can lead to major changes in the reactive pathway chosen by reactants. Within our library, two of the four Diels-Alder reactions, were shown to proceed mainly *via* an ABC-mediated pathway, one was moderately enhanced and the cofactor had little impact upon the reaction rate of another. These observations suggested that cofactor **193** was very selective in the reactions which it promoted, ideal for our dynamic library studies.

Whilst assigning the reactive pathways present in our Diels-Alder reactions the calculation of the association between carboxylic acid and amidopicoline recognition motifs was required. The K_a value for dienes **216** and **217** was calculated to be ~ 40 M^{-1} and the association constant for dienophiles **195** and **197** was calculated to be ~ 250 M^{-1}. In order to ascertain the reason for the large difference in K_a values, electrostatic potential energy maps were generated. These studies suggested that the extra amide moiety on dienophiles **195** and **197** affected the compounds ability to accept hydrogen bonds, thus, leading to the observed

reduction in association constant values. Within our library it would have been desirable to have similar binding affinities for all diene and dienophile library building blocks, as the components with a greater binding affinity will be bound more efficiently to the cofactor. In this case, two sets of dienophile could be preferentially bound as a consequence of their higher binding constant values, leading to the increase in the production of unproductive ternary complexes. Ideally, all components would have the same affinity for the cofactor molecule and would therefore compete equally for the association of cofactor **193**.

It is not possible to conduct 500 MHz ^{1}H NMR kinetic experiments over the long periods of time needed to observe library evolution. Therefore, we wished to simulate what would happen within our library over a period of days. The simulation package within SimFit allowed the generation of rate profiles for competition and full library predicted rate profiles. Simulations were generated by deriving kinetic models for competition reactions and inserting the rate constant data calculated from the previous kinetic studies. In order to ascertain whether the data generated from the simulations were accurate, NMR scale reactions were also set up and monitored each day by 500 MHz ^{1}H NMR spectroscopy. The results showed that the predicted data fitted reasonably well to the experimental data. The distribution of products produced was very similar, however, deviations from the predicted data did occur in terms of the overall concentrations of the products produced.

This result could be attributed to a number of factors:

(i) initial rate data at low conversions concentrations are subject to error
(ii) association constant values between cycloadduct products and cofactor **193** were estimated
(iii) we may not have accounted for all reactions occurring within our library in our kinetic model

One or all of these factors may be the reason for the deviations observed in the experimental data from the predicted data.

Using models derived from competition experiments, the full library was simulated using Simfit. Once again, one expected that the experimental library data would vary from the kinetically simulated data as described previously. The full library simulation showed the

selection and acceleration of two library members above all others in the presence of cofactor **193**.

Molecular modelling studies substantiated the selectivity calculated for the library, as only the cycloadduct which is produced at the fastest rate and in the greatest concentration can form the maximum four hydrogen bonds with cofactor **193**, leading to its stabilisation and preferential production.

On varying the concentration of cofactor **193** we have shown that large changes in the concentrations and selectivity of the three most abundant library members is possible. These studies show variations in product production which would be impossible to predict without the use of a kinetic modelling package.

Our study has highlighted the challenges in predicting the outcome of library studies. Within our relatively small library the kinetic model for the full library simulation relies upon 80 different rate equations. In order to achieve accurate simulation data all 80 of these values must be as accurate as possible. Therefore, on increasing library size the kinetic models required to describe them will become more complex and increasingly difficult to accurately establish all the necessary parameters. However, the step-wise kinetic approach that we have adopted to studying this library, has proven to be successful and this strategy can be adapted to investigate any dynamic library which can be monitored by ^{1}H NMR spectroscopy.

Chapter 4

Modelling Sequence Stability in Synthetic Analogues of DNA

4.1 The Structure and Mode of Replication of DNA

4.1.1 The Components of DNA

DNA (Deoxyribose Nucleic Acid) is a polymer composed of monomer nucleotide units.[214] Each nucleotide consists of a 5-carbon sugar (deoxyribose), a nitrogen containing base attached to the sugar, and a phosphate group. There are four different types of nucleotide found in DNA, differing only in heterocyclic base - adenine and guanine are purines, thymine and cytosine are pyrimidines **(Figure 88)**.

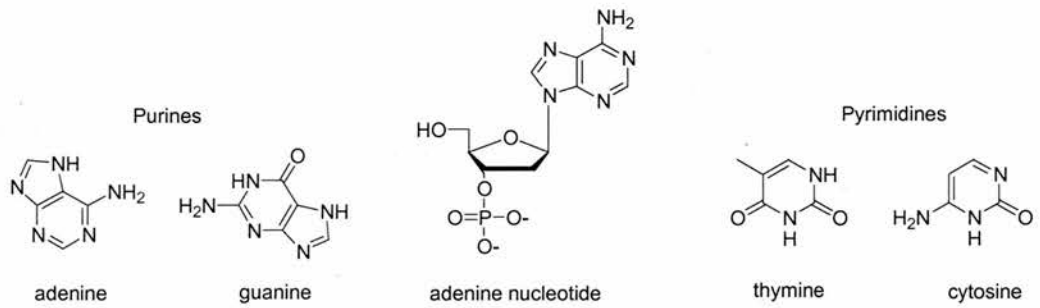

Figure 88: DNA monomers are nucleotides, shown here, an adenine nucleotide. The four bases required for DNA formation; purines – adenine and guanine; pyrimidines - thymine and cytosine.

4.1.2 The DNA Double Helix

In 1953, the helical superstructure of DNA was proposed by Watson and Crick.[215] Their deductions were based on the work of a number of eminent scientists. Pauling, Corey and Furberg had previously proposed[216-217] the structure of DNA, however, there were flaws in each of their suggestions. Wilkins first produced[218] an X-ray diffraction photograph from DNA indicating that the polymer might have a regular structure, however, the X-ray pattern was not conclusive. A well-resolved X-ray diffraction photograph of the pure B-form of DNA showing clear helical characteristics was later obtained by Franklin.[219] In 1947, Chargaff had observed[220] regularities in the percentages of heterocyclic bases in the DNA of a variety of species. Chargaff observed: (i) the total mole percentage of purines/pyrimidines $\approx$ 1, (ii) the mole percentage of adenine/thymine $\approx$ 1 and the mole percentage of guanine/thymine $\approx$ 1. The results of Chargaff's studies convinced Watson and Crick that base pairing was the key to the structure of DNA. According to their model, two nucleic acid chains would be held together by hydrogen bonds between base pairs on opposite strands. The two nucleic strands would form a helical structure, winding around an axis in a right-

handed manner, the two polynucleotide chains running in opposite directions. The bases of the individual nucleotides would be on the inside of the helix and the sugar-phosphate backbone on the outside. Watson and Crick noted that "...the specific pairing we have postulated immediately suggests a possible copying mechanism for the genetic material." Indeed, this copying mechanism was later established.

4.1.3 DNA Replication

Proof of the semi-conservative mode of replication hinted at by Watson and Crick[221] was later established by the experiments of Meselson and Stahl in 1958.[222] DNA replication[214] **(Figure 89)** begins with a portion of the double helix being unwound by a helicase. A molecule of a DNA polymerase then binds to one strand of the DNA and moves along it in the 3' to 5' direction. Thus, one strand of DNA acts as a template for the assembly of the nucleotides of the other strand and then the helix reforms. DNA synthesis can only occur in the 5' to 3' direction. Therefore, a second type of DNA polymerase binds to the complementary template strand on unwinding of the helix. This polymerase synthesizes discontinuous segments of polynucleotides, Okazaki fragments, DNA ligase then stitches these together into the lagging strand.

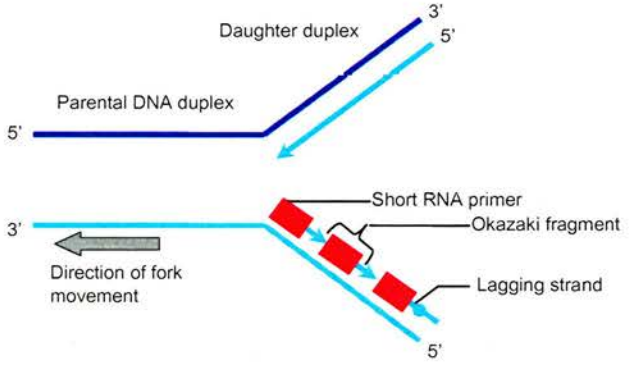

Figure 89: A schematic representation of a DNA replication fork. Adapated from Ref. 214.

When the replication process is complete, two DNA molecules, identical to each other and identical to the original, have been produced. Each strand of the original molecule has remained intact and has served as a template for the synthesis of the complementary strand. This mode of replication is described as semi-conservative **(Scheme 87)** because: one-half of each new molecule of DNA is old; one-half new. The mode of replication used by DNA is a reciprocal form of replication, it requires two inter-linked cycles, with one strand of DNA acting as a template for the formation of other. However, the simplest form of replication is

not that of reciprocal replication, it is direct or self-replication in which a molecule can template its own formation.

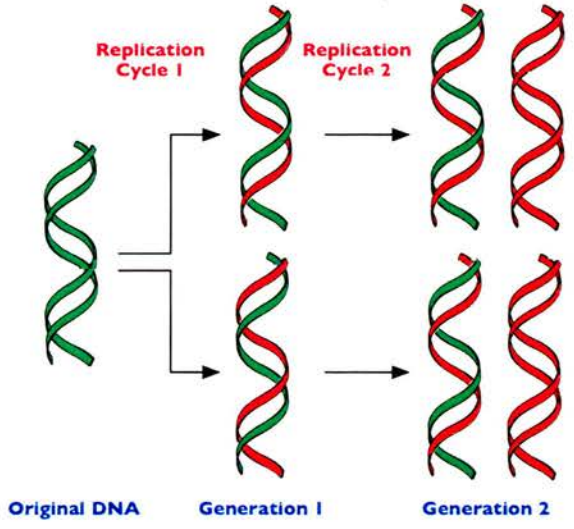

Scheme 87: The semi-conservative model. Adapted from Ref. 214.

4.2 Self-Replication

4.2.1 The Minimal Model of Self-Replication

The simplest model devised to represent self-replication[223] is that of the minimal self-replicating cycle **(Scheme 88)**. Although self-replication is less complex than reciprocal replication, there are three possible reaction channels available to the starting materials **A** and **B**.

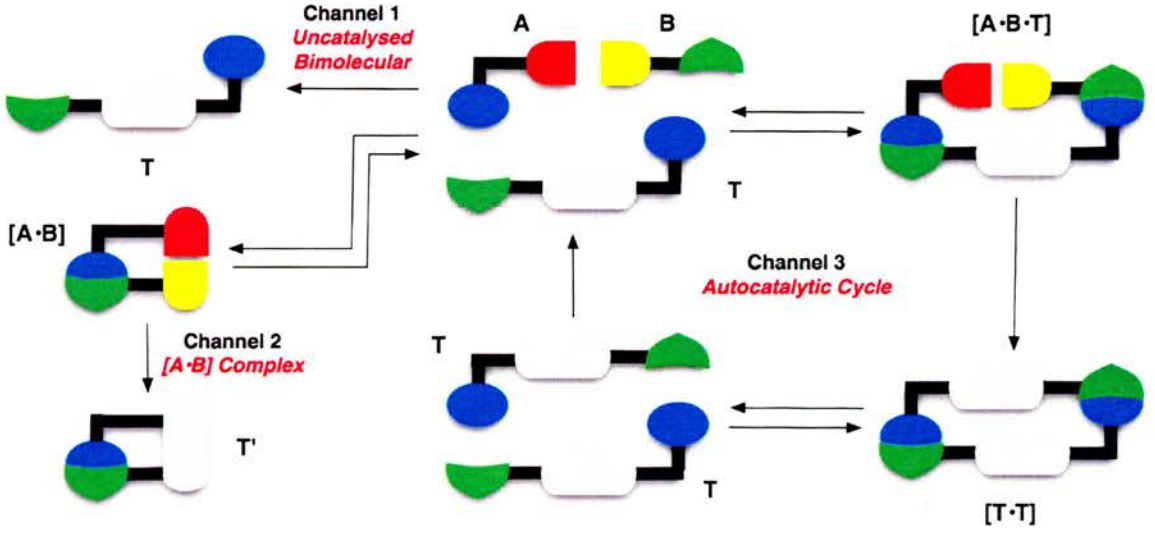

Scheme 88: The minimal model for self-replication. Green and blue blocks represent the recognition sites, red and yellow blocks represent the reactive sites and the black lines represent spacer groups.

The first channel available to the starting materials is reaction *via* the uncatalysed bimolecular pathway, this occurs when **A** and **B** react in solution to form the product **T**. The second channel is the AB recognition-mediated pathway discussed previously in **Chapter 2**. Starting materials **A** and **B** each contain one of two complementary recognition sites, and so, may bind reversibly together to form a binary [**A·B**] complex. If, whilst held in the [**A·B**] complex the reactive sites are brought into close proximity, covalent bond formation will occur forming product **T'**. In this scenario, the reaction between the two starting materials will be rendered *pseudo*-unimolecular, therefore, regio- and/or stereochemical control of the product may occur. Although control and acceleration of the reaction may occur, the AB reaction channel does not exhibit autocatalysis, as any template formed by this route usually retains the complementary binding between recognition sites within the product, and therefore, turnover cannot be achieved. The product formed from the AB channel is therefore termed the closed template **T'** as a consequence of the closed conformation it adopts. The third reaction channel is that of an autocatalytic cycle. In this pathway, **A** and **B** bind reversibly to template **T** *via* the complementary recognition sites, a ternary complex [**A·B·T**] is then formed. The termolecular complex can bring the reactive sites on **A** and **B** into close proximity allowing the covalent bond forming reaction between them to yield the product duplex [**T·T**]. Once again, as in the AB complex channel, the use of recognition renders the reaction *pseudo*-unimolecular, and therefore acceleration of the reaction, and/or regio- and stereochemical control of the product can be achieved. Once the product duplex [**T·T**] has been formed the system can be considered self-replicating. If the duplex [**T·T**] subsequently dissociates to return two free molecules of template **T** to the start of the cycle, the reaction can then be considered autocatalytic.

The autocatalytic cycle gives a characteristic sigmoidal rate profile **(Figure 90)**. In the initial stages of the reaction the biomolecular uncatalysed pathway is prevalent. On sufficient production of template molecule the reaction rate accelerates because the template molecule acts as a catalyst for its own formation. As the starting material stocks decrease, this becomes the rate-limiting factor and the reaction rate decreases.

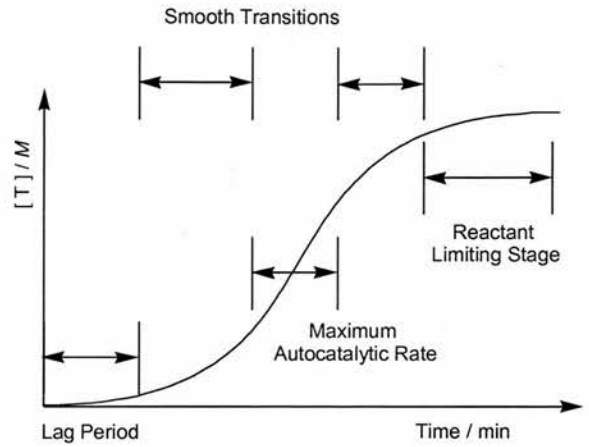

Figure 90: The classic sigmodial rate profile observed for self-replicating reactions.

The process of self-replication represents for the biologist a link with the origins of life.[224] Inspired by nature, the first examples of minimal self-replicating systems were based upon deoxyribonucleotide oligomers.

4.2.2 Natural Product Approach

In 1986, von Kiedrowski reported[225] the first example of a self-replicating hexadeoxynucleotide **(Scheme 89)**. Hexadeoynucleotide **227** with a 5'-CCGCGG-3' base sequence was utilized as a template. Building blocks were two trideoxyribonucleotides of sequence 5'-CCG-3' **229** and 5'-CGG-3' **228**. Recognition between the template and the building blocks occurred *via* strong cytosine-guanine base pairing. The hydroxy group at the 3'-phosphate position of **229** was activated using 1-(3-dimethylaminopropyl)-3-ethylcarbodiimide (CDI). The activated hydroxyl group of **230** and phosphate group of **228** were then brought into close proximity by assembly upon template **227** forming a ternary complex. The condensation reaction between **230** and **228** was therefore rendered *pseudo*-intramolecular, catalysing the reaction. Hexamer **227** which was formed was an exact copy of the template oligomer **227**. Analysis of this system by HPLC did not result in the indicative sigmoidal rate profile **(Figure 90)** for the production of product **227**.

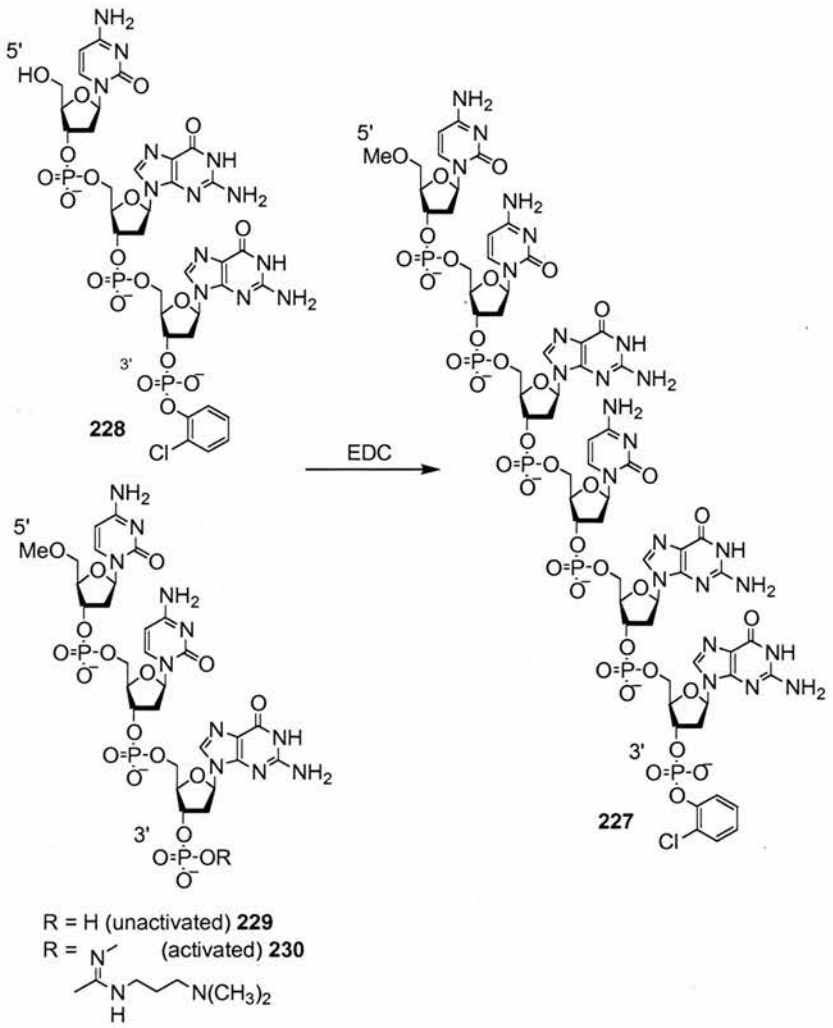

Scheme 89: A minimal self-replicating system based upon a hexadeoxynucleotide.

The kinetic behaviour of this system can be explained by considering several factors. The rate of formation of **227** was extremely slow, with only a 12% formed after 4 days leading to the hydrolysis of the feedstock. Also, non-activated **229** could couple to activated **230** giving a non-productive hexadeoxynucleotide. It is also likely that the self-replicating pathway is not the exclusive route by which this system operates, as an AB pathway is also open to the system. Although a sigmoidal curve was not observed, on doping the reaction mixture with a small amount of template **227**, the initial rate of reaction was increased, showing that the system was subject to autocatalysis.

In an attempt to observe an efficient self-replicating system von Kiedrowski modified the previous system.[226] The base sequence of the original system was maintained, the 5' hydroxyl of **228 (Scheme 90)** was replaced by an amine group **231** and the 5' terminus of **230** was protected with a methylthiomethyl group **232**. This system does indeed give a sigmodial

rate profile. In contrast to the original system the reaction between **231** and **232** reached ~ 50% conversion to template **227** within 2 hours and the only product detected was that of desired template **227**. On doping this system with a preformed template **227**, a disappearance of the lag period is observed due to a rate enhancement of the initial rate of reaction.

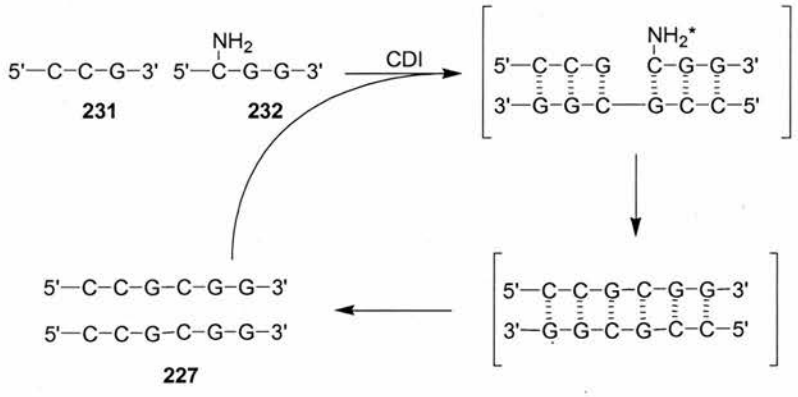

Scheme 90: Schematic representation of von Kiedrowski's self-replicating system.

Work upon natural self-replicating systems has since been reported in the groups of Ghadiri[227] and Chmielewski.[228]

4.2.3 The Synthetic Approach

For the synthetic chemist self-replicating molecules represent the ultimate synthetic system, a molecule which can template the production of a large amount of perfect copies of itself from a single molecule. The synthetic approach to self-replicating systems has been investigated by a small group of scientists including Rebek,[229-233] Menger[234-235], Sutherland[236] and Reinhoudt.[237] In the late 90's Philp and co-workers became interested in whether: "...nucleic acids were unique in their ability to store and transmit information at a molecular level?"

Philp and co-workers[238] monitored the reaction between **233** and **148 (Scheme 91)** at 10 °C at a concentration of 25 m*M* in $CDCl_3$ by ^1H NMR kinetics. The reaction was reasonably slow a 17% overall conversion to a diastereoisomeric mixture of isoxazolidines **234** and **236** was observed. The reaction showed little selectivity the ratio of *trans*:*cis* being 3:1. The kinetic rate profile for the reaction was fitted to a simple bimolecular model.

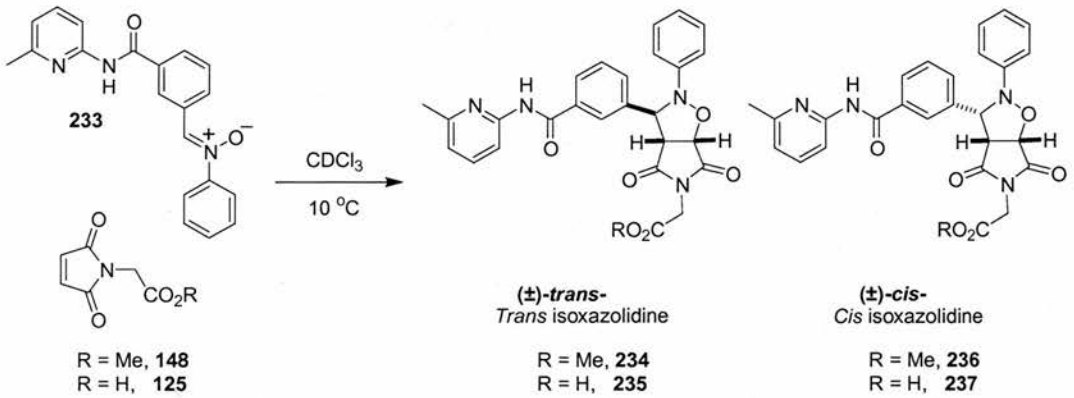

R = Me, **148**
R = H, **125**

R = Me, **234**
R = H, **235**

R = Me, **236**
R = H, **237**

Scheme 91: Reaction between maleimides **125** or **148** and nitrone **233** resulting in the production of diastereoisomeric isoxazolidines **234**, **235**, **234** or **235**.

The effect of recognition upon the reaction was investigated by substituting maleimide ester **148** with maleimide acid **125** under the experimental conditions described previously. The potential recognition-mediated reaction proceeded at a significantly faster rate than that of the bimolecular reaction **(Figure 91)**. A sigmodial curve profile was observed for the concentration/rate profile of the reaction, indicating self-replicating characteristics for the reaction.

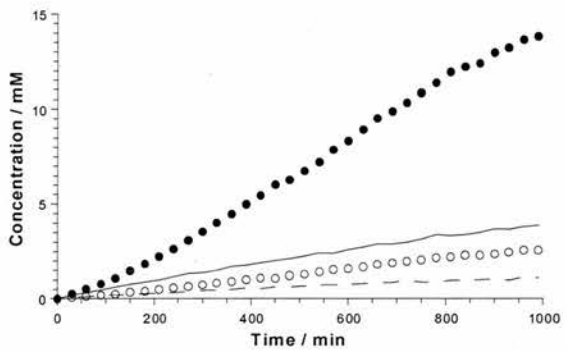

Figure 91: Comparison of the data obtained for the reaction between nitrone **233** and maleimides **125** and **148** (*trans* isomer represented as filled circles, *cis* isomer as open circles) and the average rate for the uncatalysed bimolecular reaction (*trans* isoxazolidine represented as a solid line, *cis* isoxazolidine as a dashed line).

In order to ascertain whether this reaction was self-replicating a series of control reactions were undertaken **(Figure 92)**. The addition of 40% of pre-synthesized *trans* template **235** at the beginning of the reaction, resulted in the loss of the initial lag period in rate of production of only *trans*-isoxalidine **235**, no rate enhancement was observed in the production of *cis*-isoxalidine **237**. Therefore, it was concluded that *trans*-isoxalidine **235** was acting as a selfish autocatalyst enhancing only the formation of itself. In contrast the addition of pre-synthesized *cis*-isoxalidine **237** had no effect on the rate of production of either diastereoisomer. A further control experiment was designed to disrupt the inherent recognition within the system,

thus allowing the effect of the binding events to be assessed. 4 eq. of benzoic acid were added to the reaction between **233** and **125** as a competitive inhibitor for the amidopyridine recognition unit present in nitrone **233**. Under these conditions there was a significant decrease in the rate and selectivity of the reaction. The sigmodial nature of the concentration/rate profile also disappeared on addition of benzoic acid, demonstrating the recognition-mediated nature of the native reaction between nitrone **233** and maleimide **125**.

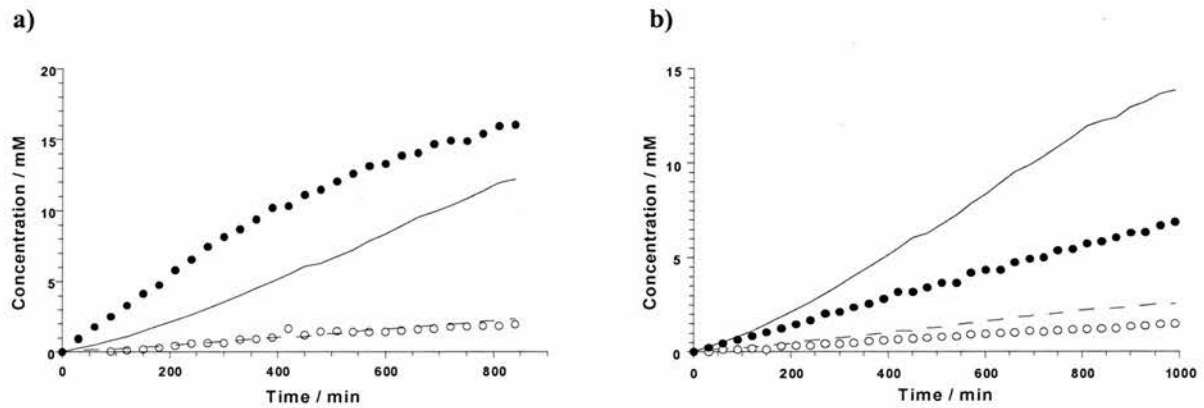

Figure 92: Data for the reaction between nitrone **233** and maleimide **125**; **a)** undoped (original data) (*trans* isoxazolidine represented as a solid line, *cis* isoxazolidine as a dashed line), and doped with preformed template at 40 mol% at t = 0 min (*trans* isoxazolidine represented as filled cirlces, *cis* isoxazolidine as open circles); **b)** Rate profile for the reactions between nitrone **233** and maleimide **125** (*trans* isoxazolidine represented as a solid line, *cis* isoxazolidine as a dashed line) and nitrone **233** and maleimide **125** with 4 eq. of benzoic acid (*trans* isoxazolidine represented as filled circles, *cis* isoxazolidine as open circles).

4.3 Reciprocal Replication

Why is DNA replication not based upon the simplest form of replication – self-replication? In terms of atom efficiency, direct replication methods are more efficient at producing template and therefore in evolutionary terms, direct replication offers a selective advantage over reciprocal replication. However, if one uses an analogy, comparing the bases of DNA to the letters in the alphabet, the limits of self-replication can be appreciated. If languages were based only upon words which are palindromic, the number of words which could be formed would be greatly limited. In a simple example **(Figure 93)** where we have the bases **A** and **T**, under self-replicating conditions, two possible products could be formed. In a reciprocal system four combinations of **A** and **T** are possible. If the example is expanded and we have two base **A**'s and two bases **T**'s, within a self-replicating system still only two palindromic sequences are possible. However, using reciprocal replication six combinations are achievable. Self-replication has the same limitations, as the sequence produced is always a palindrome of the original template. The reason why nature chose a reciprocal method of replication to sustain the basis of life may be related to the argument above.

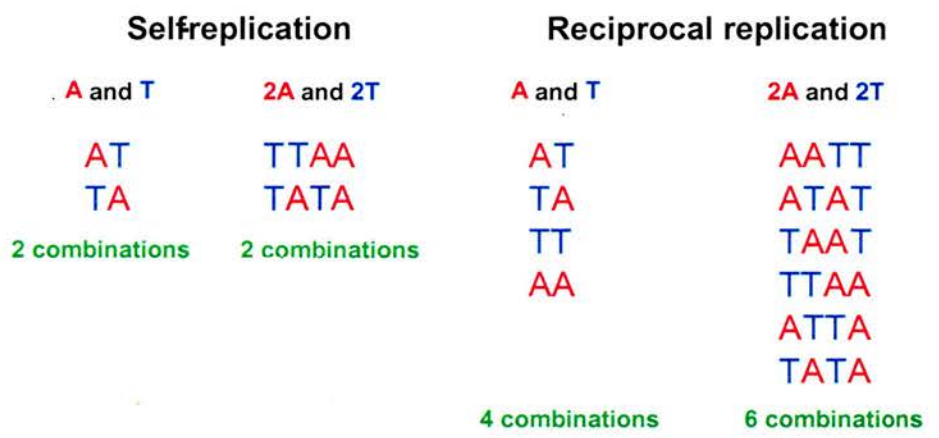

Figure 93: A schematic representation of the limitations of a self-replicating systems diversity in comparision with a reciprocal replicating system.

Reciprocal systems are also capable of storing information in a more stable manner than their self-replicating counterparts. The way in which synthetic systems have been designed to mimic DNA replication can be described simply in terms of a reciprocal replication model **(Scheme 92)**.

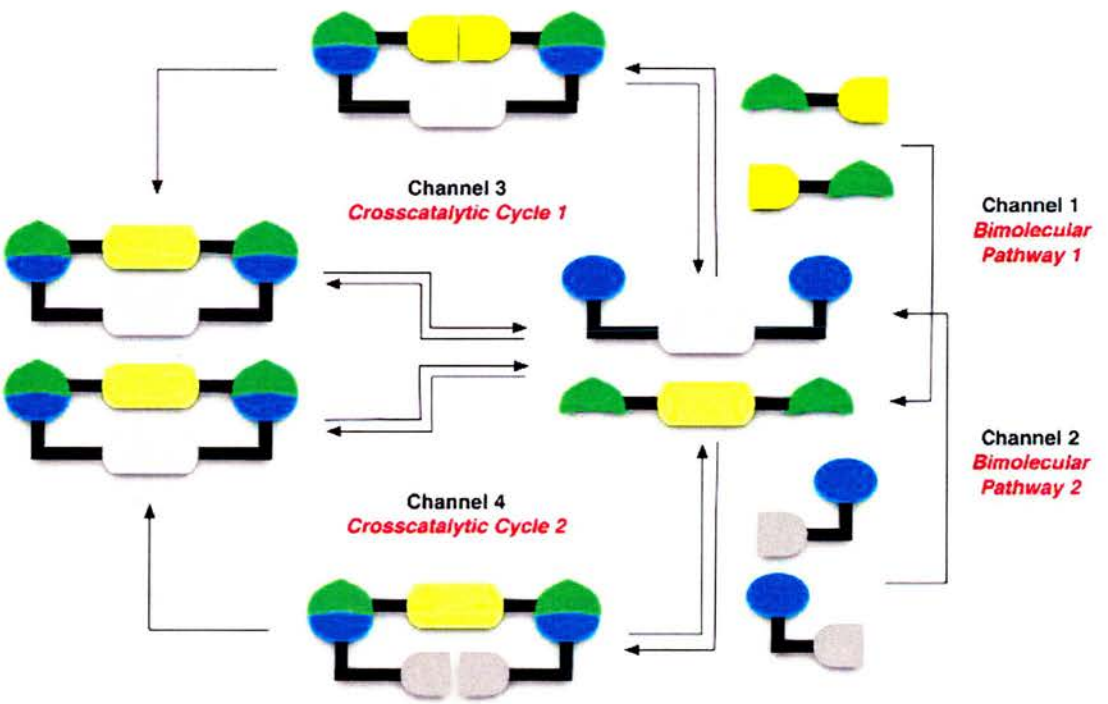

Scheme 92: A schematic representation of a reciprocal replicating system.

In this cycle, one mole of each grey molecule (reactive sites shown in grey) both containing identical recognition sites (blue) react together to form one mole of grey template *via* the bimolecular pathway 2. It is then possible that one mole of each yellow molecule could assemble upon the grey template, held by its complementary recognition sites (green), thus,

forming a ternary reactive complex. The termolecular complex could potentially bring the reactive sites on the yellow molecules into close proximity to facilitate the covalent bond forming reaction between them. This binding event would render the reaction *pseudo*-unimolecular, and by controlling the approach of the reactive sites regio- and/or stereochemical acceleration and control of the product could be achieved. It is possible that the product duplex would be unstable and therefore dissociate to give 1 mole of each template back into the cycle. In order for this cycle to be replicating, two crosscatalytic cycles must be present. Therefore, the same process must be followed in the formation of the yellow template. Template formation, followed by the subsequent reaction of two grey molecules upon the template allowing a *pseudo*-intramolecular reaction to proceed, on producing an unstable product duplex, dissociation would occur releasing two template molecules back into solution. Only on completion of both of these crosscatalytic cycles would a reciprocal replication cycle be complete.

4.3.1 An Example of Synthetic Reciprocal Replication

In 1995, Rebek and co-workers reported[239] reciprocal template effects in bisubstrate systems. Rebek chose two *p*-nitrophenylesters **240** and **241** and two amines **238** and **239** for his study **(Figure 94)**.

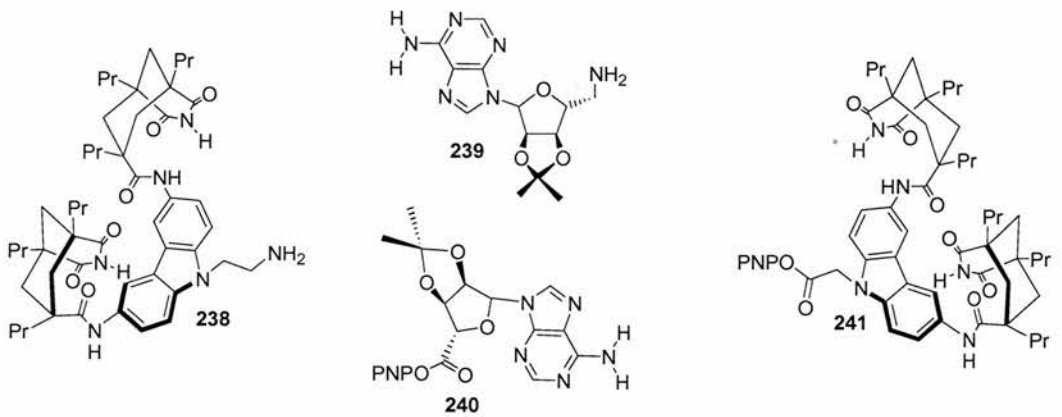

Figure 94: The four components chosen for Rebek's study on reciprocal replication. Amides **238** and **239** and esters **240** and **241** chosen as a result of their high binding specificity for one another.

Firstly the reaction between amine **239** and *p*-nitrophenylester **240** at equimolar concentrations of 0.05 m*M* in $CHCl_3$ was monitored spectrophotometrically by the release of *p*-nitrophenol. The reaction was repeated in the presence of 1 equivalent of template molecule **242 (Figure 95)**. The presence of compound **242** accelerated the formation of amide **243** ten-fold. To test the theory that one template molecule was enhancing the formation of the other, competition experiments were carried out. In the presence of 1

equivalent of preformed template **243** the reaction is accelerated only three-fold. In a similar competition experiment addition of 10 equivalents of 9-ethyladenine resulted in a decrease in acceleration to two-fold. It was noted that the rate of the uncatalysed reaction was unaffected by the competitive binders. The template directed synthesis of amide **242** was next investigated. Firstly, the rate of the uncatalysed reaction between **238** and **241** was measured spectrophotometrically under reaction conditions of 0.05 m*M* of each starting material in $CHCl_3$. Secondly, an identical reaction in the presence of 1 equivalent of template **243** was monitored. In this case, a five-fold increase in the initial rate of the reaction was observed. Once again, competition experiments were carried out using product **242** and 9-ethyladenine as competitive binders. Both of which reduced the acceleration of the template-mediated reaction whilst having no significant effect upon the corresponding bimolecular reaction. One can therefore envisage, these two templates forming a reciprocal replicating cycle as the product of each reaction is a template for the formation of the other template.

a) **b)**

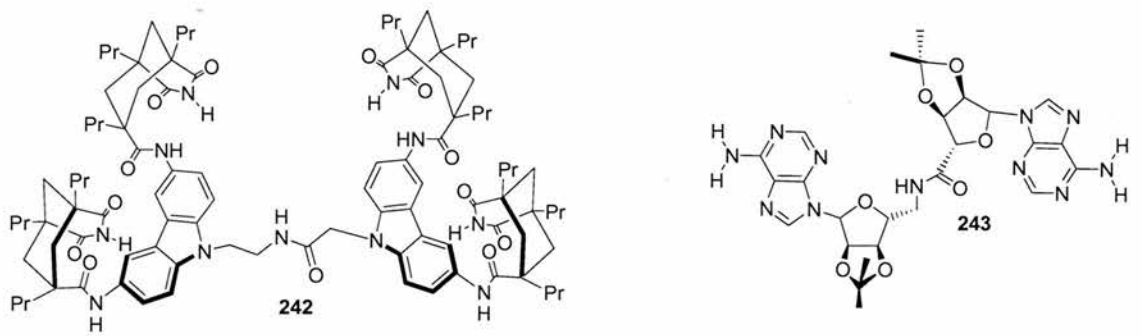

Figure 95: Templates formed by the reaction between; **a)** amine **238** and ester **241** and **b)** amine **239** and ester **240**.

4.4 The Design and Synthesis of a System Capable of Self- or Reciprocal Replication

The previous examples describe synthetic systems capable of self- or reciprocal replication. The aim of this project was to probe the interplay between direct and reciprocal replication, we wished to design a system which could potentially amplify *via* either replication route. In conjunction with the principles of dynamic combinatorial chemistry, we wished this process to be under thermodynamic control and therefore be error checking.

Dynamic libraries which utilize disulfide exchange conditions have been widely reported[113-120] **(Section 1.8.6)**. Disulfide exchange was chosen as the reaction of choice for this system. Under basic disulfide formation conditions chains of disulfides may be formed,

the form that these chains adopt would be governed by the relative stability of the helices. Questions we wished to address:

- Is replication possible within this system?
- Will it take the form of self-replication or reciprocal replication?
- Which sequence combination proves to be most stable?
- Will chains of disulfide be formed?
- If so, will helical structures be formed?

4.4.1 Target Compounds

Our library building blocks were designed loosely upon the structure of DNA **(Figure 96)**.

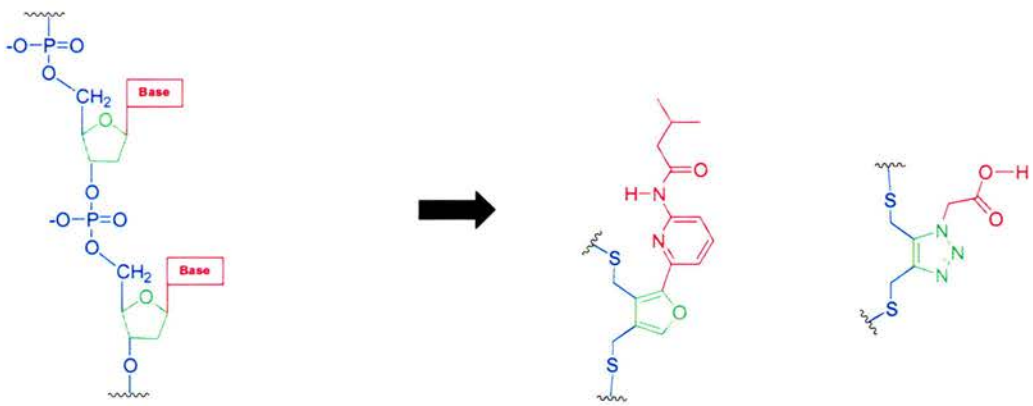

The backbone of DNA is made up of 5-membered deoxyribose sugars → A 5-membered triazole/furan ring replaces the deoxyribose sugar

Deoxyriboses are linked by phosphodiester bridges → Disulfide formation could form chains of building blocks

Strands of DNA form helices *via* specific hydrogen bonding between base pairs → A carboxylic acid/aminopicoline recognition motif will be used to allow one strand to recognise the other

Before undertaking the synthesis and study of larger chains of disulfides, the study of a simpler system was initiated. Each of the target components contain a recognition site suitable for hydrogen bonding, either in the form of a carboxylic acid or an amidopicoline group. Building blocks contain thiol moieties, which under basic conditions can undergo disulfide exchange. Considering a situation in which building blocks **244** and **246** are present there are two potential methods in which amplification maybe achieved.

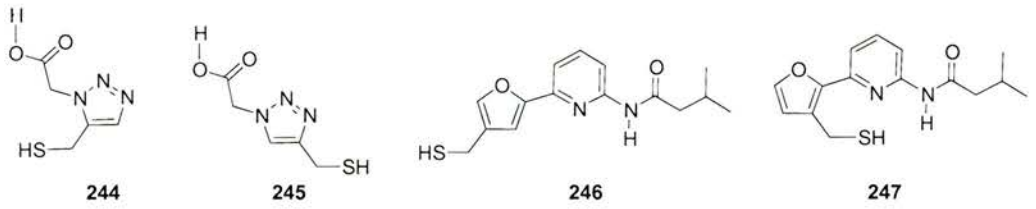

Figure 96: Synthetic targets.

If disulfide **248** is formed and assembles library building blocks **244** upon it **(Scheme 93)**, thus, rendering the disulfide bond forming reaction that ensues *pseudo*-intramolecular, formation of duplex **249** will be accelerated. Conversely, one can imagine disulfide **249** assembling library building blocks **246** upon it, allowing *pseudo*-intramolecular kinetic control of the reaction resulting in the amplification of duplex **248**. Concurrent turns of each of these two interdependent crosscatalytic cycles would generate exact copies of both duplexes.

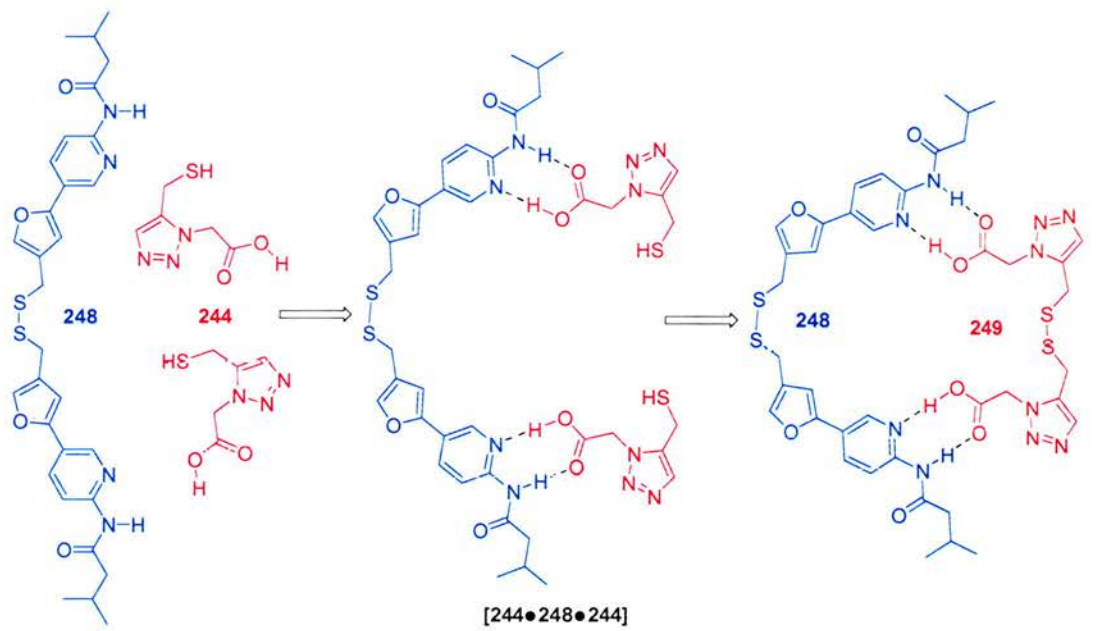

Scheme 93: One possible outcome within our system, synthetic reciprocal replication.

Another method by which building blocks **244** and **246** could amplify is *via* self-replication **(Scheme 94)**. If heterodisulfide **250** assembles building blocks **244** and **246** upon it, allowing disulfide formation to take place *pseudo*-intramolecularly, the reaction between them will be accelerated. Upon dissociation an exact copy of template **250** would be formed.

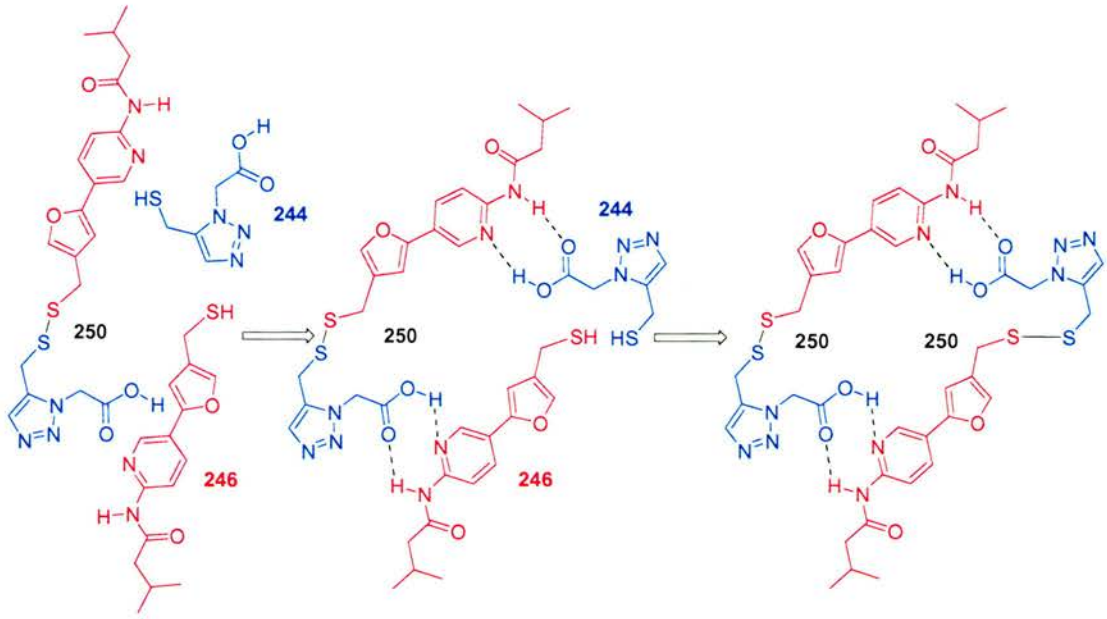

Scheme 94: One possible outcome within the system, synthetic self-replication.

4.4.2 Synthesis of Thiol 246

Synthesis of thiol **246** was attempted in 10 steps *via* the synthetic strategy shown in **Scheme 95**. Furan-3-carboxylic acid **251** was converted to the corresponding bromide **252** *via* a bromination[240] reaction involving *n*-bromosuccinimide in acetic acid to afford the desired product in 30% yield after recrystallisation from water. Carboxylic acid **252** was then reduced to the corresponding alcohol **253** using lithium aluminium hydride. Over reduction of the carboxylic acid to (4,5-dihydro-furan-3-yl)-methanol occurred initially with reaction conditions of 15 minutes at 0 °C, however, on reduction of the reaction time (10 minutes) and a decrease in the reaction temperature to -10 °C, alcohol **253** was produced in 36% yield. Alcohol **253** was then silyl protected in 53% yield.

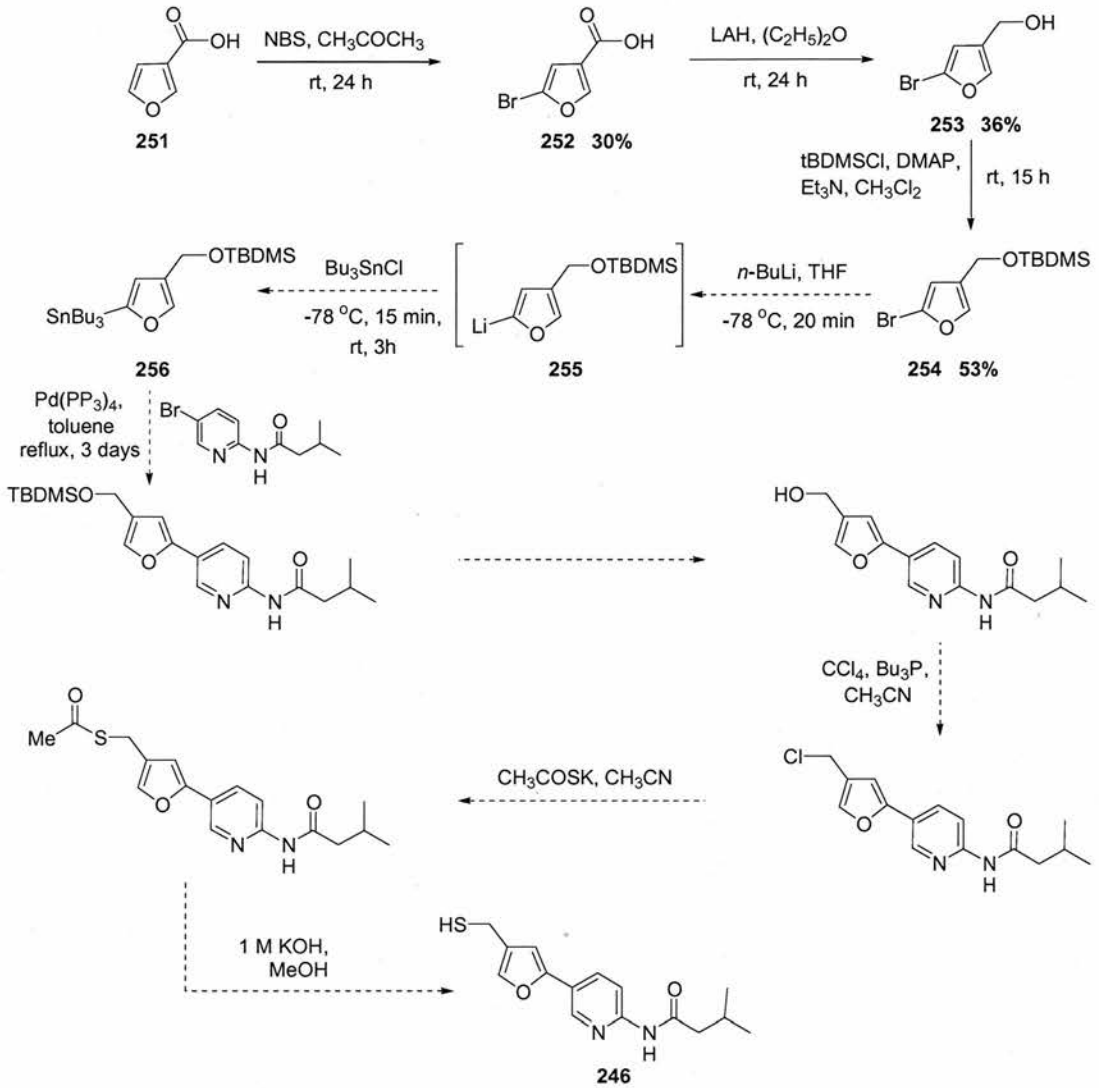

Scheme 95: Synthetic pathway for the preparation of *N*-[5-(4-mercaptomethyl-furan-2-yl)-pyridin-2-yl]-3-methyl-butyramide **246**.

The next stage of the reaction sequence involved a two-stage process; lithiation, follow by conversion to tributylstanane **256**. Bromide **254** was reacted with *n*-butyl lithium followed by addition of tributyl tin chloride. A variety of reaction times were investigated in order to facilitate the two-step process, however, all attempts failed, the major product recovered in all cases was de-brominated starting material.

The problems encountered with the conversion of bromide to stanane and the low yields obtained for the initial steps of the reaction sequence led to this synthetic strategy being abandoned. Two new synthetic targets were proposed **(Scheme 96)**.

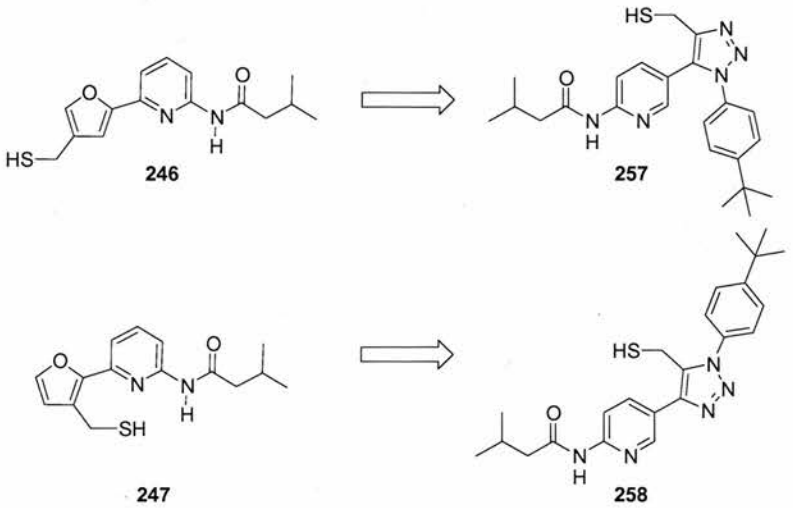

Scheme 96: New synthetic targets.

4.4.3 Synthesis of Arene 262

Amide **262** was synthesised in two simple high yielding steps **(Scheme 97)**. 2-Amino-5-bromopyridine was converted to amide **260** *via* standard coupling conditions with acid chloride isovaleryl chloride, after purification by silica gel flash column chromatography, **260** was obtained in 73% yield. Amide **260** was then reacted with freshly distilled propargyl alcohol **261** *via* a palladium-catalysed Sonogashira coupling reaction to yield amide **262** in 93% yield.

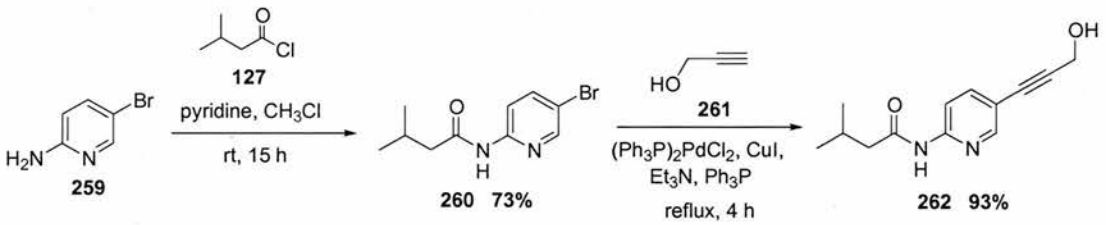

Scheme 97: Synthetic route for the preparation of *N*-[5-(3-hydroxy-prop-1-ynyl)-pyridin-2-yl]-3-methyl-butyramide **262**.

4.4.4 Synthesis of Azide 265

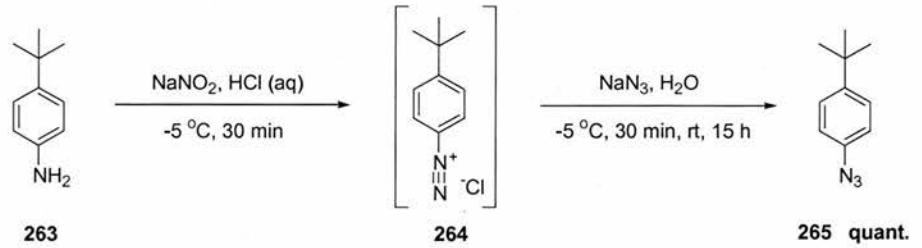

Scheme 98: One-pot synthetic sequence for the preparation of 1-azido-4-*tert*-butyl-benzene **265**.

tert-Butyl aniline was converted to the corresponding azide in a one-pot high yielding procedure **(Scheme 98)**. Azide **265** was prepared *via* intermediate diazonium salt **262**. *tert*-Butyl aniline was added to a solution of aqueous hydrochloric acid and the pH checked to be 1. Subsequent addition of 1 equivalent of sodium nitrite facilitated the formation of diazonium salt intermediate **262** on stirring at – 5 °C for 30 minutes. After this time, sodium azide was added dropwise at – 5 °C, the solution stirred for 30 minutes and then allowed to warm to room temperature and stir for a further one hour. After work-up, the reaction mixture was carefully reduced *in vacuo* to yield the desired azide **265** in quantitative yield.

4.4.5 Synthesis of Triazoles 266 and 267

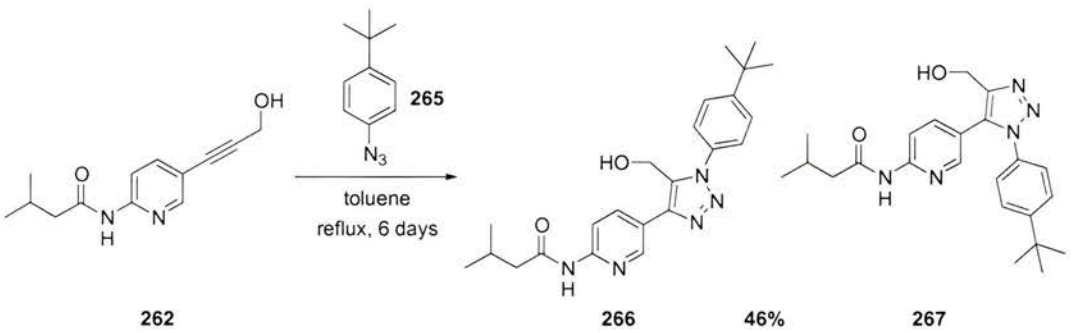

262 **266** **46%** **267**

Scheme 99: Triazole regioisomers formed in the reaction between azide **265** and arene **262**.

1,3-dipole azide **265** and dipolarophile aryne **262** reacted in a [3+2] cycloaddition reaction[242] **(Scheme 99)** to form regioisomeric triazoles **266** and **267**. The reaction between **262** and **265** was complete after six days refluxing in the minimum volume of toluene required to dissolve the starting materials. One major and one minor isomer were obtained from the reaction as a result of the influence of the bulky *tert*-butyl group. Triazoles **266** and **267** were obtained in an overall yield of 46% after purification by column chromatography.

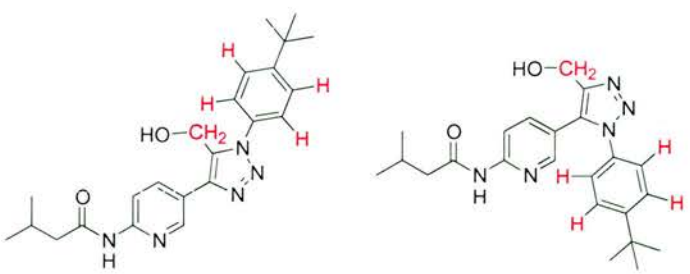

Figure 97: Potential detectable nOe difference NMR signals for triazoles **266** and **267**.

Nuclear Overhauser Effect (nOe) NMR experiments[210] were undertaken in order to establish the structure of each regioisomer. Unlike COSY experiments NOESY experiments detect through space rather than through bond couplings. nOe interactions are detected when a single resonance is irradiated at its resonance frequency and the atom which is close in space appears as a more intense signal than usual. However, in this case nOe difference experiments proved futile; there were no detectable changes in the spectra of either isomer **266** or **267 (Figure 97)** when irradiated at different frequencies. As a result, the synthesis of triazoles **268** and **269 (Figure 98)** was undertaken, in the hope that it would be possible to assign regioisomers by nOe difference experiments as a result of their additional $-CH_2$ moieties.

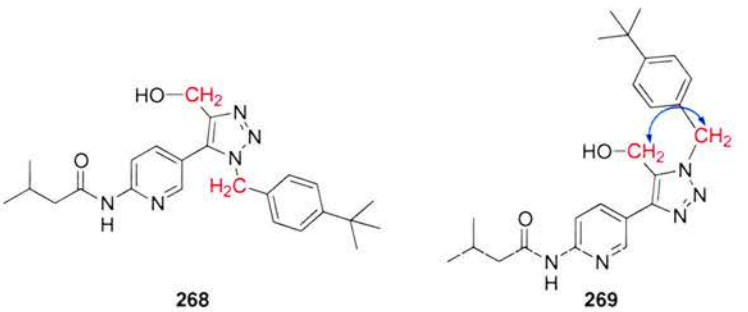

Figure 98: Potential nOe difference NMR signals for the assignment of triazoles **268** and **269**.

4.4.6 Synthesis of Azide 271

The synthesis of azide **271** was undertaken in a simple one-step process **(Scheme 100)**. 4-(*tert*-butyl) benzyl bromide was refluxed with sodium azide in acetone, by t.l.c the reaction had reached completion. The reaction mixture was then carefully reduced *in vacuo* to yield the desired azide **271** in a quantitative yield.

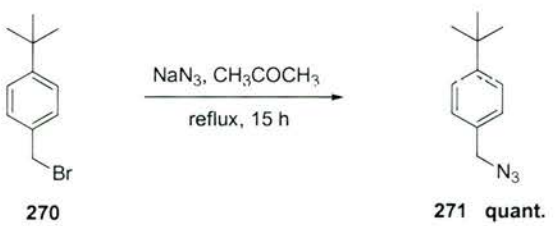

Scheme 100: Synthesis of 1-azidomethyl-4-*tert*-butyl-benzene **271**.

4.4.7 Synthesis of Triazoles 268 and 269

Azide **271** and aryne **262** were then reacted in a [3+4] cycloaddition reaction to form triazoles **268** and **269 (Scheme 101)**. Reaction between **271** and **262** was complete after refluxing overnight in the minimum volume of toluene required to dissolve the starting materials. Regioisomers were obtained in a 1:1 ratio, in an overall quantitative yield after column chromatography. In this case it was possible to assign regioisomers **268** and **269** by NMR nOe difference experiments as described in **Figure 98**.

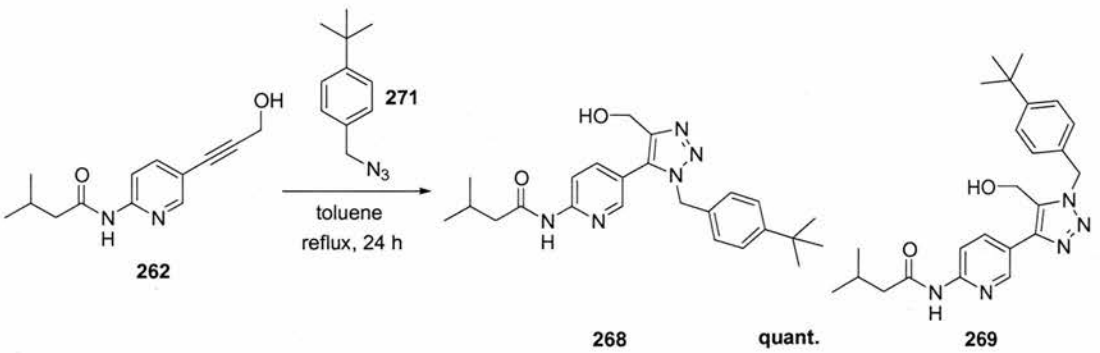

Scheme 101: The [3+4] cycloaddition reaction between 1,3-dipole azide **271** and dipolarophile aryne **262** yielding regioisomeric triazole products **268** and **269**.

4.4.8 Synthesis of Thiol 273

Successful assignment of the triazole alcohols allowed the preparation of thiol **273** to be undertaken **(Scheme 102)**. Thiol **273** was synthesised in a one-pot procedure *via* thiouronium salt intermediate[243] **272**. The corresponding chloride was prepared *in situ*, by reaction of alcohol **268** with *tri*-butyl phosphine and carbon tetrachloride the reaction was monitored by t.l.c. On full conversion of alcohol **268** to the chloride by t.l.c., thiourea was then added and the reaction mixture refluxed to yield the corresponding thiouronium salt **272**. On completion, the reaction was cooled at – 18 °C for 16 hours, after this time, addition of hexane to the reaction mixture, resulted in the precipitation of thiouronium salt **272** from solution, which was obtained by filtration under reduced pressure. Thiouronium salt **272** was then deprotected with sodium metabisulfite to yield the desired thiol **273** in 33% yield over three steps.

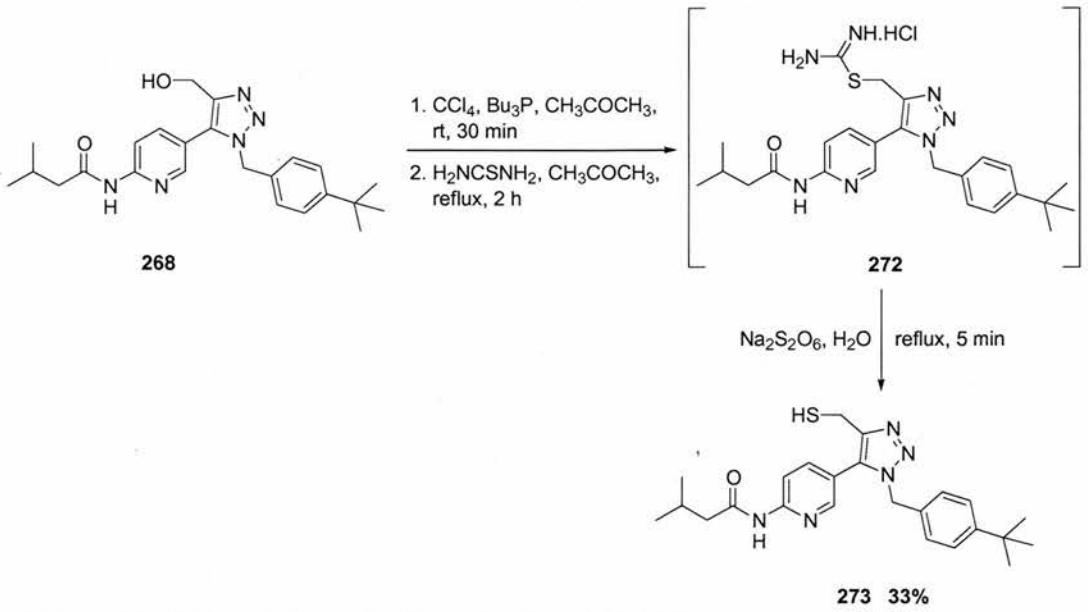

Scheme 102: Synthetic procedures for the preparation of thiol **273**.

4.4.9 Synthesis of Triazoles 276 and 277

tert-Butylbromoacetate **274 (Scheme 103)** was converted to the corresponding azide[31] **275** *via* reaction with sodium azide in acetone. The reaction mixture was filtered to remove the resulting NaBr salt, the filtrate was then concentrated *in vacuo* to yield desired azide **275** in quantitative yield. The formation of triazoles **276** and **277** was facilitated by the reaction of azide **275** in the presence of freshly distilled propargyl alcohol.

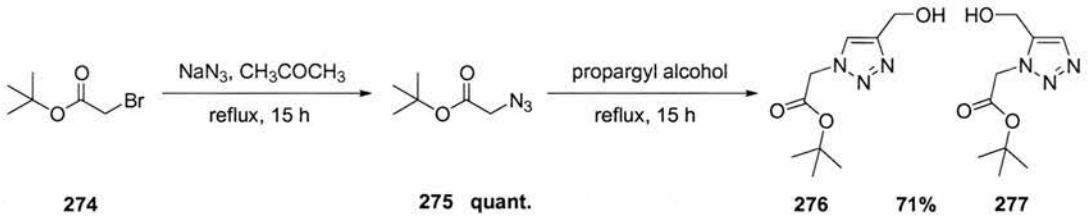

Scheme 102: Synthetic procedure for the production of triazoles **276** and **277** *via* a [3+4] cycloaddition reaction.

The resulting regioisomers were separated *via* silica gel flash column chromatography. Regioisomers **276** and **277** were formed in a 1:1 ratio, as there was no steric hindrance to invoke the preferential production of one isomer over the other. Regioisomers **276** and **277** were assigned by a set of nOe difference NMR experiments **(Figure 99)**.

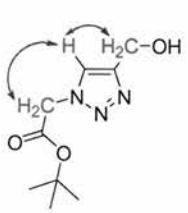

276

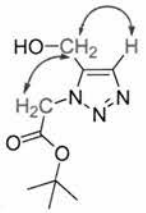

277

Figure 99: nOe signals detected for the assignment of triazole regioisomers **276** and **277**.

4.4.10 Synthesis of Thiol 283

Alcohol **276 (Scheme 104)** was chlorinated using carbon tetrachloride and *tri*-butyl phosphine, to yield chlorinated intermediate **278**, as observed by t.l.c. Intermediate chloride **278** was converted to the corresponding thioacetate **279** *via* reaction with potassium thioacetate the desired product was afforded in 57% yield after purification *via* silica gel flash column chromatography. Thioacetate **279** was de-S-acetylated under standard conditions, however, rather than obtaining desired thiol **280**, the deprotection conditions led to the formation of alcohol **281**.

A different synthetic route was therefore investigated. Chloride **278** was prepared as described previously and then converted to the corresponding thiouronium salt **282** on reaction with thiourea. The reaction mixture was then refluxed for 1.5 hours and then cooled at -18 °C for 16 hours. On addition of hexane to the reaction mixture, thiouronium salt **282** precipitated from solution and was obtained by filtration under reduced pressure. Thiouronium **282** was then deprotected with sodium metabisulfite, unfortunately under the deprotection conditions it proved impossible to obtain free thiol **280**, instead disulfide **283** was formed. The formation of disulfide rather than thiol was not seen as a major difficulty as it would be possible to reduce disulfide **283** back to its thiol counterparts at a later stage. Finally, the *tert*-butyl protecting group was removed under acidic conditions to afford disulfide **250** in 88% yield.

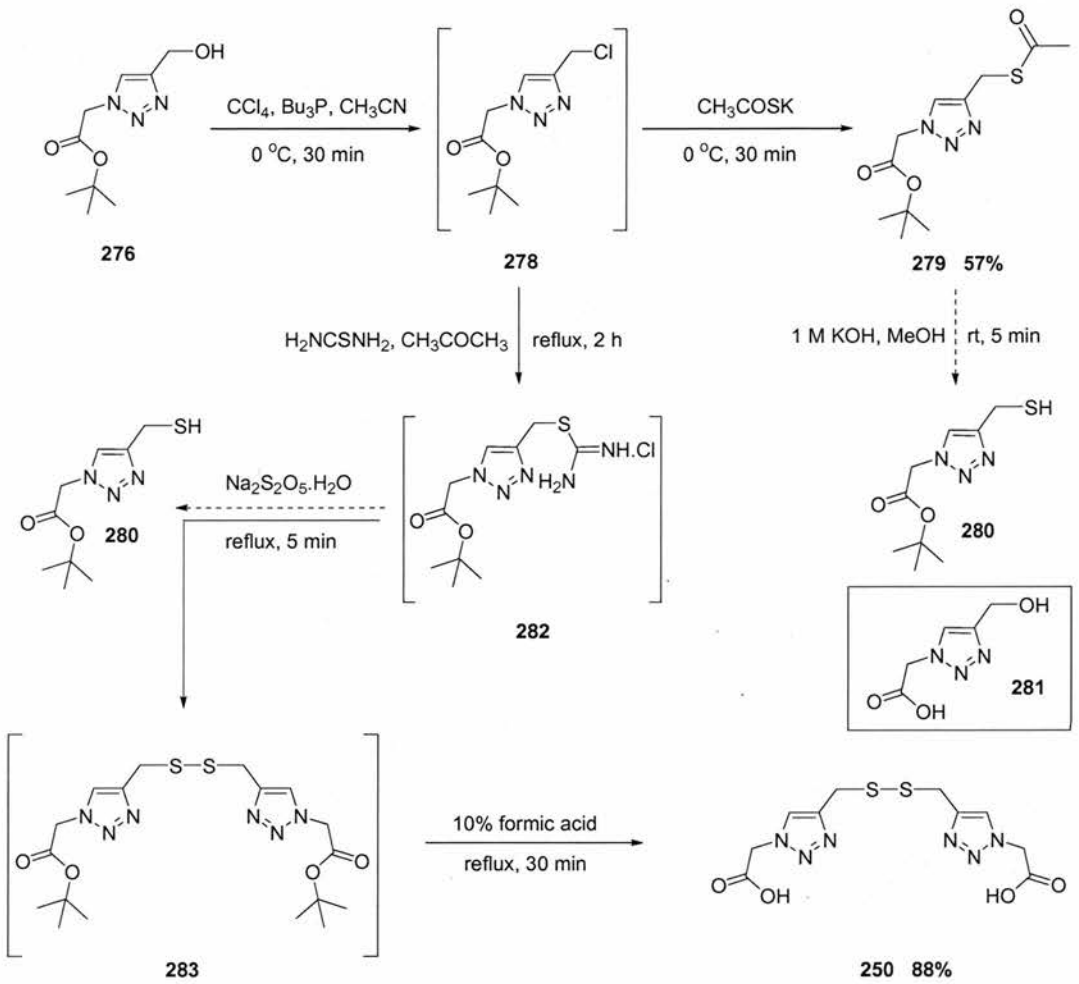

Scheme 103: Proposed synthetic sequence for the production of mercaptomethyl-[1,2,3]triazole-1-yl)-acetic acid.

Disulfide **250** proved to be insoluble at any concentration in $CDCl_3$. Disulfide **250** was only soluble in polar solvents such as methanol and DMSO. Disulfide **250** would be produced in the course of our library experiments and therefore its solubility was of great importance. All library members are required to be available for exchange and reaction with each library component, therefore one library member precipitating from solution deems the library unsuitable for study. As our studies must be conducted in non-polar solvents in order that hydrogen bonding is not disrupted, therefore this library strategy was abandoned.

4.5 Further Studies

Reflecting upon the synthetic studies conducted previously, a dynamic library which did not use disulfide exchange as the reversible reaction was designed. Target molecules shown in **Figure 100** were devised as synthetic targets. Library building blocks once again contain either amidopyridine or carboxylic acid recognition groups, in order to allow association between components. This library has been designed to use the fast reversible reaction of

aldehydes and amines to generate an imine library. The recognition features incorporated into library building blocks will allow the preference of the system to adopt reciprocal or self-replicating associations to be explored **(Figure 100)**.

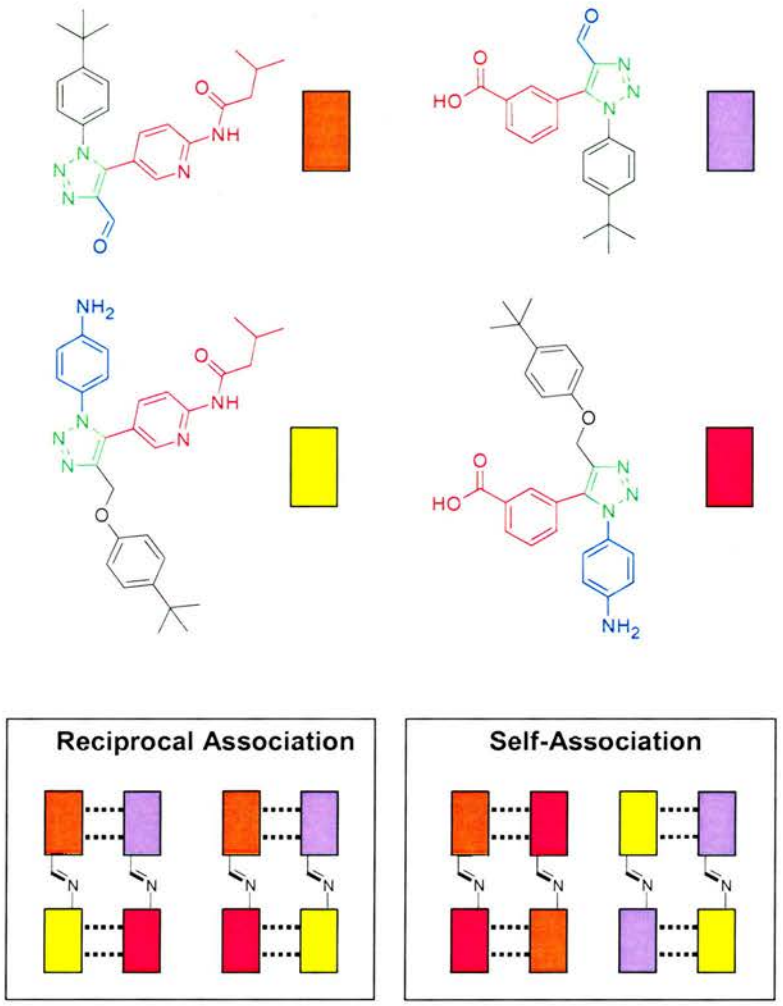

Figure 100: Target library members and the possible recognition patterns available to the library building blocks.

Indeed, in a similar manner to the proposed disulfide system, bifunctionalising the building blocks would allow the possibility of chain formation **(Figure 101)**. Molecular modelling studies were undertaken to assess the possibility of the imine chains forming a helix. Monte Carlo conformational searches were performed using the AMBER* forcefield and the GB/SA solvation model for $CDCl_3$. Molecular modelling studies show **(Figure 101)** that the hydrogen bonding recognition motifs incorporated into both imine 'strands' could potentially hold the chains together. The short imine chains **(Figure 101)** display the beginnings of helical characteristics.

Once again this study will be undertaken to answer key questions such as; (i) is replication possible and is self-replication or reciprocal replication the favoured mode of copying within

this system?, (ii) Will a helix be formed and how many imine units will it take to form a stable helix? This project is now being continued within the Philp group.

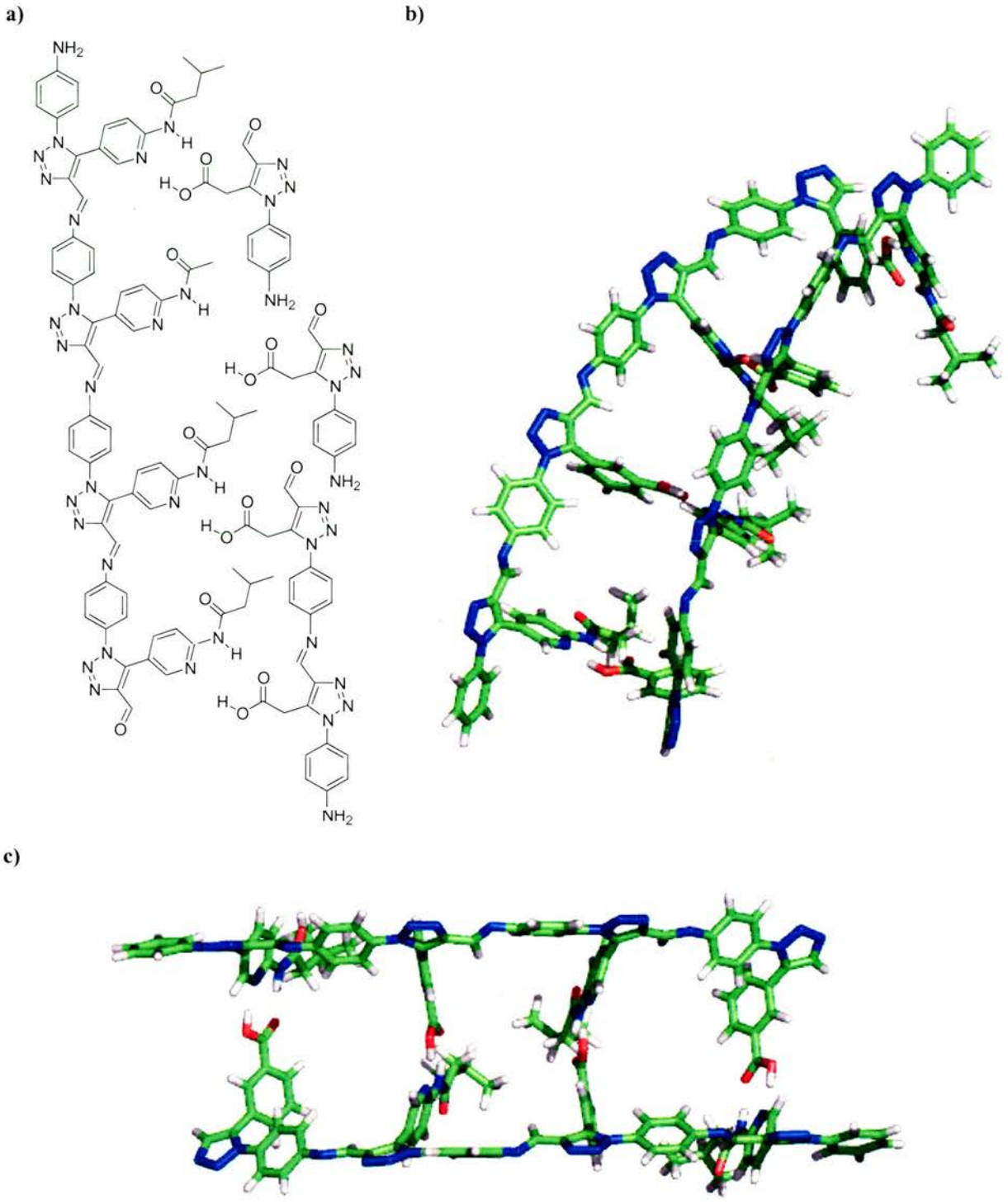

Figure 101: **a)** Imine chain formation, two chains held together by complementary hydrogen bonding interactions on each strand. Models derived from molecular mechanics calculations using the AMBER* forcefield. Carbon, oxygen, nitrogen and hydrogen atoms are coloured green, red, blue and white respectively. Hydrogen bonds are represented by dashed lines and hydrogen bond donor and acceptor distances are given in Å; **b)** the beginnings of helix formation can be observed; **c)** another view showing the hydrogen bonding interactions between chains.

4.6 The Design and Synthesis of a Diels-Alder Dynamic System Capable of Reciprocal and/or Self-Replication

The aim of this project was to probe the relationship between direct and reciprocal replication. We wished to design a system which could potentially amplify *via* either replication route. In conjunction with the principles of dynamic combinatorial chemistry, we wished this process to be under thermodynamic control and therefore be error checking.

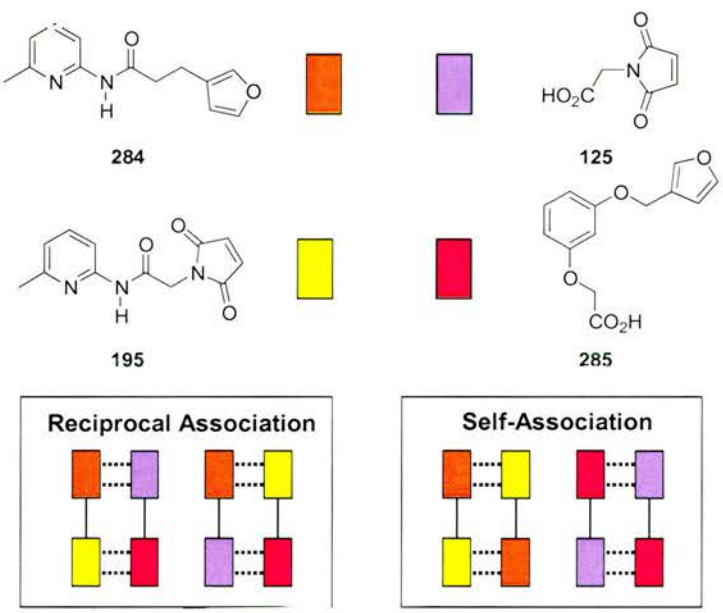

Figure 102: Target library members and the possible recognition patterns available to the library building blocks.

The Diels-Alder reaction was chosen as the reversible reaction within our new system. The target molecules **(Figure 102)** contain either amidopicoline or carboxylic acid motifs suitable for complementary hydrogen bonding. Each molecule contains either a furyl moiety (diene) or a maleimide moiety (dienophile). This small library can generate up to eight products, four cycloadducts each with an *endo* and *exo* diastereoisomer. The library may operate in a self-replicating or reciprocally replicating manner; the four possible association patterns are shown in **Figure 102**. During our studies we hoped to probe whether self- or reciprocal association would be favoured within the system and whether this would lead to the amplification of members within the library.

If adduct **286** is formed and assembles library building blocks **125** and **285** upon it **(Figure 103)**, thus, rendering the Diels-Alder bond forming reaction that ensues *pseudo*-intramolecular, formation of cycloadduct **287** will be accelerated. Conversely, one can

imagine adduct **287** assembling library building blocks **195** and **284** upon it, allowing *pseudo*-intramolecular kinetic control of the reaction amplification of duplex **286**. Concurrent turns of each of these two interdependent crosscatalytic cycles would generate exact copies of both duplexes through a reciprocal replicating pathway.

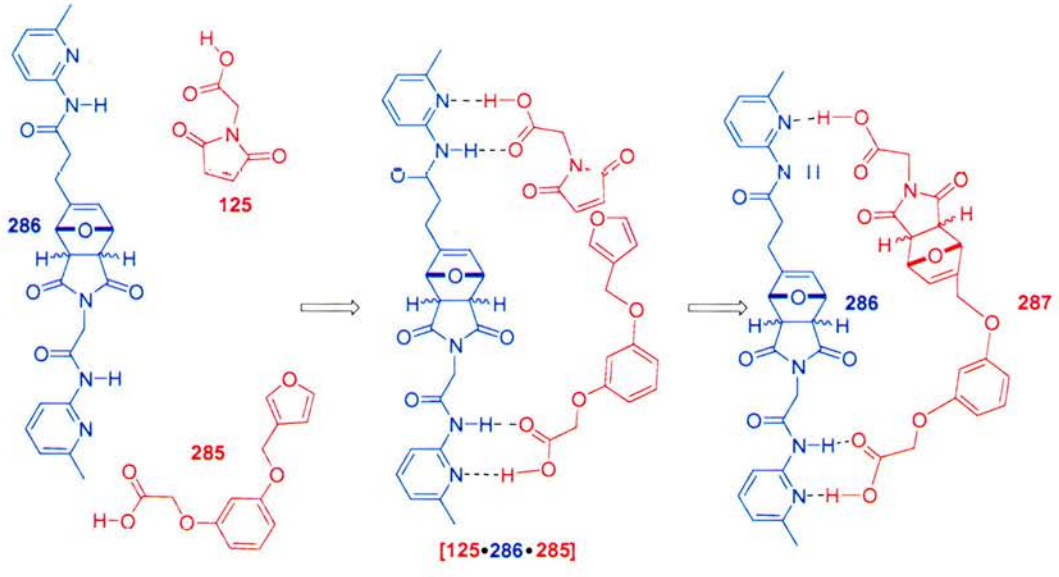

Figure 103: One possible outcome within our system; reciprocal replication.

Building blocks **195** and **285** could also amplify is *via* self-replication **(Figure 104)**. If cycloadduct **288** assembles building blocks **195** and **285** upon it, allowing covalent bond formation to take place *pseudo*-intramolecularly, the reaction between them will be accelerated. Upon dissociation an exact copy of **288** would be formed *via* a self-replicating pathway.

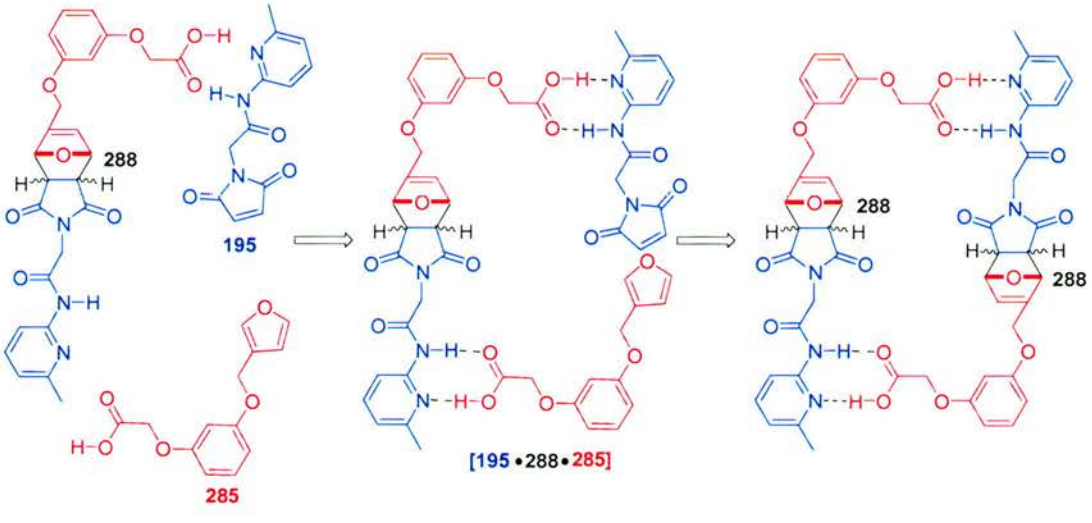

Figure 104: One possible outcome within our system; self-replication.

4.6.1 Synthesis of Carboxylic Acid 285

The synthesis of carboxylic acid **285** was attempted in 4 steps **(Scheme 105)**. The coupling between resorcinol **289** and *tert*-butyl bromoacetate **290** was carried out in the presence of potassium carbonate, the reaction mixture was refluxed in CH_3CN for 48 hours. After this time, the reaction mixture was filtered, the filtrate reduced *in vacuo* and the crude residue purified *via* silica gel flash column chromatography to yield the desired product **291** as an oil in 53% yield. 3-Chloromethyl chloride **141** was prepared from the corresponding alcohol **140** using carbon tetrachloride and *tri*-butyl phosphine in acetonitrile. Crude chloride **141** was then added to a suspension of alcohol **291** and potassium carbonate in CH_3CN. The reaction mixture was refluxed for 48 hours, after which time the reaction mixture was worked-up and purified by column chromatography to afford product **292** in good yield.

A *tert*-butyl ester groups can be deprotected under acidic conditions.[244] However, all attempts to deprotect ester **292** in a variety of acids including formic, trifluroacetic and *p*-tolyl sulfonic, under varying reaction times and solvents did not yield clean acid **285**. The majority of the material recovered from the reaction was diol **293** the acidic deprotection conditions had destroyed the furan moiety on compound **292**. Therefore, a second synthetic route for the production of **285** was devised. **Scheme 106** shows the revised synthetic sequence utilising a methyl ester group for the protection of the carboxylic acid moiety as methyl esters can be removed under basic reaction conditions.

The synthesis of alcohol **295** from diol **289** was attempted under the same conditions reported above for the conversion of **289** to **291 (Scheme 105)**. Problems in the monitoring of the reaction mixture quickly became apparent. Reaction starting material resorcinol **289**, monoester **295** and the corresponding diester products all had very similar R_f values on t.l.c in all solvent conditions attempted. This visualisation problem translated into a purification problem. Attempts to separate the three compounds (resorcinol **289**, monoester **295** and the corresponding diester) in a variety of solvent systems failed. Therefore, this synthetic pathway was abandoned at the first stage.

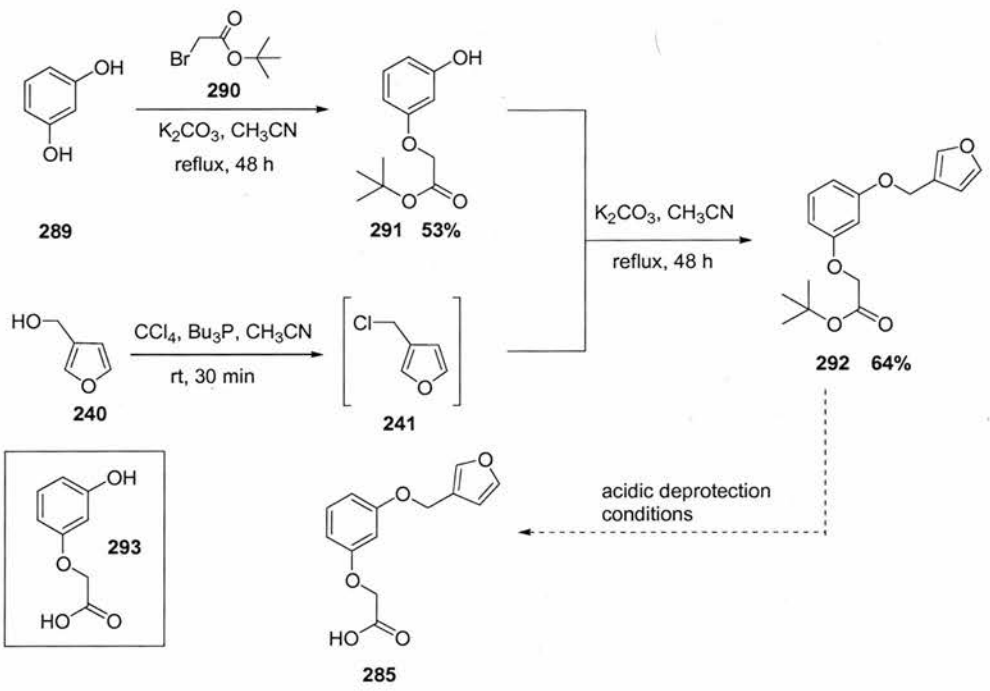

Scheme 105: Synthetic pathway for the preparation of [3-(furan-3-ylmethoxy)-phenoxy]-acetic acid **285**.

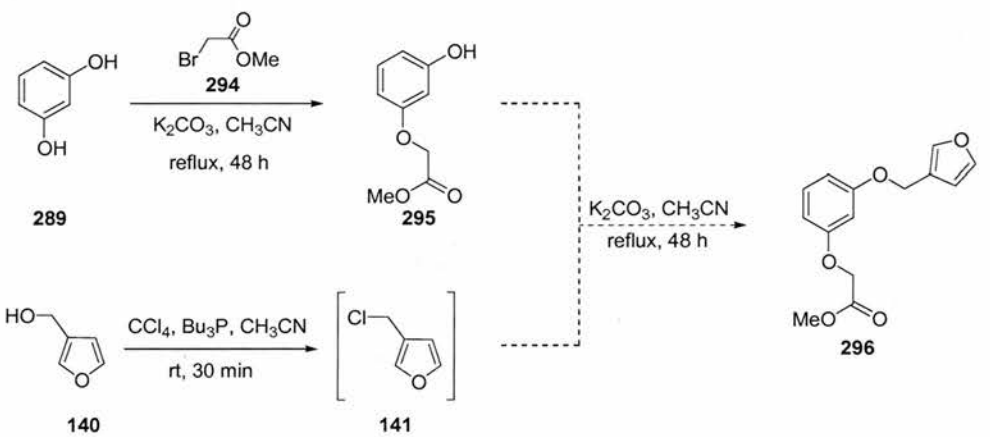

Scheme 106: Synthetic pathway towards the preparation of [3-(furan-3-ylmethoxy)-phenoxy]-acetic acid **285**.

The obvious next choice of protecting group was an ethyl ester, as it could also be removed under basic conditions and it was hoped that the increase in carbon chain length would lead to a larger difference in polarity of the mono- and disubstituted products. Indeed this was the case and monoester **298 (Scheme 107)** was isolated in 34% yield after purification *via* silica gel column chromatography. Alcohol **140** yielded the corresponding chloride **141** on reaction with carbon tetrachloride and *tri*-butyl phosphine in acetonitrile, the reaction had reached completion after 30 minutes and was carried through to the next stage without further purification. Crude chloride **141** was then added to a suspension of alcohol **298** and

potassium carbonate in CH_3CN. The reaction mixture was refluxed for 48 hours, after which time the reaction mixture was worked-up and purified by column chromatography to yield desired product **299** 64% yield. The final step in the reaction path, involved the basic deprotection of the ethyl ester **299** to yield target acid **285**. This was achieved under standard hydrolysis conditions, 1 *M* KOH in a 1:1 THF:H_2O, subsequent acidification and extraction into CH_2Cl_2, afforded acid **285** in 70% yield.

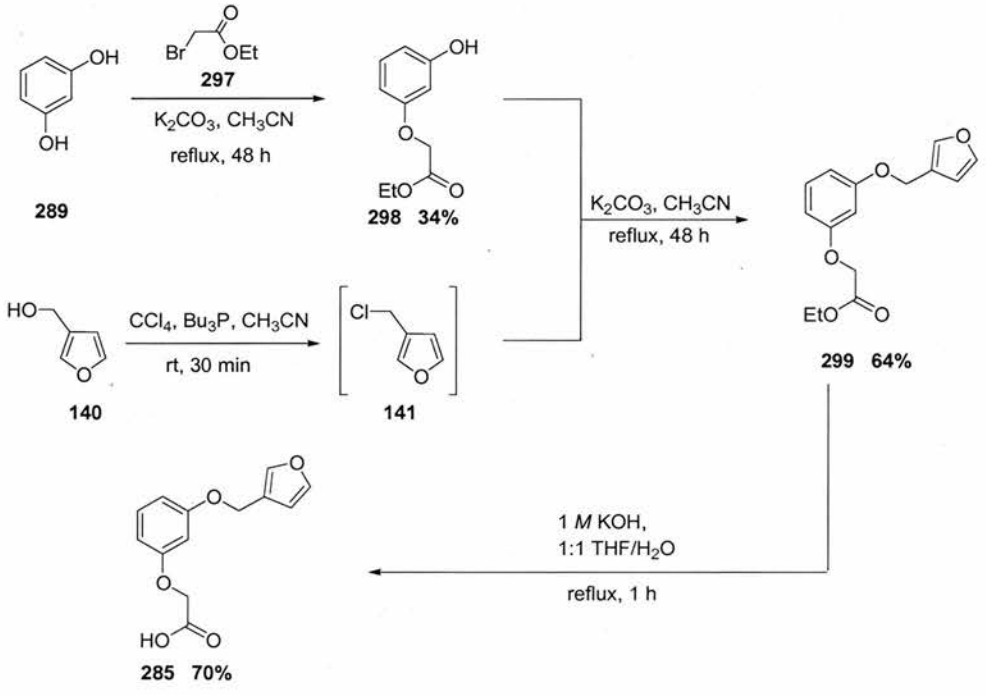

Scheme 107: Synthetic pathway for the preparation of [3-(furan-3-ylmethoxy)-phenoxy]-acetic acid **285**.

4.6.2 Synthesis of Amide 284

The synthesis of amide **284** was achieved in three high-yielding steps **(Scheme 108)**.

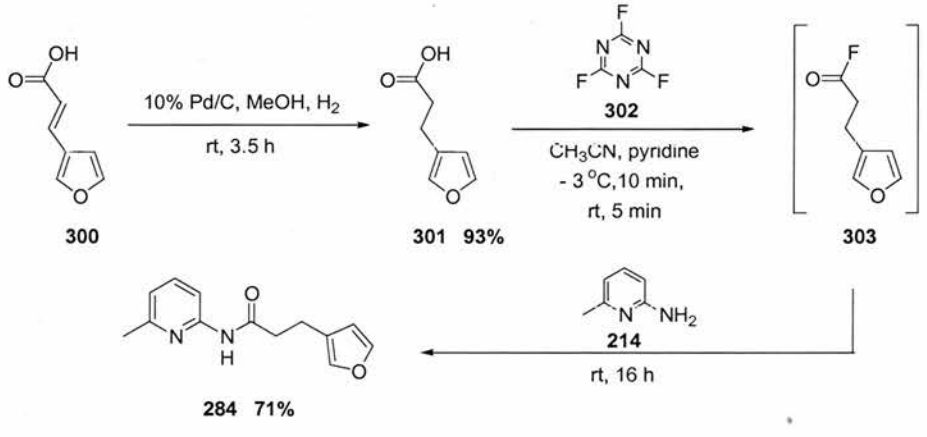

Scheme 108: Synthetic pathway for the production of 3-furan-3-yl-*N*-(6-methyl-pyridin-2-yl)-propionamide **284**.

Commercially available *trans*-3-furanacrylic acid **300** was converted to the corresponding saturated compound **301** *via* a palladium on carbon catalysed hydrogenation reaction. The reaction time was varied depending upon the activity of the palladium/carbon reagent. Monitoring this reaction proved problematic as the product and starting material both have the same retention time when run on silica gel t.l.c plate. The only indication of reaction completion was a change in the UV intensity of the spots by t.l.c. The problems in monitoring the reaction and inconsistent reaction times, led to either under or over reduced acid being present on cessation of the reaction. Impurities were removed from the desired product *via* Kugelröhr distillation followed by recrystallisation in hexane to yield the acid **301** in 93% yield. Acid **301** was converted to corresponding fluoride **303** using cyanuric fluoride **302** as a fluorinating agent, the fluoride was not isolated, the crude mixture was extracted with CH_2Cl_2/brine, dried and the organic layer reduced to half its original volume. To the crude fluoride **303** in CH_2Cl_2, aminopicoline **214** was added and the reaction mixture stirred overnight. Desired amide **284** was obtained in 71% over the two-steps after purification *via* silica gel column chromatography.

4.6.3 Synthesis of Maleimides 125, 148 and Amide 195

Maleimide **125** was prepared in a one-pot procedure as discussed in **Section 2.7.4**. Control maleimide **148** was prepared in a one-pot procedure as discussed in **Section 2.7.4**. Amide **195** was prepared in a one-pot process as discussed fully in **Section 3.5.3**.

4.7 Kinetic Analysis of the System

It was important to understand the behaviour of each pair of diene and dienophiles before conducting library based studies. Kinetic experiments were carried out in accordance with the procedure outlined in the general experimental section **(Chapter 6)**. Kinetic experiments were set up at 25 °C with each component at an initial concentration of 25 m*M* in $CDCl_3$ and monitored for a period of 16 hours by 500 MHz ^{1}H NMR spectroscopy.

4.7.1 The Diels-Alder reaction between Diene 284 and Dienophile 195

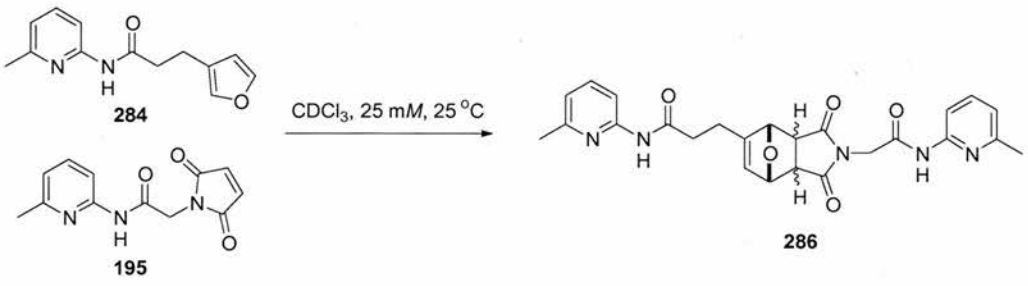

Scheme 109: Reaction conditions chosen to facilitate the Diels-Alder reaction between **284** and **195**.

The reaction between diene **284** and dienophile **195 (Scheme 109)** at 25 °C and 25 m*M* of each reagent in $CDCl_3$, was monitored by 500 MHz ^1H NMR spectroscopy, the extent of reaction was determined by deconvolution the appropriate resonances corresponding to the *exo* and *endo* cycloadduct bridgehead protons. The ratio of *exo*:*endo* cycloadducts after 16 hours was calculated to be ~1:1.

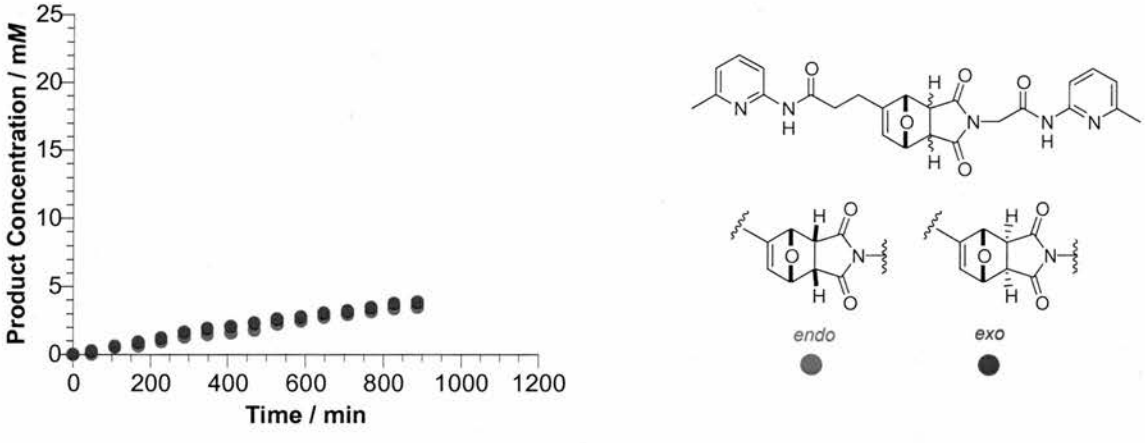

Figure 105: Rate profile for the reaction between **284** and **195** over 16 hours. The *endo* cycloadduct is depicted as full red circles and the *exo* cycloadduct is depicted as full blue circles.

The reaction between **284** and **195** was then attempted in the presence of 1 equivalent of template **287 (Scheme 110)**. However, template **287** proved to be completely insoluble in $CDCl_3$ under the reaction conditions.

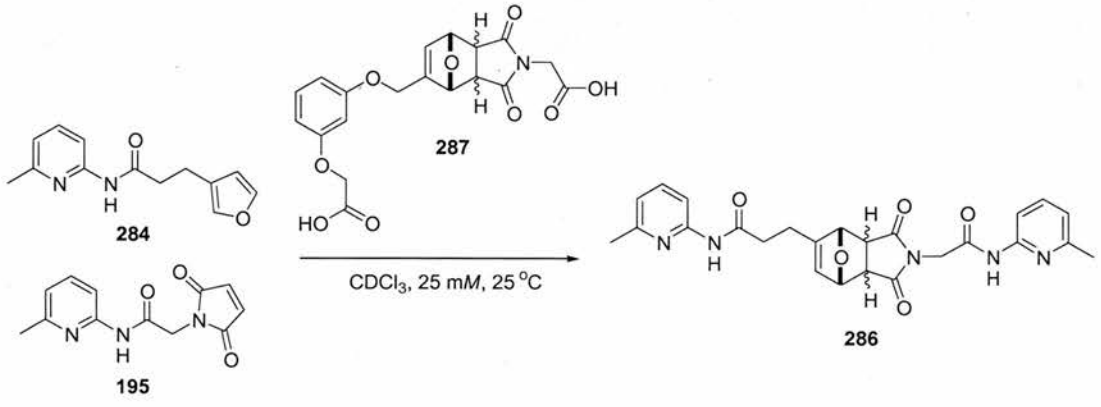

Scheme 110: Reaction conditions chosen to facilitate the Diels-Alder reaction between **285** and **195** in the presence of template **287**.

4.7.2 The Diels-Alder reaction between Diene 285 and Dienophile 125

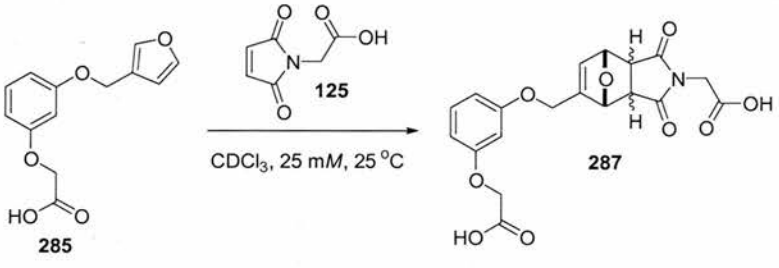

Scheme 111: Reaction conditions chosen to facilitate the Diels-Alder reaction between **125** and **285**.

The reaction between diene **285** and dienophile **125 (Scheme 111)** at 25 °C and 25 m*M* of each reagent in $CDCl_3$, was monitored by 500 MHz ^1H NMR spectroscopy, the extent of reaction completion was determined using the deconvolution tool available in 1D WINNMR. The reaction between diene and dienophile after 16 hours had reached only ~ 10% completion, with the *endo* isomer being formed in slight preference to the *exo* diastereoisomer **(Figure 106)**.

It was hoped that the reaction between **125** and **285** would be accelerated in the presence of template molecule **286 (Scheme 112)**. In this case, there were no problems with solubility and 1 equivalent of template **286** was added to the reaction between diene **125** and dienophile **285** at the beginning of the reaction.

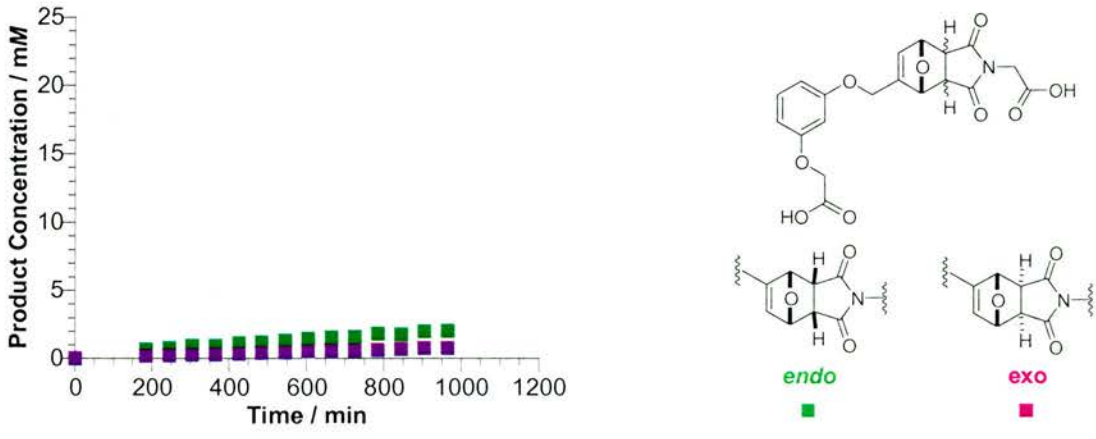

Figure 106: Rate profile for the reaction between **125** and **285** over 16 hours. The *endo* cycloadduct is depicted as full green squares and the *exo* cycloadduct is depicted as full purple squares.

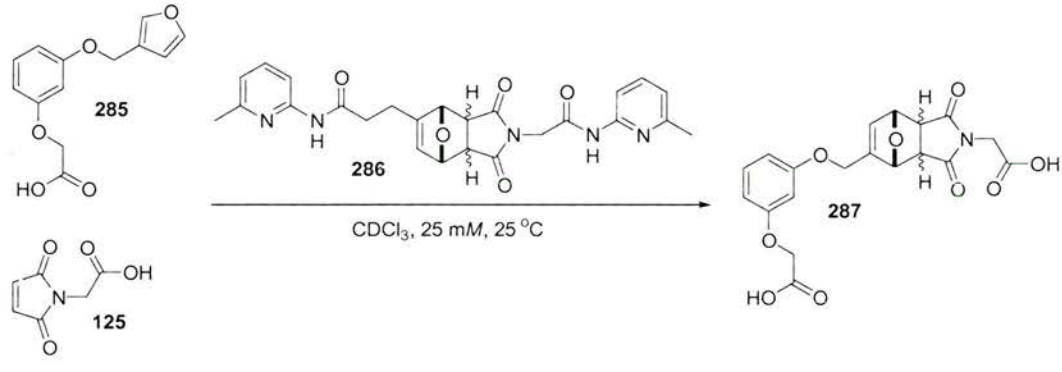

Scheme 112: Reaction conditions chosen to facilitate the Diels-Alder reaction between **125** and **285** in the presence of template **286**.

However, on addition of template **286** to the reaction mixture, little change in the rate profile was observed. A slight decrease in the concentration of the *endo* adduct and a slight increase in the extent of *exo* cycloadduct formation was observed over the 16 hour period. The extent to which the reaction proceeded was unaffected by the presence of template **286**. It is possible that template **286** is enhancing the formation of *endo* cycloadduct **287** at the expense of *exo* adduct **287**. The error in kinetic experiments is generally assumed to be ~ 5%, however at such low concentrations this error may indeed be greater. Therefore, the assumption of a template directed affect would have to be carefully considered in light of the low conversion of starting materials to product in this case.

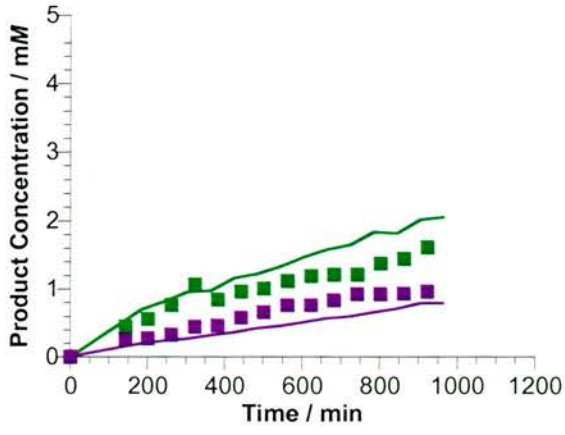

Figure 107: Rate profile for the reaction between **125** and **285** over 16 hours; the *endo* cycloadduct is depicted as a solid green line and the *exo* cycloadduct is depicted as a solid purple line. Rate profile for the reaction between **125** and **285** in the presence of template **286** over 16 hours; the *endo* cycloadduct is depicted as filled green squares and the *exo* cycloadduct is depicted as filled purple squares.

4.7.3 The Diels-Alder reaction between Diene 284 and Dienophile 125

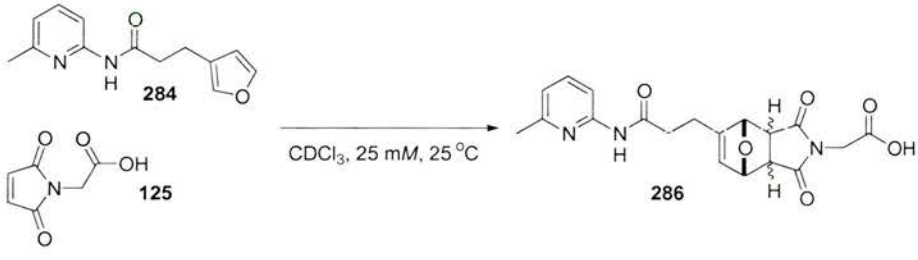

Scheme 113: Reaction conditions chosen to facilitate the Diels-Alder reaction between **284** and **125**.

In order to determine the effect of recognition on the Diels-Alder reaction described above **(Scheme 113)** a control experiment was undertaken in which the carboxylic acid recognition site was removed, replaced by a methyl ester, disrupting the recognition-mediated pathway. The reaction between diene **284** and control dienophile **148** at 25 °C and 25 m*M* of each reagent in $CDCl_3$, was monitored by 500 MHz ^{1}H NMR spectroscopy, the extent of reaction completion was determined using the deconvolution tool available in 1D WINNMR. The reaction between diene and dienophile after 16 hours had reached ~ 20% completion, with the *endo* isomer being formed in slight preference to the *exo* isomer **(Figure 108)**. The Diels-Alder reaction was then carried out under identical conditions in the presence of recognition dienophile **125**. The reaction profile for the recognition mediated reaction is shown in **Figure 109a**.

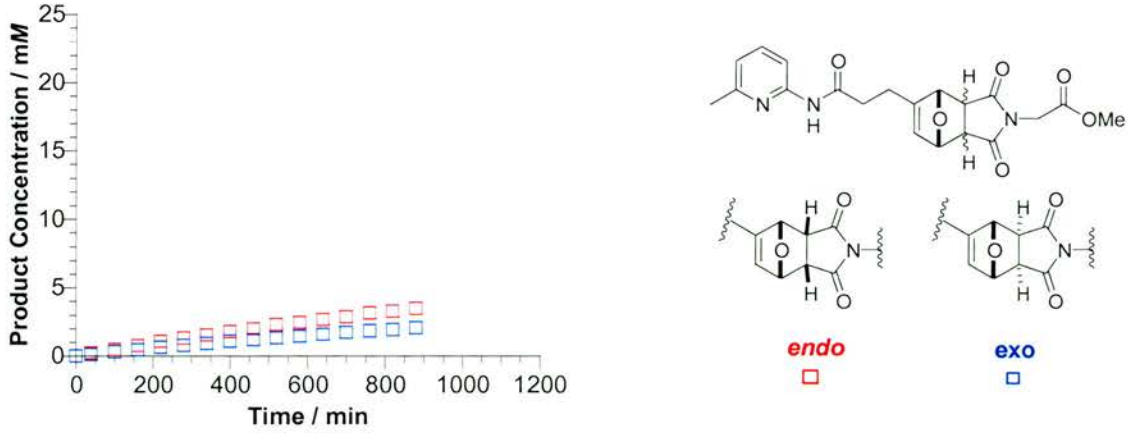

Figure 108: Rate profile for the reaction between **148** and **284** over 16 hours. The *endo* cycloadduct is depicted as open red squares and the *exo* cycloadduct is depicted as open blue squares.

The reaction is indeed effected by recognition, as the presence of the carboxylic acid moiety upon dienophile **125** has greatly enhanced the production of the *endo* adduct and barely changed the rate of production of the *exo* adduct, suggesting that the reaction is recognition-mediated, with a strong preference for the *endo* cycloadduct.

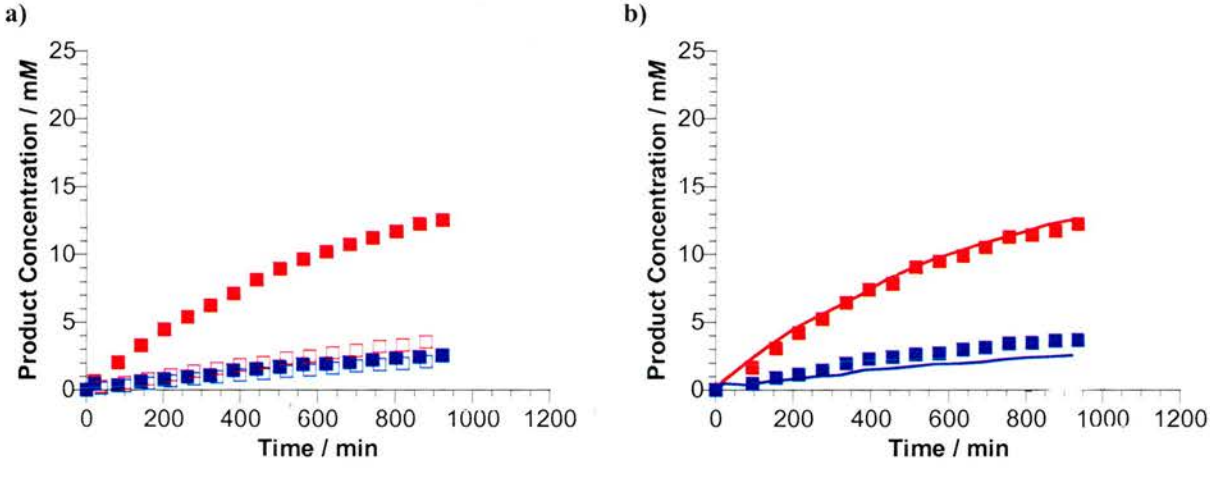

Figure 109: **a)** Rate profile for the bimolecular reaction between **284** and **125**; the *endo* cycloadduct is depicted as open red squares and the *exo* cycloadduct is depicted as open blue squares. The rate profile for the recognition-mediated reaction between **284** and **148**; the *endo* cycloadduct is depicted as filled red squares and the *exo* cycloadduct is depicted as filled blue squares. **b)** Rate profile for the recognition-mediated reaction; the *endo* cycloadduct is depicted as red lines and the *exo* cycloadduct is depicted as blue lines. The rate profile for the reaction between **125** and **284** in the presence of template **286** is depicted as filled red squares (*endo* cycloadduct) and as blue filled squares (*exo* cycloadduct).

In order to determine whether the reaction was accelerated by a template effect, the reaction was doped with 1 equivalent of its own template. The results of the reaction are shown in **Figure 109b**. The addition of template had no effect on the rate of the reaction and therefore it can be concluded that the reaction is not following a self-replicating pathway. A further

template experiment was undertaken 1 eq. of template **288** was added to the reaction between diene **284** and dienophile **125**.

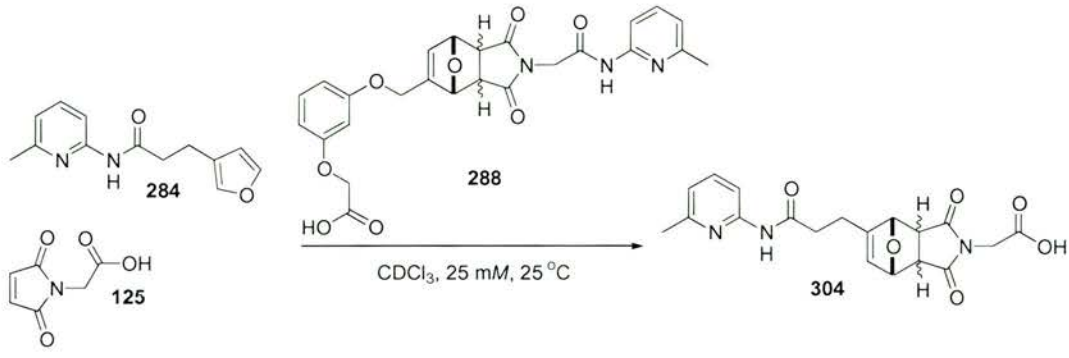

Scheme 113: Reaction conditions chosen to facilitate the Diels-Alder reaction between **284** and **125**.

The results of the Diels-Alder reaction in the presence of template **288** are shown in **Figure 110**. Once again, the template has little effect on the rate profile of the reaction, indicating that the reaction is not template directed. Template **288** does not act as a reciprocal template for the formation of cycloadduct **286**. It can be concluded from these kinetic experiments that the bimolecular reaction between diene **284** and dienophile **125** is recognition-mediated, but is not however, template directed.

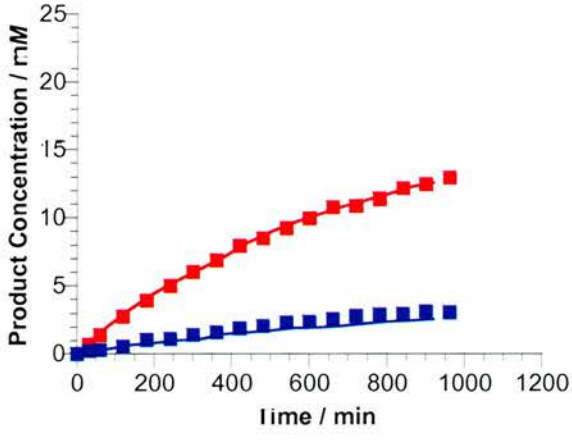

Figure 110: Rate profile for the recognition-mediated reaction; the *endo* cycloadduct is depicted as red lines and the *exo* cycloadduct is depicted as blue lines. The rate profile for the reaction between **125** and **284** in the presence of template **288** is depicted as filled red squares (*endo* cycloadduct) and as blue filled squares (*exo* cycloadduct).

In order to determine whether the reaction was indeed proceeding *via* an AB pathway, kinetic modelling studies were undertaken. In order to determine the rate constants for the bimolecular control reaction, it was necessary to define a kinetic model that would describe the chemical pathways leading to the products. The kinetic model for the control reaction

involves the reversible formation of the cycloadducts (*exo* and *endo*) from the reaction of the diene and dienophile **(Scheme 115)**.

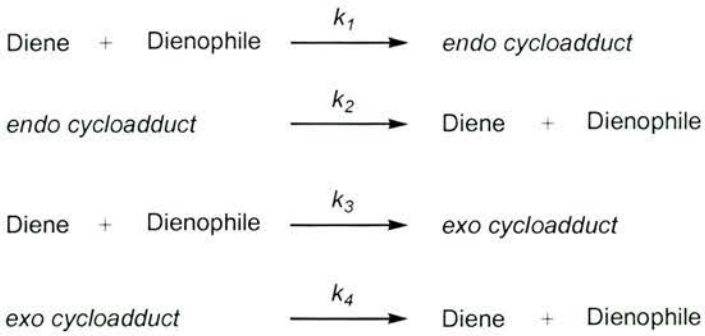

Scheme 115: A kinetic model for the bimolecular reaction between a diene and dienophile. k_1 and k_3 represent the forward rates resulting in the production of the *endo* and *exo* cycloadduct respectively, k_2 and k_4 describe the rate for the retro Diels-Alder reaction.

This model was used in conjunction with simulation and fitting package SimFit. SimFit is designed to simulate and fit experimental data as defined by a kinetic model, the programme allows the extraction of kinetic parameters from the observed rate profiles. **Figure 111** shows the experimental data as open squares, the solid lines represent the fitted data. A good fit between experimental data and model was obtained and allowed the extraction of kinetic parameters from the observed rate profiles.

a)

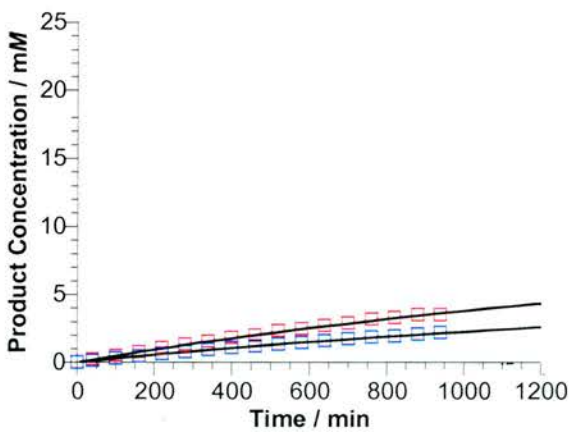

b)

cycloadduct	Control Reaction 148 + 284
endo	k_1 1.34 x 10^{-4} $M^{-1}s^{-1}$
	k_2 1.40 x 10^{-8} s^{-1}
exo	k_3 7.90 x 10^{-5} $M^{-1}s^{-1}$
	k_4 1.09 x 10^{-8} s^{-1}

Figure 111: **a)** Rate profile for the reaction between **148** and **284** over 16 hours at 25 °C. The *endo* cycloadduct is depicted as open red squares and the *exo* cycloadduct is depicted as open blue squares. **b)** The table depicts the rate constants calculated for the bimolecular reaction between diene **148** and dienophile **284**.

Once again, in order to generate estimations of the rate constants for the recognition-mediated reaction, it was necessary to define a kinetic model describing the chemical pathways leading to the production of the products. The model for an AB reaction involves 10 rate constants,

including the reversible formation of *exo* and *endo* cycloadducts as described in the simple bimolecular reaction **(Scheme 116)**.

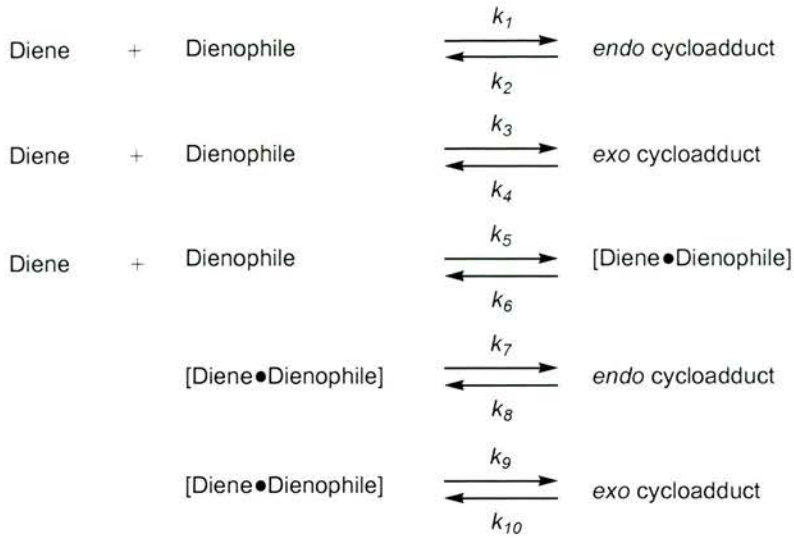

Scheme 116: Kinetic model for an AB-mediated *pseudo*-intramolecular reaction.

a)

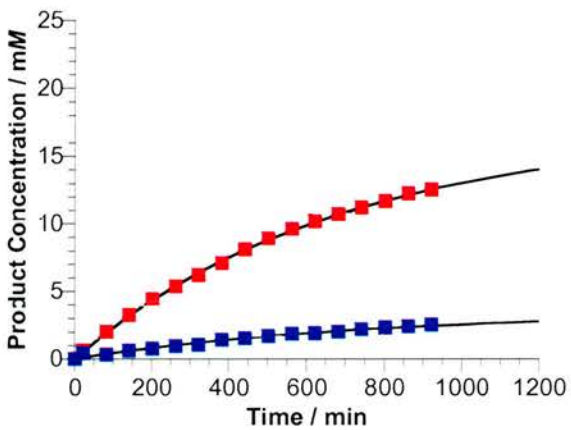

b)

cycloadduct	Recognition-Mediated Reaction 125 + 284	*kEM*/ m*M*	*tEM*/ m*M*
endo	k_7 2.14 x 10^{-5} s^{-1}	160	0.7
	k_8 2.19 x 10^{-6} s^{-1}		
exo	k_9 4.01 x 10^{-6} s^{-1}	50	0.3
	k_{10} 2.11 x 10^{-6} s^{-1}		

Figure 112: **a)** Rate profile for the reaction between **125** and **284** over 16 hours at 25 °C. The *endo* cycloadduct is depicted as open red squares and the *exo* cycloadduct is depicted as open blue squares. **b)** The table depicts the rate constants calculated for the *pseudo*-intramolecular reaction between diene **285** and dienophile **125**.

The derived kinetic model **(Scheme 116)** was used in conjunction with the SimFit the kinetic modelling package. The kinetic model gave an excellent fit to the experimentally determined rate profiles **(Figure 112a)**, enabling the rate constants for the *pseudo*-intramolecular reaction to be extracted. The EM values calculated are shown in **Figure 112b**. These results suggest that the recognition-mediated reaction between maleimide **125** and amide **284** is governed by a kinetic effect. Recognition serves to stabilise the two starting materials in the transition state in such a way that the preferential formation of *endo* **304** occurs. Identical reactions

were also carried out at 50 °C in order to assess the effect of temperature upon our recognition-mediated reactions. At 50 °C, the production of *endo* adduct was greatly enhanced in the presence of recognition. The bimolecular reaction data fitted well to the bimolecular kinetic model **(Scheme 115)**, allowing rate constant data to be extracted **(Figure 114)**. The recognition-mediated reaction data also fitted well to the experimental data allowing the calculation of effective molarities for the *pseudo*-intramolecular system. The results suggest that the presence of recognition within molecules **125** and **284** serves to stabilise the reactants at the transition-state (*kEM* = 158 m*M*) in an orientation which encourages the formation of *endo* **304**.

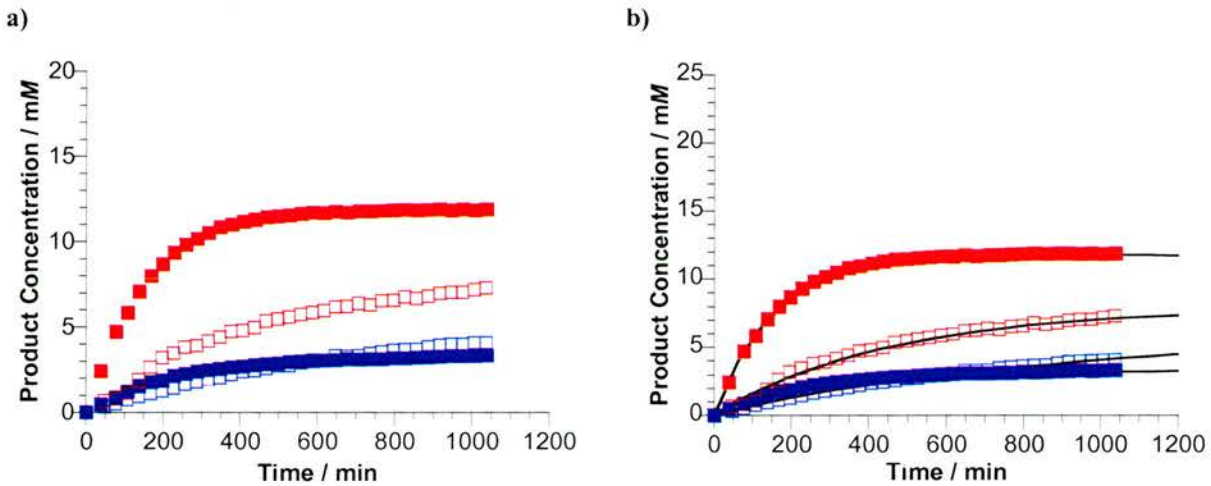

Figure 113: **a)** Rate profiles for the bimolecular reaction between compound **148** and **284** and recognition-mediated reaction between **125** and **284** at 50 °C are shown; the bimolecular reaction *endo* cycloadduct is depicted as open red squares and the *exo* cycloadduct is depicted as open blue squares, the recognition-mediated reaction data are depicted as filled red squares and the *exo* cycloadduct is depicted as filled blue sqaures. **b)** The bimolecular reaction data are shown *endo* cycloadduct is depicted as open red squares and the *exo* cycloadduct is depicted as open blue squares, the solid line represents the fitted data.

Molecular modelling studies were undertaken in order to gain insight into the strong preference for the *endo* cycloadduct under recognition-mediated reaction conditions. Molecular modelling studies were carried out using the AMBER* forcefield and the GB/SA solvation model for $CDCl_3$. These studies show **(Figure 115)** that the lowest energy conformation adopted by the *exo* isomer is unable to form hydrogen bonds between the carboxylic acid and amidopicoline recognition sites. Conversely, the lowest energy conformation adopted by the *endo* adduct is a closed structure, allowing the possibility of two hydrogen bonds being formed between the amidopyridine and carboxylic acid recognition sites.

a)

cycloadduct	Control Reaction 148 + 284
endo	k_1 5.02 x 10^{-4} $M^{-1}s^{-1}$
	k_2 9.13 x 10^{-6} s^{-1}
exo	k_3 2.16 x 10^{-4} $M^{-1}s^{-1}$
	k_4 5.54 x 10^{-7} s^{-1}

b)

cycloadduct	Recognition-Mediated Reaction 125 + 284	*kEM* / m*M*	*tEM* / m*M*
endo	k_7 7.95 x 10^{-5} s^{-1}	158	51
	k_8 2.82 x 10^{-5} s^{-1}		
exo	k_9 1.69 x 10^{-5} s^{-1}	78	1.6
	k_{10} 2.72 x 10^{-5} s^{-1}		

Figure 114: **a)** Table depicting the rate constants calculated for the bimolecular reaction between diene **284** and dienophile **125** at 50 °C. **b)** The table depicts the rate constants calculated for the *pseudo*-intramolecular reaction between diene **284** and dienophile **125** at 50 °C.

a) **b)**

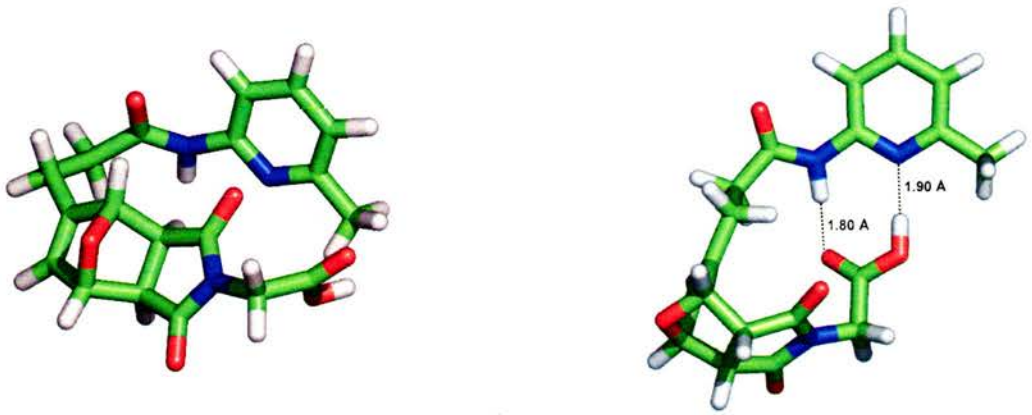

Figure 115: Models representative of the minimum energy conformation of each adduct derived from molecular mechanics calculations using the AMBER* forcefield. Carbon, oxygen, nitrogen and hydrogen atoms are coloured green, red, blue and white respectively. Hydrogen bonds are represented by dashed lines and and hydrogen bond donor and acceptor distances are given in Å: **a)** *exo* cycloadduct **304**; **b)** *endo* cycloadduct **304**.

4.7.4 The Diels-Alder Reaction between 195 and 285

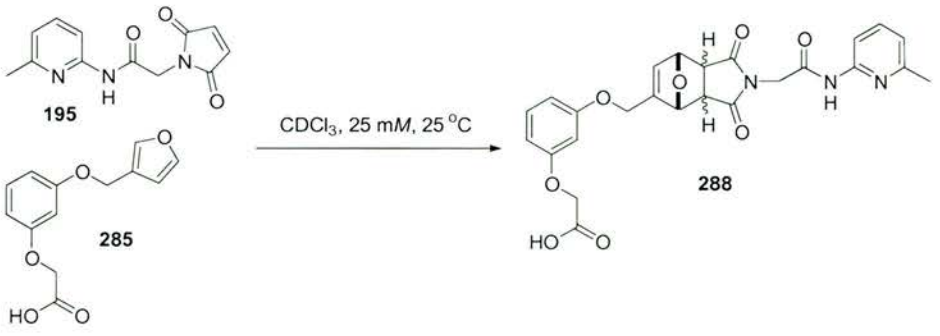

Scheme 117: Reaction conditions chosen to facilitate the Diels-Alder reaction between **195** and **285**.

In order to determine the effect of recognition on the Diels-Alder reaction shown in **Scheme 117** a control experiment was undertaken in which the carboxylic acid recognition site was removed. The control reaction used t-butyl protected compound **292** in place of carboxylic acid containing **285**. The reaction between control diene **292** and dienophile **195** at 25 °C and 25 m*M* of each reagent in $CDCl_3$, was monitored by 500 MHz ^1H NMR spectroscopy, the extent of reaction completion was determined using the deconvolution tool available in 1D WINNMR. The reaction between diene and dienophile after 16 hours had reached ~ 10% completion, with *endo*:*exo* cycloadduct products formed in a ratio of ~1:1 **(Figure 116)**. The Diels-Alder reaction was then carried out under identical conditions in the presence of recognition diene **285**. The reaction profile for the recognition mediated reaction is shown in **Figure 117a**.

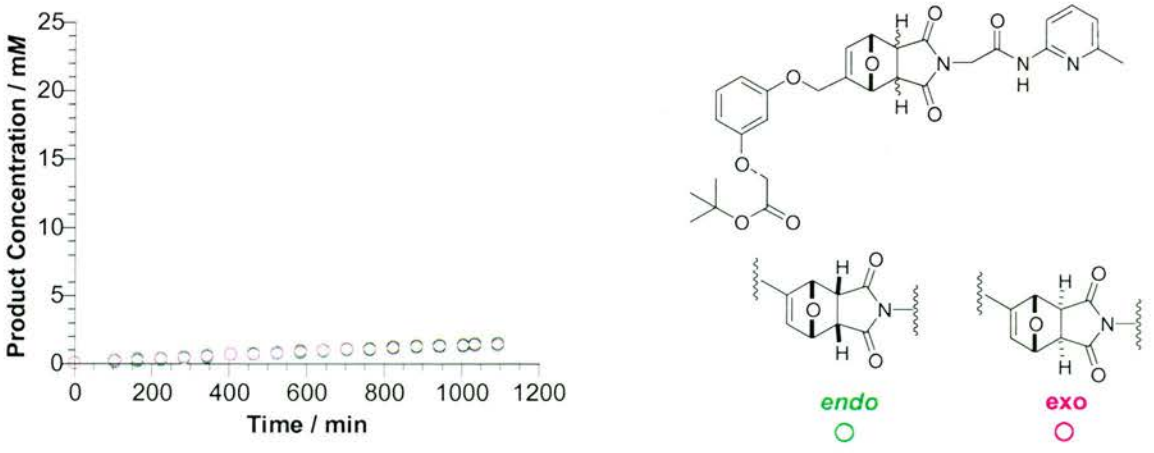

Figure 116: Rate profile for the reaction between **195** and **292** over 16 hours at 25 °C. The *endo* cycloadduct is depicted as open purple circles and the *exo* cycloadduct is depicted as open green circles.

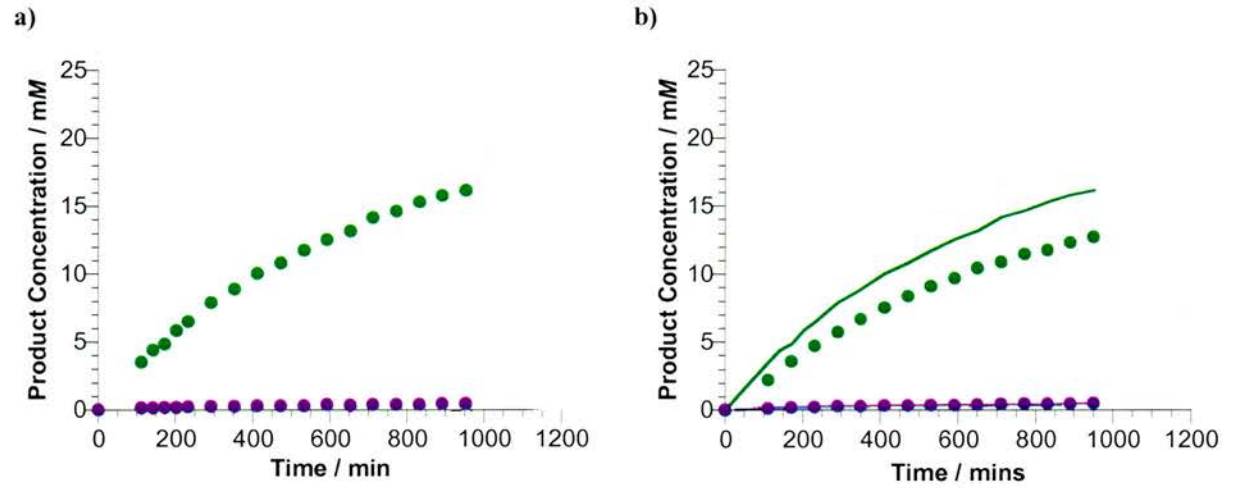

Figure 117: **a)** Rate profile for the reaction of diene **195** with dienophile **285** at 25 °C; the *endo* cycloadduct is depicted as filled green circles and the *exo* cycloadduct is depicted as filled purple circles. **b)** Rate profile for the recognition-mediated reaction; the *endo* cycloadduct is depicted as green lines and the *exo* cycloadduct is depicted as purple lines. The rate profile for the reaction between **195** and **285** in the presence of template **288** is depicted as filled green circles (*endo* cycloadduct) and as filled purple circles (*exo* cycloadduct).

The reaction is indeed effected by recognition as the presence of the carboxylic acid moiety on diene **285** has greatly enhanced the production of the *endo* adduct. The reaction is therefore recognition mediated, with a strong preference for the *endo* cycloadduct. In order to determine whether the reaction was accelerated by a template effect, the reaction was doped with 1 equivalent of its own template. The results of the reaction are shown in **Figure 117b**. The addition of template **288** reduced the rate of production of the *endo* isomer whilst not affecting the rate profile for the production the *exo* isomer. Therefore, it can be concluded that the reaction is not following a self-replicating pathway.

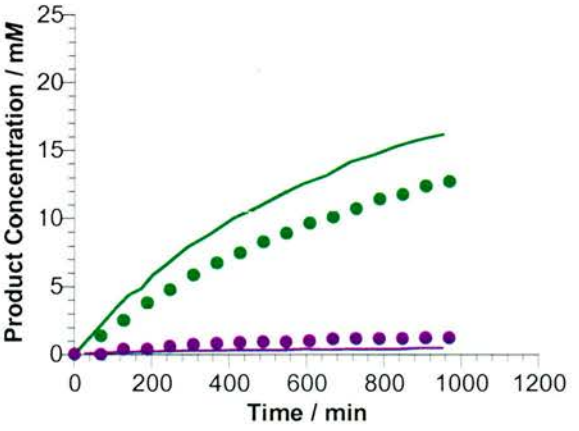

Figure 118: Rate profile for the recognition-mediated reaction between **195** and **284** at 25 °C; the *endo* cycloadduct is depicted as a green line and the *exo* cycloadduct is depicted as a purple line. The rate profile for the reaction between **195** and **284** in the presence of template **304** is depicted as filled green circles (*endo* cycloadduct) and as purple filled circles (*exo* cycloadduct).

A further template experiment was undertaken with diene **285** and dienophile **195** both with initial concentrations of 25 m*M* at 25 °C in $CDCl_3$, in addition 1 equivalent of template **304** was added. Template **304** had an inhibitory effect upon the reaction. In order to determine whether the reaction was proceeding *via* an AB pathway, kinetic modelling studies were undertaken.

a)

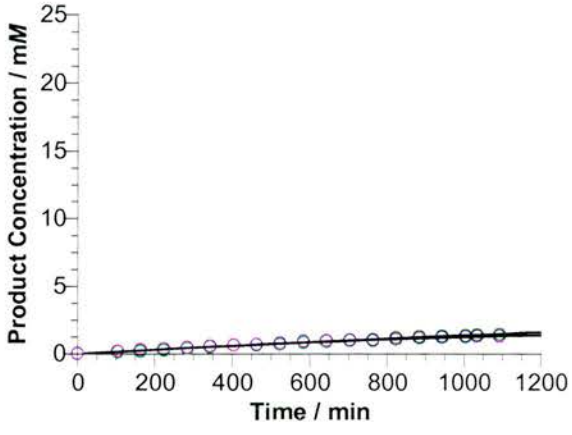

b)

cycloadduct	Control Reaction 195 + 292
endo	k_1 4.40 x 10^{-5} $M^{-1}s^{-1}$
	k_2 1.64 x 10^{-6} s^{-1}
exo	k_3 4.74 x 10^{-5} $M^{-1}s^{-1}$
	k_4 7.65 x 10^{-6} s^{-1}

Figure 119: **a)** Rate profile for the reaction between **195** and **292** over 16 hours at 25 °C. The *endo* cycloadduct is depicted as open green circles and the *exo* cycloadduct is depicted as open purple circles. **b)** The table depicts the rate constants calculated for the bimolecular reaction between diene **292** and dienophile **195**.

Once again, in order to generate estimations of the rate constants for the recognition-mediated reaction, an AB model **(Scheme 115)** was used in conjunction with the fitting package SimFit.

a)

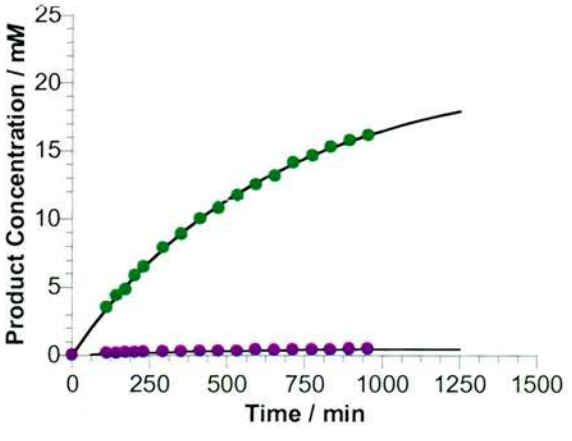

b)

cycloadduct	Recognition-Mediated Reaction 195 + 285	*kEM* / m*M*	*tEM* / m*M*
endo	k_7 2.96 x 10^{-5} s^{-1}	664	854
	k_8 1.29 x 10^{-6} s^{-1}		
exo	k_9 2.31 x 10^{-6} s^{-1}	49	5.8
	k_{10} 6.46 x 10^{-5} s^{-1}		

Figure 120: **a)** Rate profile for the reaction between **195** and **285** over 16 hours at 25 °C. The *endo* cycloadduct is depicted as filled green circles and the *exo* cycloadduct is depicted as filled purple squares. **b)** The table depicts the rate constants calculated for the *pseudo*-intramolecular reaction between diene **285** and dienophile **195**.

The simulation gave an excellent fit to the experimentally determined rate profiles **(Figure 120a)**, enabling the rate constants for the *pseudo*-intramolecular reaction to be extracted. The EM values calculated are shown in **Figure 120b**. These results suggest that the recognition-mediated production of the *endo* cycloadduct is as a consequence of the starting materials becoming arranged in a suitable configuration at the transition state for the reaction between them to be controlled and enhanced. Also, the recognition which is present in the transition state persists within the cycloadduct product, resulting in the *endo* adduct being preferentially stabilised. Identical reactions were carried out at 50 °C in order to gauge the effect of temperature upon the recognition-mediated reaction. Once again, the production of *endo* adduct was greatly enhanced by in the presence of recognition diene **285** and the *exo* adduct was suppressed by 33% relative to the analogous control reaction. The bimolecular reaction data fitted well **(Figure 121)** to the bimolecular kinetic model **(Scheme 115)**, allowing reliable rate constant data to be extracted **(Figure 122)**. The recognition-mediated reaction data also fitted well to experimental data allowing the calculation of effective molarities for the system **(Figure 122)**. The data suggests that the presence of recognition within molecules **195** and **285** serves to stabilise the reactants at the transition-state in a manner which promotes the production of the *endo* cycloadduct (kEM = 362 mM) and also stabilises the product itself (tEM = 472 mM).

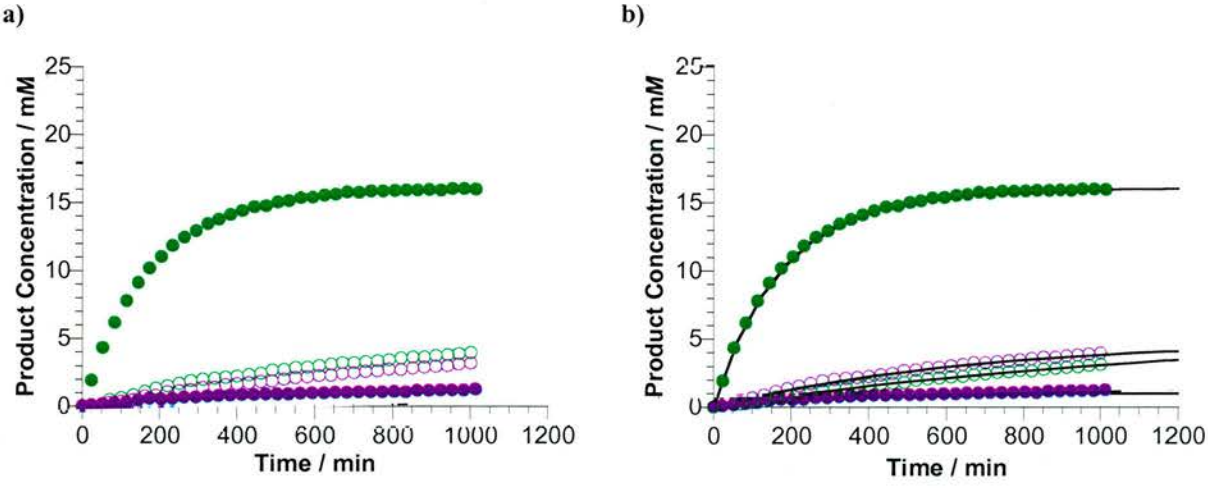

Figure 121: **a)** Rate profile for the bimolecular and recognition mediated reactions at 50 °C are shown; the bimolecular reaction *endo* cycloadduct is depicted as open green circles and the *exo* cycloadduct is depicted as open purple circles, the recognition-mediated reaction data is depicted as filled green circles and the *exo* cycloadduct is depicted as filled purple circles. **b)** The bimolecular reaction data is shown *endo* cycloadduct is depicted as open green circles and the *exo* cycloadduct is depicted as open purple circles, the solid line represents the fitted data.

a)

cycloadduct	Control Reaction 195 + 292
endo	k_1 2.06 x 10^{-4} $M^{-1}s^{-1}$
	k_2 1.05 x 10^{-5} s^{-1}
exo	k_3 1.30 x 10^{-4} $M^{-1}s^{-1}$
	k_4 2.64 x 10^{-6} s^{-1}

b)

cycloadduct	Recognition-Mediated Reaction 195 + 285	*kEM* / m*M*	*tEM* / m*M*
endo	k_7 9.72 x 10^{-5} s^{-1}	362	472
	k_8 1.37 x 10^{-5} s^{-1}		
exo	k_9 6.72 x 10^{-6} s^{-1}	5	52
	k_{10} 2.77 x 10^{-5} s^{-1}		

Figure 122: **a)** The table depicts the rate constants calculated for the bimolecular reaction between diene **292** and dienophile **195** at 50 °C. **b)** The table depicts the rate constants calculated for the *pseudo*-intramolecular reaction between diene **285** and dienophile **195** at 50 °C.

a)

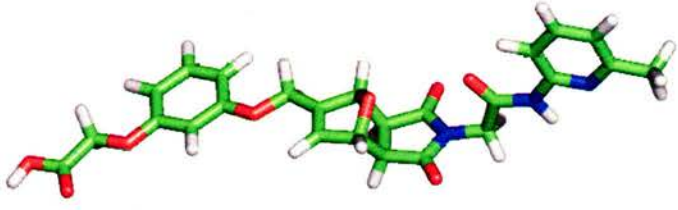

b)

Figure 123: Models representative of the minimum energy conformation of each adduct derived from molecular mechanics calculations using the AMBER* forcefield. Carbon, oxygen, nitrogen and hydrogen atoms are coloured green, red, blue and white respectively. Hydrogen bonds are represented by dashed lines and and hydrogen bond donor and acceptor distances are given in Å: **a)** *exo* cycloadduct **288**; **b)** *endo* cycloadduct **288**.

Once again, molecular modelling studies were undertaken in order to gain insight into the strong preference for the *endo* cycloadduct under recognition-mediated reaction conditions. Molecular modelling studies showed that the lowest energy conformation adopted by the *exo* isomer is a open and extended no hydrogen bonds are formed. Conversely, the lowest energy conformation adopted by the *endo* adduct is a closed structure, leading to the possibility of two hydrogen bonds being formed between the amidopyridine and carboxylic acid recognition sites.

4.8 Library Studies

The original design of this library was to generate reciprocal and self-replicating systems, however, **Section 1.7** shows that the Diels-Alder reactions which we have studied do not exhibit replicating characteristics. In order to ascertain what effect AB recognition-mediated reactions would have upon the library we conducted high pressure liquid chromatography (HPLC) experiments. Firstly, conditions were found for the separation of all library members and components under HPLC automation. An NMR scale experiment which included all library building blocks at initial concentrations of 25 m*M* was set up at 25 °C, the corresponding Diels-Alder products were allowed to form over 1 week. After this time, the library solution (10μL of a 25 m*M* solution in 0.25 cm^3 H_2O) was injected onto a XTerra Reverse Phase C18 3.0 x 50 mm, 5 μm column. Each of the starting materials and cycloadducts were separated **(Figure 124)** under mobile phase conditions of MeCN and aqueous formic acid, from 2% organic to 98% organic.

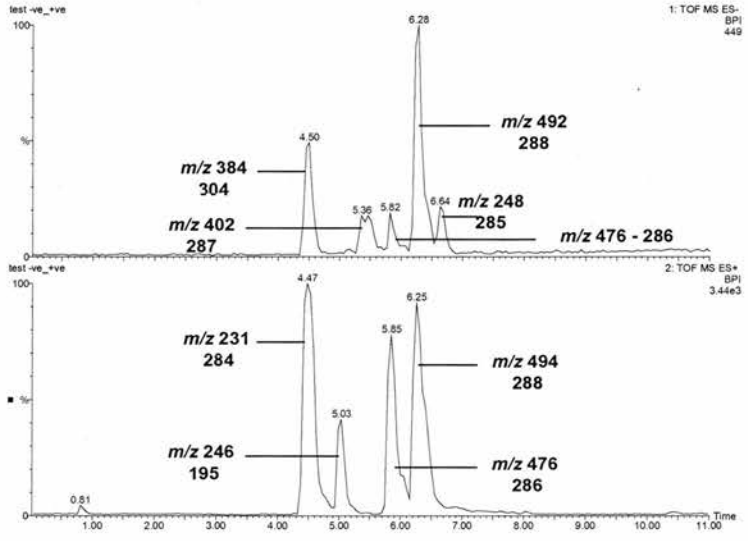

Figure 124: HPLC trace showing the separation of all library members and building blocks.

From our kinetic results one could imagine that within a library situation the main products would be generated *via* the efficient AB systems to give cycloadducts **288** and **304**. We wished to study the effect of adding preformed cycloadduct templates to an evolving library.

In order to follow the effects of pre-formed cycloadduct upon the library members a simplified library situation was setup. Only three of the four library building blocks (**125**, **284** & **285**) were reacted at 25 m*M* in $CDCl_3$ at 25 °C for 1 week. The reaction mixture was monitored every day by HPLC. After one week each pre-formed cycloadduct **304**, **286** & **288**, excluding cycloadduct **287** on solubility grounds was added to the library mixture. Each template was formed at 50 °C for one week and the remaining concentration of starting materials factored into any change detected within the library. The reaction mixture was then monitored by HPLC every day for a further one week.

Addition of templates **304** and **288** appeared to have no effect on the reaction mixture. Addition of template **286** however, led to a small but detectable decrease in diene starting material **285**. It was decided to investigate the library further at higher temperatures. Once again, three components **(125**, **284** & **285)** were reacted at 25 m*M* in $CDCl_3$ at 25 °C for one week, and the reaction monitored by HPLC each day. After this time, pre-formed templates **304**, **286** & **288** were added and the temperature of the reaction mixture raised to 50 °C. The reaction mixture was monitored by HPLC every day for a further one week. Once again, addition of templates **304** & **288** appeared to have no effect on the reaction mixture, however, the addition of template **286** led, once more, to a decrease in diene **285**. In order to fully understand the effects of template **286** upon the reaction experiments were set up on an NMR scale as follows;

(i) Template **286** was allowed to form over the period of 1 week at 50 °C, a ^{1}H NMR spectrum was recorded. After this time, 1 equivalent of diene **285** was added and the reaction mixture heated at 50 °C, for a further day and a ^{1}H NMR spectrum recorded

(ii) Template **286** was allowed to form over the period of 1 week at 50 °C, a ^{1}H NMR spectrum was recorded. After this time, 1 equivalent of diene **285** was added and the reaction mixture heated at 25 °C, for a further day and a ^{1}H NMR spectrum recorded

It was clear that in both cases the amount of *endo* cycloadduct has decreased. The decrease in *endo* cycloadduct **286** led to a comparable increase in the production of *endo* cycloadduct **288**. At the time of addition of diene **285** only 7% of *endo* cycloadduct **286** was present. It appeared that the *endo* diastereoisomer was degrading and any starting materials were being channelled *via* an AB recognition-mediated route **(Figure 125)**.

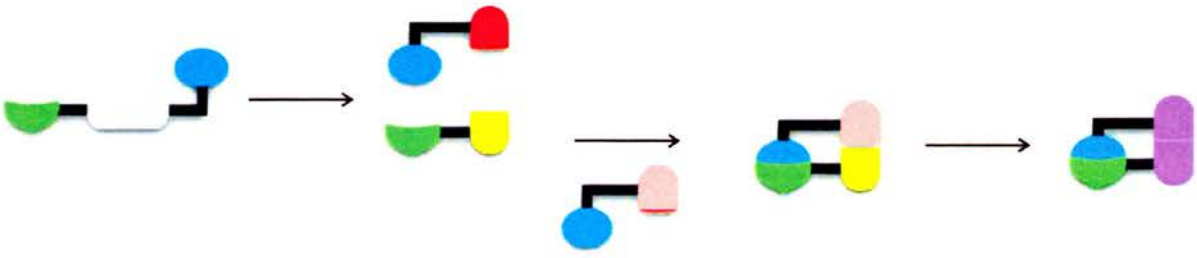

Figure 125: A schematic representation of a retro-Diels-Alder reaction 'feeding' an AB-mediated pathway. Green and blue blocks represent recognition sites, red, yellow and pink blocks represent reactive sites and black lines represent spacer units.

In order to confirm that this was indeed the case a situation in which more *endo* adduct was present was next investigated. In order to assess when the *endo* cycloadduct was at its highest concentration in the reaction between **195** and **284** at 50 °C and 25 m*M* of each reagent, predictive kinetic modelling studies were undertaken. Firstly, the reaction between diene **284** and dienophile **195** was carried out at 25 m*M* in $CDCl_3$ at 50 °C, the reaction was monitored for a period of 16 hours by 500 MHz ^{1}H NMR spectroscopy, the rate profile obtained on deconvolution of the experimental data is shown in **Figure 126**. The data was fitted to a bimolecular kinetic model using SimFit and a good fit with the experimental data obtained. The rate constants for the formation of the *endo* and *exo* cycloadducts were extracted and inserted into the simulation package isosim available within SimFit. The formation of both *endo* **286** and *exo* **286** was then predicted over a ten day period. The predicted data suggested that the time at which optimum amount of *endo* cycloadduct **286** was present was 27 hours after mixing diene **284** and dienophile **195**.

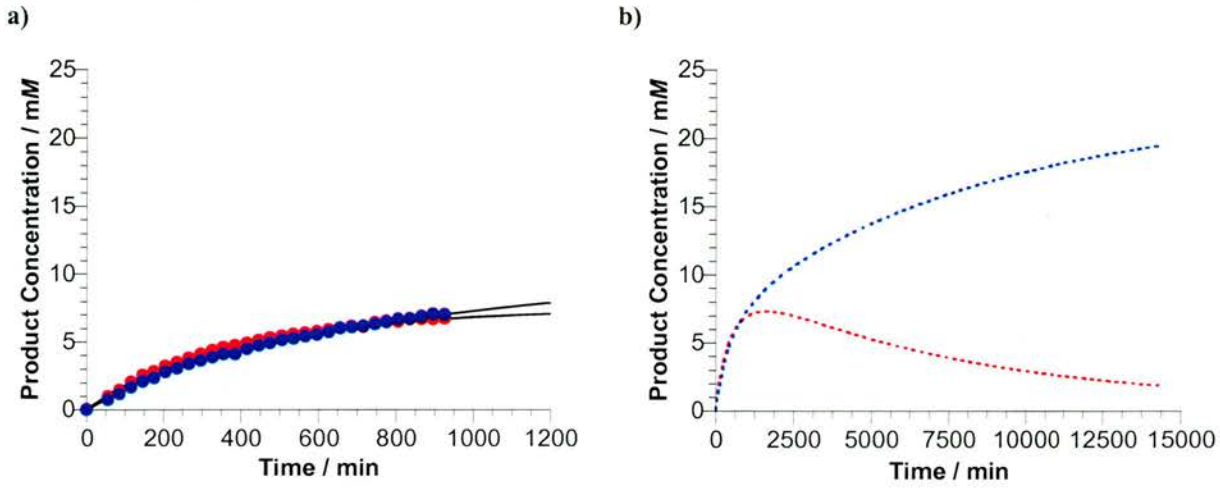

Figure 126: **a)** Rate profile for the reaction between **195** and **284** over 16 hours. The *endo* cycloadduct is depicted as filled red circles and the *exo* cycloadduct is depicted as filled blue circles. **b)** Simulation profile for the reaction of diene **284** and dienophile **195** over ten days, the *endo* and *exo* adducts are shown as a red and blue dashed line respectively.

Once again, experiments were set up on an NMR scale as follows;

(i) Template **286** was allowed to form for 27 hours at 50 °C, and a ^{1}H NMR spectrum was recorded. After this time, 1 equivalent of diene **285** was added and the reaction mixture heated at 50 °C, for a further day and a ^{1}H NMR spectrum recorded

(ii) Template **286** was allowed to form for 27 hours at 50 °C, and a ^{1}H NMR spectrum was recorded. After this time, 1 equivalent of diene **285** was added and the reaction mixture heated at 25 °C, for a further day and a ^{1}H NMR spectrum recorded.

Once again it was clear that in both cases the amount of *endo* cycloadduct **286** had decreased, in conjunction with a comparable increase in the production of *endo* cycloadduct **288**. **Figure 127** shows the partial NMR spectrum of the reaction between diene **284** and dienophile **195** at 27 hours. **Figure 128a** depicts a partial ^{1}H NMR spectrum of the reaction between **195** and **284** one day after the addition of diene **285** at 25 °C. **Figure 128b** depicts a partial ^{1}H NMR spectrum of the reaction between **195** and **284** one day after the addition of diene **285** at 50 °C.

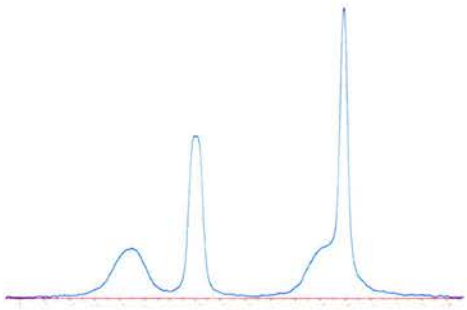

Figure 127: A partial 300 MHz ^{1}H NMR spectrum showing the cycloadduct diastereoisomeric distribution in the reaction between **195** and **284** after 27 hours.

a) **b)**

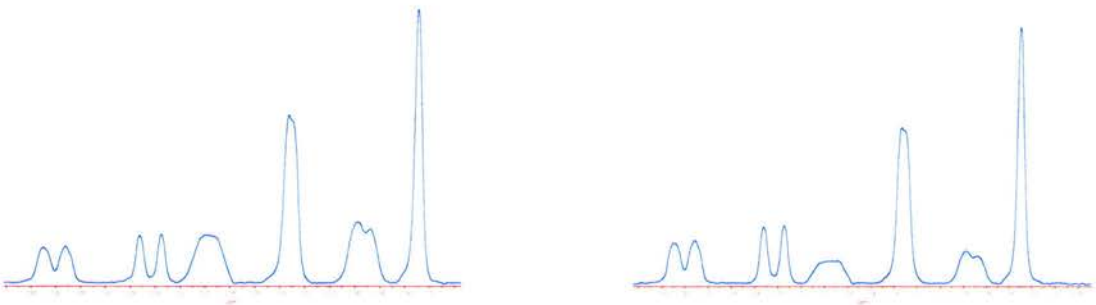

Figure 128: **a)** A partial 300 MHz ^{1}H NMR spectrum showing the cycloadduct diastereoisomeric distribution in the reaction between **195** and **284** after 27 hours, on subsequent addition of **285** after 24 hours at 25 °C. **b)** A partial 300 MHz ^{1}H NMR spectrum showing the cycloadduct diastereoisomeric distribution in the reaction between **195** and **284** after 27 hours, on subsequent addition of **285** after 24 hours at 50 °C.

These results suggest that kinetic amplification of one library member using a reversible Diels-Alder library may indeed be possible. Within this small library the use of a recognition-mediated AB pathway allows the preferential formation of an adduct *via* the degradation of an unfavourable bimolecular reaction forming adduct **(Figure 128)**.

4.8 The Design of a Dynamic Reciprocal Replicating System

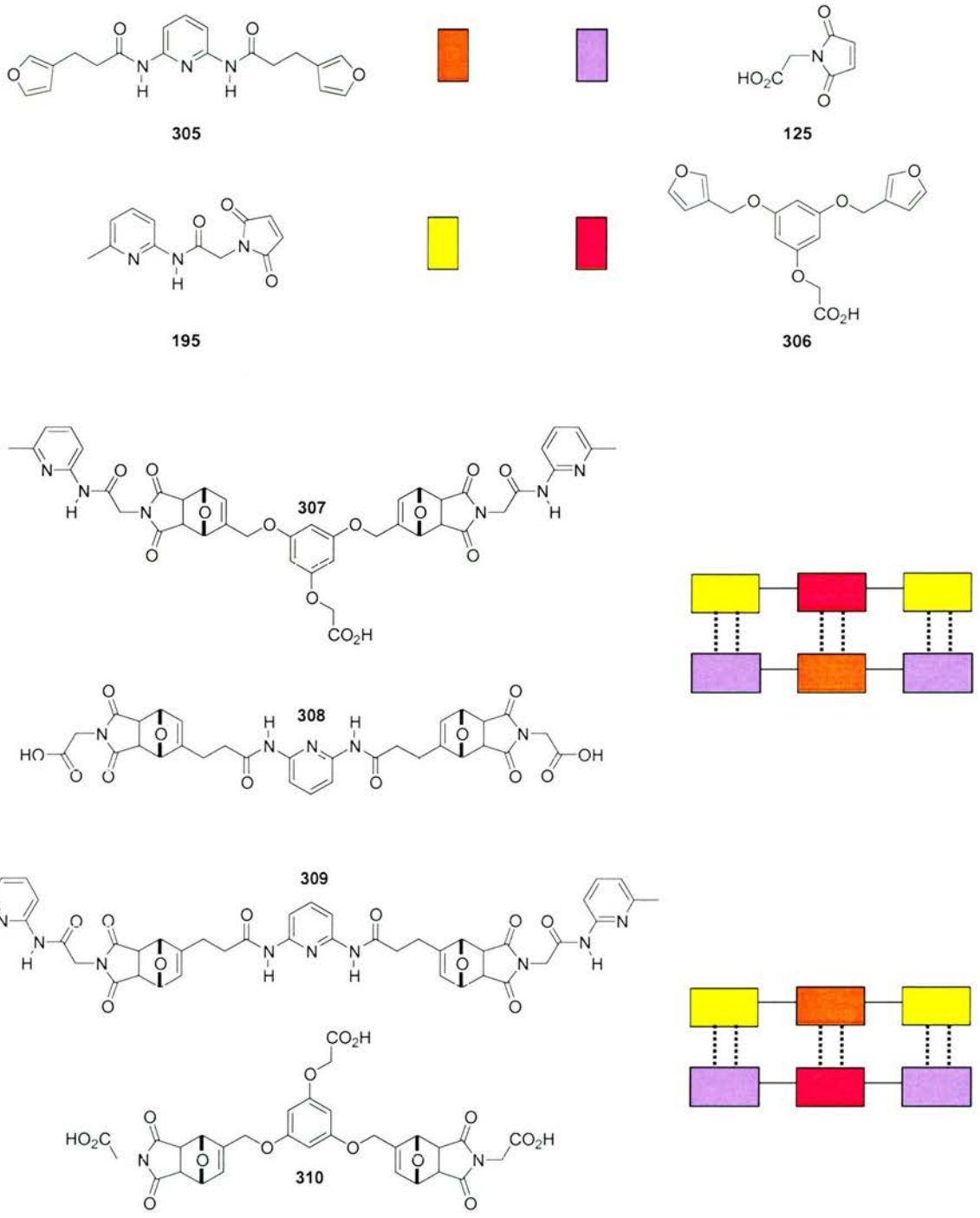

Figure 129: Target library building blocks **125**, **195**, **305-306** and library members **307-310**. A schematic representation of the possible reciprocal association patterns which could occur between library members.

The Diels-Alder reaction was chosen as the reversible reaction once again within this system. The building block molecules **(Figure 129)** contain either amidopicoline or carboxylic acid motifs suitable for complementary hydrogen bonding. Each molecule contains either a furyl moiety (diene) or a maleimide moiety (dienophile). This small library can generate up to

twenty possible cycloadduct products. The library has been designed to operate *via* reciprocal replication; the possible association patterns are shown in **Figure 129**. There are two potential reciprocal replication routes open to the building blocks. The study of this system will determine whether the library reacts in a random fashion, giving rise to up to twenty products or whether the library exploits the potential recognition-mediated pathways open to it. We shall first investigate whether specific Diels-Alder reactions can be accelerated in the presence of pre-formed templates **307-310**.

4.10 Synthesis of Carboxylic Acid 306

In a similar strategy to the synthesis of furyl acid **285 (Scheme 107)**, the synthesis of difuryl acid **306** was undertaken in 4-steps **(Scheme 117)**.

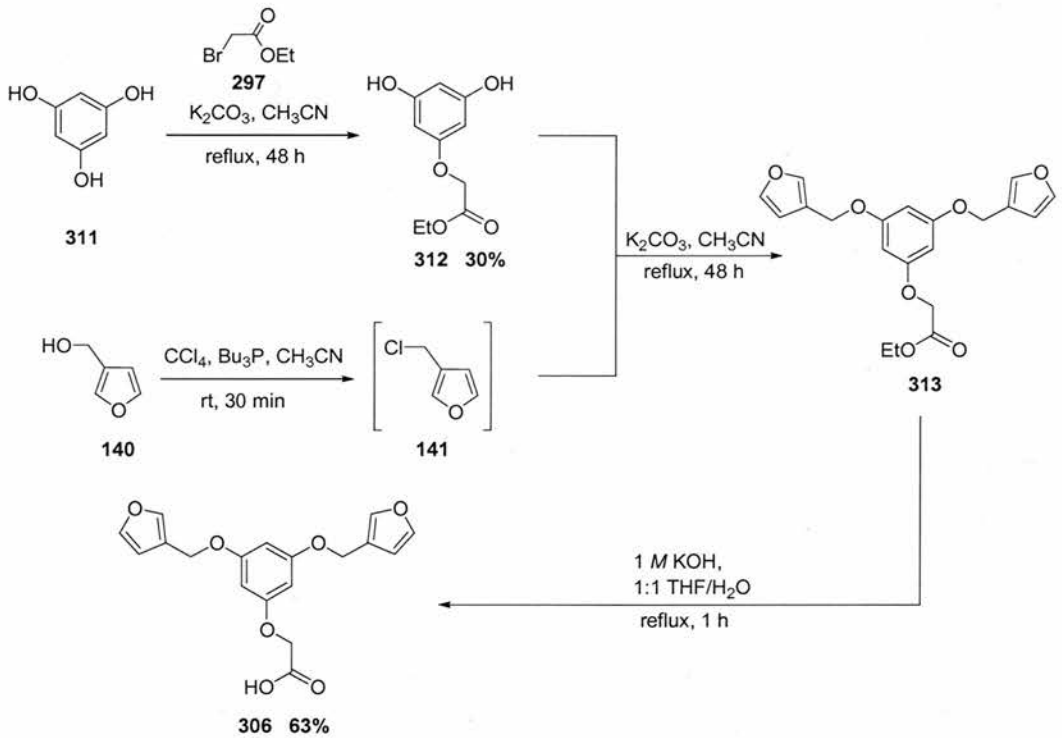

Scheme 117: Synthetic sequence for the production of [3,5-bis-(furan-3-ylmethoxy)-phenoxy]-acetaldehyde.

Phloroglucinol **311** was converted to dihydroxy ethyl ester **312** in 30% yield, following isolation of the desired compound from its di- and tri-ethyl ester counterparts *via* flash column chromatography. Alcohol **140** was converted the corresponding chloride **141** using carbon tetrachloride as a chlorinating agent, **141** was carried through to the next step of the reaction sequence without further purification. Crude chloride **141** was then added to a suspension of alcohol **312** and potassium carbonate in CH_3CN. The reaction was refluxed for 48 hours and

yielded the desired compound in good yield. Deprotection of the aryl ethyl ester **313** under basic hydrolysis conditions, led to the isolation of desired acid **306** in 63% yield. The building blocks for this project have been successfully synthesised. Time constraints have dictated that further studies upon the system were not able to be performed.

4.11 Synthesis of Amide 305

Amide **305** was synthesised in a similar fashion to compound **284 (Scheme 108)**. *trans*-Furanacrylic acid **300** was converted to propionic acid **301** *via* a catalytic hydrogenation reaction to afford the product in 93% yield. Acid **301** was converted to the acid fluoride using cyanuric fluoride as the fluorinating agent. 2,6-diaminopyridine was then added to the crude fluoride and the resulting reaction mixture stirred at room temperature for 16 hours. After this time, the resulting reaction mixture was worked-up (CH_2Cl_2/$HNaCO_3$), the organic phase dried ($MgSO_4$) and reduced *in vacuo*, the resulting yellow solid was recrystallised from hexane/ethyl acetate to afford amide **305** in 22% yield.

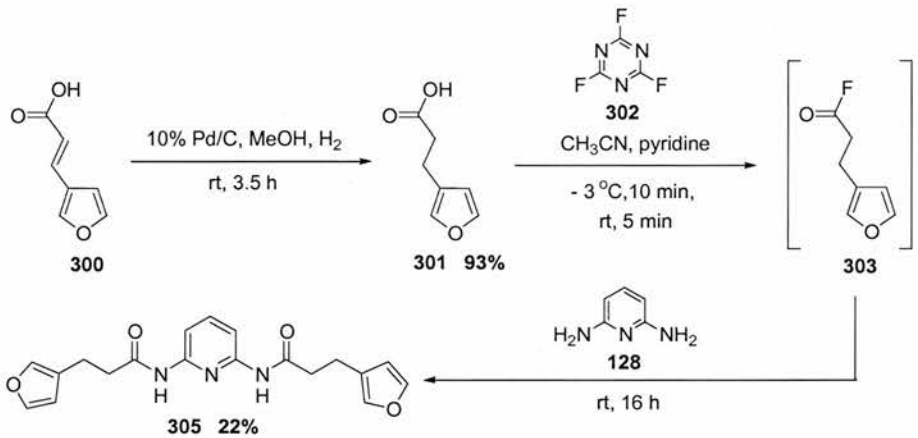

Scheme 118: Synthetic pathway for the preparation of 3-furan-3-yl-*N*-[6-(3-furan-3-yl-propionylamino)-pyridin-2-yl]-propionamide.

The synthesis of maleimide acid **125** is discussed fully in **Section 2.7.4**. The synthesis of amide **195** is discussed fully in **Section 3.5.3**.

4.12 Conclusions

The projects discussed within this Chapter highlight many of the problems faced in the design of supramolecular systems to function in a desired fashion. When many reactive pathways are open to the starting materials, predicting the outcome of recognition-mediated reactions, whether it is by AB-complex methodology, self-replication or reciprocal replication is a challenging prospect.

Initial studies upon the thiol based system **(Section 4.4)** were stopped as a result of solubility problems. The design of our system relied on hydrogen bonding to provide recognition between each library member therefore studies could have only been conducted in non-polar solvents. Library member **250** was insoluble in deuterated chloroform the solvent of choice for the monitoring of reactions by ^{1}H NMR spectroscopy. The outcome of this project emphasizes another important issue in the rational design of supramolecular projects. One cannot easily predict the solubility of compounds and although within this project the preparation of all target compounds was successful, as a result of the insolubility of one library member the project was halted. This project has been redesigned, the synthesis and study of a similar system which relies on reversible imine linkages to facilitate dynamic conditions will be synthesised and studied within the Philp group.

The library building blocks within the Diels-Alder system described in **Section 4.6** were designed with the potential for self- and reciprocal replication to take place. However, ^{1}H NMR kinetic studies have shown that an AB-mediated pathway was favoured over the corresponding self-replicating pathway in the reactions between diene **284** and dieneophile **125**, and also in the reaction between diene **285** and dieneophile **195**. In the case of potential reciprocal replicating systems, no reciprocal replicating character was observed.

The effect of AB-mediated recognition upon a library situation was investigated. On addition of templates **304** & **288** no change in the library profile was observed on analysis by HPLC. However, on addition of diamide template **286** a change in the distribution of products was observed by HPLC. The introduction of template **286** was shown to increase the production of *endo* cycloadduct **288** which is formed *via* a fast AB-mediated pathway. It was shown by ^{1}H NMR spectroscopy studies that *endo* cycloadduct template **286** was reverting back to its starting material components and that any free dienophile **195** was being preferentially consumed to form *endo* cycloadduct **288** the *via* a recognition-mediated pathway. These results show that within a reversible competing library, the reversal of an unproductive reaction pathway, returning starting material components back to the library mixture, can lead to the increased production of a library member which operates *via* a recognition-mediated route. This suggests that recognition properties incorporated within dynamic library members could, under the correct circumstances, lead to the production of one library member above all others under dynamic library conditions. These observations are analogous to a 'survial of the

fittest strategy', or in this case, 'an amplification of the component *via* the most productive route' strategy.

A second library was designed in which the AB and self-replicating modes of reaction were unavailable to the starting materials **(Section 4.8)**. This system has been designed to exploit two independent reciprocal replicating cycles. The successful synthesis of all library building blocks has been achieved. Further, studies will centre upon whether the library chooses to amplify certain library members using replication processes.

Chapter 5
General Conclusions

The field of dynamic combinatorial chemistry has emerged as a forceful addition to the supramolecular chemistry 'toolbox' since its formal classification nine years ago.

Reversibility in chemical reactions, once seen as an inconvenience by chemists has since been harnessed and has been developed into an effective means of obtaining new target molecules.

During the course of my three year study, the area of dynamic combinatorial chemistry has developed from a 'proof of principle' concept to a methodology which has afforded many novel structures - ranging from receptors with biological activity to new materials with novel architectures. Not only have new structures been developed – new reversible reactions have also emerged to effectively generate dynamic libraries.

Recent studies in the Sanders group have probed the limits of dynamic combinatorial chemistry. Their studies suggest that dynamic libraries could potentially be effective at one million members - the challenge will be in developing experimental conditions capable of allowing such large diversity.

The Michael addition reaction has yet to be reported as an effective dynamic combinatorial reaction. During my studies we have developed methodology for the study of AB mediated Michael addition reactions within a dynamic combinatorial chemistry context.

The Diels-Alder reaction has recently been reported as an effective dynamic combinatorial reaction by Lehn and co-workers. During my investigations the Diels-Alder reaction has been shown to be an effective reaction within a dynamic combinatorial framework in conjunction with AB and ABC complex methodology.

Dynamic combinatorial chemistry has a very bright future. The continuing development of suitable reversible reactions and a greater understanding of the limitations and capabilities of such systems will no doubt lead dynamic combinatorial chemistry to be a highly useful and influential tool in the years to come.

Chapter 6
Experimental Section

6.1 General Procedures

Chemicals and solvents were purchased from Acros Organics, Avocado, Bamford Laboratories, Fisher Scientific, Lancaster or Sigma-Aldrich and were used as received unless otherwise stated. Diethyl ether (Et_2O) and tetrahydrofuran (THF) were dried by refluxing with sodium-benzophenone under an atmosphere of nitrogen and collected by distillation. Acetonitrile (CH_3CN), dichloromethane (CH_2Cl_2) and dimethylformamide (DMF) were dried by heating under reflux over calcium hydride and distilled under an atmosphere of nitrogen. Pyridine was dried over KOH pellets. Thin-layer chromatography (TLC) was performed on aluminium plates coated with Merck Kieselgel 60 F_{254}. Developed plates were air dried and scrutinised under a UV lamp (366 nm), and where necessary, stained with iodine, PMA (phosphomolybdic acid), Ninhydrin or Potassium permanganate to aid identification. Column chromatography was performed using MP Silica (0.032-0.063 mm mesh). Melting points were determined using an Electrothermal 9200 melting point apparatus and are uncorrected. Microanalyses (CHN) were carried out at the University of St. Andrews. Infra-red spectra were recorded on PTFE plates/KBr disks using a Perkin-Elmer Paragon spectrometer. Chemicals and samples used prior to kinetic experiments were weighed using a Sartorius balance (MC1 Analytical AC 120S) with an accuracy of ±0.1mg.

6.2 NMR Spectroscopy

^1H Nuclear magnetic resonance (NMR) spectra were recorded on a Bruker Avance 300 (300.13 MHz) or a Varian Gemini 2000 (299.98 MHz) spectrometer using the deuterated solvent as the lock and the residual solvent as the internal reference in all cases. ^{13}C NMR spectra using the PENDANT sequence were recorded on a Bruker Avance 300 (75.5 MHz) spectrometer. All other ^{13}C spectra were recorded on a Varian Gemini 2000 (75.5 MHz) spectrometer using composite pulse ^1H decoupling. ^{19}F NMR spectra were recorded on a Bruker Avance 300 (282.3 MHz) spectrometer. All NMR samples were acquired using the deuterated solvent as the lock and the residual solvent as the internal reference. All coupling constants are quoted to the nearest 0.1 Hz. The symbols s, d, t, q used in the assignment of ^1H NMR spectra denotes singlet, doublet, triplet and quartet respectively. In the assignment of ^1H NMR spectra the abbreviations quat and Ar are used to denote quaternary and aromatic respectively. In the assignment of ^{13}C NMR spectra the abbreviation quat and the symbols

CH, CH_2 and CH_3 are used to denote a quaternary, primary, secondary and tertiary carbon centres respectively.

6.3 Mass Spectrometry

Electron impact mass spectrometry (EIMS) and high-resolution mass spectrometry (HRMS) were carried out on a VG AUTOSPEC mass spectrometer or on a Micromass GCT orthogonal acceleration time of flight mass spectrometer. Chemical Ionisation Mass Spectrometry (CIMS) was carried out on a VG AUTOSPEC instrument or on a Micromass GCT orthogonal acceleration time of flight mass spectrometer. Electrospray mass spectrometry (ESMS) and high-resolution mass spectrometry was carried out on a Micromass LCT orthogonal time of flight mass spectrometer.

6.4 NMR Scale Reactions and Kinetic Procedures

Reactions were carried out on an NMR scale. All stock solutions were prepared by dissolving the appropriate amount of a given reagent in the appropriate deuterated solvent using a 2 cm^3 (2 cm^3 ± 0.02 ml accuracy) volumetric flask. Subsequent experimental samples were obtained by mixing a fixed amount of appropriate stock solutions using a Hamilton gas tight syringe in a Wilmad 507/528PP NMR tube, which was then fitted with a polyethylene pressure cap to minimise solvent evaporation. All stock solutions were pre-equilibrated at the appropriate reaction temperature for 1 hour prior to mixing. After mixing, the sample was analysed by 500 MHz ^1H NMR spectrometry every thirty minutes for 16 hours by either a Bruker Avance or a Varian UNITYplus 500 MHz NMR spectrometer. Spectra were analysed using the deconvolution tool available within 1D WINNMR. Errors derived for the concentration of product, either by deconvolution of the analytical data or by experimental manipulation when preparing the solution for analysis are estimated to be ±4 %. Kinetic simulation and fitting of the results data to the appropriate kinetic models was achieved using SimFit. Rate constant data obtained by SimFit are calculated to be < ± 3 % RMS.

6.5 Synthetic Procedures

4-Mercaptomethyl-*N*-[6-(3-methylbutyrylamino)pyridin-2-yl]benzamide 121

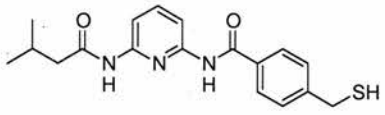

1 *M* aqueous KOH (100 cm^3) was added to a stirred solution of thioacetic acid *S*-{4-[6-(3-methylbutyrylamino)pyridin-2-ylcarbamoyl]benzyl}ester **133** (1.00 g, 2.40 mmol) in MeOH (100 cm^3). After 10 minutes, the reaction mixture was partitioned between CH_2Cl_2 and 1 *M* aqueous HCl (2 x 50 cm^3), the resulting organic layer was then washed with saturated aqueous $NaHCO_3$ (1 x 50 cm^3), dried ($MgSO_4$) and the solvent removed *in vacuo* to yield product as a colourless solid (800 mg, 98%); mp 164-165 °C; (Found: C, 62.8; H, 6.1; N, 12.0. $C_{18}H_{21}N_3O_2S$ requires C, 62.95; H, 6.2; N, 12.2%); υ_{max}(film)/cm^{-1} 3293 (N-H), 2949, 2867 (C-H), 2568 (S-H), 1663 (C=O); δ_H(300 MHz; $CDCl_3$) 8.15 (1H, bs, NH), 7.98 (1H, d, $^3J_{H,H}$ 8.1, Ar), 7.89 (1H, d, $^3J_{H,H}$ 8.1, Ar), 7.78-7.73 (2H, m, Ar), 7.69 (1H, dd, $^3J_{H,H}$ 8.1, $^3J_{H,H}$ 8.1, Ar), 7.54 (1H, bs, NH), 7.38-7.33 (2H, m, Ar), 4.09 (2H, d, $^2J_{H,S}$ 7.8, SCH_2), 2.19-2.15 (2H, m, CH_2, CH), 1.75 (1H, t, $^2J_{H,S}$ 7.8, SH), 0.96 (6H, d, $^3J_{H,H}$ 6.7, 2 x CH_3); δ_C(75 MHz; $CDCl_3$) 171.34 (C, quat, C=O), 165.4 (C, quat, C=O), 149.9 (2 x C, quat, Ar), 146.0 (C, quat, Ar), 141.4 (CH, Ar), 133.2 (C, quat, Ar), 128.9 (2 x CH, Ar), 127.9 (2 x CH, Ar), 110.1 (CH, Ar), 109.9 (CH, Ar), 47.5 (CH_2), 29.0 (CH_2), 26.5 (CH), 22.9 (2 x CH_3); *m/z* (CI) 344.1429 ($M+H^+$ - $C_{18}H_{22}N_3O_2S$ requires 344.1433), 343 (9%), 326 (5), 310 (5).

3-Mercapto-*N*-[6-(2-*p*-tolylacetylamino)pyridin-2-yl]benzamide 122

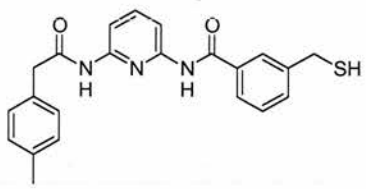

1 *M* aqueous KOH (20 cm^3) was added to a stirred solution of thioacetic acid *S*-{3-[6-(2-*p*-tolylacetylamino)pyridin-2-ylcarbamoyl]benzyl}ester **139** (500 mg, 1.30 mmol) in MeOH (20 cm^3). After 10 minutes, the reaction mixture was partitioned between CH_2Cl_2 (1 x 20 cm^3) and 1 *M* aqueous HCl (1 x 20 cm^3). The resulting organic layer was washed with saturated

aqueous $NaHCO_3$ (1 x 20 cm^3), dried ($MgSO_4$) and the solvent removed *in vacuo* to yield the product as a colourless solid (800 mg, 98%); mp 187-188 °C; (Found: C, 67.2; H, 5.4; N, 10.7. $C_{22}H_{21}N_3O_2S$ requires C, 67.5; H, 5.4; N, 10.7%); υ_{max}(film)/cm^{-1} 3250 (N-H), 2585 (S-H), 1670 (C=O); δ_H(300 MHz; $CDCl_3$) 8.18 (1H, bs, NH), 8.04 (1H, d, $^3J_{H,H}$ 7.9, Ar), 7.96 (1H, d, $^3J_{H,H}$ 7.9, Ar), 7.83-7.82 (1H, m, Ar), 7.77-7.74 (1H, m, Ar), 7.73-7.69 (1H, m, Ar), 7.54-7.51 (2H, m, NH, Ar), 7.43 (1H, dd, $^3J_{H,H}$ 7.9, $^3J_{H,H}$ 7.9, Ar), 7.22-7.23 (4H, m, Ar), 3.73 (2H, d, $^2J_{H,S}$ 7.8, SCH_2), 3.66 (2H, s, CH_2), 2.32 (3H, s, CH_3), 1.75 (1H, t, $^2J_{H,S}$ 7.8, SH); δ_C(75 MHz; $CDCl_3$) 170.0 (C, quat, C=O), 165.5 (C, quat, C=O), 149.9 (C, quat, Ar), 149.7 (C, quat, Ar), 142.5 (C, quat, Ar), 141.3 (CH, Ar), 137.9 (C, quat, Ar), 134.9 (C, quat, Ar), 132.4 (CH, Ar), 131.2 (C, quat, Ar), 130.4 (2 x CH, Ar), 129.8 (2 x CH, Ar), 129.6 (CH, Ar), 127.3 (CH, Ar), 126.1 (CH, Ar), 110.2 (CH, Ar), 110.0 (CH, Ar), 44.9 (CH_2), 29.1 (CH_2), 21.6 (CH_3); *m/z* (CI) 392.1432 ($M+H^+$ - $C_{22}H_{22}N_3O_2S$ requires 392.1433), 391 (10%).

Furan-3-yl-methanethiol 123

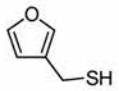

1 *M* aqueous KOH (50 cm^3) was added to a stirred solution of thioacetic acid *S*-furan-3-ylmethyl ester **142** (1.70 g, 10.9 mmol) in MeOH (50 cm^3) the reaction mixture was stirred for 5 minutes. After this time, the reaction mixture was partitioned between CH_2Cl_2 (75 cm^3) and 1 *M* aqueous HCl (1 x 50 cm^3), the resulting organic layer was then washed with saturated aqueous $NaHCO_3$ (1 x 50 cm^3), dried ($MgSO_4$) and solvent removed *in vacuo* to afford the product as a green/brown liquid (1.06 g, 85%); δ_H(300 MHz; $CDCl_3$) 7.32-7.28 (2H, m, FurylH), 6.35-6.32 (1H, m, FurylH), 3.52 (2H, d, $^2J_{H,S}$ 7.5, CH_2), 1.66 (1H, t, $^2J_{H,S}$ 7.5, SH); δ_C(75 MHz; $CDCl_3$) 143.8 (CH, Furyl), 139.7 (CH, Furyl), 125.4 (C, quat, Furyl), 110.9 (CH, Furyl), 19.3 (CH_2); *m/z* (EI) 114.0139 (M^+ - C_5H_6OS requires 114.0139), 81 (87%).

Functionalised Malemides, General Procedure

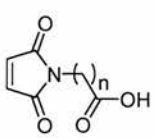

Maleic anhydride (1.0 eq.) and the appropriate amino acid (1.0 eq.) were dissolved in acetic

acid and stirred for 8 hours under a positive pressure of nitrogen, during this time a precipitate of insoluble intermediate had formed. The reaction mixture was then refluxed for 16 hours, after this time, the acetic acid was removed *in vacuo*.

(2,5-Dioxo-2,5-dihydropyrrol-1-yl)acetic acid, n=1 125

The general procedure outlined above was followed using maleic anhydride (13.00 g, 133 mmol), glycine (10.00 g, 133 mmol) and acetic acid (500 cm^3). The crude maleimide was purified *via* a short pad of silica (SiO_2, 19:1 v/v CH_2Cl_2:AcOH) and subsequent crystallisation from CH_2Cl_2/hexane, to yield large colourless crystals (8.66 g, 42%); mp 114–115 °C (lit.,[193] 113.0-113.5 °C); (Found: C, 46.2; H, 2.9; N, 8.7. $C_6H_5NO_4$ requires C, 46.5; H, 3.25; 9.0%); ν_{max}(film)/cm^{-1} 3099 (C-H), 2921 (O-H), 1746 (C=O), 1683, 922 (C=C); δ_H(300 MHz; $CDCl_3$) 6.74 (2H, s, 2 x CH, Mal), 4.26 (2H, s, CH_2); δ_C(75 MHz; $CDCl_3$) 172.8 (C, quat, C=O), 170.0 (2 x C, quat, C=O), 134.9 (2 x CH, Mal), 38.7 (CH_2); *m/z* (CI) 156.0291 ($M+H^+$ - $C_6H_6NO_4$ requires 156.0297), 138 (73%), 110 (100).

3-(2,5-Dioxo-2,5-dihydropyrrol-1-yl)propionic acid, n=2 126

The general procedure outlined above was followed using maleic anhydride (5.00 g, 50.9 mmol) and β-alanine (4.90 g, 50.9 mmol) in acetic acid (250 cm^3). The crude maleimide was purified *via* a short pad of silica (SiO_2, 19:1 v/v CH_2Cl_2:AcOH) and subsequent crystallisation from CH_2Cl_2/hexane to yield the product as a colourless solid (4.02 g, 47%); mp 105-106 °C (lit.,[193] 105.0-105.5 °C); (Found: C, 49.5; H, 4.0; N, 8.0. $C_7H_7NO_4$ requires C, 49.7; H, 4.2; N, 8.3%); υ_{max}(film)/cm^{-1} 3090 (C-H), 2724 (O-H), 1705 (C=O), 1696, 958, 926 (C=C); δ_H(300 MHz; $CDCl_3$) 6.65 (2H, s, 2 x CH, Mal), 3.78 (2H, t, $^3J_{H,H}$ 7.3, CH_2), 2.64 (2H, t, $^3J_{H,H}$ 7.3, CH_2); δ_C(75 MHz; CD_3Cl_3) 176.9 (C, quat, C=O), 170.7 (2 x C, quat, C=O), 134.6 (2 x CH, Mal), 33.6 (CH_2), 32.8 (CH_2); *m/z* (CI) 170.0452 ($M+H^+$ - $C_7H_8NO_4$ requires 170.0453).

***N*-(6-Aminopyridin-2-yl)-3-methylbutyramide 129**

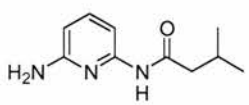

Isovaleryl chloride (1.80 cm^3, 15.2 mmol) was added dropwise at 0 °C to a stirred solution of 2,6-diaminopyridine (5.00 g, 46.0 mmol) in dry THF (200 cm^3) under a positive pressure of

nitrogen. The reaction mixture was stirred at room temperature for 15 hours. After this time, the reaction mixture was filtered under reduced pressure and the resulting filtrate reduced *in vacuo* to afford a dark brown oil which was purified *via* flash column chromatography (SiO_2, 1:1 v/v EtOAc:hexane) to yield the product as a colourless solid (2.72 g, 93%); mp 113–114 °C (lit.,[188] 110-113 °C); (Found: C, 61.9; H, 7.9; N, 21.4. $C_{10}H_{15}N_3O$ requires C, 62.15; H, 7.8; N, 21.7%); υ_{max}(film)/cm^{-1} 3444 (N-H), 3348 (N-H), 3201 (N-H), 2954 (C-H), 1671 (C=O); δ_H(300 MHz; $CDCl_3$), 8.18 (1H, bs, NH), 7.53 (1H, d, $^3J_{HH}$ 7.9, Ar), 7.40 (1H, dd, $^3J_{HH}$ 7.9, $^3J_{HH}$ 7.9, Ar), 6.21 (1H, d, $^3J_{HH}$ 7.9, Ar), 4.42 (2H, bs, NH_2), 2.16-2.06 (3H, m, CH_2, CH), 0.91 (6H, d, $^3J_{HH}$ 6.6, 2 x CH_3); δ_C(75 MHz; $CDCl_3$) 171.6 (C, quat, C=O), 157.5 (C, quat, Ar), 150.3 (C, quat, Ar), 140.6 (CH, Ar), 104.6 (CH, Ar), 103.7 (CH, Ar), 47.3 (CH_2), 26.5 (CH), 22.8 (2 x CH_3); *m/z* (CI) 193 (M^+, 35%), 109 (100).

4-Chloromethyl-*N*-[6-(3-methylbutyrylamino)pyridin-2-yl]benzamide 131

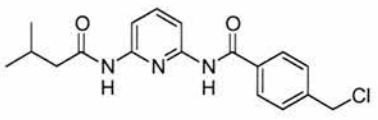

N-(6-Amino-pyridin-2-yl)-3-methyl-butyramide **129** (1.00 g, 5.20 mmol) was dissolved in dry THF (50 cm^3). To this solution, 4-(chloromethyl)benzoylchloride (0.97 g, 5.20 mmol) in dry THF (10 cm^3) was added dropwise and the reaction mixture allowed to stir for 16 hours under a positive pressure of nitrogen. After this time, the reaction mixture was filtered and the solvent removed *in vacuo* to afford the crude product as a yellow oil, which was purified *via* flash column chromatography (SiO_2, 2:1 v/v Hexane:EtOAc) to afford the product as colourless plate-like crystals (1.37 g, 71%); mp 117–118 °C; υ_{max}(film)/cm^{-1} 3274 (N-H), 2952, 2868 (C-H), 1665 (C=O); δ_H(300 MHz; $CDCl_3$) 8.01 (1H, bs, NH), 7.99 (1H, d, $^3J_{H,H}$ 7.9, Ar), 7.90 (1H, d, $^3J_{H,H}$ 7.9, Ar), 7.86-7.80 (2H, m, Ar), 7.70 (1H, dd, $^3J_{H,H}$ 7.9, $^3J_{H,H}$ 7.9, Ar), 7.53 (1H, bs, NH), 7.50-7.44 (2H, m, Ar), 4.57 (2H, s, CH_2), 2.20-2.19 (3H, m, CH_2, CH), 0.96 (6H, d, $^3J_{H,H}$ 6.7, 2 x CH_3); δ_C(75 MHz; $CDCl_3$,) 171.4 (C, quat, C=O), 165.2 (C, quat, C=O), 149.9 (C, quat, Ar), 149.8 (C, quat, Ar), 142.1 (C, quat, Ar), 141.4 (CH, Ar), 134.4 (C, quat, Ar), 129.4 (2 x CH, Ar), 127.9 (2 x CH, Ar), 110.2 (CH, Ar), 110.0 (CH_2, Ar), 47.5 (CH_2), 45.6 (CH_2), 26.5 (CH), 22.9 (2 x CH_3); *m/z* (CI) 346 ($M+H^+$, 74%), 312 (100), 194 (59), 102 (7).

Thioacetic acid *S*-{4-[6-(3-methylbutyrylamino)pyridin-2-ylcarbamoyl]benzyl} ester 133

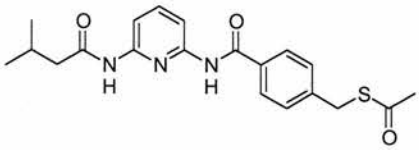

Potassium thioacetate (2.64 g, 23.1 mmol) was added to a stirred solution of 4-chloromethyl-*N*-[6-(3-methylbutyrylamino)pyridin-2-yl]benzamide **131** (2.00 g, 5.80 mmol) in acetone (75 cm^3). The reaction mixture was stirred under nitrogen for 2 hours. After this time, the reaction mixture was partitioned between CH_2Cl_2 (1 x 75 cm^3) and $NaHCO_3$ (1 x 50 cm^3). The resulting organic phase was decolourised with activated charcoal, filtered through a short pad of Celite and then dried ($MgSO_4$). The solvent was removed *in vacuo*, to afford an orange/yellow crude solid which was purified *via* flash chromatography (SiO_2, 2:1 v/v hexane:EtOAc) to yield an pale orange solid (2.21 g, quant.); mp 147-148 °C; (Found: C, 62.3; H, 6.0; N, 10.7. $C_{20}H_{23}N_3O_3S$ requires C, 62.3; H, 6.0; N, 10.9%); υ_{max}(film)/cm^{-1} 3240 (N-H), 1683 (C=O), 1583, 1506 (C=C, Ar); δ_H(300 MHz; $CDCl_3$) 8.16 (1H, bs, NH), 7.98 (1H, d, $^3J_{H,H}$ 7.9, Ar), 7.89 (1H, d, $^3J_{H,H}$ 7.9, Ar), 7.78-7.72 (2H, m, Ar), 7.69 (1H, dd, $^3J_{H,H}$ 7.9, $^3J_{H,H}$ 7.9, Ar), 7.55 (1H, bs, NH), 7.44-7.41 (2H, m, Ar), 4.09 (2H, s, CH_2), 2.30 (3H, s, CH_3), 2.19-2.15 (3H, m, CH_2, CH), 0.96 (6H, d, $^3J_{H,H}$ 6.7, 2 x CH_3); δ_C(75 MHz; $CDCl_3$) 171.4 (2 x C, quat, C=O), 165.4 (C, quat, C=O), 149.9 (2 x C, quat, Ar), 142.9 (C, quat, Ar), 141.4 (CH, Ar), 133.4 (C, quat, Ar), 129.7 (2 x CH, Ar), 127.9 (2 x CH, Ar), 110.1 (CH, Ar), 109.9 (CH, Ar), 47.5 (CH_2), 33.4 (CH_2), 30.7 (CH), 26.5 (CH_3), 22.9 (2 x CH_3); *m/z* (CI) 386 ($M+H^+$, 100%), 312 (35).

***p*-Tolyl acetyl fluoride 135**

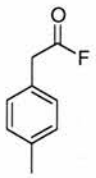

p-Tolylacetic acid (10.00 g, 66.6 mmol), dry pyridine (1.80 cm^3, 22.2 mmol) and cyanuric fluoride (1.90 cm^3, 22.2 mmol) were stirred for 16 hours in dry CH_3CN (100 cm^3) under a positive pressure of dry nitrogen. After this time, the reaction mixture was partitioned between CH_2Cl_2 (100 cm^3) and brine (2 x 50 cm^3), the organic layer dried ($MgSO_4$) and

solvent removed *in vacuo*. The fluoride product was carried through to the next stage without further purification; δ_F(282.3 MHz; $CDCl_3$) +44.1 (1F, t, $^3J_{H,F}$ 2.2, F).

_N_-6-(Amino-pyridin-2-yl)-2-_p_-tolyl acetamide 136

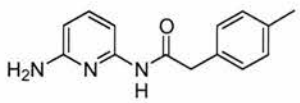

_p_-Tolyl acetyl fluoride **135** (9.00 g, 59.1 mmol) was added dropwise to a stirred solution of 2,6-diaminopyridine (19.36 g, 177 mmol) in CH_2Cl_2 (200 cm^3). The reaction mixture was stirred for 16 hours under a positive pressure of nitrogen. The reaction mixture was then filtered under reduced pressure and the resulting filtrate reduced *in vacuo* to yield a crude brown oil which was purified *via* flash column chromatography (SiO_2, 1:1 v/v EtOAc:Hexane) to afford the product as an off-white solid (13.59 g, 95%); mp 75–76 °C; δ_H(300 MHz; $CDCl_3$) 7.60 (1H, bs, NH), 7.47 (1H, d, $^3J_{H,H}$ 8.0, Ar), 7.41-7.33 (1H, m, Ar), 7.19-7.17 (4H, m, Ar), 6.16 (1H, d, $^3J_{H,H}$ 8.0, Ar), 4.29 (2H, bs, NH_2), 3.61 (2H, s, CH_2), 2.29 (3H, s, CH_3); δ_C(75 MHz; $CDCl_3$) 169.9 (C, quat, C=O), 157.4 (C, quat, Ar), 149.9 (C, quat, Ar), 140.5 (CH, Ar), 137.7 (C, quat, Ar), 131.4 (C, quat, Ar), 130.3 (2 x CH, Ar), 129.8 (2 x CH, Ar), 104.8 (CH, Ar), 103.6 (CH, Ar), 44.9 (CH_2), 21.5 (CH_3); *m/z* (CI) 242 ($M+H^+$, 50%), 152 (35), 89 (100).

3-Chloromethyl-_N_-[6-(2-_p_-tolylacetlamino)pyridin-2-yl]benzamide 138

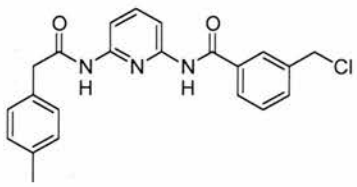

_N_-6-(Aminopyridin-2-yl)-2-_p_-tolyl acetamide **136** (13.59 g, 56.3 mmol) was dissolved in dry THF (80 cm^3). To this solution, 3-(chloromethyl)benzoylchloride (5.34 cm^3, 37.6 mmol) was added dropwise and the reaction mixture allowed to stir for 16 hours under a positive pressure of nitrogen. After this time, the reaction mixture was filtered and then the solvent removed *in vacuo* to afford the crude product as an oil, which was purified *via* recrystallisation (CH_2Cl_2:Hexane) to afford the product as a colourless solid (14.26 g, 96%); mp 118-120 °C; (Found: C, 66.8; H, 5.1; N, 10.7. $C_{22}H_{20}ClN_3O_2$ requires C, 67.1; H, 5.1; N, 10.7%);

υ_{max}(film)/cm^{-1} 3287 (N-H), 1666 (C=O), 1581, 1505 (C=C, Ar); δ_H(300 MHz; $CDCl_3$) 8.19 (1H, bs, NH), 8.04 (1H, d, $^3J_{H,H}$ 8.0, Ar), 7.96 (1H, d, $^3J_{H,H}$ 8.0, Ar), 7.87-7.88 (1H, m, Ar), 7.81-7.78 (1H, m, Ar), 7.75-7.72 (1H, m, Ar), 7.61-7.58 (1H, m, Ar), 7.55 (1H, bs, NH), 7.48 (1H, dd, $^3J_{H,H}$ 7.7, $^3J_{H,H}$ 7.7, Ar), 7.22 (4H, m, Ar), 4.64 (2H, s, CH_2), 3.72 (2H, s, CH_2), 2.37 (3H, s, CH_3); δ_C(75 MHz; $CDCl_3$) 170.0 (C, quat, C=O), 165.2 (C, quat, C=O), 149.8 (2 x C, quat, Ar), 141.3 (CH, Ar), 138.8 (C, quat, Ar), 137.9 (C, quat, Ar), 135.1 (C, quat, Ar), 132.7 (CH, Ar), 131.2 (C, quat, Ar), 130.4 (2 x CH, Ar), 129.8 (2 x CH, Ar), 129.7 (CH, Ar), 127.7 (CH, Ar), 127.4 (CH, Ar), 110.2 (CH, Ar), 110.1 (CH, Ar), 45.8 (CH_2), 44.9 (CH_2), 21.6 (CH_3); *m/z* (CI) 394 ($M+H^+$, 10%), 360 (21), 326 (12), 301 (79), 242 (100), 227 (15).

Thioacetic acid *S*-{3-[6-(2-*p*-tolyl acetylamino)pyridin-2-ylcarbamoyl]benzyl} ester 139

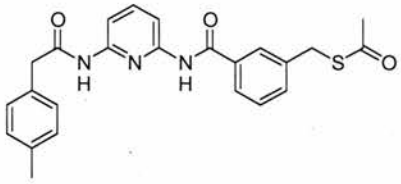

Potassium thioacetate (5.79 g, 50.8 mmol) was added to a stirred solution of 3-chloromethyl-*N*-[6-(2-*p*-tolyl acetlamino)pyridin-2-yl]benzamide **138** (5.00 g, 12.7 mmol) in acetone (150 cm^3). The reaction mixture was stirred under nitrogen for 2 hours. After this time, the reaction mixture was partitioned between CH_2Cl_2 (1 x 75 cm^3) and saturated aqueous $NaHCO_3$ (1 x 50 cm^3). The resulting organic phase was decolourised with activated charcoal, filtered through a short pad of Celite, then dried ($MgSO_4$) and the solvent removed *in vacuo*, to afford an orange/yellow crude solid which was purified *via* flash column chromatography (SiO_2, 2:1 v/v Hexane:EtOAc) to yield the product as a pale orange solid (4.83 g, 88%); mp 103-105 °C; (Found: C, 66.3; H, 5.3; N, 9.6. $C_{24}H_{23}N_3O_3S$ requires C, 66.5; H, 5.35; N, 9.7%); υ_{max}(film)/cm^{-1} 3249 (N-H), 1683 (C=O), 1582, 1506 (C=C, Ar); δ_H(300 MHz; $CDCl_3$) 8.18 (1H, bs, NH), 8.03 (1H, d, $^3J_{H,H}$ 7.7, Ar), 7.95 (1H, d, $^3J_{H,H}$ 7.7, Ar), 7.78-7.70 (3H, m, Ar), 7.56 (1H, bs, NH), 7.51-7.48 (1H, m, Ar), 7.42 (1H, dd, $^3J_{H,H}$ 7.7, $^3J_{H,H}$ 7.7, Ar), 7.23 (4H, m, Ar), 4.16 (2H, s, CH_2), 3.70 (2H, s, CH_2), 2.37 (3H, s, CH_3), 2.36 (3H, s, CH_3); δ_C(75 MHz; $CDCl_3$) 169.9 (C, quat, C=O), 165.5 (C, quat, C=O), 149.8 (C, quat, Ar), 149.7 (C, quat, Ar), 141.3 (CH, Ar), 139.2 (C, quat, Ar), 137.9 (C, quat, Ar), 134.9 (C, quat, Ar), 133.1 (CH, Ar), 131.2 (C, quat, Ar), 130.4 (2 x CH, Ar), 129.8 (2 x CH, Ar), 129.5 (CH, Ar), 127.8 (CH, Ar), 126.3 (CH, Ar), 110.2 (CH, Ar), 110.0 (CH, Ar), 45.0 (CH_2), 33.4 (CH_2), 30.7 (CH_3), 21.6 (CH_3); *m/z* (CI) 433 (M^+, 100%), 374 (10), 359 (40), 341 (15), 281 (20), 248

(23), 165 (15), 120 (30).

General procedure, 3-Chloromethyl furan 141

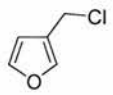

Carbon tetrachloride (1.5 eq.) was added dropwise to a stirring solution of 3-furan methanol (1 eq.) and tributyl phosphine (2 eq.) in dry acetonitrile. The reaction mixture was allowed to stir at room temperature for 30 minutes. After this time, the reaction was complete by t.l.c and the crude acid chloride used without further purification.

Thioacetic acid *S*-furan-3-ylmethyl ester 142

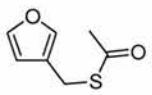

3-Furan methanol (3.52 cm^3, 40.8 mmol) and tributylphosphine (10.15 cm^3, 40.8 mmol) were stirred at room temperature in CH_3CN (50 cm^3) under an atmosphere of dry nitrogen for 30 minutes. The reaction mixture was then cooled to 0 °C before the dropwise addition of carbon tetrachloride (4.32 cm^3, 44.9 mmol) over 15 minutes. The reaction mixture was warmed to room temperature over a 60 minute period, to allow the formation of the chloride intermediate. After this time, potassium thioacetate (13.98 g, 122 mmol) was added and the reaction mixture stirred for 16 hours. After this time, reaction mixture was partitioned between CH_2Cl_2 (1 x 60 cm^3) and saturated aqueous $NaHCO_3$ (2 x 25 cm^3), the organic phase dried ($MgSO_4$) and the solvent removed *in vacuo*. The resulting crude red liquid was purified *via* flash column chromatography (SiO_2, 30:1 v/v Hexane:EtOAc) to afford the product as a brown liquid (3.67 g, 57%); δ_H(300 MHz; $CDCl_3$) 7.31-7.90 (1H, m, FurylH), 7.28-7.27 (1H, m, FurylH), 6.26-6.24 (1H, m, FurylH), 3.87 (2H, s, CH_2), 2.28 (3H, s, CH_3); δ_C(75 MHz; $CDCl_3$) 195.6 (C, quat, C=O), 143.6 (CH, Furyl), 140.8 (CH, Furyl), 121.6 (C, quat, Furyl), 111.2 (CH, Furyl), 30.8 (CH_3), 24.0 (CH_2); *m/z* (EI) 156.0244 (M^+ - $C_7H_8O_2S$ requires 156.0245), 114 (100%).

(2,5-Dioxo-2,5-dihydro-pyrrol-1-yl) acid methyl esters, General Procedure

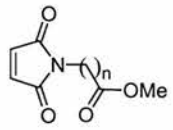

Methyl iodide (2.0 eq.) was added dropwise to a stirred solution of the appropriate maleimide (1.0 eq.) and cesium carbonate (0.5 eq.) in dry DMF. The resulting reaction mixtures were then left to stir at room temperature for 16 hours under atmosphere of dry nitrogen. After this time, the reaction mixture was partitioned between EtOAc and H_2O and washed with brine, before drying the organic layer ($MgSO_4$). The solvent was then removed *in vacuo* to afford the crude products as yellow oils, which were purified *via* flash column chromatography (SiO_2, v/v Hexane:EtOAc) to afford the products as oils.

(2,5-Dioxo-2,5-dihydropyrrol-1-yl)acetic acid methyl ester, n=1 148

The general procedure outlined above was followed using methyl iodide (3.45 cm^3, 37.2 mmol), (2,5-dioxo-2,5-dihydropyrrol-1-yl)acetic acid **125** (2.88 g, 18.6 mmol) and cesium carbonate (3.03 g, 9.30 mmol) in dry DMF (50 cm^3) to afford (2,5-dioxo-2,5-dihydropyrrol-1-yl)acetic acid methyl ester as a pale yellow oil (2.72 g, 87%); υ_{max}(film)/cm^{-1} 2954 (C-H), 1750 (C=O), 1715 (C=O); δ_H(300 MHz; $CDCl_3$) 6.78 (2H, s, 2 x CH, Mal), 4.28 (2H, s, CH_2), 3.75 (3H, s, CH_3); δ_C(75 MHz; $CDCl_3$) 170.1 (C, quat, C=O), 168.0 (2 x C, quat, C=O), 134.9 (2 x CH, Mal), 53.1 (CH_3), 38.9 (CH_2); *m/z* (CI) 170.0453 ($M+H^+$ - $C_7H_8NO_4$ requires 170.0453), 138 (100%), 110 (90).

(2,5-Dioxo-2,5-dihydropyrrol-1-yl)propionic acid methyl ester, n=2 149

The general procedure outlined above was followed using methyl iodide (2.39 cm^3, 25.8 mmol) (2,5-dioxo-2,5-dihydropyrrol-1-yl)propionic acid **126** (2.18 g, 12.9 mmol) and cesium carbonate (2.10 g, 6.40 mmol) in dry DMF (45 cm^3) to afford (2,5-dioxo-2,5-dihydropyrrol-1-yl)propionic acid methyl ester as a colourless oil (1.41 g, 60%); υ_{max}(film)/cm^{-1} 2952 (N-H), 1736 (C=O), 1704 (C=O); δ_H(300 MHz; $CDCl_3$) 6.65 (2H, s, 2 x CH, Mal), 3.76 (2H, t, $^3J_{H,H}$ 7.0, CH_2), 3.61 (3H, s, CH_3), 2.56 (2H, t, $^3J_{H,H}$ 7.0, CH_2); δ_C(75 MHz; $CDCl_3$) 171.5 (C, quat, C=O), 170.7 (2 x C, quat, C=O), 134.6 (2 x CH, Mal), 52.3 (CH_3), 33.9 (CH_2), 33.1 (CH_2);

m/z (CI) 184.0607 ($M+H^+$ - $C_8H_{10}NO_4$ requires 184.0607), 152 (100%).

3-(2,5-Dioxo-3-{3-[6-(2-*p*-tolylacetylamino)pyridin-2-ylcarbamoyl]benzylsulfanyl} pyrrolidin-1-yl)propionic acid

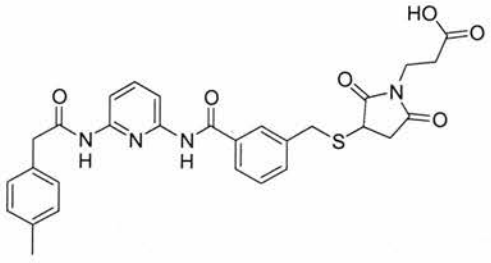

Colourless oil; δ_H(300 MHz; $CDCl_3$) 9.07 (1H, bs, NH), 8.47 (1H, bs, NH), 8.10 (1H, d, $^3J_{HH}$ 7.5, Ar), 8.03 (1H, d, $^3J_{HH}$ 7.5, Ar), 7.92-7.86 (2H, m, 2 x Ar), 7.81-7.76 (1H, m, Ar), 7.62-7.58 (1H, m, Ar), 7.49 (1H, dd, $^3J_{HH}$ 7.5, $^3J_{HH}$ 7.5, Ar), 7.22 (4H, s, 4 x CH), 4.14 (2H, dd, $^3J_{HH}$ 93.0, $^3J_{HH}$13.5, CH_2S), 3.85 (2H, t, $^3J_{HH}$ 6.4, CH_2), 3.72 (2H, s, CH_2), 3.50 (1H, dd, $^3J_{HH}$ 4.8, $^3J_{HH}$ 4.3, CH), 2.96 (1H, dd, $^3J_{HH}$ 9.2, $^3J_{HH}$ 9.2, CH), 2.60 (2H, t, $^3J_{HH}$ 6.4, CH_2), 2.40 (1H, dd, $^3J_{HH}$ 15.1, $^3J_{HH}$ 4.9, CH), 2.36 (3H, s, CH_3); δ_C(75 MHz; $CDCl_3$) 176.5 (C, quat, C=O), 175.6 (C, quat, C=O), 174.3 (C, quat, C=O), 170.0 (C, quat, C=O), 165.8 (C, quat, C=O), 149.6 (C, quat, Ar), 149.5 (C, quat, Ar), 142.6 (CH, Ar), 137.5 (C, quat, Ar), 137.4 (C, quat, Ar), 134.0 (C, quat, Ar), 133.1 (CH, Ar), 130.8 (C, quat, Ar), 129.8 (2 x CH, Ar), 129.7 (CH, Ar), 129.5 (2 x CH, Ar), 128.1 (CH, Ar), 127.5 (CH, Ar), 110.7 (CH, Ar), 110.4 (CH, Ar), 44.5 (CH_2), 37.8 (CH), 35.3 (CH_2), 34.9 (CH_2), 34.7 (CH_2), 32.2 (CH_2), 28.7 (CH_2), 21.2 (CH_3); *m/z* (ES) 559.1641 ($M-H^+$ - $C_{29}H_{27}N_4O_6S$ requires 559.1651), 390 (55%).

(2,5-Dioxo-3-{3-[6-(2-*p*-tolylacetylamino)pyridin-2-ylcarbamoyl]benzylsulfanyl} pyrrolidin-1-yl)acetic acid 163

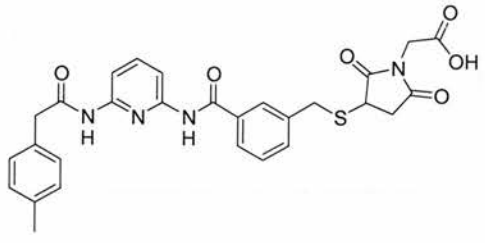

Colourless oil; δ_H(300 MHz; $CDCl_3$) 9.45 (1H, bs, NH), 8.93 (1H, bs, NH), 8.12 (1H, d, $^3J_{HH}$ 7.5, Ar), 8.05-7.70 (4H, m, 4 x Ar), 7.58-7.41 (2H, m, 2 x Ar), 7.22-7.23 (4H, m, 4 x Ar), 4.07 (2H, dd, $^3J_{HH}$ 45.9, $^3J_{HH}$ 11.4, CH_2S), 3.65 (2H, s, CH_2), 3.58 (1H, dd, $^3J_{HH}$ 4.8, $^3J_{HH}$ 4.3, CH),

2.96 (1H, dd, $^3J_{HH}$ 9.1, $^3J_{HH}$ 9.1, CH), 2.39 (1H, dd, $^3J_{HH}$ 4.8, $^3J_{HH}$ 13.8, CH), 2.27 (3H, s, CH_3); δ_C(75 MHz; $CDCl_3$) 176.5 (C, quat, C=O), 173.7 (C, quat, C=O), 172.1 (C, quat, C=O), 170.4 (C, quat, C=O), 165.4 (C, quat, C=O), 149.5 (C, quat, Ar), 149.1 (C, quat, Ar), 142.5 (CH, Ar), 137.9 (C, quat, Ar), 137.2 (C, quat, Ar), 134.0 (C, quat, Ar), 133.9 (CH, Ar), 131.0 (C, quat, Ar), 130.0 (CH, Ar), 129.7 (2 x CH, Ar), 129.4 (2 x CH, Ar), 128.0 (CH, Ar), 126.9 (CH, Ar), 110.3 (CH, Ar), 110.1 (CH, Ar), 44.1 (CH_2), 40.9 (CH_2), 38.4 (CH), 35.3 (CH_2), 34.9 (CH_2), 21.1 (CH_3); *m/z* (ES) 545.1500 ($M\text{-}H^+$ - $C_{28}H_{25}N_4O_6S$ requires 545.1495).

(2,5-Dioxo-3-{3-[6-(2-*p*-tolylacetylamino)pyridin-2-ylcarbamoyl]benzylsulfanyl} pyrrolidin-1-yl)acetic acid methyl ester 164

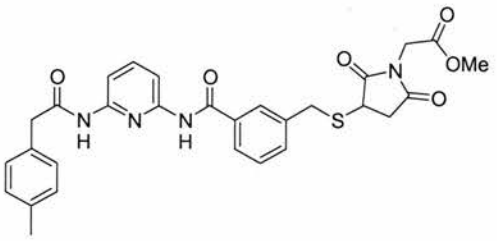

Yellow oil; δ_H(300 MHz; $CDCl_3$) 8.24 (1H, bs, NH), 8.03 (1H, d, $^3J_{HH}$ 7.9, Ar), 7.96 (1H, d, $^3J_{HH}$ 7.9, Ar), 7.92-7.90 (1H, m, Ar), 7.80-7.59 (5H, m, 4 x Ar, NH), 7.23-7.21 (4H, m, Ar), 4.27 (2H, s, CH_2), 4.09 (2H, dd, $^3J_{HH}$ 86.5, $^3J_{HH}$ 13.7, CH_2S), 3.68 (3H, s, CH_3), 3.65 (2H, s, CH_2), 3.59 (1H, dd, $^3J_{HH}$ 5.6, $^3J_{HH}$ 3.7, CH), 3.10 (1H, dd, $^3J_{HH}$ 9.3, $^3J_{HH}$ 9.3, CH), 2.49 (1H, dd, $^3J_{HH}$ 3.7, $^3J_{HH}$ 15.1, CH), 2.37 (3H, s, CH_3); δ_C(75 MHz; $CDCl_3$) 175.7 (C, quat, C=O), 173.6 (C, quat, C=O), 169.6 (C, quat, C=O), 170.0 (C, quat, C=O), 165.1 (C, quat, C=O), 149.5 (C, quat, Ar), 149.4 (C, quat, Ar), 140.9 (CH, Ar), 137.9 (C, quat, Ar), 137.5 (C, quat, Ar), 134.8 (C, quat, Ar), 133.0 (CH, Ar), 130.8 (C, quat, Ar), 130.8 (2 x CH, Ar), 129.4 (2 x CH, Ar), 129.3 (CH, Ar), 127.8 (CH, Ar), 126.5 (CH, Ar), 109.8 (CH, Ar), 109.7 (CH, Ar), 54.4 (CH_3), 44.6 (CH_2), 39.6 (CH_2), 37.7 (CH), 35.4 (CH_2), 21.2 (CH_3); *m/z* (ES) 559.1638 ($M\text{-}H^+$ - $C_{29}H_{27}N_4O_6S$ requires 559.1651), 390 (100%), 236 (30).

(3-{4-[6-(3-Methylbutyrylamino)pyridin-2-ylcarbamoyl]benzylsulfanyl}-2,5-dioxopyrrolidin-1-yl)acetic acid 165

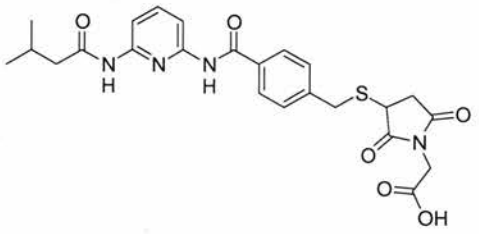

Colourless oil; δ_H(300 MHz; $CDCl_3$) 8.50 (1H, bs, NH), 8.25 (1H, bs, NH), 8.08-7.96 (2H, m, Ar), 7.86-7.72 (3H, m, Ar), 7.47-7.42 (2H, m, Ar), 4.23 (2H, bs, CH_2), 3.75 (2H, dd, $^3J_{HH}$ 93.0, $^3J_{HH}$ 13.6, CH_2S), 3.53 (1H, dd, $^3J_{HH}$ 5.3, $^3J_{HH}$ 3.8, CH), 3.03 (1H, dd, $^3J_{HH}$ 9.6, $^3J_{HH}$ 9.2, CH), 2.39 (1H, dd, $^3J_{HH}$ 15.1, $^3J_{HH}$ 3.8, CH), 2.36-2.11 (3H, m, CH_2, CH), 0.96 (6H, d, $^3J_{HH}$ 6.5, 2 x CH_3); δ_C(75 MHz; $CDCl_3$) 176.2 (C, quat, C=O), 174.2 (C, quat, C=O), 171.4 (2 x C, quat, 2 x C=O), 165.3 (C, quat, C=O), 149.6 (C, quat, Ar), 149.3 (C, quat, Ar), 141.5 (C, quat, Ar), 141.4 (CH, Ar), 133.2 (C, quat, Ar), 127.8 (2 x CH, Ar), 127.6 (2 x CH, Ar), 109.7 (CH, Ar), 109.6 (CH, Ar), 44.1 (CH_2), 41.0 (CH_2), 37.7 (CH), 35.5 (CH_2), 35.3 (CH_2), 26.2 (CH), 22.5 (2 x CH_3); *m/z* (ES) 497.1489 ($M\text{-}H^+$ - $C_{24}H_{25}N_4O_6S$ requires 497.1495), 342 (97%).

(3-{4-[6-(3-Methylbutyrylamino)pyridin-2-ylcarbamoyl]benzylsulfanyl}-2,5-dioxo-pyrrolidin-1-yl)acetic acid methyl ester 166

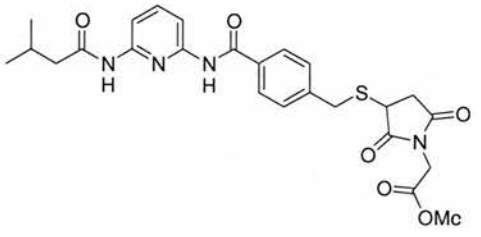

Yellow oil; υ_{max}(film)/cm^{-1} 3260 (N-H), 2953 (C-H), 1712, 1688 (C=O); δ_H(300 MHz; $CDCl_3$) 8.26 (1H, bs, NH), 8.05 (1H, d, $^3J_{HH}$ 7.7, Ar), 7.97 (1H, d, $^3J_{HH}$ 7.7, Ar), 7.88-7.84 (2H, m, Ar), 7.76 (1H, dd, $^3J_{HH}$ 7.7, $^3J_{HH}$ 7.7, Ar), 7.62 (1H, bs, NH), 7.56-7.53 (2H, m, Ar), 4.28 (2H, bs, CH_2), 4.10 (2H, dd, $^3J_{HH}$ 102.9, $^3J_{HH}$ 13.6, CH_2S), 3.77 (3H, s, CH_3), 3.58 (1H, dd, $^3J_{HH}$ 5.5, $^3J_{HH}$ 3.7, CH), 3.10 (1H, dd, $^3J_{HH}$ 9.3, $^3J_{HH}$ 9.3, CH), 2.51 (1H, dd, $^3J_{HH}$ 15.1, $^3J_{HH}$ 3.7, CH), 2.27-2.17 (3H, m, CH_2, CH), 1.03 (6H, d, $^3J_{HH}$ 6.5, 2 x CH_3); δ_C(75 MHz; $CDCl_3$) 175.8 (C, quat, C=O), 173.6 (C, quat, C=O), 170.9 (C, quat, C=O), 166.9 (C, quat,

C=O), 164.9 (C, quat, C=O), 149.6 (C, quat, Ar), 149.5 (C, quat, Ar), 141.5 (C, quat, Ar), 141.0 (CH, Ar), 133.5 (C, quat, Ar), 129.7 (2 x CH, Ar), 127.6 (2 x CH, Ar), 109.8 (CH, Ar), 109.6 (CH, Ar), 52.9 (CH_3), 47.1 (CH_2), 39.6 (CH_2), 37.4 (CH), 35.4 (CH_2), 35.3 (CH_2), 26.2 (CH), 22.5 (2 x CH_3); *m/z* (ES) 511.1653 ($M\text{-}H^+$ - $C_{25}H_{28}N_4O_6S$ requires 511.1651).

3-(3-{4-[6-(3-Methylbutyrlamino)pyridin-2-ylcarbamoyl]benzylsulfanyl}-2,5-dioxo pyrrolidin-1-yl)propionic acid 167

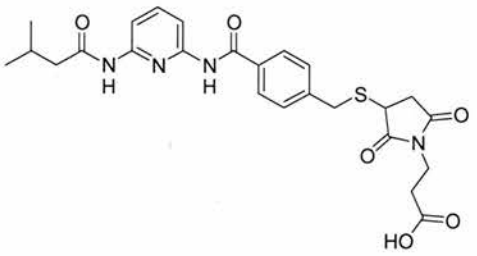

Colourless oil; δ_H(300 MHz; $CDCl_3$) 8.68 (1H, bs, NH), 8.05 (1H, bs, NH), 8.03 (1H, d, $^3J_{HH}$ 7.8, Ar), 8.00 (1H, d, $^3J_{HH}$ 7.8, Ar), 7.86-7.84 (2H, m, 2 x Ar), 7.76 (1H, dd, $^3J_{HH}$ 7.8, $^3J_{HH}$ 7.8, Ar), 7.51-7.45 (2H, m, Ar), 4.04 (2H, dd, $^2J_{HH}$ 106.5, $^3J_{HH}$ 13.1 CH_2S), 3.84 (2H, t, $^3J_{HH}$ 7.5, CH_2), 3.48 (1H, dd, $^2J_{HH}$ 5.4, $^3J_{HH}$ 3.8, CH), 2.99 (1H, dd, $^3J_{HH}$ 9.3, $^3J_{HH}$ 9.3, CH), 2.65 (2H, t, $^3J_{HH}$ 7.1, CH_2), 2.40 (1H, dd, $^3J_{HH}$ 14.9, $^3J_{HH}$ 3.8, CH), 2.30-2.16 (3H, m, CH_2, CH_2), 1.02 (6H, d, $^3J_{HH}$ 6.5, 2 x CH_3); δ_C(75 MHz; $CDCl_3$) 176.5 (C, quat, C=O), 175.5 (C, quat, C=O), 174.4 (C, quat, C=O), 171.5 (C, quat, C=O), 165.2 (C, quat, C=O), 149.8 (C, quat, Ar), 149.4 (C, quat, Ar), 141.5 (C, quat, Ar), 141.4 (CH, Ar), 134.3 (C, quat, Ar), 129.6 (2 x CH, Ar), 127.8 (2 x CH, Ar), 110.2 (CH, Ar), 109.9 (CH, Ar), 46.9 (CH_2), 37.4 (CH), 35.4 (CH_2), 35.3 (CH_2), 32.8 (CH_2), 26.1 (CH), 22.5 (2 x CH_3); *m/z* (ES) 511.1660 ($[M\text{-}H]^+$ - $C_{25}H_{27}N_4O_6S$ requires 511.1651), 340 (100%).

3-(3-{4-[6-(3-Methylbutyrylamino)pyridin-2-ylcarbamoyl]benzylsulfanyl}-2,5-dioxo pyrrolidin-1-yl)propionic acid methyl ester 168

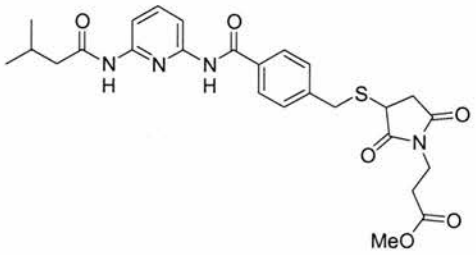

Yellow oil; δ_H(300 MHz; $CDCl_3$) 8.25 (1H, bs, NH), 8.05 (1H, d, $^3J_{HH}$ 7.5, Ar), 7.97 (1H, d, $^3J_{HH}$ 7.5, Ar), 7.88-7.83 (2H, m, Ar), 7.76 (1H, dd, $^3J_{HH}$ 7.5, $^3J_{HH}$ 7.5, Ar), 7.62 (1H, bs, NH), 7.56-7.53 (2H, m, Ar), 4.10 (2H, dd, $^2J_{HH}$ 109.2, $^3J_{HH}$ 13.7, CH_2S), 3.82 (2H, t, $^3J_{HH}$ 7.2, CH_2), 3.68 (3H, s, CH_3), 3.47 (1H, dd, $^2J_{HH}$ 5.5, $^3J_{HH}$ 3.7, CH), 3.00 (1H, dd, $^3J_{HH}$ 9.4, $^3J_{HH}$ 9.4, CH), 2.64 (2H, t, $^3J_{HH}$ 7.2, CH_2), 2.42 (1H, dd, $^3J_{HH}$ 15.1, $^3J_{HH}$ 3.7, CH), 2.27-2.16 (3H, m, CH_2, CH), 1.02 (6H, d, $^3J_{HH}$ 6.5, 2 x CH_3); δ_C(75 MHz; $CDCl_3$) 176.2 (C, quat, C=O), 174.1 (C, quat, C=O), 171.0 (2 x C, quat, C=O), 164.9 (C, quat, C=O), 149.6 (C, quat, Ar), 149.5 (C, quat, Ar), 141.5 (C, quat, Ar), 141.0 (CH, Ar), 134.7 (C, quat, Ar), 129.7 (2 x CH, Ar), 127.6 (2 x CH, Ar), 109.8 (CH, Ar), 109.6 (CH, Ar), 52.0 (CH_3), 47.1 (CH_2), 37.1 (CH), 35.5 (CH_2), 35.2 (CH_2), 34.8 (CH_2), 31.7 (CH_2), 26.2 (CH), 22.5 (CH_3); *m/z* (ES) 525.1802 ($M\text{-}H^+$ - $C_{26}H_{29}N_4O_6S$ requires 525.1808).

3-(2,5-Dioxo-3-{3-[6-(2-*p*-tolylacetylamino)pyridin-2-ylcarbomoyl]benzylsulfanyl} pyrrolidin-1-yl)propionic acid methyl ester 169

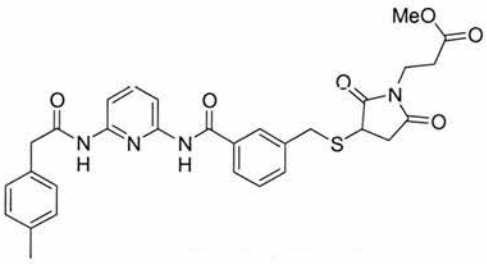

Yellow oil; υ_{max} (thin film)/cm^{-1} 3260 (N-H), 2953 (C-H), 1712, 1688 (C=O); δ_H(300 MHz; $CDCl_3$) 8.25 (1H, bs, NH), 8.03 (1H, d, $^3J_{HH}$ 7.5, Ar), 7.96 (1H, d, $^3J_{HH}$ 7.5, Ar), 7.92-7.90 (1H, m, Ar), 7.79-7.71 (2H, m, Ar), 7.66 (1H, bs, NH), 7.63-7.58 (1H, m, Ar), 7.46 (1H, dd, $^3J_{HH}$ 7.5, $^3J_{HH}$ 7.5, Ar), 7.22-7.20 (4H, m, Ar), 4.10 (2H, dd, $^3J_{HH}$ 99.3, $^3J_{HH}$13.7, CH_2S), 3.82

(2H, t, $^3J_{HH}$ 6.5, CH_2), 3.72 (2H, s, CH_2), 3.67 (3H, s, CH_3), 3.47 (1H, dd, $^3J_{HH}$ 5.5, $^3J_{HH}$ 3.7, CH), 3.00 (1H, dd, $^3J_{HH}$ 9.4, $^3J_{HH}$ 9.4, CH), 2.65 (2H, t, $^3J_{HH}$ 6.4, CH_2), 2.42 (1H, dd, $^3J_{HH}$ 15.1, $^3J_{HH}$ 3.7, CH), 2.37 (3H, s, CH_3); δ_C(75 MHz; $CDCl_3$) 176.3 (C, quat, C=O), 174.1 (C, quat, C=O), 171.1 (C, quat, C=O), 169.6 (C, quat, C=O), 165.1 (C, quat, C=O), 149.5 (2 x C, quat, Ar), 140.9 (CH, Ar), 137.8 (C, quat, Ar), 137.5 (C, quat, Ar), 134.8 (C, quat, Ar), 133.1 (CH, Ar), 131.0 (C, quat, Ar), 130.0 (2 x CH, Ar), 129.5 (2 x CH, Ar), 129.3 (CH, Ar), 127.8 (CH, Ar), 126.4 (CH, Ar), 109.8 (CH, Ar), 109.7 (CH, Ar), 52.0 (CH_3), 44.6 (CH_2), 37.3 (CH), 35.6 (CH_2), 35.3 (CH_2), 34.8 (CH_2), 31.7 (CH_2), 21.2 (CH_3); *m/z* (ES) 573.1808 ($M\text{-}H^+$ - $C_{30}H_{29}N_4O_6S$ requires 573.1808), 390 (7%), 178 (100).

Functionalised Dimethylmaleimides – General Procedure

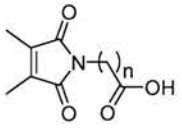

Dimethylmaleic anhydride (1.0 eq.) and the appropriate amino acid (1.0 eq.) were dissolved in acetic acid and refluxed for 8 hours under a positive pressure of nitrogen. The reaction mixture was then allowed to stir at room temperature for 16 hours, after this time, the acetic acid was removed *in vacuo*.

(3,4-Dimethyl-2,5-dioxo-2,5-dihydropyrrol-1-yl)acetic acid, n=1 174

The general procedure outlined above was followed using dimethylmaleic anhydride (3.00 g, 23.8 mmol) and glycine (1.79 g, 23.8 mmol) in acetic acid (80 cm^3). The crude maleimide was purified *via* column chromatography (SiO_2, 19:1 v/v CH_2Cl_2:AcOH) to yield the product as a colourless solid (1.98 g, 45%); mp 100-102 °C; (Found: C, 52.4; H, 4.7; N, 7.4. $C_8H_9NO_4$ requires C, 52.5; H, 4.95; N, 7.65%); ν_{max}(film)/cm^{-1} 2937 (C-H), 2820 (OH), 1713 (C=O); δ_H(300 MHz; $CDCl_3$) 10.02 (1H, bs, OH), 4.28 (2H, s, CH_2), 1.98 (6H, s, 2 x CH_3); δ_C(75 MHz; $CDCl_3$) 176.5 (2 x C, quat, C=O), 171.1 (C, quat, C=O), 138.0 (2 x C, quat, Mal), 38.5 (CH_2), 8.8 (2 x CH_3); *m/z* (CI) 184.0608 ($M+H^+$ - $C_8H_{10}NO_4$ requires 184.0610), 166 (21%), 138 (100).

3-(3,4-Dimethyl-2,5-dioxo-2,5-dihydropyrrol-1-yl)propionic acid, n=2 175

The general procedure outlined above was followed using dimethylmaleic anhydride (3.00 g, 23.8 mmol) and β-alanine (2.12 g, 23.8 mmol) in acetic acid (80 cm^3). The crude maleimide was purified *via* column chromatography (SiO_2, 19:1 v/v CH_2Cl_2:AcOH) to yield the product as a colourless solid (1.69 g, 37%); mp 167-168 °C; (Found: C, 55.1; H, 5.3; N, 6.8. $C_9H_{11}NO_4$ requires C, 54.8; H, 5.6; N, 7.1%); ν_{max}(film)/cm^{-1} 2932 (OH), 1696 (C=O); δ_H(300 MHz; $CDCl_3$) 3.79 (2H, t, $^3J_{HH}$ 7.3, CH_2), 2.68 (2H, t, $^3J_{HH}$ 7.3, CH_2), 1.96 (6H, s, 2 x CH_3); δ_C(75 MHz; $CDCl_3$) 176.5 (2 x C, quat, C=O), 171.8 (C, quat, C=O), 137.4 (2 x C, quat, Mal), 33.3 (CH_2), 32.7 (CH_2), 8.7 (2 x CH_3); *m/z* (CI) 198.0761 ($M+H^+$ - $C_9H_{12}NO_4$ requires 198.0766), 180 (100%).

3,4-Dimethyl furan-2,5-dione 178

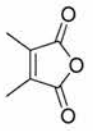

Maleic anhydride (10.40 g, 110 mmol) in acetic acid (30 cm^3) was added dropwise to a solution of 2-aminopyridine (5.00 g, 53.0 mmol) in acetic acid (30 cm^3) at reflux. After addition was complete the reaction mixture was refluxed for a further 2 hours. After this time, the solvent was removed *in vacuo*. The resulting residue was dissolved in 2 M H_2SO_4 (60 cm^3) and refluxed for a further 1 hour. Upon cooling, the product crystallised from solution, was filtered under reduced pressure, whilst being washed thoroughly with cold H_2O. The product was dried under vacuum over P_2O_5, to yield the product as large colourless crystals (4.81 g, 72%); mp 91-92 °C (lit.,[201] 93.0-95.0 °C); ν_{max}(film)/cm^{-1} 1746 (C=O); δ_H(300 MHz; $CDCl_3$) 2.06 (6H, s, 2 x CH_3); δ_C(75 MHz; $CDCl_3$) 166.6 (2 x C, quat, C=O), 141.2 (2 x C, quat, Mal), 9.9 (2 x CH_3); *m/z* (CI) 127.0396 ($M+H^+$ $C_6H_7O_3$ requires 127.0395).

Functionalised Methylmaleimides – General Procedure

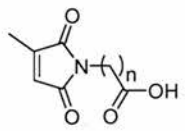

Citraconic anhydride (1.0 eq.) and the appropriate amino acid (1.0 eq.) were dissolved in acetic acid and refluxed for 8 hours under a positive pressure of nitrogen. The reaction mixture was then allowed to stir at room temperature for 16 hours, after this time, the acetic acid was removed *in vacuo*.

(3-Methyl-2,5-dioxo-2,5-dihydropyrrol-1-yl)acetic acid, n=1 181

The general procedure outlined above was followed using citraconic anhydride (3.00 g, 26.8 mmol) and glycine (2.01 g, 26.8 mmol) in acetic acid (80 cm^3). The crude maleimide was purified *via* column chromatography (SiO_2, 19:1 v/v CH_2Cl_2:AcOH) to yield the product as a colourless solid (3.04 g, 67%); mp 118-120 °C; (Found: C, 49.3; H, 3.7; N, 8.4. $C_7H_7NO_4$ requires C, 49.7; H, 4.2; N, 8.3%); ν_{max}(film)/cm^{-1} 2800 (vb, OH), 1706 (C=O); δ_H(300 MHz; $CDCl_3$) 10.06 (1H, bs, OH), 6.42 (1H, m, MalH), 4.29 (2H, s, CH_2), 2.11 (3H, d, $^3J_{HH}$ 1.9, CH_3); δ_C(75 MHz; $CDCl_3$) 173.0 (C, quat, C=O), 170.8 (C, quat, C=O), 169.8 (C, quat, C=O), 146.3 (C, quat, Mal), 127.8 (CH, Mal), 38.4 (CH_2), 11.1 (CH_3); *m/z* (ES) 168.0291 ($[M-H]^+$ - $C_7H_6NO_4$ requires 168.0297), 124 (100%).

3-(3-Methyl-2,5-dioxo-2,5-dihydropyrrol-1-yl)propionic acid, n=2 182

The general procedure outlined above was followed using citraconic anhydride (3.00 g, 26.8 mmol) and β-alanine (2.39 g, 26.8 mmol) in acetic acid (80 cm^3). The crude maleimide was purified *via* column chromatography (SiO_2, 19:1 v/v CH_2Cl_2:AcOH) to yield the product as a colourless solid (2.41 g, 49%); mp 88-89 °C; (Found: C, 52.5; H, 5.0; N, 7.6. $C_8H_9NO_4$ requires C, 52.5; H, 4.95; N, 7.65%); ν_{max}(film)/cm^{-1} 2950 (vb, OH), 1706 (C=O); δ_H(300 MHz; $CDCl_3$) 10.77 (1H, bs, OH), 6.32 (1H, m, MalH), 3.78 (2H, t, $^3J_{HH}$ 7.3, CH_2), 2.66 (2H, t, $^3J_{HH}$ 7.3, CH_2), 2.06 (2H, d, $^3J_{HH}$ 1.9, CH_3); δ_C(75 MHz; $CDCl_3$) 176.7 (C, quat, C=O), 171.4 (C, quat, C=O), 170.5 (C, quat, C=O), 145.9 (C, quat, Mal), 127.5 (CH, Mal), 33.3 (CH_2), 32.6 (CH_2), 11.0 (CH_3); *m/z* (ES) 182.0456 ($M-H^+$ - $C_8H_8NO_4$ requires 182.0453), 110

(100%).

3-(4-*tert*-Butylbenzyloxy)pentanedioic acid 193

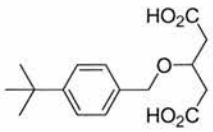

1 *M* aqueous NaOH (20 cm^3) was added to a solution of 3-(4-*tert*-butylbenzyloxy)pentanedioic acid diethyl ether (1.50 g, 4.30 mmol) in EtOH (25 cm^3) and the resulting reaction mixture was left to stir at room temperature for 16 hours. After this time, the reaction was quenched with 1 *M* aqueous HCl, the organic layer extracted with EtOAc (1 x 60 cm^3) and the combined organic extracts washed with brine (1 x 25 cm^3) and dried ($MgSO_4$). The solvent was then removed *in vacuo* to afford the crude product as a colourless solid, which was purified *via* recrystallisation from CH_2Cl_2/hexane to afford 3-(4-*tert*-butyl-benzyloxy)-petanedioic acid as a colourless solid (1.10 g, 87%); mp 108-110 °C (lit.,[246] 111-112 °C); (Found: C, 65.8; H, 7.8. $C_{16}H_{22}O_5$ requires C, 65.3; H, 7.5%); ν_{max}(film)/cm^{-1} ~2953vb (CO_2H), 1706 (C=O); δ_H(300 MHz; $CDCl_3$) 10.11 (2H, bs, 2 x OH), 7.29-7.26 (2H, m, Ar), 7.19-7.16 (2H, m, Ar), 4.51 (2H, s, CH_2), 4.28-4.19 (1H, m, alkyl), 2.73-2.57 (4H, m, 2 x CH_2), 1.22 (9H, s, *t*Bu); δ_C(75 MHz; $CDCl_3$) 177.4 (2 x C, quat, C=O), 151.4 (C, quat, Ar), 134.8 (C, quat, Ar), 128.2 (2 x CH, Ar), 125.8 (2 x CH, Ar), 72.4 (2 x CH_2), 72.3 (CH), 39.6 (CH_2), 34.9 (C, quat, *t*Bu), 31.7 (3 x CH_3, *t*Bu); *m/z* (ES) 293.1394 ($M\text{-}H^+$ - $C_{16}H_{21}O_5$ requires 293.1389).

Furan-2-yl-*N*-[6-(3-methylbutyrylamino)pyridin-2-yl]benzamides, General procedure

The appropriate iodo compound (1.0 eq.), 2- or 3-furyl boronic acid (1.5 eq.), palladium tetrakis (0.05 eq.) and lithium chloride (2.0 eq.) were dissolved in EtOH. A solution of 2 *M* aqueous $NaHCO_3$ (3.0 eq) was added, and the resulting solution stirred under an atmosphere of dry nitrogen at 90 °C for 15 hours. After this time, the reaction mixture was allowed to cool to room temperature and was subsequently washed with H_2O, 2 *M* aqueous $NaHCO_3$ and extracted with CH_2Cl_2. The combined organic extracts were then dried ($MgSO_4$) and the solvent removed *in vacuo* to yield the crude products as brown oils. These residual oils were purified *via* column chromatography to afford the desired products.

4-Furan-2-yl-*N*-[6-(3-methylbutyrylamino)pyridin-2-yl]benzamide 194

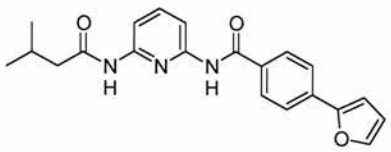

The general procedure outlined above was followed using 4-iodo-*N*-[6-(3-methylbutyrylamino)pyridin-2-yl]benzamide **200** (0.5 g, 1.20 mmol), 2-furyl boronic acid **203** (201 mg, 1.80 mmol), palladium tetrakis (69 mg, 0.06 mmol) and lithium chloride (102 mg, 2.40 mmol) in EtOH (25 cm^3). To this reaction mixture was added a solution of $NaHCO_3$ (302 mg, 3.60 mmol) in H_2O (2 cm^3). The resulting residual oil was purified *via* column chromatography (SiO_2, v/v 4:1 hexane:EtOAc) to afford **194** as a colourless solid (0.39 g, 89%); mp 208-210 °C; ν_{max}(film)/cm^{-1} 3307 (N-H), 2978 (C-H), 1673 (C=O), 1584, 1447 (C=C, Ar); δ_H(300 MHz; $CDCl_3$) 8.26 (1H, bs, NH), 8.07 (1H, d, $^3J_{H,H}$ 8.0, Ar), 8.00 (1H, d, $^3J_{H,H}$ 8.0, Ar), 7.93-7.89 (2H, m, Ar), 7.80-7.74 (3H, m, Ar), 7.62 (1H, bs, NH), 7.53 (1H, d, $^3J_{H,H}$ 1.6, FurylH), 6.80 (1H, d, $^3J_{H,H}$ 3.4, FurylH), 6.52 (1H, dd, $^3J_{H,H}$ 1.6, $^3J_{H,H}$ 3.4, FurylH), 2.27-2.17 (3H, m, CH_2, CH), 1.03 (6H, d, $^3J_{H,H}$ 6.4, 2 x CH_3); δ_C(75 MHz; $CDCl_3$) 171.4 (C, quat, C=O), 165.3 (C, quat, C=O), 153.0 (C, quat, Ar), 150.0 (2 x C, quat, Ar, Furyl), 143.6 (CH, Furyl), 141.4 (CH, Ar), 134.8 (C, quat, Ar), 132.7 (C, quat, Ar), 128.1 (2 x CH, Ar), 124.3 (2 x CH, Ar), 112.5 (CH, Furyl), 110.1 (CH, Ar), 110.0 (CH, Ar), 107.7 (CH, Furyl), 47.5 (CH_2), 26.6 (CH), 22.9 (2 x CH_3); *m/z* (ES) 386.1496 ($M+Na^+$ - $C_{21}H_{21}N_3O_3Na$ requires 386.1481), 364 ($M+H^+$, 55%).

3-Furan-2-yl -*N*-[6-(4-*tert*-butylbenzamino)pyridin-2-yl]benzamide 196

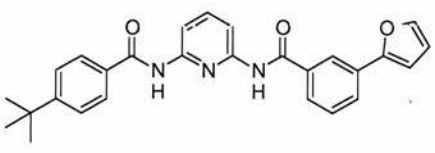

The general procedure outlined above was followed using, 3-iodo-*N*-[6-(4-*tert*-butylbenzamino)pyridin-2-yl]benzamide **207** (1.00 g, 2.00 mmol), 2-furyl boronic acid **203** (340 mg, 3.00 mmol), palladium tetrakis (120 mg, 0.10 mmol) and lithium chloride (170 mg, 4.00 mmol) in EtOH (50 cm^3). To this reaction mixture was added a solution of $NaHCO_3$ (500 mg, 6.00 mmol) in H_2O (4 cm^3). The resulting residual oil was purified *via* column

chromatography (SiO_2, v/v 4:1 hexane:EtOAc) to afford **196** as a colourless solid (0.69 g, 78%); ν_{max}(film)/cm^{-1} 3305 (N-H), 1676 (C=O), 1583, 1523 (C=C, Ar), 749 (C-H, furan); δ_H(300 MHz; $CDCl_3$) 8.50 (1H, bs, NH), 8.39 (1H, bs, NH), 8.20-8.19 (1H, m, Ar), 8.14-8.10 (2H, m, Ar), 7.92-7.74 (5H, m, Ar), 7.52-7.47 (4H, m, Ar), 6.77 (1H, d, $^3J_{H,H}$ 3.4, FurylH), 6.50 (1H, dd, $^3J_{H,H}$ 1.8, $^3J_{H,H}$ 3.4, FurylH), 1.35 (9H, s, *t*Bu); δ_C(75 MHz; $CDCl_3$) 165.8 (C, quat, C=O), 165.7 (C, quat, C=O), 156.5 (C, quat, Ar), 153.1 (C, quat, Furyl), 150.2 (C, quat, Ar), 150.0 (C, quat, Ar), 143.1 (CH, Furyl), 141.5 (CH, Ar), 135.1 (C, quat, Ar), 132.0 (C, quat, Ar), 131.5 (C, quat, Ar), 129.7 (2 x CH, Ar), 127.7 (2 x CH, Ar), 127.4 (CH, Ar), 126.2 (CH, Ar), 126.1 (CH, Ar), 122.9 (CH, Ar), 112.3 (CH, Furyl), 110.4 (CH, Ar), 110.2 (CH, Ar), 106.7 (CH, Furyl), 35.5 (C, quat, *t*Bu), 31.5 (*t*Bu); *m/z* (ES) 440.1981 ($M+H^+$ - $C_{27}H_{26}N_3O_3$ requires 440.1974).

2-(2,5-Dioxo-2,5-dihydropyrrol-1-yl)-*N*-(6-methylpyridin-2-yl)acetamide 195

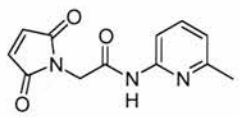

2-Amino-6-picoline (0.42 g, 3.66 mmol) was added to a stirring solution of crude acid fluoride **213**. The reaction mixture was then stirred at room temperature overnight. After this time, the reaction mixture was diluted with CH_2Cl_2 (15 cm^3) and brine (1 x 10 cm^3) added, the resulting organic layer was then dried ($MgSO_4$) and solvent removed *in vacuo*. The resulting crude yellow foam was purified *via* column chromatography (SiO_2, 1:1 v/v EtOAc:pet. ether) to afford the product as a colourless solid (0.57 g, 63%); mp 134-135 °C; υ_{max}(KBr)/cm^{-1} 3332 (N-H), 2945 (C-H), 1712 (C=O); δ_H(300 MHz; $CDCl_3$) 8.15 (1H, bs, NH), 7.92 (1H, d, $^3J_{H,H}$ 7.8, Ar), 7.59 (1H, dd, $^3J_{H,H}$ 7.8, $^3J_{H,H}$ 7.8, Ar), 6.92 (1H, d, $^3J_{H,H}$ 7.8, Ar), 6.83 (2H, s, 2 x CH, Mal), 4.36 (2H, bs, CH_2), 2.45 (3H, s, CH_3); δ_C(75 MHz; $CDCl_3$) 170.0 (2 x C, quat, C–O), 164.4 (C, quat, C=O), 156.8 (C, quat, Ar), 149.8 (C, quat, Ar), 138.9 (CH, Ar), 134.6 (2 x CH, Mal), 119.8 (CH, Ar), 111.1 (CH, Ar), 41.1 (CH_2), 23.9 (CH_3); *m/z* (ES) 246.0879 ($M+H^+$ - $C_{12}H_{12}N_3O_3$ requires 246.0885).

3-(2,5-Dioxo-2,5-dihydropyrrol-1-yl)-*N*-(6-methylpyridin-2-yl)propionamide 197

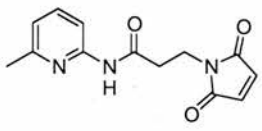

2-Amino-6-picoline (1.95 g, 18.1 mmol) was added to a stirred solution of crude acid fluoride **215**. The reaction mixture was then stirred at room temperature overnight. After this time, the reaction mixture was diluted with CH_2Cl_2 (25 cm^3) and brine (1 x 20 cm^3) added, the resulting organic layer was then dried ($MgSO_4$) and solvent removed *in vacuo*. The resulting crude yellow foam was purified *via* column chromatography (SiO_2, 1:1 v/v CH_2Cl_2:Et_2O) to afford the product as a colourless solid (2.56 g, 55%); mp 166-167 °C; (Found: C, 60.2; H, 4.8; N, 16.2. $C_{13}H_{13}N_3O_3$ requires C, 60.2; H, 5.05; N, 16.2%); υ_{max}(KBr)/cm^{-1} 3330 (N-H), 3073, 2948 (C-H), 1714 (C=O); δ_H(300 MHz; $CDCl_3$) 8.05 (1H, bs, NH), 7.97 (1H, d, $^3J_{HH}$ 7.8, Ar), 7.60 (1H, dd, $^3J_{HH}$ 7.8, $^3J_{HH}$ 7.8, Ar), 6.91 (1H, d, $^3J_{HH}$ 7.8, Ar), 6.71 (2H, s, 2 x CH, Mal), 3.87 (2H, t, $^3J_{HH}$ 7.1, CH_2), 2.67 (2H, t, $^3J_{HH}$ 7.1, CH_2), 2.39 (3H, s, CH_3); δ_C(75 MHz; $CDCl_3$) 170.8 (2 x C=O, quat), 168.5 (C=O, quat), 257.1 (CH, Ar), 134.7 (2 x CH, Mal), 119.9 (CH, Ar), 111.32 (CH, Ar), 36.0 (CH_2), 34.2 (CH_2), 24.3 (CH_3); *m/z* (ES) 260.1035 ($M+H^+$ - $C_{13}H_{14}N_3O_3$ requires 260.1035).

4-Iodo-*N*-[6-(3-methylbutyrylamino)pyridin-2-yl]benzamide 200

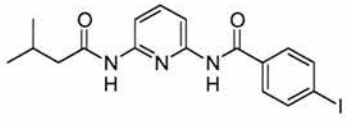

4-Iodobenzoyl chloride (4.14 g, 15.5 mmol) was added dropwise to a stirred solution of ***N***-(6-aminopyridin-2-yl)-3-methylbutyramide **129** (3.00 g, 15.5 mmol) in dry CH_2Cl_2 (70 cm^3) at 0 °C. The reaction mixture was subsequently stirred under nitrogen at room temperature for 15 hours. After this time, the solvent was removed *in vacuo* to afford a dark brown oil which was purified *via* flash column chromatography (SiO_2, 1:1 v/v EtOAc:hexane) to yield the product as a colourless solid (5.32 g, 81%); mp 168-169 °C; ν_{max}(film)/cm^{-1} 3305 (N-H), 1652 (C=O), 1581, 1516 (C=C, Ar); δ_H(300 MHz; $CDCl_3$) 8.18 (1H, bs, NH), 8.04 (1H, d, $^3J_{H,H}$ 7.9, Ar), 7.98 (1H, d, $^3J_{H,H}$ 7.9, Ar), 7.88-7.84 (2H, m, Ar), 7.77 (1H, dd, $^3J_{H,H}$ 7.9, $^3J_{H,H}$ 7.9,

Ar), 7.63-7.59 (2H, m, Ar), 7.57 (1H, bs, NH), 2.27-2.22 (3H, m, CH_2, CH), 1.03 (6H, d, $^3J_{H,H}$ 6.5, 2 x CH_3); δ_C(75 MHz; $CDCl_3$) 171.4 (C, quat, C=O), 165.1 (C, quat, C=O), 150.0 (C, quat, Ar), 149.7 (C, quat, Ar), 141.4 (CH, Ar), 138.5 (2 x CH, Ar), 133.9 (C, quat, Ar), 129.1 (2 x CH, Ar), 110.3 (CH, Ar), 110.1 (CH, Ar), 99.9 (C, quat, Ar), 47.5 (CH_2), 26.6 (CH), 22.9 (2 x CH_3); *m/z* (ES) 446.0349 ($M+H^+$ - $C_{17}H_{18}N_3O_2NaI$ requires 446.0341), 424 (M^+, 14%).

2-Furylboronic acid 203

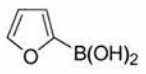

A 2.5 *M* solution of n-BuLi in hexane (30.0 cm^3, 75.0 mmol) was syringed dropwise into a cooled solution (-15 °C) of furan (8.0 cm^3, 125 mmol) in dry THF (30 cm^3) under a positive pressure of nitrogen. The reaction mixture was warmed to room temperature and stirred for 1 hour before the dropwise addition of trimethyl borate (8.58 cm^3, 75.0 mmol) at -78 °C. The solution was allowed to warm to room temperature and the reaction mixture was partitioned between Et_2O (1 x 125 cm^3) and 10 % aqueous HCl (1 x 125 cm^3). The ethereal extract was separated, washed with H_2O (1 x 50 cm^3) and dried ($MgSO_4$). After this time, the solvent was removed *in vacuo* and the resulting residue recrystallised from Et_2O/hexane (1:10) to afford 2-furylboronic acid as a pale yellow solid (4.04 g, 53%); mp 112–113 °C (lit.,[206] 110 °C); ν_{max}(film)/cm^{-1} 3310 (OH), 1577 (C=C, furan); δ_H(300 MHz; CD_3OD) 7.20 (1H, d, $^3J_{HH}$ 1.4, FurylH), 7.01 (1H, d, $^3J_{HH}$ 3.3, FurylH), 6.43 (1H, dd, $^3J_{HH}$ 1.4, $^3J_{HH}$ 3.3, FurylH); δ_C(75 MHz; CD_3OD) 148.9 (CH, Furyl), 125.1 (CH, Furyl), 111.9 (CH, Furyl); *m/z* (EI) 282 (3M–$3H_2O^+$, 100%), 188 (2M–$2H_2O^+$, 10), 112 (M^+, 8).

***N*-(6-Aminopyridin-2-yl)-4-*tert*-butylbenzamide 205**

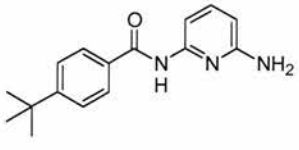

t-Butyl benzoyl chloride (4.18 cm^3, 21.4 mmol) was added dropwise to a stirred solution of 2,6-diaminopyridine (7.00 g, 64.1 mmol) in dry THF (200 cm^3) at 0 °C. The reaction mixture was subsequently stirred under nitrogen at room temperature for 15 hours. After this time, the reaction mixture was filtered under reduced pressure and the resulting filtrate dried ($MgSO_4$). The solvent was then removed *in vacuo* to afford a dark brown oil which was purified *via*

flash column chromatography (SiO_2, 1:1 v/v EtOAc:hexane) to afford the product as a pale yellow solid (5.70 g, 99%); mp 58-60 °C; ν_{max}(film)/cm^{-1} 3354 (N-H), 3216 (N-H), 2960 (C-H), 1665 (C=O); δ_H(300 MHz; $CDCl_3$) 8.25 (1H, bs, NH), 7.84-7.81 (2H, m, Ar), 7.72 (1H, d, $^3J_{H,H}$ 7.5, Ar), 7.52-7.47 (3H, m, Ar), 6.23 (1H, d, $^3J_{H,H}$ 7.5, Ar), 4.35 (2H, bs, NH_2), 1.34 (9H, s, *t*Bu); δ_C(75 MHz; $CDCl_3$) 165.7 (C, quat, C=O), 157.5 (C, quat, Ar), 156.0 (C, quat, Ar), 150.5 (C, quat, Ar), 140.6 (CH, Ar), 127.4 (4 x CH, Ar), 126.1 (C, quat, Ar), 104.8 (CH, Ar), 103.9 (CH, Ar), 35.4 (C, quat), 31.5 (*t*Bu); *m/z* (ES) 270.1607 ($M+H^+$ $C_{16}H_{20}N_3O$ requires 270.1606).

3-Iodo-*N*-[6-(4-*tert*-buylbenzamino)pyridin-2-yl]benzamide 207

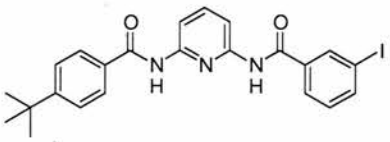

3-Iodo benzoyl chloride (1.07 cm^3, 7.4 mmol) was added dropwise to a stirred solution of *N*-(6-aminopyridin-2-yl)-4-*tert*-butylbenzamide (2.00 g, 7.40 mmol) in dry CH_2Cl_2 (50 cm^3) at 0 °C. The reaction mixture was subsequently stirred under nitrogen at room temperature for 15 hours. After this time, the solvent removed *in vacuo* to afford a dark brown oil which was purified *via* flash column chromatography (SiO_2, 1:1 v/v EtOAc:hexane) to afford the products as a colourless solid (2.83 g, 76%); mp 151-152 °C; (Found: C, 55.1, H, 4.5, N, 8.0. $C_{23}H_{22}IN_3O_2$ requires C, 55.3; H, 4.4; N, 8.4%); ν_{max}(film)/cm^{-1} 3253 (N-H), 2950 (C-H), 1682 (C=O); δ_H(300 MHz; $CDCl_3$) 8.24 (1H, bs, NH), 8.19-8.18 (2H, m, Ar), 8.08 (1H, d, $^3J_{H,H}$ 7.9, Ar), 8.01 (1H, d, $^3J_{H,H}$ 7.9, Ar), 7.86-7.73 (5H, m, Ar, NH), 7.48-7.43 (2H, m, Ar), 7.19 (1H, dd, $^3J_{H,H}$ 7.9, $^3J_{H,H}$ 7.9, Ar), 1.29 (9H, s, *t*Bu); δ_C(75 MHz; $CDCl_3$,) 165.4 (C, quat, C=O), 164.9 (C, quat, C=O), 156.1 (C, quat, Ar), 149.8 (C, quat, Ar), 149.3 (C, quat, Ar), 141.2 (2 x CH, Ar), 136.2 (CH, Ar), 136.1 (C, quat, Ar), 131.1 (C, quat, Ar), 130.5 (CH, Ar), 127.4 (2 x CH, Ar), 126.3 (CH, Ar), 125.9 (2 x CH, Ar), 110.2 (CH, Ar), 109.8 (CH, Ar), 94.5 (C, quat, Ar), 35.5 (C, quat, *t*Bu), 31.1 (*t*Bu); *m/z* (ES) 522.0655 ($M+Na^+$ - $C_{23}H_{22}IN_3O_2Na$ requires 522.0654), 500 ($M+H^+$, 100%).

2,2,2-Trichloroacetimidic acid *tert*-butyl benzyl ester 210

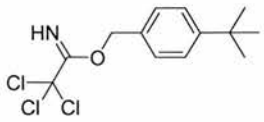

A solution of 4-*tert*-butylbenzylalcohol (4.70 cm^3, 26.4 mmol) in CH_2Cl_2 (40 cm^3) was cooled to –15 °C. To this solution was added a 50 % aqueous KOH (40 cm^3) and a catalytic amount of *tetra*-n-butylammonium hydrogen sulfate (120 mg, 0.40 mmol) was added. The resulting solution was stirred vigorously whilst maintaining this temperature for 15 minutes. After this time, trichloroacetonitrile (3.20 cm^3, 31.6 mmol) was added dropwise and the resulting reaction mixture left to stir at -15 °C for 30 minutes and then at room temperature for a further 30 minutes. The organic layer was then separated and the aqueous layer further extracted with CH_2Cl_2 (2 x 100 cm^3). The combined organic extracts were then dried ($MgSO_4$), before filtering through a short pad of Celite. The filtrate was reduced *in vacuo* to afford the crude product as yellow oil which was purified *via* flash column chromatography (SiO_2, v/v 2.5:1 hexane:CH_2Cl_2) to afford 2,2,2-trichloroacetimidic acid *tert*-butyl benzyl ester **210** as a colourless oil (7.81 g, 96%); ν_{max}(film)/cm^{-1} 2974 (NH), 1662 (C=NH), 1076 (R-O-R), 796 (C-Cl); δ_H(300 MHz; $CDCl_3$) 8.30 (1H, bs, NH), 7.44-7.35 (4H, m, Ar), 5.31 (2H, s, CH_2), 1.33 (9H, s, *t*Bu); δ_C(75 MHz; $CDCl_3$) 163.1 (C, quat, C=NH), 151.8 (C, quat, Ar), 132.9 (C, quat, Ar), 127.9 (2 x CH, Ar), 125.9 (2 x CH, Ar), 91.9 (C, quat, CCl_3), 71.1 (CH_2), 35.0 (C, quat, *t*Bu), 31.8 (3 x CH_3, *t*Bu); *m/z* (CI) 311 ($M+5H^+$, 28%), 309 ($M+3H^+$, 90), 307.0293 (M^+ - $C_{13}H_{16}NOCl_3$ requires 307.0297).

3-(4-*tert*-Butylbenzyloxy)pentanedioic acid diethyl ether 212

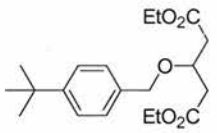

Boron trifluoride diethyl ether (0.25 cm^3, 1.37 mmol) was added to a solution of diethyl-3-hydroxyglutarate (1.60 cm^3, 13.0 mmol) and 2,2,2-trichloroacetimidic acid *t*-butyl benzyl ester (8.00 g, 26.1 mmol) in cyclohexane (100 cm^3). The resulting reaction mixture was left to stir at room temperature for 3 hours, after which time more cyclohexane (100 cm^3) was added. The reaction mixture was then filtered and washed with saturated aqueous $NaHCO_3$ (2

x 50 cm^3) and brine (1 x 100 cm^3). The combined organic extracts were dried ($MgSO_4$) and the solvent removed *in vacuo* to yield the crude product as a yellow oil, which was purified *via* column chromatography (SiO_2, v/v 15:1 hexane:EtOAc) to afford 3-(4-*tert*-butylbenzyloxy)pentanedioic acid diethyl ether **212** as a colourless oil (1.85 g, 92%); ν_{max}(film)/cm^{-1} 1733 (C=O), 1194 and 1149 (R-O-R); δ_H(300 MHz; $CDCl_3$) 7.29-7.26 (2H, m, Ar), 7.18-7.15 (2H, m, Ar), 4.48 (2H, s, CH_2), 4.30-4.22 (1H, m, CH), 4.10-4.03 (4H, m, 2 x CH_2), 2.64-2.48 (4H, m, CH_2), 1.22 (9H, s, *t*Bu), 1.17 (6H, m, $^3J_{H,H}$ 7.2, 2 x CH_3); δ_C(75 MHz; $CDCl_3$) 171.4 (2 x C, quat, C=O), 151.1 (C, quat, Ar), 135.4 (C, quat, Ar), 128.1 (2 x CH, Ar), 125.7 (2 x CH, Ar), 73.2 (CH_2), 72.4 (CH), 61.0 (2 x CH_2), 40.2 (2 x CH_2), 34.9 (C, quat, *t*Bu), 31.7 (3 x CH_3, *t*Bu), 14.6 (2 x CH_3); *m/z* (CI) 351.2166 ($M+H^+$ - $C_{20}H_{31}O_5$ requires 351.2171), 350 (M^+, 11%), 349 (35), 335 (100).

(2,5-Dioxo-2,5-dihydropyrrol-1-yl)acetyl fluoride 213

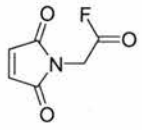

Cyanuric fluoride (0.19 cm^3, 2.30 mmol) was added dropwise to a stirring solution of (2,5-dioxo-2,5-dihydropyrrol-1-yl)acetic acid **125** (0.60 g, 3.90 mmol) in dry CH_3CN (8 cm^3) at -3 °C. The reaction mixture was then stirred for 5 minutes at -3 °C and subsequently warmed to room temperature for 2 minutes. The reaction mixture was then partitioned between CH_2Cl_2 (15 cm^3) and brine (1 x 10 cm^3), dried ($MgSO_4$) and solvent removed reduced *in vacuo* to 5 cm^3. The crude acid fluoride was reacted on to the next stage without further purification; δ_F(282.3 MHz; $CDCl_3$) +30.8 (1F, s, COF).

3-(2,5-Dioxo-2,5-dihydropyrrol-1-yl)propionyl fluoride 215

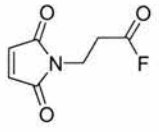

Cyanuric fluoride (0.92 cm^3, 10.8 mmol) was added dropwise to a stirring solution of 3-(2,5-dioxo-2,5-dihydropyrrol-1-yl)propionic acid **126** (3.00 g, 18.1 mmol) in dry CH_3CN (30 cm^3) at -3 °C. The reaction mixture was then stirred for 5 minutes at -3 °C and subsequently

warmed to room temperature for 2 minutes. The reaction mixture was then partitioned between CH_2Cl_2 (15 cm^3) and brine (1 x 10 cm^3), dried ($MgSO_4$) and solvent removed reduced *in vacuo* to 10 cm^3. The resulting crude acid fluoride was reacted on to the next stage without further purification; δ_F(282.3 MHz; $CDCl_3$) +30.7 (1F, s, COF).

Furan-3-yl-*N*-[6-(3-methylbutyrylamino)pyridin-2-yl]benzamides, General procedure

The appropriate iodo compound (1.0 eq.), 2- or 3-furyl boronic acid (1.5 eq.), palladium tetrakis (0.05 eq.) and lithium chloride (2.0 eq.) were dissolved in EtOH. A solution of 2 *M* aqueous $NaHCO_3$ (3.0 eq) was added, and the resulting solution stirred under an atmosphere of dry nitrogen at 90 °C for 15 hours. After this time, the reaction mixture was allowed to cool to room temperature and was subsequently washed with H_2O, 2 *M* aqueous $NaHCO_3$ and extracted with CH_2Cl_2. The combined organic extracts were then dried ($MgSO_4$) and the solvent removed *in vacuo* to yield the crude products as brown oils. These residual oils were purified *via* column chromatography to afford the desired products.

4-Furan-3-yl-*N*-[6-(3-methylbutyrylamino)pyridin-2-yl]benzamide 216

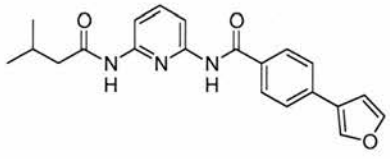

The general procedure outlined above was followed using, 4-iodo-*N*-[6-(3-methylbutyrylamino)pyridin-2-yl]benzamide **200** (1.00 g, 2.40 mmol), 3-furyl boronic acid **221** (403 mg, 3.6 mmol), palladium tetrakis (139 mg, 0.10 mmol) and lithium chloride (203 mg, 4.8 mmol) in EtOH (50 cm^3). To this reaction mixture was added a solution of $NaHCO_3$ (605 mg, 7.2 mmol) in H_2O (4 cm^3). The resulting residual oil was purified *via* column chromatography (SiO_2, 4:1 v/v hexane:EtOAc) to afford 4-furan-3-yl-*N*-[6-(3-methylbutyrylamino)pyridin-2-yl]benzamide as a colourless solid (0.64 g, 74%); mp 188-190 °C; ν_{max}(film)/cm^{-1} 3294 (N-H), 1668 (C=O), 1608, 1583 (C=C, Ar), 764, 749 (C-H, Furyl); δ_H(300 MHz; $CDCl_3$) 8.27 (1H, bs, NH), 8.08 (1H, d, $^3J_{H,H}$ 8.0, Ar), 7.97 (1H, d, $^3J_{H,H}$ 8.0, Ar), 7.92-7.88 (2H, m, Ar), 7.83 (1H, dd, $^4J_{H,H}$ 0.9, $^4J_{H,H}$ 1.3, FurylH), 7.77 (1H, dd, $^3J_{H,H}$ 8.0, $^3J_{H,H}$ 8.0, Ar), 7.63-7.59 (3H, m, NH, 2 x Ar), 7.52 (1H, dd, $^4J_{H,H}$ 1.3, $^3J_{H,H}$ 1.7, FurylH), 6.75 (1H, dd, $^4J_{H,H}$ 0.9, $^3J_{H,H}$ 1.7, FurylH), 2.53-2.28 (3H, m, CH_2, CH), 1.03 (6H, d, $^3J_{H,H}$ 6.5, 2 x CH_3);

δ_C(75 MHz; $CDCl_3$) 171.4 (C, quat, C=O), 165.4 (C, quat, C=O), 149.0 (2 x C, quat, Ar), 144.6 (CH, Furyl), 141.4 (CH, Ar), 139.9 (CH, Furyl), 136.9 (C, quat, Ar), 132.7 (C, quat, Ar), 128.2 (2 x CH, Ar), 126.4 (2 x CH, Ar), 125.8 (C, quat, Furyl), 110.1 (CH, Ar), 110.0 (CH, Ar), 109.0 (CH, Furyl), 47.5 (CH_2), 26.6 (CH), 22.9 (2 x CH_3); *m/z* (ES) 364.1659 ($M+H^+$ - $C_{21}H_{22}N_3O_3$ requires 364.1661).

3-Furan-3-yl -*N*-[6-(4-*tert*-butylbenzamino)pyridin-2-yl]benzamide 217

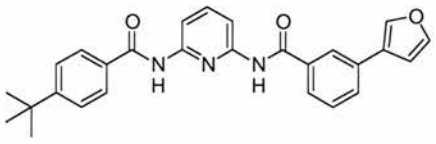

The general procedure outlined above was followed using 3-iodo-*N*-[6-(4-*tert*-buylbenzamino)pyridin-2-yl]benzamide **207** (0.50 g, 1.00 mmol), 3-furyl boronic acid **221** (168 mg, 1.50 mmol), palladium tetrakis (58 mg, 0.05 mmol) and lithium chloride (85 mg, 2.00 mmol) in EtOH (25 cm^3). To this reaction mixture was added a solution of $NaHCO_3$ (252 mg, 3.00 mmol) in H_2O (2 cm^3). The resulting residual oil was purified *via* column chromatography (SiO_2, v/v 4:1 hexane:EtOAc) to afford **217** as a colourless solid (380 mg, 86%); mp 128-130 °C; ν_{max}(film)/cm^{-1} 3326 (N-H), 2962 (C-H), 1672 (C=O), 1607, 1583 (Ar, C=C), 738 (C-H, furyl); δ_H(300 MHz; $CDCl_3$) 8.35-8.32 (2H, bs, 2 x NH), 8.16-8.11 (2H, m, Ar), 8.05-8.04 (1H, m, Ar), 7.87-7.81 (4H, m, Ar), 7.78-7.75 (1H, m, FurylH), 7.71-7.68 (1H, m, FurylH), 7.54-7.49 (4H, m, Ar), 6.70 (1H, dd, $^4J_{H,H}$ 0.9, $^4J_{H,H}$ 1.0, FurylH), 1.29 (9H, s, *t*Bu); δ_C(75 MHz; $CDCl_3$) 165.4 (2 x C, quat, C=O), 156.1 (C, quat, Ar), 149.8 (C, quat, Ar), 149.6 (C, quat, Ar), 144.1 (CH, Furyl), 141.2 (CH, Ar), 139.1 (CH, Furyl), 134.8 (C, quat, Ar), 133.5 (C, quat, Ar) 131.1 (C, quat, Ar), 129.6 (CH, Ar), 129.3 (CH, Ar), 127.0 (2 x CH, Ar), 125.9 (2 x CH, Ar), 125.2 (C, quat, Furyl), 124.9 (CH, Ar), 124.9 (CH, Ar), 110.0 (CH, Ar), 109.8 (CH, Ar), 108.7 (CH, Furyl), 35.1 (C, quat, *t*Bu), 31.1 (3 x CH_3, *t*Bu); *m/z* (ES) 440.1973 ($M+H^+$ - $C_{27}H_{26}N_3O_3$ requires 440.1974).

exo-N-(6-(4-_tert_-butylbenzamino)pyridin-2-yl]-3-{4-[6-methylpyridin-2-ylcarbamoyl) ethyl-3,5-dioxo-10-oxa-4-aza-tricyclo[5.2.1.$0^{2,6}$]dec-8-en-8-yl 218

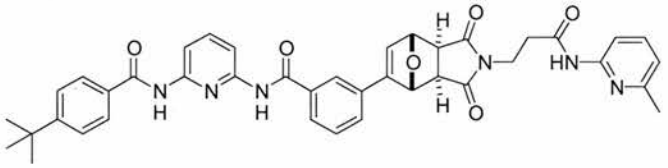

Yellow oil; υ_{max}(film)/cm^{-1} 3340 (N-H), 1702 (C=O), 1579 (C=CH), 1197, 1145 (R-O-R, bridgehead); δ_H(300 MHz; TCE) 8.47 (1H, bs, NH), 8.37 (1H, bs, NH), 8.03-7.42 (15H, m, 14 x Ar, NH), 6.67-6.66 (1H, m, alkene), 5.61-5.60 (1H, m, bridgeheadH), 5.34-5.32 (1H, m, bridgeheadH), 3.82 (2H, t, $^3J_{HH}$ 6.9, CH_2), 2.97 (2H, dd, $^3J_{HH}$ 6.5, $^3J_{HH}$ 4.6, CH), 2.66 (2H, t, $^3J_{HH}$ 6.9, CH_2), 2.37 (3H, s, CH_3), 1.27 (9H, s, *t*Bu); δ_C(75 MHz; TCE) 176.1 (C, quat, C=O), 175.7 (C, quat, C=O), 170.6 (C, quat, C=O), 168.8 (C, quat, C=O), 165.7 (C, quat, C=O), 165.0 (C, quat, Ar), 156.4 (C, quat, Ar), 150.0 (C, quat, alkene), 149.9 (C, quat, Ar), 148.7 (C, quat, Ar), 141.1 (CH, Ar), 139.8 (CH, Ar), 135.0 (C, quat, Ar), 134.3 (CH, alkene), 132. 6 (C, quat, Ar), 131.5 (C, quat, Ar), 131.0 (C, quat, Ar), 129.7 (CH, Ar), 129.2 (CH, Ar), 129.2 (CH, Ar), 129.0 (2 x CH, Ar), 127.5 (2 x CH, Ar), 126.0 (CH, Ar), 124.8 (CH, Ar), 119.8 (CH, Ar), 111.4 (CH, Ar), 110.0 (CH, Ar), 109.9 (CH, Ar), 82.7 (CH), 81.6 (CH), 49.1 (CH, bridgehead), 47.5 (CH, bridgehead), 35.6 (C, quat, *t*Bu), 35.1 (CH_2), 33.8 (CH_2), 31.2 (3 x CH_3, *t*Bu), 23.6 (CH_3); *m/z* (ES) 721.2731 ($M+Na^+$ - $C_{40}H_{38}N_6O_6Na$ requires 712.2716), 699 (100%).

3-Furylboronic acid 221

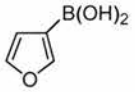

A 2.5 *M* solution of n-BuLi in hexane (13.60 cm^3, 34.0 mmol) was added dropwise to a cooled solution (-78 °C) of 3-bromofuran (5.00 g, 34.0 mmol) in dry THF (50 cm^3) under a positive pressure of nitrogen. The reaction mixture was stirred at -78 °C for 1 hour before adding dropwise a solution of trimethylborate (3.9 cm^3, 34.0 mmol) in dry THF (50 cm^3). Once the addition complete, the solution was stirred at -40 °C for 3 hours and warmed to room temperature overnight. The reaction mixture was partitioned between Et_2O (1 x 100 cm^3) and 10 % aqueous HCl (1 x 120 cm^3). The ethereal extract was separated, washed with

H_2O (1 x 50 cm^3) and dried ($MgSO_4$). Removal of the solvent under reduced pressure followed by recrystallisation from Et_2O/hexane (1:10) afforded 3-furylboronic acid as a brown solid (1.53 g, 46%); Decomp >120 °C (lit.,[206] 126-128 °C); ν_{max}(film)/cm^{-1} 3311 (O-H), 1574 (C=C, Ar); δ_H(300 MHz; CD_3OD) 7.72 (1H, dd, $^4J_{HH}$ 1.1, $^4J_{HH}$ 1.5, FurylH), 7.47 (1H, dd, $^4J_{HH}$ 1.5, $^3J_{HH}$ 1.8, FurylH), 6.53 (1H, dd, $^4J_{HH}$ 1.1, $^3J_{HH}$ 1.8, FurylH); δ_C(75 MHz; CD_3OD) 152.5 (CH, Furyl), 144.7 (CH, Furyl), 115.9 (CH, Furyl); *m/z* (ES) 282 (3M–$3H_2O^+$, 100%), 188 (M–$2H_2O^+$, 32), 112 (M^+, 10).

exo-N-[6-(3-Methylbutyrylamino)pyridin-2-yl]-4-{4-[(6-methylpyridin-2-ylcarbamoyl) methyl]-3,5-dioxo-10-oxa-4-aza-tricyclo[5.2.1.$0^{2,6}$]de-yl}benzamide 222

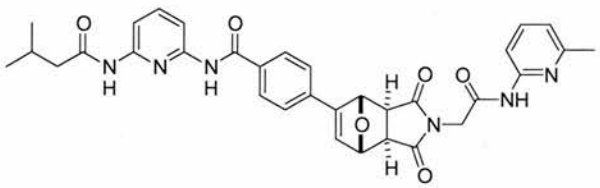

Yellow oil; υ_{max}(thin film)/cm^{-1} 3250 (N-H), 1702 (C=O), 1581 (C=CH), 1201, 1146 (R-O-R, bridgehead); δ_H(300 MHz; TCE) 8.35 (1H, bs, NH), 8.26 (1H, bs, NH), 7.97-7.42 (8H, m, Ar), 6.90-6.87 (2H, m, Ar), 6.75-6.74 (1H, m, alkene), 5.61-5.59 (1H, m, bridgeheadH), 5.46-5.43 (1H, m, bridgeheadH), 4.31 (2H, s, CH_2), 3.11 (2H, dd, $^3J_{HH}$ 14.5, $^3J_{HH}$ 6.5, CH), 2.39 (3H, s, CH_3), 2.20-2.07 (3H, m, CH_2, CH), 0.94 (6H, d, $^3J_{HH}$ 6.2, 2 x CH_3); δ_C(75 MHz; TCE) 175.6 (C, quat, C=O), 175.4 (C, quat, C=O), 171.5 (C, quat, C=O), 170.4 (C, quat, C=O), 165.0 (C, quat, C=O), 156.3 (C, quat, Ar), 156.1 (C, quat, Ar), 155.8 (C, quat, alkene), 149.8 (C, quat, Ar), 149.5 (C, quat, Ar), 148.6 (C, quat, Ar), 141.1 (CH, Ar), 139.8 (CH, Ar), 134.7 (CH, alkene), 134.3 (C, quat, Ar), 128.2 (2 x CH, Ar), 126.0 (2 x CH, Ar), 120.3 (CH, Ar), 111.4 (CH, Ar), 110.0 (CH, Ar), 109.8 (CH, Ar), 82.7 (CH), 81.6 (CH), 49.5 (CH, bridgehead), 48.0 (CH, bridgehead), 47.1 (CH_2), 42.3 (CH_2), 26.2 (CH_3), 23.5 (CH), 22.7 (2 x CH_3); *m/z* (ES) 631.2296 ($M+Na^+$ - $C_{33}H_{32}N_6O_6Na$ requires 631.2281), 609 (86%).

exo-N-[6-(3-Methylbutyrylamino)pyridin-2-yl]-4-{4-[2-(6-methylpyridin-2-ylcarbamoyl)ethyl]-3,5-dioxo-10-oxa-4-aza-tricyclo[5.2.1.0]^{2,6}dec-8-en-8-yl}benzamide 225

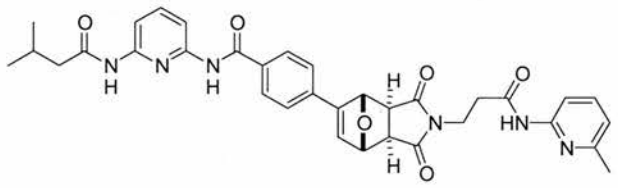

Yellow oil; υ_{max}(film)/cm^{-1} 3286 (N-H), 1697 (C=O), 1581 (C=CH), 1201, 1147 (R-O-R, bridgehead); δ_H(300 MHz; TCE) 8.55 (1H, bs, NH), 8.39 (1H, bs, NH), 7.97-7.37 (8H, m, 7 x Ar, NH), 6.87-6.83 (2H, m, Ar), 6.70-6.68 (1H, m, alkene), 5.54-5.53 (1H, m, bridgeheadH), 5.42-5.40 (1H, m, bridgeheadH), 3.83 (2H, t, $^3J_{HH}$ 6.5, CH_2), 2.98 (2H, dd, $^3J_{HH}$ 15.4, $^3J_{HH}$ 6.5, 2 x CH), 2.65 (2H, t, $^3J_{HH}$ 6.5, CH_2), 2.37 (3H, s, CH_3), 2.23-2.05 (3H, m, CH_2, CH), 0.95 (6H, d, $^3J_{HH}$ 6.4, 2 x CH_3); δ_C(75 MHz; TCE) 175.9 (C, quat, C=O), 175.8 (C, quat, C=O), 171.4 (C, quat, C=O), 168.7 (C, quat, C=O), 164.9 (C, quat, C=O), 156.3 (C, quat, Ar), 156.0 (C, quat, Ar), 150.0 (C, quat, alkene), 149.8 (C, quat, Ar), 149.5 (C, quat, Ar), 148.5 (C, quat, Ar), 141.0 (CH, Ar), 139.7 (CH, Ar), 134.4 (C, quat, Ar), 134.3 (CH, alkene), 127.8 (2 x CH, Ar), 125.9 (2 x CH, Ar), 119.8 (CH, Ar), 111.3 (CH, Ar), 109.9 (CH, Ar), 109.7 (CH, Ar), 82.7 (CH), 81.6 (CH), 49.1 (CH, bridgehead), 47.5 (CH, bridgehead), 47.0 (CH_2), 35.1 (CH_2), 35.0 (CH_2), 26.2 (CH_3), 23.6 (CH), 22.7 (2 x CH_3); *m/z* (ES) 631.2296 ($M+Na^+$ - $C_{33}H_{32}N_6O_6Na$ requires 631.2281), 609 (86%).

exo-N-(6-(4-_tert_-Butylbenzamino)pyridin-2-yl]-3-{4-[6-methylpyridin-2-yl carbamoyl)methyl-3,5-dioxo-10-oxa-4-aza-tricyclo[5.2.1.0^{2,6}]dec-8-en-8-yl 226

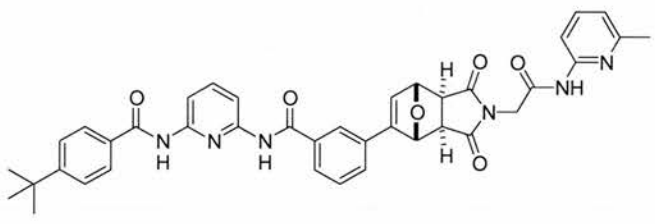

Yellow oil; υ_{max}(film)/cm^{-1} 3264 (N-H), 1706 (C=O), 1447 (C=CH), 1199, 1146 (R-O-R, bridgehead); δ_H(300 MHz; TCE) 8.48 (1H, bs, NH), 8.39 (1H, bs, NH), 8.03-7.42 (15H, m, 14 x Ar, NH), 6.88-6.86 (1H, m, alkene), 5.65-5.64 (1H, m, bridgeheadH), 5.39-5.37 (1H, m, bridgeheadH), 4.30 (2H, bs, CH_2), 3.09 (2H, dd, $^3J_{HH}$ 6.5, $^3J_{HH}$ 3.1, 2 x CH), 2.39 (3H, s,

CH_3), 1.28 (9H, s, 3 x CH_3); δ_C(75 MHz; TCE) 175.7 (C, quat, C=O), 175.3 (C, quat, C=O), 170.3 (C, quat, C=O), 165.7 (C, quat, C=O), 165.1 (C, quat, C=O), 156.6 (C, quat, Ar), 150.0 (C, quat, alkene), 149.7 (C, quat, Ar), 149.6 (C, quat, Ar), 149.5 (C, quat, Ar), 141.1 (C, quat, Ar), 139.8 (CH, Ar), 135.0 (C, quat, Ar), 134.6 (CH, alkene), 131.5 (C, quat, Ar), 131.0 (C, quat, Ar), 129.8 (CH, Ar), 129.4 (CH, Ar), 127.3 (CH, Ar), 127.2 (2 x CH, Ar), 126.0 (2 x CH, Ar), 124.8 (CH, Ar), 120.2 (CH, Ar), 111.4 (CH, Ar), 110.0 (CH, Ar), 109.8 (CH, Ar), 82.7 (CH), 81.6 (CH), 49.5 (CH, bridgehead), 47.9 (CH, bridgehead), 41.0 (CH_2), 35.1 (C, quat, *t*Bu), 31.2 (3 x CH_3, *t*Bu), 23.6 (CH_3); *m/z* (ES) 707.2584 ($M+Na^+$ - $C_{39}H_{36}N_6O_6Na$ requires 707.2594), 685 (17%).

[5-(3-Carboxymethyl-3H-[1,2,3]triazol-4-ylmethyldisulfanylmethyl)[1,2,3]triazol-1-yl] acetic acid 249

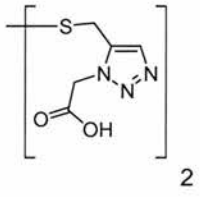

(5-Mercaptomethyl-[1,2,3]triazol-1-yl)acetic acid *tert*-butyl ester **283** (50 mg, 0.11 mmol) was refluxed in 10% formic acid (2 cm^3) for 30 minutes. On cooling, the reaction mixture was partitioned between CH_2Cl_2 (8 cm^3) and H_2O (10 cm^3). The water layer was then acidified with 1 *M* HCl until a pH of ~1-2 was obtained and the product was then extracted with CH_2Cl_2 (10 cm^3), the organic phase dried ($MgSO_4$) and concentrated *in vacuo* to yield the product as a colourless solid (33 mg, 88%); mp 108-109 °C; δ_H(300 MHz; $CDCl_3$) 8.00 (2H, s, 2 x triazole), 5.23 (4H, s, 2 x CH_2), 3.97 (4H, s, 2 x CH_2); δ_C(75 MHz; $CDCl_3$) 169.3 (2 x C, quat, C=O), 144.0 (2 x C, quat, triazole), 125.5 (2 x CH, triazole), 51.9 (2 x CH_2), 33.9 (2 x CH_2); *m/z* (ES) 343.0286 ($M+H^+$ - $C_{10}H_{11}N_6O_4S_2$ requires 343.0283).

5-Bromofuran-3-carboxylic acid 252

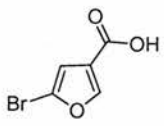

N-Bromosuccinimide (14.25 g, 127 mmol) was added with stirring to a solution of 3-furan

carboxylic acid (10.00 g, 84.8 mmol) in AcOH (70 cm^3) at room temperature. The reaction mixture was stirred for 48 hours, before the solvent was removed *in vacuo*. On addition of Et_2O excess *N*-bromosuccinimide precipitated from solution and was filtered under reduced pressure. The resulting filtrate was concentrated *in vacuo* and subsequently triturated with H_2O, the resulting solid was filtered under reduced pressure and recrystallised from H_2O to yield the product as a yellow solid (4.80 g, 30%); mp 133–134 °C (lit.,[240] 136.0 °C); (Found: C, 31.45; H, 1.4. $C_5H_3BrO_3$ requires C, 31.4; H, 1.6%); υ_{max}(film)/cm^{-1} 2978 (O-H), 1688 (C=O), 636, 501 (C-H, Furyl); δ_H(300 MHz; $CDCl_3$) 8.06 (1H, d, $^4J_{HH}$ 1.0, FurylH), 6.69 (1H, d, $^4J_{HH}$ 1.0, FurylH); δ_C(75 MHz; $CDCl_3$) 167.7 (C, quat, C=O), 150.3 (CH, Furyl), 124.8 (C, quat, Furyl), 121.5 (C, quat, Furyl), 111.8 (CH, Furyl); *m/z* (CI) 193 ($M+2H^+$, 100%), 191 (M^+, 100).

(5-Bromofuran-3-yl)methanol 253

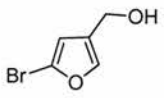

A solution of 5-bromo-3-furan carboxylic acid (1.00 g, 5.20 mmol) in dry Et_2O (50 cm^3) was added dropwise to a stirring solution of lithium aluminium hydride (180 mg, 4.80 mmol) in dry Et_2O (50 cm^3) at -20 °C. The reaction mixture was stirred under a positive pressure of nitrogen for 10 minutes. After this time, the reaction mixture was partitioned between 2 *M* aqueous NaOH (1 x 70 cm^3), the organic layer then washed with brine (1 x 30 cm^3), dried ($MgSO_4$) and solvent removed *in vacuo* to yield the product as a colourless oil which was reacted on without further purification (310 mg, 36%); δ_H(300 MHz; $CDCl_3$) 7.34-7.32 (1H, m, FurylH), 6.30-6.29 (1H, m, FurylH), 4.45 (2H, s, CH_2), 1.60 (1H, bs, OH).

(5- Bromofuran-3-ylmethoxy)*tert*-butyldimethylsilane 254

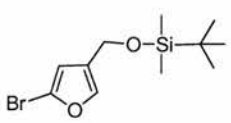

A solution of *tert*-butyldimethylsilyl chloride (0.65 g, 4.30 mmol) in dry CH_2Cl_2 (5 cm^3) was added dropwise to a stirred solution of 5-bromo-3-furyl methanol (0.70 g, 3.90 mmol) and imidazole (0.59 g , 8.70 mmol) in dry CH_2Cl_2 (25 cm^3) at 0 °C over a 30 minute period. The

reaction mixture was then stirred for a further 10 minutes at 0 °C and then warmed to room temperature over 15 hours. After this time, the reaction mixture was the partitioned between CH_2Cl_2 and saturated aqueous $NaHCO_3$ (1 x 10 cm^3) and H_2O (2 x 10 cm^3), the resulting organic phases combined, dried ($MgSO_4$) and the solvent removed *in vacuo*. The resulting crude yellow oil was purified using column chromatography (SiO_2, pet. ether) to afford the desired product as a colourless oil (0.61 g, 53%); δ_H(300 MHz; $CDCl_3$) 7.33-7.31 (1H, m, FurylH), 6.26 (1H, d, $^4J_{HH}$ 1.0, FurylH), 4.50 (2H, s, CH_2), 0.91 (9H, s, *t*Bu), 0.08 (6H, s, 2 x CH_2); δ_C(75 MHz; $CDCl_3$) 141.1 (CH, Furyl), 129.0 (C, quat, Furyl), 122.7 (C, quat, Furyl), 111.5 (CH, Furyl), 57.6 (CH_2), 26.2 (3 x CH_3, *t*Bu), 18.7 (C, quat, *t*Bu), 0.0 (2 x CH_3); *m/z* 179 (M-TBDMS+2H^+, 100%), 177 (M^+, 100%).

_N_-(5-Bromopyridin-2-yl)-3-methylbutyramide 260

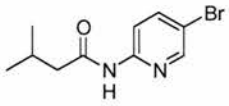

Isovaleryl chloride (10.1 cm^3, 82.9 mmol) was added dropwise at 0 °C to a stirred solution of 2-amino-5-bromopyridine (21.52 g, 124 mmol) in dry CH_2Cl_2 (500 cm^3) under a positive pressure of nitrogen. The reaction mixture was subsequently stirred at room temperature for 15 hours. After this time, the reaction mixture was filtered under reduced pressure and the solvent removed *in vacuo* to afford a dark brown oil which was purified *via* flash column chromatography (SiO_2, 1:1 v/v EtOAc:hexane) to yield the product as a colourless solid (15.62 g, 73%); mp 98-100 °C; (Found: C, 46.8; H, 5.2; N, 10.9. $C_{10}H_{13}N_2O$ requires C, 46.7; H, 5.1; N, 10.9%); υ_{max}(film)/cm^{-1} 3222 (N-H), 2950 (C-H), 1653 (C=O), 1567, 1520 (C=C, Ar); δ_H(300 MHz; $CDCl_3$), 11.76 (1H, bs, NH), 8.66 (1H, d, $^3J_{HH}$ 7.0, Ar), 8.29 (1H, d, $^4J_{HH}$ 2.2, Ar), 8.21 (1H, dd, $^3J_{HH}$ 7.0, $^4J_{HH}$ 2.2, Ar), 2.48 (2H, d, $^3J_{HH}$ 7.2, CH_2), 2.34-2.20 (1H, m, CH), 1.02 (6H, d, $^3J_{HH}$ 6.6, 2 x CH_3); δ_C(75 MHz; $CDCl_3$) 171.6 (C, quat, C=O), 150.4 (C, quat, Ar), 148.7 (CH, Ar), 141.4 (CH, Ar), 115.7 (CH, Ar), 114.8 (C, quat, Ar), 47.4 (CH_2), 26.5 (CH), 22.8 (2 x CH_3); *m/z* (CI) 259 (M+2H^+, 100%), 257 (M^+, 97).

_N_-[5-(3-Hydroxyprop-1-ynyl)pyridin-2-yl]-3-methylbutyramide 262

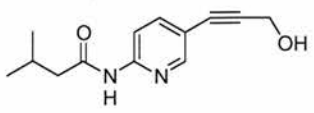

Triphenylphosphine (200 mg, 0.70 mmol), palladium(II)bistriphenylphosphine dichloride (270 mg, 0.4 mmol) and copper(I)iodide (70 mg, 0.40 mmol) were added to a stirred degassed solution of *N*-(5-bromopyridin-2-yl)-3-methylbutyramide **260** (2.00 g, 7.80 mmol) in triethylamine (20 cm^3). After addition, the reaction mixture was degassed further, warmed to dissolve solids at 60 °C and then cooled to room temperature before dropwise addition of propargyl alcohol (0.99 cm^3, 17.1 mmol) over a 30 minute period. The reaction mixture was then refluxed for 4 hours. After this time, the reaction mixture was cooled, filtered at reduced pressure and solvent removed *in vacuo*. The resulting oil was partitioned between CH_2Cl_2 (1 x 20 cm^3) and 2 *M* aqueous HCl (1 x 10 cm^3), the organic phase washed with H_2O (2 x 10 cm^3), then dried ($MgSO_4$) and solvent removed *in vacuo*. The resulting crude brown oil was purified using column chromatography (SiO_2, 1:1 v/v EtOAc:hexane) to afford the product as a colourless solid (1.68 g, 93%); mp 133-135 °C; δ_H(300 MHz; $CDCl_3$) 8.27 (1H, d, $^4J_{HH}$ 2.0, Ar), 8.15 (1H, d, $^3J_{HH}$ 7.6, Ar), 7.95 (1H, bs, NH), 7.66 (1H, dd, $^3J_{HH}$ 7.6, $^4J_{HH}$ 2.0, Ar), 4.44 (2H, s, CH_2), 2.21-2.09 (3H, m, CH_2, CH), 0.95 (6H, d, $^3J_{HH}$ 6.5, 2 x CH_3); δ_C(75 MHz; $CDCl_3$) 171.7 (C, quat, C=O), 150.9 (CH, Ar), 150.8 (C, quat, Ar), 141.6 (CH, Ar), 115.7 (C, quat, Ar), 113.6 (CH, Ar), 90.2 (C, quat, arene), 82.6 (C, quat, arene), 51.8 (CH_2), 47.4 (CH_2), 26.5 (CH), 22.8 (2 x CH_3), *m/z* (ES) 233.1282 ($M+H^+$ $C_{13}H_{17}N_2O_2$ requires 233.1290).

1-Azido-4-*tert*-butyl benzene 265

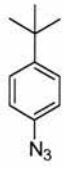

tert-Butyl aniline (7.5 cm^3, 46.9 mmol) was added dropwise to a stirred solution of 10 *M* HCl (45 cm^3) and H_2O (60 cm^3) at -5 °C and the pH measured to ensure a pH of 1. A solution of sodium nitrite (3.24 g, 46.9 mmol) in H_2O (25 cm^3) was then added dropwise ensuring the temperature did not rise above -5 °C and the reaction mixture stirred for 30 minutes in order

to facilitate the formation of intermediate diazonium salt. A solution of sodium azide (3.05 g, 46.9 mmol) in H_2O (25 cm^3) was then added dropwise at -5 °C and the reaction mixture stirred for 30 minutes and subsequently at room temperature for a further 60 minutes. After this time, the reaction mixture was diluted with CH_2Cl_2 (2 x 75 cm^3) the organic phases combined, partitioned with water (2 x 25 cm^3), dried ($MgSO_4$) and solvent removed *in vacuo* to yield the crude azide which was reacted on without further purification; δ_H(300 MHz; $CDCl_3$) 7.40-7.35 (2H, m, 2 x Ar), 6.99-6.95 (2H, m, 2 x Ar), 1.35 (9H, s, *t*Bu); δ_C(75 MHz; $CDCl_3$) 148.5 (C, quat, Ar), 137.5 (C, quat, Ar), 127.1 (2 x CH, Ar), 119.0 (2 x CH, Ar), 34.9 (C, quat, *t*Bu), 31.7 (3 x CH_3, *t*Bu).

_N_-{5-3-/5-1-(4-*tert*-Butylbenzyl)-5-hydroxymethyl-3*H*-[1,2,3]triazole-4-yl]pyridin-2-yl}3-methyl butyramide

268

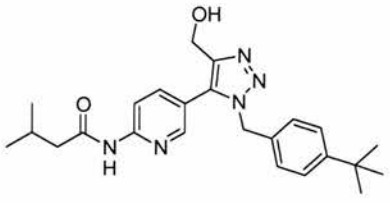

269

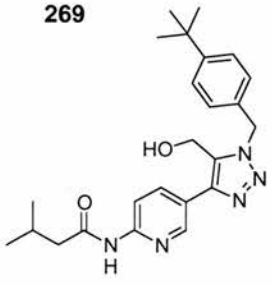

A solution of *N*-[5-(3-hydroxyprop-1-ynyl)pyridin-2-yl]-3-methyl butyramide **262** (0.60 g, 2.30 mmol) and 1-azidomethyl-4-*tert*-butyl benzene **265** (440 mg, 2.30 mmol) in toluene (1.0 cm^3) was stirred and refluxed under a positive pressure of nitrogen for 16 hours. After this time, solvent was removed *in vacuo* to afford a dark brown oil which was purified *via* flash column chromatography (SiO_2, 1:1 v/v EtOAc:hexane) to yield the product regioisomers as colourless solids (**268**, 500.00 mg; **269**, 480.00 mg; quant. yield);

268 - mp 184-185 °C; υ_{max}(film)/cm^{-1} 3400 (O-H), 3212 (N-H), 2987 (C-H), 1698 (C=O), 1591, 1576 (C=C, Ar); δ_H(300 MHz; $CDCl_3$) 8.32 (1H, d, $^3J_{HH}$ 7.4, Ar), 8.18-8.17 (2H, m, NH, Ar), 7.56 (1H, dd, $^3J_{HH}$ 7.4, $^4J_{HH}$ 2.3, Ar), 7.33-7.28 (2H, m, Ar), 7.05-7.01 (2H, m, Ar), 5.43 (2H, s, CH_2), 4.67 (2H, s, CH_2), 2.34-2.17 (3H, m, CH_2, CH), 1.28 (9H, s, *t*Bu), 1.04 (6H, d, $^3J_{HH}$ 6.4, 2 x CH_3); δ_C(75 MHz; $CDCl_3$) 172.1 (C, quat, C=O), 152.6 (C, quat, Ar), 152.0 (C, quat, Ar), 148.6 (CH, Ar), 146.1 (C, quat, triazole), 140.0 (CH, Ar), 132.9 (C, quat, triazole), 132.3 (C, quat, Ar), 127.4 (2 x CH, Ar), 126.5 (2 x CH, Ar), 118.8 (C, quat, Ar), 114.1 (CH, Ar), 55.9 (CH_2), 52.8 (C, quat, *t*Butyl), 52.4 (CH_2), 47.4 (CH_2), 31.6 (CH_3, *t*Bu),

26.6 (CH), 22.9 (2 x CH_3); *m/z* (ES) 420 ($M\text{-}H^+$, 100%).

269 - mp 206-207 °C; υ_{max}(film)/cm^{-1} 3413 (O-H), 3217 (N=NH), 2952 (C-H), 1672 (C=O), 1586, 1538 (C=C, Ar); δ_H(300 MHz; $CDCl_3$) 8.59 (1H, d, $^4J_{HH}$ 2.0, Ar), 8.28 (1H, d, $^3J_{HH}$ 7.6, Ar), 8.02 (1H, dd, $^3J_{HH}$ 7.6, $^4J_{HH}$ 2.0, Ar), 7.98 (1H, bs, NH), 7.42-7.38 (2H, m, Ar), 7.27-7.23 (2H, m, Ar), 5.68 (2H, s, CH_2), 4.69 (2H, s, CH_2), 2.28-2.17 (3H, m, CH_2, CH), 2.0 (1H, bs, OH), 1.30 (9H, s, *t*Bu), 1.02 (6H, d, $^3J_{HH}$ 6.4, 2 x CH_3); δ_C(75 MHz; $CDCl_3$) 171.6 (C, quat, C=O), 151.9 (C, quat, Ar), 150.8 (C, quat, Ar), 146.2 (CH, Ar), 143.2 (C, quat, triazole), 137.7 (CH, Ar), 132.1 (C, quat, triazole), 131.7 (C, quat, Ar), 127.4 (2 x CH, Ar), 126.1 (2 x CH, Ar), 123.0 (C, quat, Ar), 113.9 (CH, Ar), 52.4 (2 x CH_2), 47.0 (CH_2), 34.6 (C, quat, *t*Bu), 31.2 (*t*Bu), 26.1 (CH), 22.5 (2 x CH_3); *m/z* (ES) 420 ($M\text{-}H^+$, 100%), 362 (50).

1-Azidomethyl-4-*tert*-butyl benzene 271

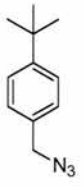

Sodium azide (11.45 g, 176 mmol) was added to a stirred solution of 4-(*tert*-butyl)benzyl bromide (8.10 cm^3, 44.0 mmol) in acetone (200 cm^3) the resulting reaction mixture was refluxed for 18 hours. After this time, the solvent was removed *in vacuo* to yield the product as a yellow oil which was reacted on to the next stage without further purification; δ_H(300 MHz; $CDCl_3$) 7.36-7.31 (2H, m, 2 x Ar), 7.20-7.16 (2H, m, 2 x Ar), 4.23 (2H, s, CH_2), 1.25 (9H, s, *t*Bu); δ_C(75 MHz; $CDCl_3$) 151.8 (C, quat, Ar), 132.8 (C, quat, Ar), 128.4 (2 x CH, Ar), 126.2 (2 x CH, Ar), 54.9 (CH_2), 36.0 (C, quat, *t*Bu), 31.7 (3 x CH_3, *t*Bu).

***N*-[6-(5-Mercaptomethyl-4*H*-[1,2,3]triazole-4-yl)pyridin-2-yl]-3-methyl butyramide 273**

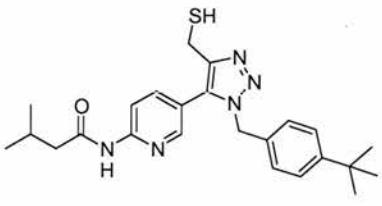

Carbon tetrachloride (0.087 cm^3, 0.9 mmol) was added dropwise to a stirred solution of *N*-{5-[3-(4-*tert*-butylbenzyl)-5-hydroxymethyl-3*H*-[1,2,3]triazole-4-yl]pyridin-2-yl}-3-methyl

butyramide **268** (250 mg, 0.60 mmol) and tri-butyl phosphine (0.29 cm^3, 1.20 mmol) in acetone (5.0 cm^3). The reaction mixture was stirred for 30 minutes at room temperature. After this time, the reaction mixture was partitioned between CH_2Cl_2 (1 x 10 cm^3) and brine (1 x 5 cm^3) the organic phase dried ($MgSO_4$) and solvent removed *in vacuo*. Thiourea (50 mg, 0.7 mmol) was then added to a stirred solution of the crude chloride in acetone (5 cm^3) and the reaction mixture refluxed for 2 hours. After this time, the mixture was allowed to cool at -18 °C for 16 hours. On subsequent addition of hexane the thiourea intermediate precipitated from solution, the resulting solid was filtered under reduced pressure. Sodium metabisulfite (220 mg, 1.2 mmol) was then added to the thiourea intermediate in water (5 cm^3) and the reaction mixture refluxed for 5 minutes. After this time, the reaction mixture was cooled to room temperature and CH_2Cl_2 (1 x 15 cm^3) added, the organic phase was then washed with H_2O (1 x 10 cm^3), dried ($MgSO_4$) and solvent removed *in vacuo*. The resulting yellow oil was recrystallised from hexane to yield the product as a yellow solid (85 mg, 33%); δ_H(300 MHz; $CDCl_3$) 8.33 (1H, d, $^3J_{HH}$ 7.0, Ar), 8.17 (1H, bs, NH), 8.14-8.12 (1H, m, Ar), 7.52 (1H, dd, $^3J_{HH}$ 7.0, $^4J_{HH}$ 2.3, Ar), 7.33-7.27 (2H, m, Ar), 7.04-6.96 (2H, m, Ar), 5.38 (2H, s, CH_2), 4.67 (2H, d, $^3J_{HS}$ 7.7, CH_2SH), 2.34-2.17 (3H, m, CH_2, CH), 2.00 (1H, t, $^3J_{HS}$ 7.7, SH), 1.28 (9H, s, *t*Bu), 1.04 (6H, d, $^3J_{HH}$ 6.4, 2 x CH_3); δ_C(75 MHz; $CDCl_3$) 171.5 (C, quat, C=O), 152.0 (C, quat, Ar), 151.7 (C, quat, Ar), 147.8 (CH, Ar), 145.9 (C, quat, triazole), 140.0 (CH, Ar), 131.9 (C, quat, triazole), 130.9 (C, quat, Ar), 127.2 (2 x CH, Ar), 125.9 (2 x CH, Ar), 118.7 (C, quat, Ar), 113.7 (CH, Ar), 52.3 (CH_2), 47.1 (CH_2), 34.6 (C, quat, *t*Bu), 31.2 (3 x CH_3, *t*Bu), 26.2 (CH), 22.5 (2 x CH_3), 18.6 (CH_2); *m/z* (ES) 437.2233 (M^+ - $C_{24}H_{31}N_5OS$ requires 437.2243), 147 (53%), 83 (100%).

Azido acetic acid *tert*-butyl ester 275

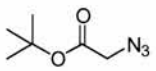

Sodium Azide (4.99 g, 76.9 mmol) was added to a stirred solution of *tert*-butyl bromoacetate (8.27 ml, 51.3 mmol) in acetone (200 cm^3). The reaction mixture was refluxed for 8 hours, the reaction mixture filtered under reduced pressure and the solvent removed *in vacuo*. The product was carried through to the next stage without further purification; δ_H(300 MHz; $CDCl_3$) 3.72 (2H, s, CH_2), 1.48 (9H, s, *t*Bu).

(3-/4-Hydroxymethyl-[1,2,3]triazole-1-yl)acetic acid *tert*-butyl ester

276 **277**

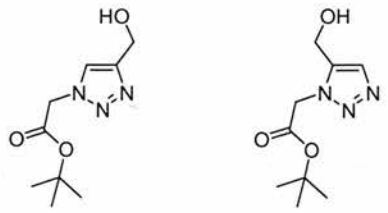

Azido acetic acid *tert*-butyl ester **275** (22.00 g, 140 mmol) in propargyl alcohol (24.4 cm^3, 420 mmol) was stirred and heated to 90 °C under a positive pressure of nitrogen for 16 hours. After this time, solvent was removed *in vacuo* to afford a dark brown oil which was purified *via* flash column chromatography (SiO_2, 4:1 v/v EtOAc:hexane) to yield the product regioisomers as colourless solids (**276** - 10.39 g, **277** - 10.84 g, overall yield, 71%);

276 – mp 106 °C–107 °C; (Found: C, 50.9; H, 7.2; N, 19.8. $C_9H_{15}N_3O_3$ requires C, 50.7; H, 7.1; N, 19.7%); υ_{max}(film)/cm^{-1} 3340 (O-H), 2972 (C-H), 1740 (C=O), 1369 (O-C-H); δ_H(300 MHz; $CDCl_3$) 7.65 (1H, s, Ar), 5.04 (2H, s, CH_2), 4.78 (2H, s, CH_2), 2.71 (1H, bs, OH), 1.47 (9H, s, *t*Bu); δ_C(75 MHz; $CDCl_3$) 165.7 (C, quat, C=O), 148.5 (C, quat, Ar), 123.6 (CH, Ar), 84.3 (C, quat, *t*Bu), 56.8 (CH_2), 51.9 (CH_2), 28.4 (*t*Bu); *m/z* (CI) 214 ($M+H^+$, 100%), 200 (10), 158 (25).

277 – mp 71–72 °C; (Found: C, 50.6; H, 7.3; N, 19.8. $C_9H_{15}N_3O_3$ requires C, 50.7; H, 7.1; N, 19.7%); υ_{max} (film)/cm^{-1} 3343 (O-H), 2975 (C-H), 1741 (C=O), 1367 (O-C-H); δ_H(300 MHz; $CDCl_3$) 7.56 (1H, s, Ar), 5.15 (2H, s, CH_2), 4.72 (2H, s, CH_2), 2.62 (1H, bs, OH), 1.47 (9H, s, *t*Bu); δ_C(75 MHz; $CDCl_3$) 166.5 (C, quat, C=O), 137.3 (C, quat, Ar), 133.3 (CH, Ar), 84.4 (C, quat, *t*Bu), 53.7 (CH_2), 50.7 (CH_2), 28.3 (*t*Bu); *m/z* (CI) 214 ($M+H^+$, 100%), 158 (19).

(4-Acetylsulfanylmethyl-[1,2,3]triazole-1-yl)acetic acid *tert*-butyl ester 279

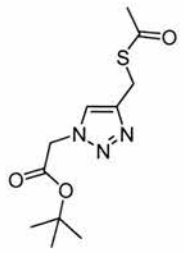

Carbon tetrachloride (0.25 cm^3, 2.60 mmol) and tributyl phosphine (0.64 cm^3, 2.60 mmol) were added to a stirred solution of potassium thioacetate (0.80 g, 7.00 mmol) and 18-crown-6 (190 mg, 0.70 mmol) in dry CH_3CN (30 cm^3). A solution of 4-hydroxymethyl-[1,2,3]triazole-1-yl)acetic acid *tert*-butyl ester **276** (0.50 g, 2.30 mmol) in dry CH_3CN (10 cm^3) was the added dropwise at 0 °C. The reaction mixture was allowed to reach room temperature over 16 hours. After this time, the reaction mixture was partitioned between CH_2Cl_2 and saturated aqueous $NaHCO_3$ (2 x 20 cm^3), dried ($MgSO_4$) and solvent removed *in vacuo*. The resulting red solid was purified using column chromatography (SiO_2, 1:1 v/v hexane:EtOAc) to afford the product as a yellow solid (357 mg, 57%); mp sublimes > 65 °C; υ_{max}(film)/cm^{-1} 3153 (N=N), 2979, 2943 (C-H), 1740 (C=O); δ_H(300 MHz; $CDCl_3$) 7.73 (1H, s, triazoleH), 5.16 (2H, s, CH_2), 5.15 (2H, s, CH_2), 2.07 (3H, s, CH_3), 1.47 (9H, s, *t*Bu); δ_C(75 MHz; $CDCl_3$) 170.9 (C, quat, C=O), 165.7 (C, quat, C=O), 135.2 (CH, triazole), 133.0 (C, quat, triazole), 84.3 (C, quat, *t*Bu), 54.1 (CH_2), 50.6 (CH_2), 28.3 (3 x CH_3, *t*Bu), 20.9 (CH_3), *m/z* (ES) 278 ($M+Na-O^+$, 100%), 222 (86).

(5-Mercaptomethyl-[1,2,3]triazol-1-yl)acetic acid *tert*-butyl ester 283

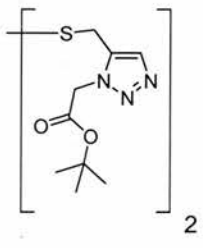

Carbon tetrachloride (0.96 cm^3) was added dropwise to a stirred solution of 3-hydroxymethyl-[1,2,3]triazole-1-yl)acetic acid *tert*-butyl ester **276** (1.40 g, 6.60 mmol) and tri-butyl

phosphine (3.27 cm^3, 13.2 mmol) in acetone (15 cm^3). The reaction mixture was stirred for 30 minutes at room temperature. After this time, the reaction mixture was partitioned between CH_2Cl_2 (1 x 15 cm^3) and brine (1 x 7 $cm^{3)}$ the organic phase dried ($MgSO_4$) and solvent removed *in vacuo*. Thiourea (0.50 g, 6.60 mmol) was then added to a stirred solution of the crude chloride in acetone (10 cm^3) and the reaction mixture refluxed for 2 hours. After this time, the mixture was allowed to cool at -18 °C for 16 hours. On subsequent addition of hexane, the thiourea intermediate precipitated from solution, this solid was filtered under reduced pressure. Sodium metabisulfite (2.49 g, 13.2 mmol) was then added to the thiourea intermediate in H_2O (10 cm^3) and the reaction mixture refluxed for 5 minutes. After this time, the reaction mixture was cooled to room temperature and CH_2Cl_2 (1 x 25 cm^3) added, the organic phase was then washed with H_2O (1 x 15 cm^3), dried ($MgSO_4$) and solvent removed *in vacuo*. The resulting yellow oil was reacted on to the next stage without further purification; δ_H(300 MHz; $CDCl_3$) 7.73 (2H, s, 2 x triazole), 5.16 (4H, s, 2 x CH_2), 5.15 (4H, s, 2 x CH_2), 1.47 (18H, s, 2 x *t*Bu); *m/z* (ES) 455 ($M\text{-}H^+$, 100%).

3-Furan-3-yl-*N*-(6-methylpyridin-2-yl)propionamide 284

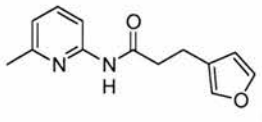

2-Amino-6-picoline (2.32 g, 21.4 mmol) was added to a stirring solution of crude acid fluoride **303** (0.67 eq.). The reaction mixture was stirred at room temperature overnight. After this time, the reaction mixture was diluted with CH_2Cl_2 (30 cm^3) and brine (1 x 15 cm^3) added, the resulting organic layer was then dried ($MgSO_4$) and solvent removed *in vacuo*. The resulting crude solid was purified *via* column chromatography (SiO_2, 5:1 v/v hexane:EtOAc) to afford the product as a colourless solid (2.34 g, 71%); mp 123-124 °C; ν_{max}(film)/cm^{-1} 3270 (N-H), 2921 (C-H), 1678 (C=O), 1601, 1576 (C=C, Ar); δ_H(300 MHz; $CDCl_3$) 8.19 (1H, bs, NH), 8.0 (1H, d, $^3J_{H,H}$ 7.8, Ar), 7.86 (1H, dd, $^3J_{H,H}$ 7.8, $^3J_{H,H}$ 7.8, Ar), 7.33 (1H, t, $^3J_{H,H}$ 1.8, FurylH), 7.25-7.24 (1H, m, FurylH), 6.87 (1H, d, $^3J_{H,H}$ 7.8, Ar), 6.26-6.25 (1H, m, FurylH), 2.85 (2H, t, $^3J_{H,H}$ 7.5, CH_2), 2.66 (2H, t, $^3J_{H,H}$ 7.5, CH_2), 2.41 (3H, s, CH_3); δ_C(75 MHz; $CDCl_3$) 171.0 (C, quat, C=O), 157.1 (C, quat, Ar), 150.9 (C, quat, Ar), 143.4 (CH, Furyl), 139.5 (CH, Ar), 139.2 (CH, Furyl), 123.8 (C, quat, Furyl), 119.7 (CH, Furyl), 111.3 (CH, Ar), 111.2 (CH, Ar), 38.5 (CH_2), 24.3 (CH_3), 20.9 (CH_2), *m/z* (ES) 231.1134 ($M+H^+$ - $C_{13}H_{15}N_2O_2$ requires 231.1134), 213 (37%).

[3-(Furan-3-ylmethoxy)phenoxy]acetic acid 285

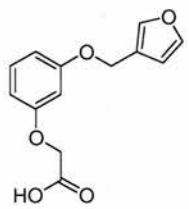

[3-(Furan-3-ylmethoxy)phenoxy]acetic acid ethyl ester **299** (0.67 g, 2.43 mmol) was added to a stirred solution of 1 *M* KOH (1:1 THF:H_2O, 20 cm^3) the reaction mixture was refluxed for 1 hour. After this time, the reaction mixture was cooled to room temperature and acidified to pH 1 with 1 *M* aqueous HCl. The organic phase was then extracted with CH_2Cl_2 (1 x 75 cm^3), dried ($MgSO_4$), and solvent removed *in vacuo* to yield the product as a colourless solid (420 mg, 70%); mp 112-113 °C; (Found: C, 63.0; H, 5.0. $C_{13}H_{12}O_5$ requires C, 62.9; H, 4.9%); ν_{max}(film)/cm^{-1} 1702 (C=O), 1159 (R-O-R), 760 (C-H, Furyl); δ_H(300 MHz; $CDCl_3$) 7.51-7.50 (1H, m, FurylH), 7.44-7.43 (1H, m, FurylH), 7.21 (1H, m, Ar), 6.66-6.62 (1H, m, Ar), 6.58-6.51 (2H, m, Ar), 6.49-6.48 (1H, m, FurylH), 4.91 (2H, s, CH_2), 4.67 (2H, s, CH_2); δ_C(75 MHz; $CDCl_3$) 174.1 (C, quat, C=O), 160.3 (C, quat, Ar), 158.9 (C, quat, Ar), 144.0 (CH, Furyl), 141.3 (CH, Furyl), 130.6 (CH, Ar), 121.5 (C, quat, Furyl), 110.6 (CH, Ar), 108.9 (CH, Ar), 107.3 (CH, Ar), 102.5 (CH, Furyl), 65.2 (CH_2), 62.3 (CH_2); *m/z* (ES) 271.0578 ($M+Na^+$ - $C_{13}H_{12}O_5$ Na requires 271.0582).

***exo-N*-(6-Methylpyridin-2-yl)-3-{4-[(6-methylpyridin-2-ylcarbamoyl)methyl]-3,5-dioxo-10-oxa-4-aza-tricyclo[5.2.1.$0^{2,6}$]dec-8-en-8-yl} 286**

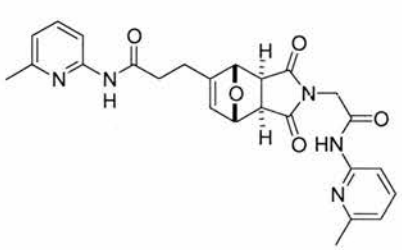

Yellow oil; υ_{max}(film)/cm^{-1} 3308 (N-H), 1701 (C=O), 1577 (C=CH), 1179, 1163 (R-O-R, bridgehead); δ_H(300 MHz; DMSO-d_6) 10.76 (1H, bs, NH), 10.46 (1H, bs, NH), 7.89 (1H, d, $^3J_{HH}$ 8.0, Ar), 7.78 (1H, d, $^3J_{HH}$ 8.0, Ar), 7.68-7.61 (2H, m, 2 x Ar), 6.99-6.92 (2H, m, 2 x Ar), 6.13-6.10 (1H, m, alkene), 5.10-5.08 (1H, m, bridgehead), 5.06-5.05 (1H, m, bridgehead),

4.24 (2H, bs, CH_2), 3.10 (2H, dd, $^3J_{HH}$ 28.2, $^3J_{HH}$ 6.5, CH), 2.63-2.49 (4H, m, 2 x CH_2), 2.41 (3H, s, CH_3), 2.39 (3H, s, CH_3); δ_C(75 MHz; DMSO-d_6) 176.0 (C, quat, C=O), 175.9 (C, quat, C=O), 171.1 (C, quat, C=O), 164.7 (C, quat, C=O), 156.6 (C, quat, Ar), 156.3 (C, quat, Ar), 151.3 (C, quat, alkene), 150.8 (C, quat, Ar), 150.4 (C, quat, Ar), 138.6 (CH, Ar), 138.4 (CH, alkene), 128.9 (CH, Ar), 118.9 (CH, Ar), 118.4 (CH, Ar), 110.3 (CH, Ar), 110.2 (CH, Ar), 82.2 (CH), 81.0 (CH), 48.9 (CH, bridgehead), 46.8 (CH, bridgehead), 41.0 (CH_2), 33.63 (CH_2), 23.48 (2 x CH_3), 22.32 (CH_2); *m/z* (ES) 476.1932 ($M+H^+$ - $C_{25}H_{26}N_5O_5$ requires 476.1934), 246 (100%), 231 (33).

exo-[8-(3-Carboxymethoxyphenoxymethyl)-2,6-dimethyl-3,5-dioxo-10-oxa-4-aza-tricyclo[5.2.1.0^{2,6}]dec-8-en-4-yl]acetic acid 287

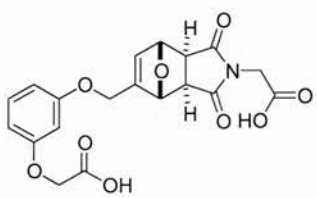

Colourless solid; mp 130-132 °C; υ_{max}(KBr)/cm^{-1} ~3000 (O-H), 2932 (C-H), 1718 (C=O), 1603 (C=CH), 1181, 1156 (R-O-R, bridgehead); δ_H(300 MHz; DMSO-d_6) 7.22-7.13 (1H, m, ArH), 6.63-6.44 (4H, m, ArH, alkeneH), 5.20-5.25 (1H, m, bridgeheadH), 5.15-5.13 (1H, m, bridgeheadH), 4.84 (2H, s, CH_2), 4.65 (2H, s, CH_2), 4.07 (2H, s, CH_2), 3.19 (2H, dd, $^3J_{HH}$ 26.0, $^3J_{HH}$ 6.6, CH); δ_H(75 MHz; DMSO-d_6) 175.6 (C, quat, C=O), 175.5 (C, quat, C=O), 170.1 (C, quat, C=O), 168.0 (C, quat, C=O), 159.2 (C, quat, Ar), 158.9 (C, quat, alkene), 146.7 (C, quat, Ar), 131.9 (CH, alkene), 130.0 (CH, Ar), 107.3 (CH, Ar), 107.1 (CH, Ar), 101.5 (CH, Ar), 64.5 (CH_2), 63.0 (CH_2), 81.0 (CH), 80.6 (CH), 41.1 (CH_2), 48.3 (CH, bridgehead), 46.8 (CH, bridgehead); *m/z* (ES) 402.0825 ($M-H^+$ - $C_{19}H_{16}NO_9$ requires 402.0825).

exo-(3-{2,6-Dimethyl-4-[(6-methylpyridin-2-ylcarbamoyl)methyl]-3,5-dioxo-10-oxa-4-aza-tricyclo[5.2.1.$0^{2,6}$]dec-8-en-ylmethoxy}phenoxy)acetic acid 288

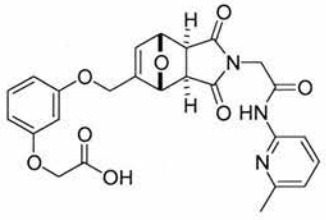

Colourless solid; mp 190-191 °C; υ_{max}(KBr)/cm^{-1} 3219 (N-H), 3081 (O-H), 2937 (C-H), 1718 (C=O), 1596 (C=CH), 1183, 1156 (R-O-R, bridgehead); δ_H(300 MHz; DMSO-d_6) 10.69 (1H, bs, NH), 7.76 (1H, d, $^3J_{HH}$ 7.8, Ar), 7.65 (1H, t, $^3J_{HH}$ 7.7, Ar), 7.19 (1H, dd, $^3J_{HH}$ 7.8, $^3J_{HH}$ 7.8, Ar), 6.98 (1H, d, $^3J_{HH}$ 7.8, Ar), 6.59-6.57 (1H, m, Ar), 6.54-6.50 (2H, m, Ar), 6.46-6.45 (1H, m, CH-alkene), 5.19-5.18 (1H, m, bridgeheadH), 5.14-5.13 (1H, m, bridgeheadH), 4.85 (2H, s, CH_2), 4.64 (2H, s, CH_2), 4.25 (2H, s, CH_2), 3.25 (1H, d, $^3J_{HH}$ 6.6, CH), 3.14 (1H, d, $^3J_{HH}$ 7.8, CH), 2.41 (3H, s, CH_3); δ_C(75 MHz; DMSO-d_6) 175.9 (C, quat, C=O), 175 (C, quat, C=O), 170.1 (C, quat, C=O), 164.7 (C, quat, C=O), 159.1 (C, quat, Ar), 158.9 (C, quat, alkene), 156.5 (C, quat, Ar), 150.8 (C, quat, Ar), 146.6 (C, quat, Ar), 138.6 (CH, Ar), 131.9 (CH, alkene), 130.0 (CH, Ar), 118.9 (CH, Ar), 110.3 (CH, Ar), 107.3 (CH, Ar), 107.2 (CH, Ar), 101.5 (CH, Ar), 81.1 (CH), 80.6 (CH), 64.5 (CH_2), 63.0 (CH_2), 48.4 (CH, bridgehead), 46.9 (CH, bridgehead), 41.1 (CH_2), 23.5 (CH_3); *m/z* (ES) 492.1407 ($M\text{-}H^+$ - $C_{25}H_{22}N_3O_8$ requires 492.1407), 247 (90%).

(3-Hydroxyphenoxy)acetic acid _tert_-butyl ester 291

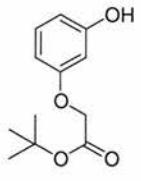

Resorcinol (5.00 g, 45.4 mmol) was added to a suspension of potassium carbonate (9.40 g, 68.1 mmol) in dry CH_3CN (150 cm^3) which had been degassed by bubbling a fast stream of nitrogen through it. The reaction mixture was then heated to 80 °C in order to dissolve the solids, cooled, before dropwise addition *tert*-butyl bromoacetate (2.36 cm^3, 21.3 mmol). The

reaction mixture was then refluxed under nitrogen for 48 hours. After this time, the reaction mixture was filtered and the filtrate reduced *in vacuo*. The resulting oil was taken up in CH_2Cl_2 (1 x 150 cm^3) washed with 1 M aqueous HCl (1 x 75 cm^3), the organic layer washed with H_2O (1 x 50 cm^3), dried ($MgSO_4$) and solvent removed *in vacuo*. The resulting colourless oil was purified *via* column chromatography (SiO_2, 10:1 v/v hexane:EtOAc) to afford the product as a yellow oil (3.10 g, 70%); ν_{max}(film)/cm^{-1}3360 (O-H), 1722 (C=O), 1579, 1478 (C=C, Ar), 1142 and 1175 (R-O-R); δ_H(300 MHz; $CDCl_3$) 7.14-7.08 (1H, m, Ar), 6.48-6.42 (3H, m, Ar), 5.54 (1H, bs, OH), 4.49 (2H, s, CH_2), 1.49 (9H, s, *t*Bu); δ_C(75 MHz; $CDCl_3$) 168.8 (C, quat, C=O), 159.5 (C, quat, Ar), 157.4 (C, quat, Ar), 130.5 (CH, Ar), 109.3 (CH, Ar), 106.6 (CH, Ar), 103.0 (CH, Ar), 83.1 (C, quat, *t*Bu), 66.1 (CH_2), 28.4 (3 x CH_3, *t*Bu); *m/z* (ES) 223.0966 ($M\text{-}H^+$ - $C_{12}H_{15}O_4$ requires 223.0966).

[3-(Furan-3-ylmethoxy)phenoxyl]acetic acid *tert*-butyl ester 292

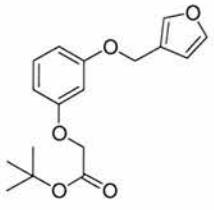

(3-Hydroxy-phenoxy)acetic acid *tert*-butyl ester **291** (1.00 mg, 4.76 mmol) was added to a suspension of potassium carbonate (1.97 g, 14.3 mmol) in dry CH_3CN (20 cm^3) which had been degassed by bubbling a fast stream of nitrogen through it. The reaction mixture was then heated to 80 °C in order to dissolve the solids, cooled, before dropwise addition of crude freshly prepared **141** (1.5 eq.). The reaction mixture was then refluxed under nitrogen for 48 hours. After this time, the reaction mixture was filtered and the filtrate reduced *in vacuo*. The resulting oil was taken up in CH_2Cl_2 (1 x 50 cm^3) washed with 1 *M* aqueous HCl (1 x 30 cm^3), the organic layer washed with H_2O (1 x 20 cm^3), dried ($MgSO_4$) and solvent removed *in vacuo*. The resulting colourless oil was purified *via* column chromatography (SiO_2, 10:1 v/v hexane:EtOAc) to afford the product as a yellow oil (1.14 g, 79%); ν_{max}(film)/cm^{-1} 1725 (C=O), 1197, 1153 (R-O-R); δ_H(300 MHz; $CDCl_3$) 7.50-7.49 (1H, m, Furyl), 7.44-7.42 (1H, m, Furyl), 7.20-7.15 (1H, m, Ar), 6.55-6.48 (4H, m, 3 x Ar, Furyl), 4.90 (2H, s, CH_2), 4.45 (2H, s, CH_2), 1.49 (9H, s, *t*Bu); δ_C(75 MHz; $CDCl_3$) 168.3 (C, quat, C=O), 160.2 (C, quat, Ar), 159.5 (C, quat, Ar), 143.9 (CH, Furyl), 141.2 (CH, Furyl), 130.3 (CH, Ar), 121.6 (C, quat, Furyl), 110.5 (CH, Furyl), 108.4 (CH, Ar), 107.2 (CH, Ar), 102.5 (CH, Ar), 82.8 (C,

quat, *t*Bu), 66.1 (CH_2), 62.3 (CH_2), 28.4 (3 x CH_3, *t*Bu); *m/z* (ES) 328 ($M+Na^+$, 100%).

(3-Hydroxyphenoxy)acetic acid ethyl ester 298

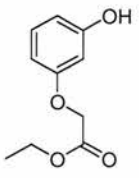

Resorcinol (7.00 g, 63.6 mmol) was added to a suspension of potassium carbonate (8.79 g, 63.6 mmol) in dry CH_3CN (200 cm^3) which had been degassed by bubbling a fast stream of nitrogen through it. The reaction mixture was then heated to 80 °C in order to dissolve the solids, then cooled, before dropwise addition addition of ethylbromoacetate (2.36 cm^3, 21.3 mmol) in dry CH_3CN (50 cm^3). The reaction mixture was then refluxed under nitrogen for 48 hours. After this time, the reaction mixture was filtered and the filtrate reduced *in vacuo*. The resulting oil was taken up in CH_2Cl_2 (50 cm^3) washed with 1 *M* aqueous HCl (1 x 30 cm^3), the organic layer washed with H_2O (1 x 20 cm^3), dried ($MgSO_4$) and solvent removed *in vacuo*. The resulting colourless oil was purified using column chromatography (SiO_2, 2:1 v/v hexane:EtOAc) to afford the product as a yellow oil (1.42 g, 34%); ν_{max}(film)/cm^{-1} 3358 (O-H), 1730 (C=O), 1597, 1489 (C=C, Ar), 1146 and 1176 (R-O-R); δ_H(300 MHz; $CDCl_3$) 7.06 (1H, m, Ar), 6.42-6.36 (3H, m, Ar), 4.59 (2H, s, CH_2), 4.27 (2H, q, $^3J_{H,H}$ 7.1, CH_2), 1.30 (3H, t, $^3J_{H,H}$ 7.1, CH_3); δ_C(75 MHz; $CDCl_3$) 167.5 (C, quat, C=O), 157.1 (C, quat, Ar), 155.0 (C, quat, Ar), 128.3 (CH, Ar), 107.2 (CH, Ar), 105.9 (CH, Ar), 105.8 (CH, Ar), 63.4 (CH_2), 59.7 (CH_2), 12.2 (CH_3); *m/z* (ES) 195.0657 ($M-H^+$ - $C_{10}H_{11}O_4$ requires 195.0659), 149 (63%).

[3-(Furan-3-ylmethoxy)phenoxy]acetic acid ethyl ester 299

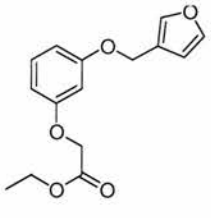

(3-Hydroxyphenoxy)acetic acid ethyl ester **298** (250 mg, 2.60 mmol) was added to a suspension of potassium carbonate (1.41 g, 10.2 mmol) in dry CH_3CN (20 cm^3) which had been degassed by bubbling a fast stream of nitrogen through it. The reaction mixture was

then heated to 80 °C in order to dissolve the solids, cooled, before dropwise addition of crude freshly prepared **141** (2.36 cm^3, 21.3 mmol). The reaction mixture was then refluxed under nitrogen for 48 hours. After this time, the reaction mixture was filtered and the filtrate reduced *in vacuo*. The resulting oil was taken up in CH_2Cl_2 (1 x 50 cm^3) washed with 1 *M* aqueous HCl (1 x 30 cm^3), the organic layer washed with H_2O (1 x 20 cm^3), dried ($MgSO_4$) and solvent removed *in vacuo*. The resulting colourless oil was purified *via* column chromatography (SiO_2, 2:1 v/v hexane:EtOAc) to afford the product as a yellow oil (460 mg, 64%); ν_{max}(film)/cm^{-1} 1733 (C=O), 1203, 1145 (R-O-R); δ_H(300 MHz; $CDCl_3$) 7.51-7.50 (1H, m, FurylH), 7.44-7.43 (1H, m, FurylH), 7.23-7.17 (1H, m, Ar), 6.64-6.60 (1H, m, Ar), 6.57-6.50 (2H, m, Ar), 6.48 (1H, dd, $^4J_{H,H}$ 0.8, $^4J_{H,H}$ 1.0, FurylH), 4.91 (2H, s, CH_2), 4.60 (2H, s, CH_2), 4.28 (2H, q, $^3J_{H,H}$ 7.1, CH_2), 1.30 (3H, t, $^3J_{H,H}$ 7.1, CH_3); δ_C(75 MHz, $CDCl_3$) 169.3 (C, quat, C=O), 160.2 (C, quat, Ar), 159.4 (C, quat, Ar), 143.9 (CH, Furyl), 141.3 (CH, Furyl), 130.4 (CH, Ar), 121.6 (C, quat, Furyl), 110.6 (CH, Ar), 108.5 (CH, Ar), 107.3 (CH, Ar), 102.5 (CH, Furyl), 65.8 (CH_2), 62.3 (CH_2), 61.8 (CH_2), 14.6 (CH_3); *m/z* (ES) 299.0902 ($M+Na^+$ - $C_{15}H_{16}O_5Na$ requires 299.0895).

3-Furan-3-yl-propionic acid 301

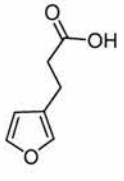

trans-3-Furanacrylic acid (5.00 g, 36.2 mmol) and 10 % palladium on carbon were flushed with nitrogen for 30 minutes before MeOH (75 cm^3) was syringed carefully into the flask. The flask was then flushed with H_2 gas and a hydrogen balloon fitted. The reaction mixture was then stirred at room temperature for 3.5 hours. After this time, the reaction mixture was filtered over Celite@, flushed with CH_2Cl_2 (20 cm^3) and the solvent then removed *in vacuo*. The resulting crude brown solid was purified *via* Kugelröhr distillation subsequent recrystallisation from hexane afforded the product as a colourless solid (4.70 g, 93%); mp 62 °C (lit.,[247] 66-67 °C); υ_{max}(film)/cm^{-1} 2932 (C-H), 2550 (O-H), 1694 (C=O), 1499 (C=C, Furyl); δ_H(300 MHz; $CDCl_3$) 7.29 (1H, m, FurylH), 7.14 (1H, m, FurylH), 6.22 (1H, m, FurylH), 2.98 (2H, t, $^3J_{HH}$ 7.2, CH_2), 2.72 (2H, t, $^3J_{HH}$ 7.2, CH_2); δ_C(75 MHz; $CDCl_3$) 179.3 (C, quat, C=O), 154.2 (C, quat, Furyl), 141.8 (CH, Furyl), 110.6 (CH, Furyl), 105.9 (CH, Furyl), 32.9 (CH_2), 23.5 (CH_2); *m/z* (CI) 141.0556 ($M+H^+$ - $C_7H_9O_3$ requires 141.0552), 140

(M^+, 45%), 123 (100).

3-Furan-3-yl-propionyl fluoride 303

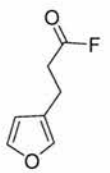

Cyanuric fluoride (0.72 cm^3, 8.60 mmol) was added dropwise to a stirring solution of 3-furan-3-yl-propionic acid (2.00 g, 14.3 mmol) in dry CH_3CN (20 cm^3) at -3 °C. The reaction mixture was then stirred for 10 minutes at -3 °C and subsequently warmed to room temperature for 5 minutes. The reaction mixture was then partitioned between CH_2Cl_2 (30 cm^3) and brine (1 x 20 cm^3), dried ($MgSO_4$) and solvent reduced to 15 cm^3 *in vacuo*. The resulting crude acid fluoride was reacted on to the next stage without further purification; δ_F(282.3 MHz; $CDCl_3$) +44.1 (1F, s, COF).

***exo*-{8-[2-(6-Methylpyridin-2-ylcarbamoyl)ethyl]-3,5-dioxo-10-oxa-4-aza-tricyclo[5.2.1.$0^{2,6}$]dec-8-en-4-yl}acetic acid 304**

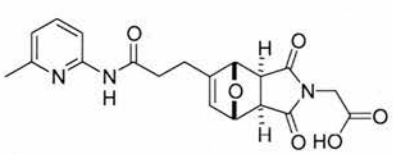

Colourless solid; mp 222-223 °C; υ_{max}(KBr)/cm^{-1} 3096.1 (N-H), 2999, 2920 (C-H), ~2750b (O-H), 1706 (C=O), 1610 (C=CH), 1181, 1160 (R-O-R, bridgehead); δ_H(300 MHz; DMSO-d_6) 10.53 (1H, bs, NH), 7.95 (1H, d, $^3J_{HH}$ 7.8, ArH), 7.70 (1H, d, $^3J_{HH}$ 7.8, ArH), 7.01 (1H, d, J_{HH}^3 7.8, ArH), 6.17 (1H, m, MalH), 5.14-5.13 (1H, m, bridgeheadH), 5.10-5.09 (1H, m, bridgehead H), 4.12 (2H, s, CH_2), 3.15 (2H, dd, $^3J_{HH}$ 26.8, $^3J_{HH}$ 6.6, CH), 2.66-2.55 (4H, m, 2 x CH_2), 2.45 (3H, s, CH_3); δ_C(75 MHz; DMSO-d_6) 175.8 (C, quat, C=O), 175.6 (C, quat, C=O), 174.3 (C, quat, C=O), 171.1 (C, quat, C=O), 156.3 (C, quat, Ar), 151.3 (C, quat, Ar), 150.4 (C, quat, alkene), 138.5 (CbH, Ar), 128.9 (CH, alkene), 118.4 (CH, Ar), 110.3 (CH, Ar), 82.2 (CH), 81.0 (CH), 48.8 (CH, bridgehead), 46.7 (CH, bridgehead), 39.3 (CH_2), 33.6 (CH_2), 23.5 (CH_3), 22.3 (CH_2); *m/z* (ES) 384.1198 (M-H^+ - $C_{19}H_{18}N_3O_6$ requires 384.1196), 322 (95%).

3-Furan-3-yl-*N*-[6-(3-furan-3-yl-propionylamino)pyridine-2-yl]propionate 305

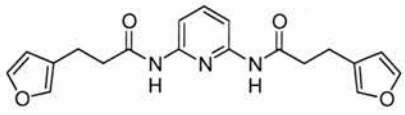

2,6 diaminopyridine (290 mg, 2.71 mmol) was added to a stirring solution of crude acid fluoride **303** (2 eq.) in acetone (50 cm^3). The reaction mixture was stirred for 16 hours under a positive pressure of nitrogen. After this time, the reaction mixture was extracted into CH_2Cl_2 (1 x 30 cm^3) washed with $NaHCO_3$ (1 x 20 cm^3), dried ($MgSO_4$) and concentrated *in vacuo*. The resulting yellow solid was recrystallised from hexane:EtOAc to yield the product as an off-white solid (211 mg, 22%); mp 144-145 °C; δ_H(300 MHz; $CDCl_3$) 7.82 (2H, d, $^3J_{H,H}$ 8.0, Ar), 7.63 (1H, dd, $^3J_{H,H}$ 8.0, $^3J_{H,H}$ 8.0, Ar), 7.49 (2H, bs, 2 x NH), 7.29 (2H, t, $^3J_{H,H}$ 1.6, 2 x FurylH), 7.21-7.20 (2H, m, 2 x FurylH), 6.23 (2H, d, $^3J_{H,H}$ 0.78, 2 x FurylH), 2.79 (4H, t, $^3J_{H,H}$ 7.2, 2 x CH_2), 2.54 (4H, t, $^3J_{H,H}$ 7.2, 2 x CH_2); δ_C(75 MHz; $CDCl_3$) 170.82 (2 x C, quat, C=O), 149.6 (2 x C, quat, Ar), 143.5 (2 x CH, Furyl), 141.3 (CH, Ar), 139.6 (2 x CH, Furyl), 123.7 (2 x C, quat, Furyl), 111.1 (2 x CH, Furyl), 109.9 (2 x CH, Ar), 38.5 (2 x CH_2), 20.8 (2 x CH_2); *m/z* (CI) 354.1461 ($M+H^+$ $C_{19}H_{20}N_3O_4$ requires 354.1454).

[3,5-Bis-(furan-3-ylmethoxy)phenoxy]acetic acid 306

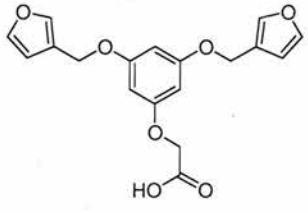

[3,5-Bis-(furan-3-ylmethoxy)phenoxy]acetic acid ethyl ester **313** (0.50 g, 1.34 mmol) was added to a stirred solution of 1 *M* KOH (1:1 THF:H_2O, 15 cm^3) the reaction mixture was refluxed for 1 hour. After this time, the reaction mixture was cooled to room temperature and acidified to pH 1 with 1 *M* aqueous HCl. The organic phase was then extracted with CH_2Cl_2 (1 x 50 cm^3), dried ($MgSO_4$), and solvent removed *in vacuo* to yield the product as a colourless solid (290 mg, 63 %); mp decomposes > 80 °C; ν_{max}(film)/cm^{-1}1733 (C=O), 1595 (Ar, C=C), 1203, 1147 (R-O-R), 873, 747 (C-H, Furyl); δ_H(300 MHz; $CDCl_3$) 7.49-7.48 (2H, m, 2 x FurylH), 7.44-7.43 (2H, m, 2 x FurylH), 6.48-6.47 (2H, m, 2 x FurylH), 6.27-6.25 (1H,

m, Ar), 6.18-6.17 (2H, m, Ar), 4.87 (4H, s, 2 x CH_2), 4.63 (2H, s, CH_2); δ_C(75 MHz; $CDCl_3$) 173.8 (C, quat, C=O), 160.9 (2 x C, quat, Ar), 159.6 (C, quat, Ar), 144.0 (CH, Furyl), 141.3 (CH, Furyl), 121.4 (2 x C, quat, Furyl), 110.6 (CH, Furyl), 96.0 (CH, Ar), 95.0 (2 x CH, Ar), 65.1 (CH_2), 62.4 (2 x CH_2); *m/z* (CI) 345.0977 ($M+H^+$ - $C_{18}H_{17}O_7$ requires 345.0974), 263 (78%), 161 (100).

(3,5-Dihydroxyphenoxy)acetic acid ethyl ester 312

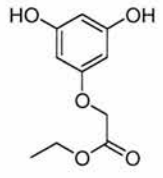

Phloroglucinol dihydrate (7.00 g, 43.2 mmol) was added to a suspension of potassium carbonate (4.47 g, 32.4 mmol) in dry CH_3CN (200 cm^3) which had been degassed by bubbling a fast stream of nitrogen through it. The reaction mixture was then heated to 80 °C in order to dissolve the solids, then cooled, before dropwise addition addition of ethylbromoacetate (1.19 ml, 10.8 mmol) in dry CH_3CN (50 cm^3). The reaction mixture was then refluxed under nitrogen for 48 hours. After this time, the reaction mixture was filtered and the filtrate reduced *in vacuo*. The resulting oil was taken up in CH_2Cl_2 (1 x 50 cm^3) washed with 1 *M* aqueous HCl (1 x 30 cm^3), the organic layer washed with H_2O (1 x 20 cm^3), dried ($MgSO_4$) and solvent removed *in vacuo*. The resulting colourless oil was purified *via* column chromatography (SiO_2, 1:1 v/v EtOAc:hexane) to afford the product as a colourless oil, traces of starting material remained as a result the compound was not fully characterised and was carried on to the next stage without further purification; δ_H(300 MHz, MeOD) 5.94-5.92 (1H, m, Ar), 5.89-5.88 (2H, m, Ar), 4.55 (2H, s, CH_2), 4.21 (2H, q, $^3J_{H,H}$ 7.1, CH_2), 1.26 (3H, t, $^3J_{H,H}$ 7.1, CH_3); δ_C(75 MHz, MeOD) 171.2 (C, quat, C=O), 161.3 (C, quat, Ar), 160.3 (2 x C, quat, Ar), 97.4 (CH, Ar), 94.8 (2 x CH, Ar), 66.1 (CH_2), 62.4 (CH_2), 14.5 (CH_3).

[3,5-Bis-(furan-3-ylmethoxy)phenoxy]acetic acid ethyl ester 317

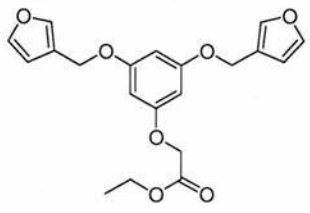

(3,5-Dihydroxyphenoxy)acetic acid ethyl ester **312** (400 mg, 1.88 mmol) was added to a suspension of potassium carbonate (1.56 g, 5.66 mmol) in dry CH_3CN (20 cm^3) which had been degassed by bubbling a fast stream of nitrogen through it. The reaction mixture was then heated to 80 °C in order to dissolve the solids, cooled, before dropwise addition of crude freshly prepared **141** (0.66g, 5.66 mmol, in 20 cm^3 CH_3CN). The reaction mixture was then refluxed under nitrogen for 48 hours. After this time, the reaction mixture was filtered and the filtrate reduced *in vacuo*. The resulting oil was taken up in CH_2Cl_2 (1 x 50 cm^3) washed with 1 *M* aqueous HCl (1 x 30 cm^3), the organic layer washed with H_2O (1 x 20 cm^3), dried ($MgSO_4$) and solvent removed *in vacuo*. The resulting colourless oil was purified *via* column chromatography (SiO_2, 2:1 v/v hexane:EtOAc) to afford the product as a yellow oil, traces of starting material and mono-furyl compound remained as a result the compound was not fully characterised and was carried on to the next stage without further purification; δ_H (300 MHz, $CHCl_3$) 7.50-7.49 (2H, m, 2 x FurylH), 7.44-7.42 (2H, m, 2 x FurylH), 6.48-6.47 (2H, m, 2 x FurylH), 6.25-6.23 (1H, m, Ar), 6.17-6.16 (2H, m, Ar), 4.87 (4H, s, 2 x CH_2), 4.56 (2H, s, CH_2), 4.27 (2H, q, $^3J_{HH}$ 7.1, CH_2), 1.30 (3H, t, $^3J_{HH}$ 7.1, CH_3).

Chapter 7
References

[1] Pedersen, C. J., *J. Am. Chem. Soc.*, **1967**, *89*, 7017-7036.

[2] Pedersen, C. J., *Angew. Chem. Int. Ed. Engl.*, **1988**, *27*, 1021-1027.

[3] Dietrich, B.; Lehn, J.-M.; Sauvage, J. P., *Tetrahedron Lett.*, **1969**, *34*, 2885-2888.

[4] Lehn, J.-M., *Angew. Chem. Int. Ed. Engl.*, **1988**, *27*, 89-112.

[5] Ball, P., *Designing the Molecular World*, Princeton University Press, New Jersey, **1994**.

[6] Kyba, E. P.; Helgeson, R. C.; Madan, K.; Gokel, G. W.; Tarnowski, T. L.; Moore, S. S.; Cram, D. J., *J. Am. Chem. Soc.*, **1997**, *8*, 2564-2571.

[7] Lehn, J.-M., *Pure Appl. Chem.*, **1978**, *50*, 872-893.

[8] Lehn, J.-M., *Supramolecular Chemistry Concepts and Perspectives*, VCH, Weinheim, **1995**.

[9] Hof, F.; Craig, S. L.; Nuckolls, C.; Rebek Jr., J., *Angew. Chem. Int. Ed.*, **2002**, *41*, 1488-1508.

[10] Menger, F. M., *Proc. Natl. Acad. Aci USA*, **2002**, *99*, 4818-4822.

[11] Swiegers, G. F.; Malefetse, T. J., *Chem. Rev.*, **2000**, *100*, 3483-3537.

[12] Hunter, C. A., *Chem. Soc. Rev.*, **1994**, 23, 101-109.

[13] Hunter, C. A., *Angew. Chem. Int. Ed.*, **2004**, *43*, 5310-5324.

[14] Castellano, R. K.; Diederich, F.; Meyer, E. A., *Angew. Chem. Int. Ed.*, **2003**, *42*, 1210-1250.

[15] Mascal, M., *Contemporary Organic Synthesis*, **1994**, *1*, 31-46.

[16] Lehn, J.-M., *Angew. Chem. Int. Ed. Engl.*, **1990**, *29*, 1304-1319.

[17] Fyfe, M. C. T.; Stoddart, J. F., *Acc. Chem. Res.*, **1997**, 30, 393-401.

[18] Lehn, J.-M., *Angew. Chem. Int. Ed.*, **1998**, *27*, 89-112.

[19] Reinhoudt, D. N.; Stoddart, J. F.; Ungaro, R., *Chem. Eur. J.*, **1998**, *4*, 1349-1352.

[20] Lavigne, J. J.; Anslyne, E. V., *Angew. Chem. Int. Ed.*, **2001**, *40*, 3118-3130.

[22] Niemeyer, C. M., *Angew. Chem. Int. Ed.*, **2001**, *40*, 4128-4158.

[23] Schalley, C. A.; Lützen, A.; Albrecht, M., *Chem. Eur. J.*, **2004**, *10*, 1072-1080.

[24] Cram, D. J., *Angew. Chem. Int. Ed.*, **1988**, *27*, 1009-1020.

[25] Rebek Jr., J., *Angew. Chem. Int. Ed. Engl.*, **1990**, *29*, 245-255.

[26] Rebek Jr., J., *Acc. Chem. Res.*, **1990**, *23*, 400-404.

[27] Nernst, W. Z., *Phys. Chem.*, **1892**, *8*, 110.

[28] Werner, A., *Liebigs. Ann. Chem.*, **1902**, *322*, 261.

[29] Huggins, M. L., *J. Org. Chem.*, **1936**, *1*, 407-456.

[30] Prins, L. J.; Reinhoudt, D. N.; Timmerman, P., *Angew. Chem. Int. Ed.*, **2001**, *40*, 2382-2426.

[31] Jorgenson, W. L.; Pranata, J., *J. Am. Chem. Soc.*, **1990**, *112*, 2008-2010.

[32] Murray, T. J.; Zimmerman, S. C., *J. Am. Chem. Soc.*, **1992**, *114*, 4010-4011.

[33] Rebek Jr., J.; Askew, B.; Ballester, C.; Buhr, C.; Jones, S.; Nemeth, D.; Williams, K., *J. Am. Chem. Soc.*, **1987**, *109*, 5033-5035.

[34] Watson, J. D.; Crick, F. H. C., *Nature*, **1953**, *171*, 737-738.

[35] Seel, C.; Galán, A.; Mendoza, J., *Top. Curr. Chem.*, **1995**, *175*, 101-132.

[36] Etter, M. C., *Acc. Chem. Res.*, **1990**, *23*, 120-126.

[37] Etter, M. C., *J. Phys. Chem.*, **1991**, *95*, 4601-4610.

[38] Rebek Jr., J., *Angew. Chem. Int. Ed. Engl.*, **1990**, *29*, 245-255.

[39] Kemp, D. S.; Petrakis, K. S., *J. Org. Chem.*, **1981**, *46*, 5140-5143.

[40] Rebek Jr., J., *Acc. Chem. Res.*, **1990**, *23*, 401-404.

[41] Galán, A.; Mendoza, J.; Toiron, C.; Bruix, M.; Deslongchamps, G.; Rebek Jr., J., *J. Am. Chem. Soc.*, **1991**, *113*, 9424-9425.

[42] Chang, S.-K.; Van Engen, D.; Fan, E.; Hamilton, A. D., *J. Am. Chem. Soc.*, **1991**, *113*, 7640-7645.

[43] Garcia-Tellado, F.; Goswami, S.; Chang, S.-K.; Geib, S. J.; Hamilton, A. D., *J. Am. Chem. Soc.*, **1990**, *112*, 7393-7394.

[44] Lindsey, J. S., *New J. Chem.*, **1991**, *15*, 153-180.

[45] Philp, D.; Stoddart, J. F., *Angew. Chem. Int. Ed. Engl.*, **1996**, *35*, 1154-1196.

[46] Greig, L. M.; Philp, D., *Chem. Soc. Rev.*, **2001**, *30*, 287-302.

[47] Klug, A., *Angew. Chem. Int. Ed. Engl.*, **1983**, *22*, 565-582.

[48] Fraenkel-Conrat, H.; Williams, R. C., *Proc. Natl. Acad. Sci. USA*, **1995**, *41*, 690-698.

[49] Philp, D.; Stoddart, J. F., *Synlett*, **1991**, 7, 445-458.

[50] Hopf, H., *Angew. Chem. Int. Ed.*, **2003**, *115*, 2928-2931.

[51] Rowan, A. E.; Nolte, R. J. M., *Angew. Chem. Int. Ed.*, **1998**, 37, 63-67.

[52] Schmuck, C., *Angew. Chem. Int. Ed.*, **2003**, *42*, 2448-2452.

[53] Constable, E. C., in *Comprehensive Supramolecular Chemistry*, Ed. J.-M. Lehn, Elseiver, **1996**.

[54] Conn, M. M.; Rebek Jr., J., *Chem. Rev.*, **1997**, *97*, 1647-1668.

[55] Hof, F.; Rebek Jr. J., *Proc. Natl. Acad. Sci. USA*, **2002**, *99*, 4775-4777.

[56] Lipkowski, P.; Bielejewska, A.; Kooijman, H.; Spek, A. L.; Timmerman, P.; Reinhoudt, D. N., *Chem. Commun.*, **1999**,1311-1312.

[57] Ruben, M.; Lehn, J.-M.; Vaughan, G., *Chem. Commun.*, **2003**, 1338-1339.

[58] Hunter, C. A., *Angew. Chem. Int. Ed. Engl.*, **1995**, *34*, 1079-1081.

[59] Albrecht, M., *Chem. Rev.*, **2001**, *101*, 3457-3497.

[60] Piguet, C.; Bernardinelli, G.; Hopfgartener, G., *Chem. Rev.*, **1997**, *97*, 2005-2062.

[61] Lehn, J.-M.; Sauvage, J.-P.; Simon, J.; Ziessel, R., *Nouveau Journal de Chimie*, **1983**, *7*, 413-420.

[62] Lehn, J.-M., *Chem. Eur. J.*, **2000**, *6*, 2097-2102.

[63] Lehn, J.-M.; Rigault, A.; Siegel, J.; Harrowfield, J.; Chevrier, B.; Moras, D., *Proc. Natl. Acad. Sci. USA*, **1987**, *84*, 2565-2569.

[64] Lehn, J.-M.; Rigault, A., *Angew. Chem. Int. Ed. Engl.*, **1988**, *27*, 1095-1097.

[65] Kramer, R.; Lehn, J.-M.; Marquis-Rigault, A., *Proc. Natl. Acad. Sci. USA*, **1993**, *90*, 5394-5398.

[66] Hasenknopf, B.; Lehn, J.-M.; Baum, G.; Kneisel, B. O.; Fenske, D., *Angew. Chem. Int. Ed. Engl.*, **1996**, *35*, 1838-1840.

[67] Hasenknopf, B.; Lehn, J.-M.; Boumediene, N.; Dupont-Gervais, A.; Van Dorsselaer, A.; Kneisel, B.; Fenske, D., *J. Am. Chem. Soc.*, **1997**, *119*, 10956-10962.

[68] Lehn, J.-M., *Chem. Eur. J.*, **1999**, *5*, 2455-2463.

[69] Terret, N. K., *Combinatorial Chemistry*, Oxford University Press, Oxford, **1998**.

[70] Fischer, E., *Ber. Dtsch. Chem. Ges.*, **1894**, *27*, 2985-2993.

[71] Moore, J. S.; Zimmerman, N. W., *Org. Lett.*, **2000**, *2*, 915-918.

[72] Corbett, P. T; Otto, S.; Sanders, J. K. M., *Org. Lett.*, **2004**, *6*, 1825-1827.

[73] Corbett, P. T.; Otto, S.; Sanders, J. K. M., *Chem. Eur. J.*, **2004**, *10*, 3139-3143.

[74] Severin, K., *Chem. Eur. J.*, **2004**, *10*, 2565-2580.

[75] Klekota, B.; Miller, B. L., *Trends in Biotechnology*, **1999**, *17*, 205-209.

[76] Cousins, G. R. L.; Poulsen, S.-A.; Sanders, J. K. M., *Curr. Opin. Chem. Bio.*, **2000**, *4*, 270-279.

[77] Karan, C.; Miller, B. L., *Drug Discov. Today*, **2000**, *5*, 67-75.

[78] Motherwell, W. B.; Bingham, M. J.; Six, Y., *Tetrahedron*, **2001**, *57*, 4663-4686.

[79] Huc, I.; Nguyen, R., *Comb. Chem. High T. Scr.*, **2001**, *4*, 109-130.

[80] Lehn, J. M.; Eliseev, A. V., *Science*, **2001**, *291*, 2331-2332.

[81] Otto, S.; Furlan, R. L. E.; Sanders, J. K. M., *Curr. Opin. Chem. Bio.*, **2002**, *6*, 321-327.

[82] Ramström, O.; Lehn, J.-M., *Nat. Rev. Drug Discov.*, **2002**, *1*, 26-36.

[83] Ramström, O.; Bunyapaiboonsri, T.; Lohmann, S.; Lehn, J.-M., *Biochim. Biophys. Acta*, **2002**, *1572*, 172-186.

[84] Otto, S.; Furlan, R. L. E.; Sanders, J. K. M., *Drug Discov. Today*, **2002**, 7, 117-125.

[85] Rowan, S. J.; Cantrill, S. J.; Cousins, R. L.; Sanders, J. K. M.; Stoddart, J. F., *Angew. Chem. Int. Ed.*, **2002**, *41*, 898-952.

[86] Brady, P. A.; Bonar-Law, R. P.; Rowan, S. J.; Suckling, C. J.; Sanders, J. K. M., *Chem. Commun*, **1996**, 319-320.

[87] Brady, P. A.; Sanders, J. K. M., *J. Chem. Soc., Perkin Trans. 1*, **1997**, 3237-3253.

[88] Kaiser, G.; Sanders, J. K. M., *Chem. Commun.*, **2000**, 1763-1764.

[89] Swann, P. G.; Casanova, R. A.; Desai, A.; Frauenhoff, M. M.; Urbancic, M.; Slomczynska, U.; Hopfinger, A. J.; Le Breton, G. C.; Venton, D. L., *Biopolymers*, **1997**, *40*, 617-625.

[90] Sakai, S.; Shigemasa, Y.; Saski, T., *Tetrahedron Lett.*, **1997**, *38*, 8145-8148.

[91] Star, A.; Goldberg, I.; Fuchs, B., *Angew. Chem. Int. Ed.*, **2000**, *39*, 2685-2689.

[92] Epstein, D. M.; Choudhary, S.; Churchill, M. R.; Keil, K. M.; Eliseev, A. V.; Morrow, J. R., *Inorg. Chem.*, **2001**, *40*, 1591-1596.

[93] Bunyapaiboonsri, T.; *ChemBioChem.*, **2001**, *2*, 438-444.

[94] Storm, O.; Lüning, U., *Chem. Eur. J.*, **2002**, *8*, 793-798.

[95] Hochgürtel, M.; Kroth, H.; Piecha, D.; Hofmann, M. W.; Nicolau, C.; Krause, S.; Schaaf, O.; Sonnenmoser, G.; Eliseev, A. V., *Proc. Natl. Acad. Sci. USA*, **2002**, *99*, 3382-3387.

[96] Mascal, M.; Wood, I. G.; Walsgrove, T., *Org. Lett.*, **2003**, *5*, 2517-2518.

[97] Giuseppone, N.; Lehn, J.-M., *J. Am. Chem. Soc.*, **2004**, *126*, 11448-11449.

[98] González-Álvarez, A.; Alfonso, I.; López-Ortiz, F.; Aguirre, Á.; Garcia-Granda, A.; Gotor, V., *Eur. J. Org. Chem.*, **2004**, 1117-11127.

[99] Huc, I.; Lehn, J.-M., *Proc. Natl. Acad. Sci. USA*, **1997**, *94*, 2106-2110.

[100] Polyakov, V. A.; Nelen, M. I.; Narzarpack-Kandlousy, N.; Ryabox, A. D.; Eliseev, A. V., *J. Phys. Org. Chem.*, **1999**, *12*, 357-363.

[101] Nazarpack-Kandlousy, N.; Zweigenbaum, J.; Henion, J.; Eliseev, A. V., *J. Comb. Chem.*, **1999**, *1*, 199-206.

[102] Cousins, G. R. L.; Poulsen, S.-A.; Sanders, J. K. M., *Chem. Commun.*, **1999**, 1575-1576.

[103] Furlan, R. L. E.; Cousins, G. R. L.; Sanders, J. K. M., *Chem. Commun.*, **2000**, *18*, 1761-1762.

[104] Cousins, G. R. L.; Furlan, R. L. E.; Ng, Y.-F; Redman, J. E.; Sanders, J. K. M., *Angew. Chem. Int. Ed.*, **2001**, *40*, 423-428.

[105] Furlan, R. L. E.; Ng, Y.-F; Cousins, G. R. L.; Redman, J. E.; Sanders, J. K. M., *Tetrahedron*, **2002**, *58*, 771-778.

[106] Kubik, S.; Goddard, R., *J. Org. Chem.*, **1999**, *64*, 9475-9486.

[107] Furlan, R. L. E.; Ng, Y.-F; Otto, S.; Sanders, J. K. M., *J. Am. Chem. Soc.*, **2001**, *123*, 8876-8877.

[108] Ramström, O.; Lehn, J.-M., *ChemBioChem.*, **2000**, *1*, 41-47.

[109] Ramström, O.; Lohmann, S.; Bunyapaiboonsri, T.; Lehn, J.-M., *Chem. Eur. J.*, **2004**, *10*, 1711-1715.

[110] Bunyapaiboonsri, T.; Ramström, O.; Lohmann, S.; Lehn, J.-M.; Peng, L.; Goeldner, M., *ChemBioChem*, **2001**, *2*, 438-444.

[111] Bunyapaiboonsri, T.; Ramström, H.; Ramström, O.; Haiech, J.; Lehn, J.-M., *J. Med. Chem.*, **2003**, *46*, 5803-5811.

[112] Patai, S., *The Chemistry of The Thiol Group*, Wiley, London, **1974**.

[113] Ganesan, A., *Angew. Chem. Int. Ed.*, **1998**, *37*, 2828-2831.

[114] Hioki, H.; Still, W. C., *J. Org. Chem.*, **1998**, *63*, 904-905.

[115] Otto, S.; Furlan, R. L. E.; Sanders, J. K. M., *J. Am. Chem. Soc.*, **2000**, *122*, 12063-12064.

[116] Otto, S.; Furlan, R. L. E.; Sanders, J. K. M., *Science*, **2002**, *297*, 590-593.

[117] Brisig, B.; Sanders, J. K. M.; Otto, S., *Angew. Chem. Int. Ed.*, **2003**, *42*, 1270-1273.

[118] Otto, S.; Kubik, S., *J. Am. Chem. Soc.*, **2003**, *125*, 7804-7805.

[119] Krishnan-Ghosh, Y.; Balasubramanian, S., *Angew. Chem. Int. Ed.*, **2003**, *42*, 2171-2173.

[120] Whitney, A. M.; Ladame, S.; Balasubramanian, S., *Angew. Chem. Int. Ed.*, **2004**, *43*, 1143-1146.

[121] Nicolaou, K. C.; Hughes, R.; Cho, S. Y.; Winssinger, N.; Smethurst, C.; Labischinski, H.; Endermann, R., *Angew. Chem. Int. Ed.*, **2000**, *39*, 3823-3828.

[122] Brändli, C.; Ward, H., *Helv. Chim. Acta.*, **1998**, *81*, 1616-1621.

[123] Larsson, R.; Pei, Z.; Ramström, O., *Angew. Chem. Int. Ed.*, **2004**, *43*, 3716-3718.

[124] Calama, M. C.; Timmerman, P.; Reinhoudt, D. N., *Angew. Chem. Int. Ed.*, **2000**, *39*, 755-758.

[125] Jolliffe, K. A.; Calma, M. C.; Fokkens, R.; Nibbering, N. M. M.; Timmerman, P.; Reinhoudt, D. N., *Angew. Chem. Int. Ed.*, **1998**, *37*, 1247-1251.

[126] Timmerman, P.; Reinhoudt, D. N., *Adv. Mater.*, **1999**, *11*, 71-74.

[127] Cardullo, F.; Calama, M. C.; Snellink-Ruel, B. H. M.; Weidmann, J.-L.; Bielejewska, A.; Fokkens, R.; Nibbering, N. M. M.; Timmerman, P.; Reinhoudt, D. N., *Chem. Commun.*, **2000**, 367-368.

[128] Hof, F.; Nuckolls, C.; Rebek Jr., J., *J. Am. Chem. Soc.*, **2000**, *122*, 4251-4252.

[129] Marsella, M. J.; Maynard, H. D.; Grubbs, R. H., *Angew. Chem. Int. Ed. Engl.*, **1997**, *36*, 1101-1103.

[130] Hiraoka, S.; Fujita, M., *J. Am. Chem. Soc.*, **1999**, *121*, 10239-10240.

[131] Albrecht, M.; Blau, O.; Frohlich, R., *Chem. Eur. J.*, **1999**, *5*, 48-56.

[132] Huc, I.; Krische, M. J.; Fueriu, D. P.; Lehn, J.-M., *Eur. J. Inorg. Chem.*, **1999**, 1415-1420.

[133] Constable, E. C.; Housecroft, C. E.; Kulke, T.; Lazzarini, C.; Schofield, E. R.; Zimmermann, Y., *J. Chem. Soc., Dalton Trans.*, **2001**, 2864-2871.

[134] Ziegler, M.; Miranda, J. J.; Andersen, U. N.; Johnson, D. W.; Leary, J. A.; Raymond, K. N., *Angew. Chem. Int. Ed.*, **2001**, *40*, 733-736.

[135] Kubota, Y.; Sakamoto, S.; Yamauchi, K.; Fujita, M., *Proc. Natl. Acad. Sci. USA*, **2002**, *99*, 4854-4856.

[136] Albrecht, M.; Blau, O.; Fröhlich, R., *Proc. Natl. Acad. Sci. USA*, **2002**, *99*, 4867-4872.

[137] Grote, Z.; Scopelliti, R.; Severin, K., *Angew. Chem. Int. Ed.*, **2003**, *42*, 3821-3825.

[138] Giuseppone, N.; Schmitt. J.-L.; Lehn, J.-M., *Angew. Chem. Int. Ed.*, **2004**, *43*, 4902-4906.

[139] Stulz, E.; Ng, Y.-F.; Scott, S. M.; Sanders, J. K. M., *Chem Commun.*, **2002**, 524-525.

[140] Stulz, E.; Scott, S. M.; Bond, A. D.; Teat, S. J.; Sanders, J. K. M., *Chem. Eur. J.*, **2003**, *9*, 6039-6048.

[141] Klekota, B.; Hammond, M. H.; Miller, B. L., *Tetrahedron Lett.*, **1997**, *38*, 8639-8642.

[142] Klekota, B.; Miller, B. L., *Tetrahedron*, **1999**, *55*, 11687-11697.

[143] Karan, C.; Miller, B. L., *J. Am. Chem. Soc.*, **2001**, *123*, 7455-7456.

[144] Berl, V.; Huc, I.; Lehn, J.-M.; DeCian, A.; Fischer, J., *Eur. J. Org. Chem.*, **1999**, 3089-3094.

[145] Eliseev, A. V.; Nelen, M. I., *J. Am. Chem. Soc.*, **1997**, *199*, 1147-1148.

[146] Goral, V.; Nelen, M. I.; Eliseev, A. V.; Lehn, J.-M., *Proc. Natl. Acad. Sci. USA*, **2001**, *98*, 1347-1352.

[147] Choudary, S.; Morrow, J. R., *Angew. Chem. Int. Ed.*, **2002**, *41*, 4096-4098.

[148] Pauling, L., *Nature*, **1948**, *161*, 707-709.

[149] Menger, F. M., *Biochemistry*, **1992**, *31*, 5368-5373.

[150] Koshland, D. E., *J. Theor. Biol.*, **1962**, *2*, 75-86.

[151] Bruice, T. C.; Pandit, U. K., *Proc. Natl. Acad. Sci. USA*, **1960**, *46*, 402-404.

[152] Bruice, T. C.; Pandit, U. K., *J. Am. Chem. Soc.*, **1960**, *82*, 5858-5865.

[153] Kirby, A. J., *Adv. Phys. Org. Chem.*, **1980**, *17*, 183-259.

[154] Beesley, R. M.; Ingold, C. K, *J. Am. Chem. Soc.*, **1915**, *107*, 1080-1105.

[155] Schleyer, P. von R., *J. Am. Chem. Soc.*, **1961**, *83*, 1368-1373.

[156] Jung, M. E.; Gervay, J., *J. Am. Chem. Soc.*, **1989**, *111*, 5469-5470.

[157] Jung, M. E.; Gervay, J., *J. Am. Chem. Soc.*, **1991**, *113*, 224-232.

[158] Menger, F. M., *Acc. Chem. Res.*, **1985**, *18*, 128-134.

[159] Menger, F. M., *Acc. Chem. Res.*, **1993**, *26*, 206-212.

[160] Page, M. I., *Angew. Chem. Int. Ed. Engl.*, **1977**, *16*, 449-459.

[161] Page, M. I., *Phil. Trans. R. Soc. Lond. B.*, **1991**, *332*, 149-156.

[162] Koshland Jr., D. E., *J. Theoret. Biol.*, **1962**, *2*, 75-86.

[163] Storm, D. R.; Koshland Jr., D. E., *J. Am. Chem. Soc.*, **1972**, 94, 5815-5825.

[164] Hoare, D. G., *Nature*, **1972**, *236*, 437-440.

[165] Menger, F. M.; Glass, L. E., *J. Am. Chem. Soc.*, **1980**, *102*, 5406-5407.

[166] Lightstone, F. C.; Bruice, T. C., *J. Am. Chem. Soc.*, **1996**, *118*, 2595-2605.

[167] Lightstone, F. C.; Bruice, T. C., *J. Am. Chem. Soc.*, **1997**, *119*, 9103-9113.

[168] Lightstone, F. C.; Bruice, T. C., *Bioorg. Chem.*, **1998**, *26*, 193-199.

[169] Bruice, T. C.; Lightstone, F. C., *Acc. Chem. Res.*, **1999**, *32*, 127-136.

[170] Page, M. I.; Jencks, W. P., *Proc. Natl. Acad. Sci. USA*, **1971**, *68*, 1678-1683.

[171] Kelly, T. R.; Bridger, G. J.; Zhao, C., *J. Am. Chem. Soc.*, **1990**, *112*, 8024-8034.

[172] Walter, C. J.; Anderson, H. L.; Sanders, J. K. M., *J. Chem. Soc., Chem. Commun.*, **1993**, 458-460.

[173] Clyde-Watson, Z.; Vidal-Ferran, A.; Twyman, L. J.; Walter, C. J.; McCallien, D. W. J.; Fanni, S.; Bampos, N.; Wylie, R. S.; Sanders, J. K. M., *New J. Chem.*, **1998**, 493-502.

[174] Diels, O.; Alder, K., *Justus Liebigs Ann. Chem.*, **1928**, *98*, 460.

[175] Fleming, I., *Frontier Orbitals and Organic Chemical Reactions*, Wiley, Oxford, **1976**.

[176] Fringuelli, F.; Taticchi, A., *Dienes in the Diels-Alder reaction*, Wiley, New York, **1990**.

[177] Sustmann, R.; Schubert, R., *Angew. Chem. Int. Ed. Engl.*, **1972**, *11*, 840.

[178] Diederich, F.; Stang, P. J., *Templated Organic Synthesis*, Wiley, Weinheim, **2000**.

[179] Jensen, F., *Introduction to Computational Chemistry*, Wiley, New York, **1998**.

[180] Philp, D.; Robertson, A., *Chem. Commun.*, **1998**, *8*, 879-880.

[181] Booth, C. A.; Philp, D., *Tetrahedron Lett.*, **1998**, *39*, 6987-6990.

[182] Robertson, A.; Philp, D.; Spencer, N., *Tetrahedron*, **1999**, *55*, 11365-11384.

[183] Bennes, R.; Philp, D.; Spencer, N.; Kariuki, B. M.; Harris, K. D. M., *Org. Lett.*, **1999**, *1*, 1087-1090.

[184] Bennes, R.; Babiloni, M. S.; Hayes, W.; Philp, D., *Tetrahedron Lett.*, **2001**, *42*, 2377-2380.

[185] Howell, S. J.; Spencer, N.; Philp, D., *Tetrahedron*, **2001**, *57*, 4945-4954.

[186] Pearson, R. J.; Kassianidis, E.; Philp, D., *Tetrahedron Lett.*, **2004**, *45*, 4777-4780.

[187] Patai, S., *The Chemistry of the Amino Group*, Interscience, London, **1968**.

[188] Sinclair, A. J., PhD Thesis, University of Birmingham, **1999**.

[189] Hu, J.; Fox, M. A., *J. Org. Chem.*, **1999**, *64*, 4959-4961.

[190] Černý, M.; Vrkoč, J.; Staněk, J., *Collect. Czech. Chem. Commun.*, **1959**, *24*, 64-69.

[191] Zheng, T-C.; Burkart, M.; Richardson, D. E, *Tetrahedron Lett.*, **1999**, *40*, 603-606.

[192] Dowden, J.; Edwards, P. D.; Flack, S. S.; Kilburn, J., *Chem. Eur. J.*, **1999**, *5*, 79-89.

[193] Rich, D. H.; Gesellchen, P. D.; Tong, A.; Cheng, A.; Buckner, C. K., *J. Med. Chem.*, **1975**, *18*, 1004-1010.

[194] Allen, V. C., PhD Thesis, University of Birmingham, **2000**.

[195] Patai, S., *The Chemistry of The Thiol Group*, Wiley, London, **1974**.

[196] Tam-Chang, S-W.; Stehouwer, J. S.; Hao, J., *J. Org. Chem.*, **1999**, *64*, 334-335.

[197] Furusho, Y.; Hasegawa, T.; Tsuboi, A.; Kihara, N.; Takata, T., *Chem. Lett.*, **2000**, *1*, 18-19.

[198] Michael, A., *J. Prakt. Chem.*, **1887**, *35*, 379.

[199] Bergmann, E. D.; Ginsburg, D.; Pappo, R., *Organic Reactions*, **1959**, *10*, 179-555.

[200] van Axel Castelli, V.; Bernardi, F.; Cort, A. D.; Mandolini, L.; Rossi, I.; Schiaffino, L., *J. Org. Chem.*, **1999**, *64*, 8122-8126.

[201] Baumann, M. E.; Bosshard, H.; Breitenstein, W.; Ribs, G.; Winkler, T., *Helv. Chim. Acta*, **1984**, *67*, 1897-1905.

[202] Bugg, T., *Introduction to Enzyme and Coenzyme Chemistry, 2nd Ed.*, Blackwell, Oxford, **2004**.

[203] Ashton, P. R.; Howell, S. J.; Spencer, N.; Philp, D., *Org. Lett.*, **2001**, *3*, 353-356.

[204] Howell, S. J.; Spencer, N.; Philp, D., *Org. Lett.*, **2002**, *4*, 273-276.

[205] Cowie, R. M., PhD Thesis, University of St Andrews, **2005**.

[206] Roques, B. P.; Florentin, D.; Callanquin, M., *J. Am. Chem. Soc.*, **1975**, *12*, 195-196.

[207] Miyaura, N.; Suzuki, A., *Chem. Rev.*, **1995**, *95*, 2457-2483.

[208] Patil, V. J., *Tetrahedron Lett.*, **1996**, *37*, 1481-1484.

[209] Lam, L. K.-P.; Jones, J. P., *Can J. Chem.*, **1988**, *66*, 1422-1424.

[210] Williams, D. H.; Fleming, I., *Spectroscopic Methods in Organic Chemistry, 5th Ed.*, McGraw-Hill, Cambridge, **1995**.

[211] Wilcox, C., *Frontiers in Supramolecular Organic Chemistry and Photochemistry*, VCH, Weinheim, **1991**, 122-143.

[212] Stewart, J. J. P., *J. Comput. Chem.*, **1989**, *10*, 209-220.

[213] Stewart, J. J. P., *J. Comp-Aided. Mol. Design*, **1990**, *4*, 1-105.

[214] Stryer, L., *Biochemistry 3rd Ed.*, W. H. Freeman and Company, New York, **1988**.

[215] Watson, J. D.; Crick, F. H. C., *Nature*, **1953**, *171*, 737-738.

[216] Pauling, L.; Corey, R. B., *Nature*, **1953**, *171*, 346.

[217] Pauling, L.; Corey, R. B., *Proc. Natl. Acad. Sci. USA*, **1953**, *39*, 84-87.

[218] Wilkins, M. H. F.; Randell, J. T., *Biochim. Biophys. Acta*, **1953**, *10*, 192-193.

[219] Franklin, R. E.; Gosling, R. G., *Nature*, **1953**, *172*, 156-157.

[220] Zamenhof, S.; Brawerman, G.; Chargaff, E., *Biochim. Biophys. Acta*, **1952**, *9*, 402-405.

[221] Watson, J. D.; Crick, F. H. C., *Nature*, **1953**, *171*, 964-967.

[222] Meselson, M.; Stahl, F. W., *Proc. Natl. Acad. Sci. USA*, **1958**, *44*, 671-682.

[223] Robertson, A.; Sinclair, A. J.; Philp, D., *Chem. Soc. Rev.*, **2000**, *29*, 141-152.

[224] Orgel, L. E., *Nature*, **1992**, *358*, 203-209.

[225] von Kiedrowski, G., *Angew. Chem. Int. Ed. Engl.*, **1986**, *25*, 932-935.

[226] von Kiedrowski, G.; Wlotzka, B.; Helbing, J.; Matzen, M.; Jordan, S., *Angew. Chem. Int. Ed. Engl.*, **1991**, *30*, 423-426.

[227] Lee, D. H.; Granja, J. R.; Martinez, J. A.; Severin, K.; Ghadiri, M. R., *Nature*, **1996**, *382*, 525-527.

[228] Yao, S.; Ghosh, I.; Zutshi, R.; Chmielewski, J., *Angew. Chem. Int. Ed. Engl.*, **1998**, 478-481.

[229] Tjivikua, T.; Ballester, P.; Rebek Jr., J., *J. Am. Chem. Soc.*, **1990**, *112*, 1249-1250.

[230] Rotello, V.; Hong, J-I.; Rebek Jr., J., *J. Am. Chem. Soc.*, **1991**, *113*, 9422-9423.

[231] Park, T. K.; Feng, Q.; Rebek Jr., J., *J. Am. Chem. Soc.*, **1992**, *114*, 4529-4532.

[232] Conn, M. M.; Wintner, E. A.; Rebek Jr., J., *J. Am. Chem. Soc.*, **1994**, *116*, 8823-8824.

[233] Wintner, E. A.; Conn, M. M.; Rebek Jr., *J. Am. Chem. Soc.*, **1994**, *116*, 8877-8884.

[234] Menger, F. M.; Eliseev, A. V.; Khanjin, N. A., *J. Am. Chem. Soc.*, **1994**, *116*, 3613-3614.

[235] Menger, F. M.; Eliseev, A. V.; Sherrod, M. J., *J. Org. Chem.*, **1995**, *60*, 2870-2878.

[236] Wang, B.; Sutherland, I. O., *Chem. Commun.*, **1997**, 1495-1496.

[237] Reinhoudt, D. N.; Rudkevich, de Jong, F., *J. Am. Chem. Soc.*, **1996**, *118*, 6880-6889.

[238] Allen, V. C.; Philp, D.; Spencer, N., *Org. Lett.*, **2001**, *3*, 777-780.

[239] Pieters, R. J.; Huc, I.; Rebek Jr., J., *Tetrahedron*, **1995**, *51*, 485-498.

[240] Aruke, J.; Undheim, K., *Acta Chem. Scand.*, **1991**, *45*, 914-918.

[241] Allen, M., *Organic Synthesis*, **1955**, *3*, 710-711.

[242] L'Abbe, G., *Bull. Soc. Chim.*, **1968**, *7*, 345-368.

[243] Bonner, W. A.; Kahn, J. E., *J. Am. Chem. Soc.*, **1951**, *73*, 2241-2245.

[244] Vollmar, A.; Dunn, M. S., *J. Org. Chem.*, **1960**, *25*, 387-390.

[245] Greene, T. W.; Wut, P. G. M., Protective groups in Organic Synthesis, Wiley, Chichester, **1991**.

[246] Howell, S. J., PhD Thesis, University of St Andrews, **2001**.

[247] Arena, G.; Cali, R.; Maccarone, E.; Passerinni, A., *J. Chem. Soc., Perkin Trans. 2*, **1993**, *10*, 1941-1945.